Reaching Ultimate Sensitivity of Autofluorescence Spectroscopy on Label-Free Single Proteins with Deep-Ultraviolet Nanophotonics

Prithu Roy

Aix*Marseille université
Socialement engagée

NNT : 2023AIXM0001

THÈSE DE DOCTORAT

Soutenue à Aix-Marseille Université
le 7 décembre 2023 par

Prithu ROY

Reaching Ultimate Sensitivity of Autofluorescence Spectroscopy on Label-Free Single Proteins with Deep-Ultraviolet Nanophotonics

Discipline
Physique et Sciences de la Matière

Spécialité
Optique, Photonique et Traitement d'Image

École doctorale
ED352-Physique et Sciences de la Matière

Laboratoire/Partenaires de recherche
Institut Fresnel,CNRS

Composition du jury

Jerker WIDENGREN KTH Royal Institute of Technology, Sweden	Rapporteur
Celine FIORINI DEBUISSCHERT CEA, France	Rapporteure
Julien PROUST UTT Troyes, France	Examinateur
Yves MELY University of Strasbourg, France	Président du jury
Jerome WENGER Institut Fresnel, Aix Marseille University, France	Directeur de thèse

cnrs

INSTITUT FRESNEL

Affidavit

I, undersigned,Prithu Roy, hereby declare that the work presented in this manuscript is my own work, carried out under the scientific supervision of Jerome Wenger, in accordance with the principles of honesty, integrity and responsibility inherent to the research mission. The research work and the writing of this manuscript have been carried out in compliance with both the french national charter for Research Integrity and the Aix-Marseille University charter on the fight against plagiarism.

This work has not been submitted previously either in this country or in aother country in the same or in a similar version to any other examination body.

Marseille, 28.08.2023

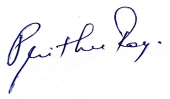

List of Publication and Conferences

Publication added in thesis

1. Prithu ROY, Siyuan ZHU et al. « Ultraviolet Resonant Nanogap Antennas with Rhodium Nanocube Dimers for Enhancing Protein Intrinsic Autofluorescence ». In : *ACS Nano* 17.22 (2023), p. 22418-22429. DOI : 10.1021/acsnano.3c05008. URL : https://doi.org/10.1021/acsnano.3c05008
2. Jerome WENGER, Prithu ROY, Jean-Benoit CLAUDE et al. « Self-Assembled Deep Ultraviolet Rhodium nanogap antenna to enhance single protein autofluorescence ». In : *Conference on Lasers and Electro-Optics/Europe (CLEO/Europe 2023) and European Quantum Electronics Conference (EQEC 2023) (2023), paper eh_p_16* (juin 2023), eh_p_16. URL : https://opg.optica.org/abstract.cfm?uri=EQEC-2023-eh_p_16
3. Jerome WENGER, Prithu ROY et Jean-Benoit CLAUDE. « Deep Ultraviolet Nanophotonics to enhance the sensitivity of autofluorescence spectroscopy on label-free proteins ». In : *Conference on Lasers and Electro-Optics/Europe (CLEO/Europe 2023) and European Quantum Electronics Conference (EQEC 2023) (2023), paper eg_5_5* (juin 2023), eg_5_5. URL : https://opg.optica.org/abstract.cfm?uri=EQEC-2023-eg_5_5
4. Prithu ROY, Jean-Benoît CLAUDE et al. « Ultraviolet Nanophotonics Enables Autofluorescence Correlation Spectroscopy on Label-Free Proteins with a Single Tryptophan ». In : *Nano Letters* 23.2 (jan. 2023), p. 497-504. DOI : 10.1021/acs.nanolett.2c03797
5. Prithu ROY, Clémence BADIE et al. « Preventing Corrosion of Aluminum Metal with Nanometer-Thick Films of Al2O3 Capped with TiO2 for Ultraviolet Plasmonics ». In : *ACS Applied Nano Materials* 4.7 (juin 2021), p. 7199-7205. DOI : 10.1021/acsanm.1c01160
6. Aleksandr BARULIN, Prithu ROY, Jean-Benoît Benoît CLAUDE et al. « Ultraviolet optical horn antennas for label-free detection of single proteins ». In : *Nature Communications* 13.1 (déc. 2022), p. 1842. URL : https://www.nature.com/articles/s41467-022-29546-4
7. Sunny TIWARI, Prithu ROY et al. « Achieving High Temporal Resolution in Single-Molecule Fluorescence Techniques Using Plasmonic Nanoantennas ». In : *Advanced Optical Materials* (avr. 2023). ISSN : 2195-1071. DOI : 10.1002/ADOM.202300168. URL : https://onlinelibrary.wiley.com/doi/10.1002/adom.202300168

8. Aleksandr BARULIN, Prithu ROY, Jean-Benoît CLAUDE et al. « Purcell radiative rate enhancement of label-free proteins with ultraviolet aluminum plasmonics ». In : *Journal of Physics D : Applied Physics* 54.42 (oct. 2021), p. 425101. ISSN : 0022-3727. DOI : 10.1088/1361-6463/ac1627. URL : https://iopscience.iop.org/article/10.1088/1361-6463/ac1627
9. Mikhail BAIBAKOV, Aleksandr BARULIN, Prithu ROY, Jean-Benoît CLAUDE et al. « Zero-mode waveguides can be made better : fluorescence enhancement with rectangular aluminum nanoapertures from the visible to the deep ultraviolet ». In : *Nanoscale Advances* 2.9 (2020), p. 4153-4160. ISSN : 2516-0230. DOI : 10.1039/d0na00366b

Publication not-included in thesis

1. Quanbo JIANG, Prithu ROY, Jean-Benoît CLAUDE et al. « Single Photon Source from a Nanoantenna-Trapped Single Quantum Dot ». In : *Nano Letters* (août 2021), p. 7030-7036. ISSN : 1530-6984. DOI : 10.1021/acs.nanolett.1c02449

Participation in conference during thesis

1. CLEO-EQEC Europe 2023, Munich,Germany (Invited talk and poster)
2. Scientific days of the Active Plasmonics GDR Marseille 2023, Marseille, France (Talk)
3. Nanophotonics and Micro/Nano Optics International Conference 2022 , Paris, France (Talk)
4. Summer School : Photothermal Effects in Plasmonics. 2021, Porquerolles, France (Poster)
5. International Workshop on Single molecule Spectroscopy and Super resolution Microscopy in Life science, PicoQuant, Berlin,Germany 2021 (Talk and Best speaker Award)

Résumé

Les études de fluorescence à l'échelle d'une molécule sont essentielles en recherche biophysique. À la différence des mesures d'ensemble, qui donnent des moyennes sur plusieurs molécules, les études monomoléculaires révèlent les comportements individuels. Toutefois, elles reposent sur l'utilisation de marqueurs fluorescents qui peuvent modifier la dynamique des molécules, comme les protéines. Il est donc crucial d'étudier la nature propre des protéines pour saisir leurs fonctions.

Cette thèse aborde des techniques avancées de spectroscopie d'autofluorescence UV sans marqueur, permettant d'étudier les protéines au niveau moléculaire sans marquage. Par la spectroscopie ultraviolette et la nanophotonique, la cinétique protéique monomoléculaire est analysée. Le texte couvre la littérature sur les méthodes monomoléculaires, les techniques sans marqueurs, et le potentiel de l'autofluorescence UV. Il aborde aussi les challenges liés au faible signal d'autofluorescence et aux spécificités des microscopes UV. On y explore aussi les guides d'ondes en mode zéro (ZMWs), le renforcement du signal par des antennes UV et l'optimisation de la détection pour les protéines avec des résidus de tryptophane.

La recherche évolue ensuite vers l'amplification du signal d'autofluorescence grâce aux plasmons de surface. Le Rhodium est identifié comme essentiel à cette amélioration. Le dernier chapitre discute de l'amélioration du signal avec les plasmons de gap, abordant les challenges de la nanofabrication.

En conclusion, la recherche propose une méthode d'autofluorescence UV sans marqueur pour détecter des protéines uniques avec un résidu de tryptophane. Cette réalisation implique des structures nanophotoniques optimisées, des ajustements chimiques, et l'usage de matériaux spécifiques pour la protection UV. Ce travail élargit les horizons de la spectroscopie UV pour les études monomoléculaires des protéines.

Mots clés : Autofluorescence UV, Sensibilité au tryptophane unique, Spectroscopie de corrélation de fluorescence (SCF), ZMWs, Nanophotonique UV,Antenne à gap UV,Détection de protéines sans marquage

Abstract

Single-molecule fluorescence studies have emerged as indispensable in biophysical research. Unlike ensemble measurements, which provide average outcomes over numerous molecules, single-molecule studies allow for the observation of individual molecular behaviors. However present studies relies on use label which are bright fluorescent molecules attached to analytes. It is reported that labelling sometimes leads to alteration in molecular dynamics of analytes like proteins. Thus investigation of proteins' intrinsic nature is crucial for understanding their functions and interactions. This thesis explores advanced methods of label-free UV autofluorescence spectroscopy, aiming to discern and study proteins at the molecular level without any external labeling.Using ultraviolet spectroscopy and nanophotonics, proteins can be observed without labeling, and their kinetics at the single-molecule level can be detailed. Initially, the work investigates the literature of single-molecule approaches, label-free techniques, and the potential of UV autofluorescence spectroscopy. Particular emphasis is given to challenges like low autofluorescence signal and the intricacies of UV microscope objectives. The next chapter delves into the functionality of Zero-Mode Waveguides (ZMWs), detailing their ability to observe single molecules at micro-molar concentration. Techniques to amplify the signal from proteins are discussed, focusing on a UV horn antenna, a unique nanophotonic structure, which magnifies the light emitted by proteins within the ZMWs. In the subsequent chapter, achieving optimum sensitivity is emphasized, touching on the challenges of detecting proteins with single tryptophan residues. As the research progresses, efforts shift to amplifying the UV autofluorescence signal. Through the use of Localized surface plasmons, it becomes possible to considerably augment this signal. The investigation then showcases Rhodium as a pivotal material for UV autofluorescence enhancement. The final chapter highlights efforts to further refine the UV autofluorescence signal using the concept of gap plasmons, coupled with the challenges in nanofabrication and material requirements for UV nanophotonics. Conclusively, this research presents a robust label-free UV autofluorescence technique, capable of detecting even a single protein containing just one tryptophan residue. Achieving this feat involved optimizing advanced nanophotonic structures, buffer chemistry adjustments, and exploring non-conventional materials for protection against UV corrosion. The culmination of this work pushes the boundaries of UV spectroscopy, ushering in a new realm of protein study at the single-molecule level.

Keywords: UV Autofluorescence, Single Tryptophan sensitivity, Fluorescence correlation spectroscopy(FCS), ZMWs, UV Nanophotonics, UV Gap antenna,label-free protein detection.

Acknowledgement

I would like to express my appreciation to the jury members of my thesis for taking the time to read and assess my work.

Jerker Widengren, KTH Sweden

Céline Fiorini Debuisschert, CEA, France

Yves Mély, University of Strasbourg, France

Julien Proust, UTT Troyes, France

Jérôme Wenger, Institut Fresnel, Aix Marseille Université, France

I am deeply appreciative of my PhD supervisor Jerome Wenger for his support and direction both as a scientific advisor and mentor. I am thankful for the three years of scientific exploration I was able to experience, during which I was able to learn and grow as a researcher.
I am grateful to have had the support of Alexandr, Mikhail, Satyjit, Jean-Benoit, Sunny and Quanbo, former team members, who taught me their skills. I would also like to express my appreciation to everyone at Insitut Fresnel for their incredible support over the past three and a half years, particularly Maelle, Eric, Ksenia, Sandro, Malavika, Baptisite, Astrid and all the members of the MEMO student association. I would also like to thanks our collaborator for rhodium nanoparticles Jie Liu, Duke University, USA and for metal oxide deposition : L. Santinacci, CINaM, Aix Marseille University, France
I would like to dedicate my thesis to my Physics professor from India, Arnab Ray. His inspiring words were the impetus for me to transition from engineering to pursuing a PhD in Physics. I am deeply grateful to my parents Suresh and Madhu for their moral support. Additionally, I am thankful to my partner Kate for her incredible backing during the last few years of highs and lows.
I am grateful to the European Research Council for providing me with the financial support to pursue my PhD through the Horizon 2020 research and innovation program of the European Union (grant agreement No. 723241).

Content

Introduction

The true character of humans is unveiled when they are invisible, argued Plato, from the story of "Ring of Gyges" in the book "Republic". Similarly to see the true nature of proteins and study their kinetics, we should see them when they are invisible (label-free) and in their physiological surroundings such as in water salt and in concentrations of μM-mM. Ultraviolet spectroscopy provides us with the ability to observe proteins without the need for labelling, and nanophotonics enables us to view them at the single-molecule level in physiological concentrations with remarkable sensitivity.

In recent years, biophysical studies have shifted from studying ensembles to single molecules in order to gain a better understanding of proteins at the molecular level. Further research is now focussing on label-free single-molecule studies, which will provide an unaltered view of kinetics at the molecular level. In the **first chapter**, we will explore the literature for single-molecule approaches, delve into label-free techniques, discuss their advantages and drawbacks, and introduce how UV autofluorescence spectroscopy can be a major player in single-molecule protein sensing. We will also examine the key challenges in UV autofluorescence spectroscopy, such as the low autofluorescence signal, the photostability of proteins and single molecule studies at μM concentrations, as well as the limitations of UV microscope objectives.

In the **second chapter**, we will introduce a versatile tool of single-molecule fluorescence spectroscopy, the Zero-Mode Waveguides (ZMWs) which provide us with the ability to study a single molecule at μM concentration and show how we can use them for UV autofluorescence spectroscopy. We will explore the state-of-the-art in ZMWs-based sensing, we also discuss the physics behind ZMWs and show how we can adapt them to deal with the challenges of single molecule Auto-fluorescence spectroscopy. BAIBAKOV, Aleksandr BARULIN, ROY, Jean-Benoît CLAUDE et al. 2020 ROY, BADIE et al. 2021 Aleksandr BARULIN, ROY, Jean-Benoît CLAUDE et al. 2021

Further in **chapter 3** we will see how we can increase the signal from proteins. The total fluorescence enhancement is the product of excitation gain, collection gain, and Purcell factor. In this chapter, we will target collection gain while keeping the screening capability of ZMWs intact. We will introduce a UV horn antenna(ZMWs embedded in conical micro-reflector), this design will focus back the light into the UV microscope objective. This will allow us to probe the molecules at the single-molecule level label-free. We will show how by using this antenna system we can collect 90% of the light emitted by the protein within the ZMWs. Aleksandr BARULIN, ROY, J.-B. B. CLAUDE et al. 2022

In **chapter 4** we will investigate how we can achieve the highest level of sensitivity with our technique. The current best practice for detection is single-molecule

detection of proteins with 24 Trp residues, however, human proteins usually have fewer than 5 Trp. Therefore, we will delve further into our method to determine the feasibility of single-molecule detection of proteins with only one Trp residue. We will analyze the signal-to-background ratio (SBR) and its essential role in attaining the ultimate sensitivity. We will show how it was not possible to reach such sensitivity by the confocal method alone, we need a signal boost as given by the UV horn antenna. Additionally, we will create a protocol to reduce the SBR and reach the unprecedented sensitivity of UV autofluorescence spectroscopy. We will show our final results by detecting proteins like TNase and LiCT with one and two Trp residues, respectively. ROY, Jean-Benoît CLAUDE et al. 2023

In the **final chapter**, we investigate how to further improve the UV autofluorescence signal. We know that fluorescence enhancement is dependent on excitation gain and the radiative emission gain (related to Purcell Factor). To increase these factors, we will use Localized surface plasmons. The concept is to use the plasmonic resonant antenna for UV autofluorescence enhancement, which has not been done before. We will examine different materials that can be used as plasmonic materials for UV and demonstrate how Rhodium is a key material. Additionally, we will design a self-assembled Rhodium dimer gap antenna inside an Aluminum ZMW. We will optimize the structure with optical simulation and then use it to detect proteins with very low quantum yields, ranging from 0.1% to 3.5%. We will also demonstrate that this configuration can provide an unprecedented 120 times enhancement in UV plasmonic antenna. Furthermore, we will prove that the antenna is robust and reusable.

Next, we will conclude our results and show the possible direction in which research may evolve. We will explore the limitation of our nanophotonics-enabled UV spectroscopy and potential methods to reduce them. We will also investigate the potential areas where our UV spectroscopy with unparalleled single Trp resolution and intense brightness enhancement can be utilised.

1 Introduction to Ultraviolet Autofluorescence Spectroscopy and its Nanophotonic Aspects

FIGURE 1.1 – UV makes the invisible proteins visible

Summary

1.1 Single Molecule Biosensing

Single-molecule biosensing refers to the detection and quantification of individual biomolecules (e.g. DNA, proteins, and enzymes) and not average over large groups, as in conventional bulk assays. These methods provide important information about the molecular level heterogeneity, structural dynamics, and reaction kinetics of biological systems, which bulk measurements cannot detect, about the heterogeneity of biological systems, structural dynamics, and reaction kinetics. Single-molecule techniques rely on the properties of individual molecules, as opposed to the averaged behavior of a collection of molecules. Single-molecule experiments have provided

fresh insights into many biological processes, including DNA replication, transcription, protein folding, and enzymatic activity RITORT 2006 Single-molecule biosensing can be achieved using various methods, including optical microcavity-based sensorsBAASKE, FOREMAN et al. 2014, solid-state nanoporesSCHMID et DEKKER 2021, single-molecule mechanochemical sensingC. HU, TAHIR et al. 2022, digital biosensing assays CURTIN, FIKE et al. 2022, single-molecule fluorescence imaging solid state single-molecule force spectroscopyJ.-F. LI, Q. X. LI et al. 2019, and plasmon-enhanced detection Jérôme WENGER 2019.P. ZHANG, MA et al. 2020 These techniques have been used for a wide range of applications, including chemical detection and biosensing. Single-molecule biosensing has the potential to revolutionise the field of biosensing by enabling the detection of low-abundance molecules and providing a deeper understanding of molecular interactions.
The most widely used technique for single-molecule spectroscopy and microscopy is the fluorescence-based technique, where red-shifted light emitted by the light-excited molecule is used for sensing. The molecule can have intrinsic light originating from electronic transitions or can be tagged with fluorophore molecules, which emit light on excitation with specific wavelengths. In the following section, we will discuss this technique in detail and its advantages, shortfalls, and how to mitigate them.

1.2 Single-Molecule Fluorescence spectroscopy

Fluorescence spectroscopy has emerged as a formidable tool, especially for biosensing LAKOWICZ 2006 with a particular advantage in the domain of protein detection. Fluorescence is a fascinating phenomenon that has been observed for centuries, but it was only in the 19th century that it began to be understood and studied scientifically. The phenomenon of fluorescence can be traced back to ancient times. For instance, the Romans were known to produce fluorite cups that glow in the dark when exposed to light. The fluorescent properties of fluorite were later used in the 16th century by Vincenzo Cascariolo, an Italian shoemaker and alchemist, who created the "Bologna Stone," a material that, after being exposed to sunlight, would glow in the dark. The term "fluorescence" itself was coined by Sir George Gabriel Stokes in 1852STOKES 1852. Stokes investigated the emission of light by substances that had absorbed light or other electromagnetic radiation. He named the phenomenon after fluorite, a mineral that exhibits this prominent property. At the core of fluorescence spectroscopy is the interaction of light with molecules, which can be visualised using a Jablonski diagram. Named after the Polish physicist Aleksander Jabłoński, this diagram provides a visual representation of the different energy states in a molecule and the transitions between them.

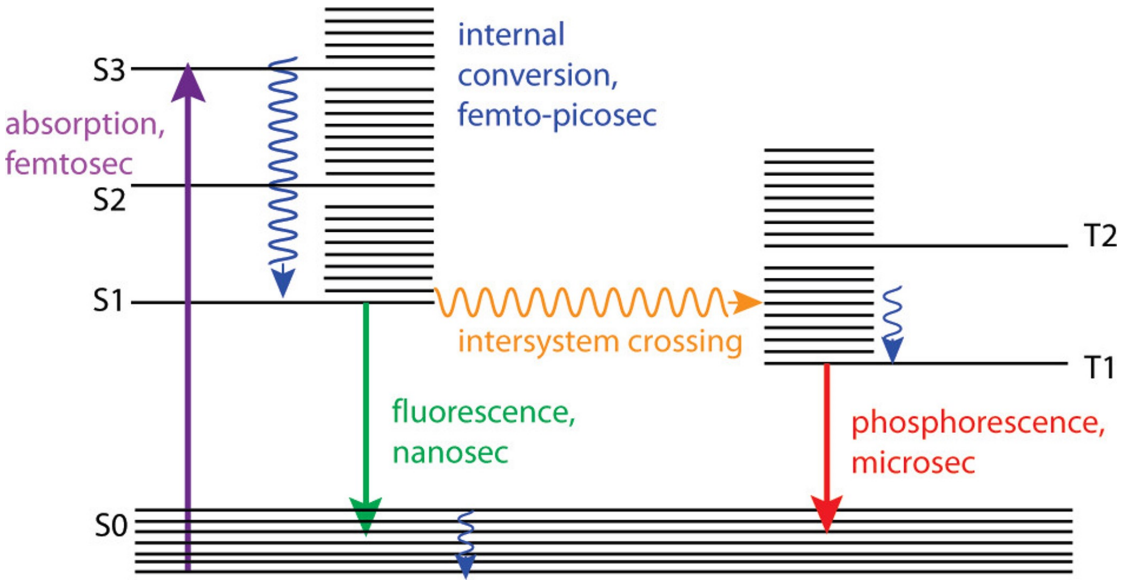

FIGURE 1.2 – Jablonski diagram and a time scale of photophysical processes for organic molecules. adapted from refBEREZIN et ACHILEFU 2010

A Jablonski diagram in Fig 1.2 typically consists of several parallel lines representing the vibrational levels within electronic states, grouped into horizontal series representing the electronic states themselves. The ground state is denoted by S0 and the excited states S1, S2, etc. The vertical transitions between these states are caused by the absorption or emission of light. When a molecule absorbs a photon, it jumps from the ground state to an excited state, typically landing at a high vibrational level of an excited electronic state. The molecule then quickly loses its excess vibrational energy through nonradiative processes such as collision with other molecules or conversion into heat. This process is known as internal conversion (IC) or vibrational relaxation.

Finally, the molecule returns to the ground state by emitting a photon, a process called fluorescence. Importantly, because the molecule loses some energy through internal conversion before it fluoresces, the emitted photon is less energetic (and therefore has a longer wavelength) than the absorbed photon. This phenomenon is known as the Stokes shift. The two important readouts in fluorescence spectroscopy are the fluorescence intensity and the lifetimeBEREZIN et ACHILEFU 2010.
The fluorescence lifetime of a molecule refers to the average time that a molecule stays in its excited state before emitting a photon.

$$\tau = \frac{1}{\Gamma_r + \Gamma_{nr}} \tag{1.1}$$

where τ is the lifetime and Γ_r is the radiative rate constant and Γ_{nr} is the non-radiative rate constant. The lifetime of emitters can be single exponential or multiple exponents due to different intermediate states or channels of the decay process from excited to ground states. To measure lifetime information, a dedicated TCSPC is requiredWAHL, RAHN et al. 2008(we will discuss TCSPC(Time-Correlated Single Photon Counting)

in the following sections). The fluorescence lifetime is a property of the fluorophore and depends on its environment, including factors such as local temperature, pH, and the presence of quenching or enhancing agents. WIDENGREN, METS et al. 1995It is typically measured in nanoseconds. An important aspect of the fluorescence lifetime is that it is not influenced by the concentration of the fluorophore or the intensity of the excitation light, making it a very useful parameter in various applications, including studies of fluorescence lifetime imaging microscopy (FLIM)GADELLA, JOVIN et al. 1993 and fluorescence resonance energy transfer (FRET) SCHULER et EATON 2008 studies.

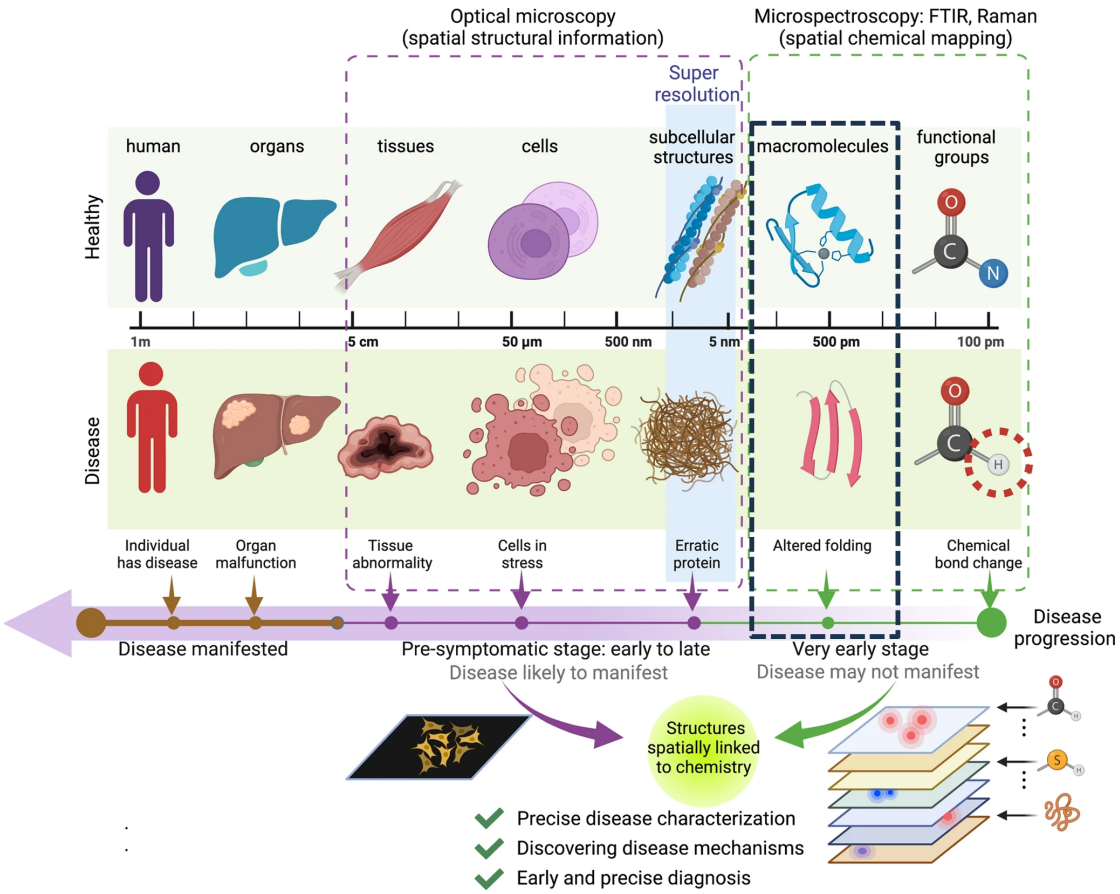

FIGURE 1.3 – Optical microscopy and spectroscopy detect different scales of organization and hence are complementary to visualize different phases of development and disease. Optical microscopy even with the super-resolution cannot go beyond 1nm. Microspectroscopy detects chemical changes occurring at levels of functional groups with spatial distribution. However, with thousands of chemical changes occurring, it is difficult to use spectroscopy alone, especially at early onset, until it is correlated with manifested structural changes occurring at micron to nano scales. This can help characterize the early onset of disease as well as understand the basis of several physiological and pathological events. Reproduced fromGHOSH et AGARWAL 2023. In this thesis our focus area will be macromolecules like proteins shown in the dotted box

Fluorescence spectroscopy provides a unique and efficient way of probing the biological world at the molecular level. This method has several distinct advantages that make it particularly suitable for biosensing applications.

1.2.1 Advantages of Fluorescence Spectroscopy

High Sensitivity and Specificity : One of the main advantages of fluorescence spectroscopy is its exceptional sensitivity. The ability to detect even single molecules in complex mixtures sets this technique apart from other analytical methods. Furthermore, the introduction of specific fluorescent tags enables the detection of individual molecular species among a wide range of biological molecules. This specificity is particularly beneficial in protein detection where identifying and quantifying specific proteins from a complex biological matrix is crucial. The fluorophore lifetime information adds to the advantages of fluorescence spectroscopy since the lifetime varies with changes in surrounding conditions such as pH, temperature, viscosity, etc. PERIASAMY, ALAM et al. 2017

Non-invasive Method : Fluorescence spectroscopy is non-destructive, meaning that the analyte is not altered or destroyed during the process. This attribute is especially important in biological applications where the functionality and integrity of the molecule under investigation, such as proteins, must be preserved.

Versatility : Fluorescence spectroscopy provides the opportunity to use different fluorophores to label different proteins. This offers the possibility of detecting and quantifying multiple proteins simultaneously within a single sample, further enhancing the efficiency and power of this technique.HANEY, WISSNER et al. 2015

Real-time Monitoring : Another notable advantage of fluorescence spectroscopy is its ability to facilitate real-time monitoring of dynamic biological processes. It offers an unparalleled opportunity to observe protein folding, conformational changes, and molecular interactions as they occur.ZOUMI, YEH et al. 2002CHALLA, PETER et al. 2018

1.2.2 Drawbacks of labelling

Fluorescence spectroscopy is a powerful tool for studying proteins' structural and dynamic properties. It involves labelling proteins with fluorescent probes or dyes that emit light upon excitation. Although labelling is a widely used technique, it is not without limitations. This section explores the challenges and drawbacks associated with labelling in fluorescence spectroscopy of proteins.

Perturbation of Protein Structure and Function : One significant limitation of labelling is the possible alteration of protein structure and functionR. YANG, Zhiwen TANG et al. 2008. Attachment of fluorescent probes to proteins can introduce steric hindrance, modify surface charges, or disrupt intermolecular interactions.GIEPMANS, ADAMS et al. 2006 These changes can affect protein folding, stability, enzymatic activity, and binding affinity, potentially leading to inaccurate conclusions about native protein behaviour.

Probe-Specific Effects : Different fluorescent probes may have distinct physicochemical properties that can affect protein behaviour. For instance, large-sized probes might interfere with protein dynamics, while hydrophobic probes can induce nonspecific binding or disrupt the local environment. ZANETTI-DOMINGUES, TYNAN et al. 2013Moreover, the electronic properties of the probe may influence the fluorescence properties of the labelled protein, which can lead to altered emission characteristics or quenching effects.HA et TINNEFELD 2012a

Labelling Site Selection : Choosing an appropriate site for the attachment of the probe is crucial but challenging. Labelling at specific residues can introduce conformational changes, disrupt active sites, or interfere with protein-protein interactionsGIEPMANS, ADAMS et al. 2006. The location and proximity of the labelling site to critical functional regions require careful consideration to minimise disturbance.STRUNK, ENDERLEIN et al. 2008

Labelling Efficiency and Homogeneity : Achieving high labelling efficiency and homogeneity across the protein sample is essential for an accurate analysisYan CHEN, L. WEI et al. 2003. Incomplete labelling or the presence of a mixture of labelled and unlabelled proteins can introduce heterogeneity, leading to variations in fluorescence signals and subsequent data interpretation challenges. Obtaining a uniformly labelled protein sample can be technically demanding and time-consuming.

Photophysical Interactions : Fluorescent probes can exhibit photophysical interactions, which can complicate the interpretation of the dataHUSER, M. YAN et al. 2000. These interactions include fluorescence resonance energy transfer (FRET), quenching, and self-aggregation. For instance, FRET can occur when two fluorophores are nearby, leading to energy transfer between them. Such interactions can affect the fluorescence intensity, lifetime, and emission spectra, and careful control experiments are required to differentiate between true protein interactions and these probe-specific phenomena.

Photostability and Photobleaching : Fluorescent probes are susceptible to photobleaching, where prolonged exposure to excitation light results in irreversible loss of fluorescence signalDEAN, LUBBECK et al. 2015. This limits the duration of experiments and may lead to incomplete data acquisition. Photostability, which refers to the ability of a probe to withstand repeated excitation without significant degradation, varies between different dyesCORDES, VOGELSANG et al. 2009. Selecting probes with sufficient photostability is crucial to ensure reliable and reproducible measurements.

Challenges in Multi-Labelling and Complex Systems : Studying protein complexes or multi-protein systems often requires simultaneous labelling of multiple components.VERDAASDONK, LAWRIMORE et al. 2014However, achieving selective and independent labelling for each component can be challenging. Cross-reactivity, nonspecific binding, or probe interference may arise, leading to difficulty in accurately dissecting the individual contributions of each protein in the complex.

Although protein labelling in fluorescence spectroscopy provides valuable information about protein structure, dynamics, and interactions, it is not without limitations. The perturbation of protein structure and function, probe-specific effects, challenges in labelling site selection, issues with labelling efficiency and homoge-

neity, photophysical interactions, photostability, and photobleaching, as well as complexities in multi-labelling and complex systems, pose significant challenges. The overcomer of these limitations and the advancement of labelling techniques will be instrumental in enhancing the accuracy and reliability of fluorescence spectroscopy in protein research. It is needless to say that we need a technique which has high contrasts, such as fluorescence spectroscopy, but does not suffer the drawbacks of labelling, thus a label-free technique.

1.3 Non-Fluorescent Techniques of Single-Molecule Label-free Spectroscopy

In the realm of single-molecule label-free spectroscopy and microscopy, there exist several techniques that exhibit notable distinctions. In this section, we will explore some prominent techniques, each with its unique approach. One such technique is iSCAT, which relies on the detection of light scattered from molecules. Nanopore employs electrical signals as probing signals to detect biomolecules. Raman scattering, another prominent label-free technique, is frequently used due to its noninvasive nature and its ability to capture intricate vibrational signatures of individual molecules. Additionally, we will delve into the autofluorescence-based approach for spectroscopy, which constitutes the main focus of this thesis.

1.3.1 Interferometric Scattering-based technique

iSCAT (interferometric scattering) microscopy is a powerful technique in the field of single-molecule spectroscopy. It allows the label-free detection and imaging of single molecules with high sensitivity and resolution TAYLOR et SANDOGHDAR 2019(Taylor Sandoghdar, 2019). iSCAT is a form of interferometric detection that measures the interference of light scattered from subwavelength objects HSIEH 2017(Hsieh, 2017). It was first introduced in 2004 by Sandoghdar and colleagues, who demonstrated its ability to detect gold nanoparticles as small as 5 nmKÜPPERS, ALBRECHT et al. 2023 . Since then, iSCAT has been widely used in various applications, including the detection and imaging of non-fluorescent matter at the single-molecule/particle levelW. YANG, Z. WEI et al. 2022 , the study of protein adsorption and desorption on surfaces BUENO-ALEJO, VEGA et al. 2022, and the imaging of single proteins secreted from living cells (Gemeinhardt et al., 2018).

Compared to fluorescence-based techniques, iSCAT offers several advantages. It is a label-free method, eliminating the need for fluorescent labelling and avoiding potential artefacts caused by the labelling processBUENO-ALEJO, VEGA et al. 2022 . This makes it particularly useful for studying biomolecules and their interactions in their native state. iSCAT also provides high sensitivity, allowing for the detection of single molecules and particlesPILIARIK et SANDOGHDAR 2014. It has been used to detect and track individual proteins, viruses, and nanoparticles. Furthermore, iSCAT can provide information about the mass of molecules, as the scattering signal is

proportional to the mass of the molecule YOUNG, HUNDT et al. 2018. This has led to the development of mass photometry, a variant of iSCAT that enables the quantification of single molecules on the basis of their mass.

The principle of iSCAT is based on the interference of light scattered by sub-wavelength objects. When a sample is illuminated with a laser beam, the scattered light interferes with the incident light, resulting in an interference pattern. When this interference pattern is detected and analysed, information about the sample can be obtained. iSCAT microscopy typically uses a common-path interferometric setup, where the reference beam and the scattered light are combined and interfere with each other ADHIKARI et ORRIT 2022 The interference pattern is then detected and analysed to extract information about the sample, such as its position, size, and dynamics, as explained in figure 1.4

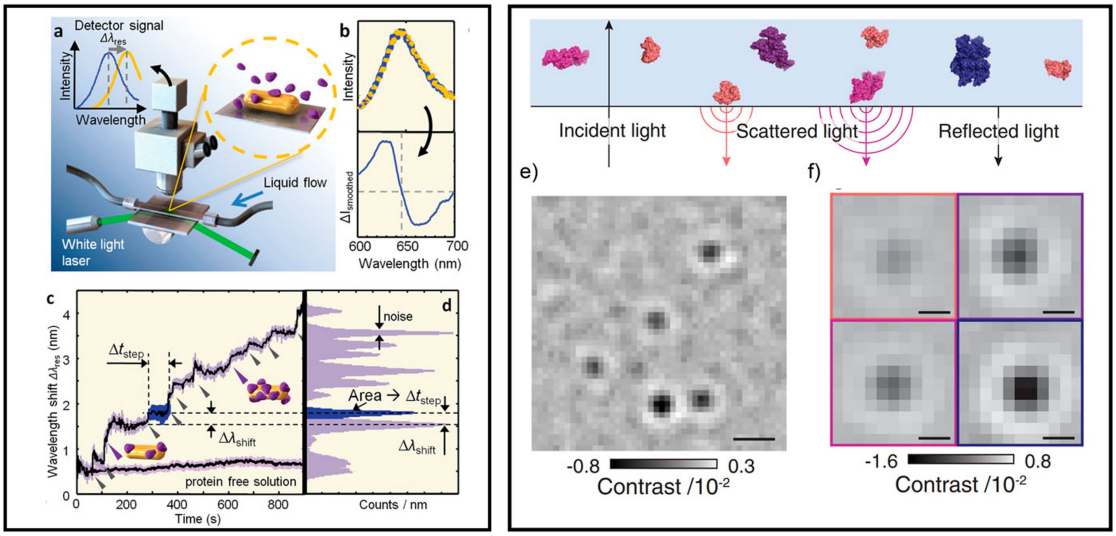

FIGURE 1.4 – Left panel : detection of a single protein molecule's attachment to a single gold nanorod. (a) Schematic diagram of the microscope with an enlarged view of the flow cell. Inset : schematic representation of the plasmonic wavelength shift. (b) The measured plasmonic spectra of a single gold nanorod before and after a single protein's attachment (upper panel) and the difference between those two spectra (bottom panel). (c) The plasmonic resonance wavelength shift of a single gold nanorod during single protein attachment events and in a protein-free solution. (d) Histogram of the time trace shown in (c), showing distinct peaks for every single binding event. Right panel : The top part shows the experimental approach. Oligomers of protein molecules in different colours are immobilized near an interface with a different refractive index. The incident light gets scattered by the molecules and reflected by the interface. (e) Interferometric scattering (iSCAT) image of BSA protein molecules. Scale bar : 500 nm. (f) Images of different BSA oligomers : monomer, dimer, trimer, and tetramer. Scale bar : 200 nm.ADHIKARI et ORRIT 2022

In summary, iSCAT is a powerful technique in single-molecule spectroscopy that allows for the label-free detection and imaging of single molecules with high

sensitivity and resolution. It has been used in various applications, including the study of protein adsorption and desorption, the imaging of nonfluorescent matter, and the quantification of single molecules based on their mass. Surface passivation techniques have been developed to improve the precision of single-molecule measurements using iSCAT. Overall, iSCAT offers a valuable tool for studying the behaviour and interactions of individual molecules in their native state.RICHARD W. TAYLOR et V. SANDOGHDAR s. d. However, iSCAT has some limitations, including background interference, limited field depth, and complex data analysis. It is susceptible to background interference caused by factors such as light scattered from the environment or imperfections in the optical setup. These interferences can reduce the signal-to-noise ratio and affect the accuracy of the measurements. The depth of field in iSCAT is limited, meaning that only objects within a specific range of distances from the focal plane can be effectively imaged. There is the limitation of the size of proteins that can be measured using iSCAT, researchers have used plasmonic to reach protein size down to 64kDa.BAASKE, ASGARI et al. 2022

1.3.2 Raman Spectroscopy of single molecules

Raman spectroscopy is a powerful analytical technique that has been used for decades to study the vibrational modes of molecules. In recent years, Raman spectroscopy has been combined with surface-enhanced techniques to achieve single-molecule sensitivity. The Raman effect occurs when a photon of light interacts with a molecule and causes a change in the polarisability of the molecule. This change in polarisability results in a shift in the energy of the scattered photon. The shift in energy is proportional to the vibrational frequency of the molecule. When the shift in the energy of the scattered photons is analysed, the vibrational modes of the molecule can be determined. Single-molecule Raman spectroscopy has several advantages, including high sensitivity, high spatial resolution, and the ability to study individual molecules. It is a non-destructive technique that can be used to analyse samples in situ. Raman spectroscopy can be used to analyse a wide range of samples, including biological cells and tissues, materials, and even the surface of MarsBEEGLE, BHARTIA et al. 2015.

One of the most promising techniques for single-molecule Raman spectroscopy is surface-enhanced Raman spectroscopy (SERS) RU et ETCHEGOIN 2012. SERS is a technique that enhances the Raman signal of molecules by several orders of magnitude through the use of plasmonic nanoparticles. SERS has been used to detect single molecules of various analytes, including DNA, proteins, and small molecules Y. ZHANG, ZHEN et al. 2014. Another technique that has been used for single-molecule Raman spectroscopy is plasmonic Fano resonance Y. ZHANG, ZHEN et al. 2014. This technique combines resonant molecular excitation with large electromagnetic field enhancements experienced by a molecule associated with an interparticle junction.

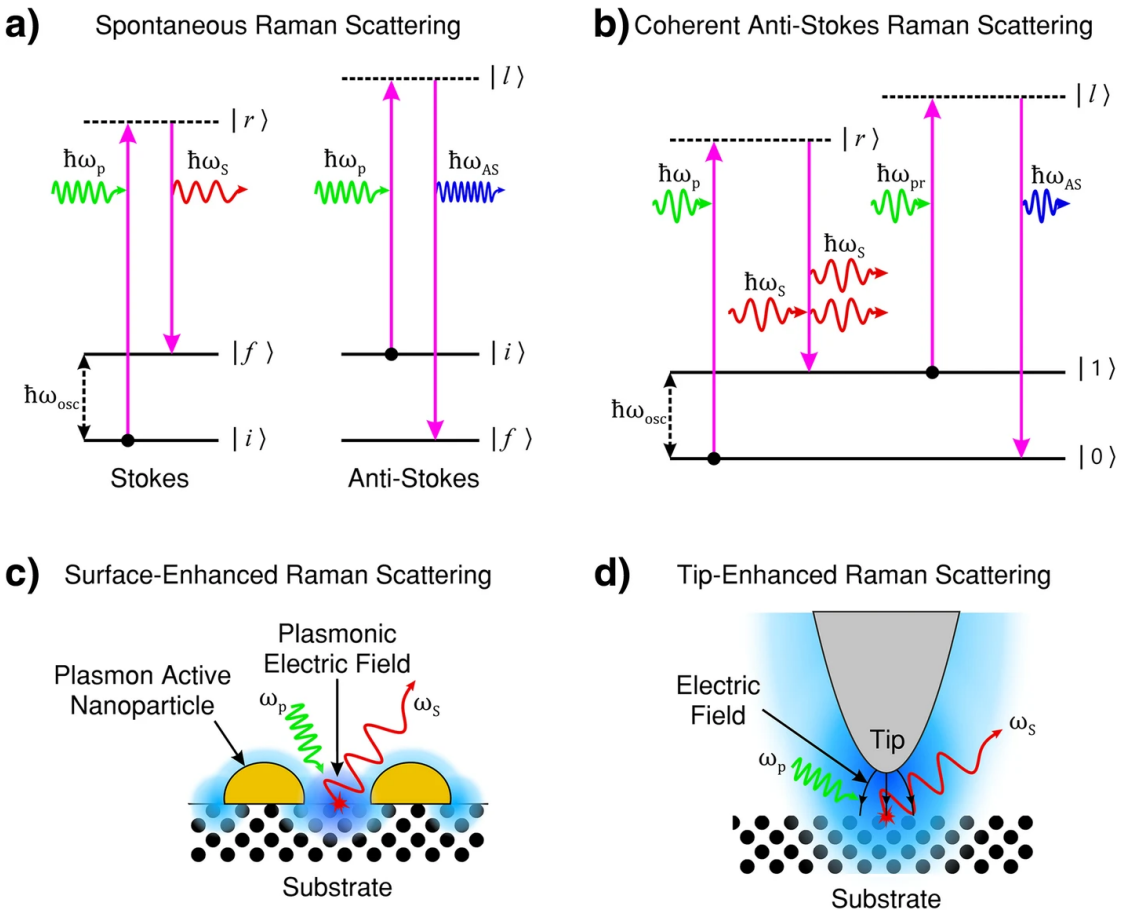

FIGURE 1.5 – Different Raman techniques commonly used for label free spectroscopy and microscopy. reproduced fromJONES, HOOPER et al. 2019

Smart plasmonic molecular traps have also been developed for single-molecule Raman spectroscopy Yuanhui ZHENG, SOERIYADI et al. 2015. These traps use thermoresponsive polymers to reversibly gate the access of molecules to the plasmonic substrate. High spatial resolution nanoslit SERS has also been used for single molecule nucleobase sensing C. W. CHEN, Y. LI et al. 2018. This technique uses an optically engineered elongated nanopore structure, a plasmonic nanoslit, to locally enable SERS.

Transient-stimulated Raman excited fluorescence spectroscopy has also been used for all-far-field single-molecule Raman spectroscopy Q. YU 2023. This technique couples Raman scattering with fluorescence emission. Direct measurement of the Raman scattering tensor of orientation-fixed single iodine molecules has also been achieved D. WANG et Zikang TANG 2015. However, for gaseous single molecules, only limited structural information can be obtained from Raman spectroscopy because of their freely rotating and randomly orientated nature.

One of the quite interesting Raman techniques is Ultraviolet Resonance Raman (UVRR) spectroscopy, a variant of Raman spectroscopy, which offers significant advantages for single-molecule biosensing. This technique uses the energy of ultraviolet light

to achieve resonance with molecular or electronic transitions, thus amplifying the Raman signal and allowing highly sensitive detection and characterisation of individual molecules.RAZZELL HOLLIS, SHARMA et al. 2023 UVRR spectroscopy has several key advantages for single-molecule sensing. First, it provides a highly molecule-specific vibrational signal. Certain functional groups, such as aromatic rings or peptide bonds in proteins, show a dramatic increase in scattering cross section when UV light is tuned into resonance with an electronic transitionJHA, AHMED et al. 2012a M. ZHANG, TAI et al. 2023. This resonance enhancement allows the direct detection and identification of these specific molecular subunits in complex biological molecules. Another advantage is the reduction in fluorescence interference. Many biomolecules, such as proteins or nucleic acids, that are fluorescent under visible or near-infrared excitation, are typically non-fluorescent under UV excitation, thus reducing the fluorescence background and improving the signal-to-noise ratio THOMAS 1999 In conclusion, Raman spectroscopy techniques for single-molecule sensing have several advantages and limitations. Raman signal compared to fluorescence is a few orders weaker and does not provide contrast as much as possible with fluorescence spectroscopy.

1.3.3 Nanopores for spectroscopy of Proteins

Nanopores are tiny, nanometre-scale channels that allow the passage of molecules on the order of single molecules or ions. They can be formed by natural biological structures, such as protein channels in cell membranes, or artificially created using synthetic materials. The key feature of nanopores is their ability to detect and analyse individual molecules as they pass through the pore. This is achieved by measuring changes in electrical or ionic current flowing through the nanopore.

Protein sensing using nanopores relies on the unique physical and electrical properties of proteins. When a protein molecule passes through a nanopore, it causes changes in the current flowing through the pore. These changes in current can be measured and correlated to specific protein characteristics, such as size, charge, and conformation. When current signals are analysed, valuable information on protein structure, interactions, and dynamics can be obtained.SCHMID et DEKKER 2021 The nanopore technique enables the real-time label-free detection of proteins, making it an invaluable tool for protein characterisation. By measuring the changes in current as a protein passes through a nanopore, researchers can determine its size, shape, and folding patterns. Furthermore, the analysis of translocation time and current blockades can provide information on protein-protein interactions, ligand binding, and conformational changes, which are vital to understanding protein function and dynamics.GAROLI, YAMAZAKI et al. 2019

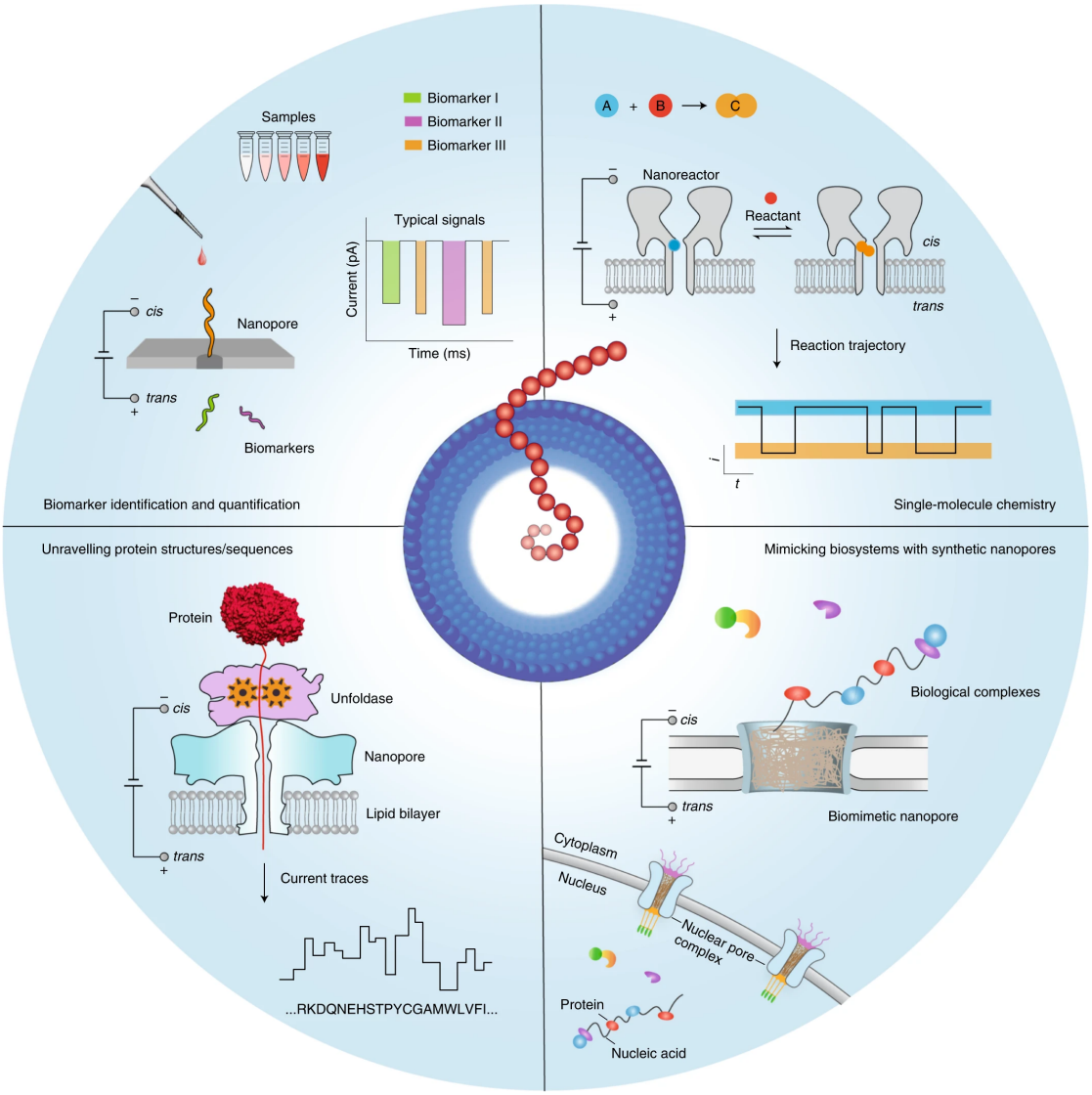

FIGURE 1.6 – Four areas of research in which nanopores have great potential to contribute to new knowledge and new technologies are shown.reproduced from YING, Z. L. HU et al. 2022

One of the most significant applications of the nanopore technique in protein sensing is the study of protein folding kinetics. Protein folding is a crucial process for determining a protein's functional structure. Nanopores offer a unique platform to investigate folding intermediates and pathways by observing the changes in current as the protein undergoes folding or unfolding. This capability opens up new possibilities for understanding protein misfolding, aggregation, and associated diseases, such as Alzheimer's and Parkinson's.

While the nanopore technique for protein sensing is revolutionary, it does have certain limitations. First, the signal-to-noise ratio can be a challenge, particularly for low-abundance proteins, which may result in lower sensitivity compared to some

other techniques. Additionally, the analysis and interpretation of current signals require sophisticated algorithms and computational models, which can be complex and time-consuming. The nanopore technique has emerged as a revolutionary method for protein sensing, enabling researchers to delve into the intricacies of protein structure, function, and interactions. The real-time and label-free capabilities of the detector, combined with the ability to analyse single molecules, provide unprecedented opportunities for scientific exploration. Although the technique has limitations, its advantages in terms of sensitivity, selectivity, and real-time analysis make it a powerful tool for protein biosensing, offering new avenues for research, diagnostics, and therapeutics in diverse fields of biology and medicine.

1.3.4 Intrinsic fluorescence-based spectroscopy

Intrinsic fluorescence-based spectroscopy is a powerful tool used in various fields, including biomedical research, pharmaceuticals, and biotechnology. This technique involves measuring the intrinsic fluorescence of molecules, which is the fluorescence emitted by molecules without the addition of any external fluorophores. Intrinsic fluorescence spectroscopy is based on the excitation of aromatic amino acids, such as tryptophan, tyrosine, and phenylalanine, which are present in many proteins and other biomolecules.LACKOWICZ 2011. Intrinsic fluorescence spectroscopy brings together the merits of fluorescence spectroscopy and label-free techniques. In the upcoming section, we will elaborate on this technique and explore it more in detail

1.4 UV Auto-fluorescence Spectroscopy of Proteins

In 1883, the Swiss scientist Soret in his work "*Analyse spectrale* : *Sur le spectre d'absorption du sang dans la partie violette et ultra-violette*", explained that the UV absorption of protein is due to aromatic amino acid BEAVEN et HOLIDAY 1952. The emission from these amino acids is prone to perturbation as a result of changes in the media or conformal orientation of proteins. These emissions from aromatic proteins were key to understanding the behaviour of proteins in different environments, their kinetics and reactions to different stimuli. Thus, the UV emission of aromatic amino acids opens a new regime of UV autofluorescence spectroscopy to explore. One of the most prominent applications of this technique is used on Mars Rover "Perseverance" (2020) which has a UV fluorescence spectroscopy unit called SHERLOC to analyze the surface of MarsBEEGLE, BHARTIA et al. 2015, they were able to study 51 different compound using this technique on Mars published in 2023 RAZZELL HOLLIS, SHARMA et al. 2023.

1.4.1 Source of protein auto-fluorescence emission

Protein fluorescence is a crucial property in biophysical studies and biological sensing, primarily derived from certain amino acid residues that absorb and emit light

in the ultraviolet (UV) range. The principal source of intrinsic protein fluorescence is from the aromatic amino acids - tryptophan (Trp), tyrosine (Tyr), and phenylalanine (Phe), with Trp being the most fluorescent and Phe the least LAKOWICZ 2006. Sometimes, post-translation modifications of certain proteins, such as the formation of disulphide bonds, can also exhibit fluorescence FIELD 1988.

The intrinsic fluorescence of these amino acids arises from their unique molecular structure and electronic properties. When a fluorescent molecule, such as Trp, Tyr, or Phe, is exposed to light of a particular wavelength, it absorbs the light energy. This energy absorption causes an electron in the molecule to become excited and jump from the ground state to a higher energy level (excited state). In the case of Trp, Tyr, and Phe, this excitation generally occurs with the absorption of UV light, with wavelengths around 280-290 nm ALBANI 2013. For Trp, Tyr, and Phe, the light emitted is typically in the range of 300-400 nm as shown in Fig 1.7, depending on the specific amino acid and its environment SMIRNOV, ENGLISH et al. 1997.
In the figure, it is evident that the absorption cross-section of tryptophan is greater than that of other amino acids, making its contribution to intrinsic fluorescence more significant. Therefore, we will mainly focus on the emission of intrinsic fluorescence from tryptophan.

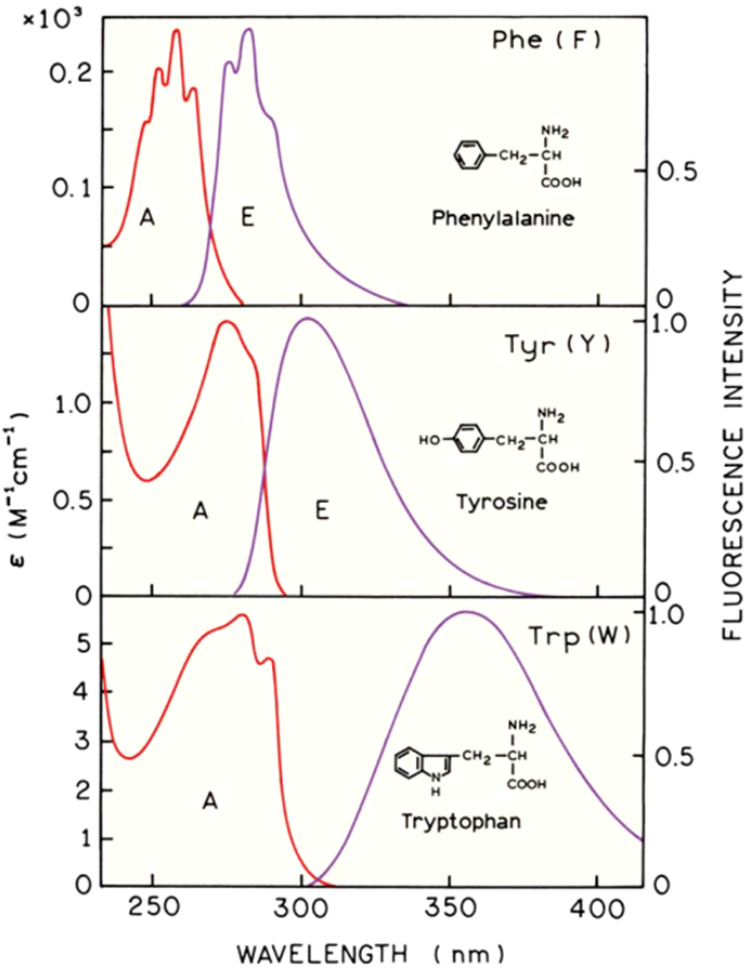

FIGURE 1.7 – The absorption and emission spectra of three main aromatic amino acids.LAKOWICZ 2006

Tryptophan Tryptophan exhibits strong fluorescence properties due to its indole side chain. When excited by a light source with a wavelength of around 280 nm, it emits light at longer wavelengths, typically between 320 nm and 350 nm. This broad and red-shifted fluorescence can be attributed to the $\pi\pi*$ transition state of the indole ring. The exact emission peak depends on the surrounding environment, solvent polarity, pH, and the presence of other nearby fluorophores.ROBBINS, FLEMING et al. 1980 When dissolved in water solution, tryptophan has an absorption cross-section of 5500 cm^{-1} and a quantum yield of 13 % at an excitation wavelength of 280 nm. However, this number changes when tryptophans are embedded within proteins; for example, the quantum yield can fall to less than 1% as in the case of haemoglobin. The fluorescence spectra of the indolic chromophore can be significantly altered in terms of position and intensity depending on the conditions of the medium, which is used in the evaluation of protein conformational states. The fluorescence properties of proteins are highly sensitive to their local environment, making fluorescence a powerful tool for studying protein structure, conformational changes, and interactions with

other molecules HEVEKERL, TORNMALM et al. 2016. Other factors, such as the polarity of the surrounding environment, pH, and the presence of quenchers, can influence the fluorescence properties of a proteinTOGASHI, SZCZUPAK et al. 2009.

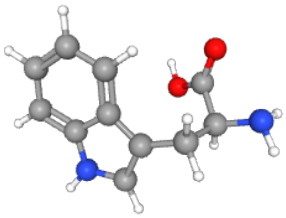

FIGURE 1.8 – The ball and stick model of tryptophan. Reproduced from Pubchem.

In conclusion, protein fluorescence is a critical property in biophysical studies and biological sensing, primarily derived from certain amino acid residues that absorb and emit light in the ultraviolet (UV) range. The intrinsic fluorescence of these amino acids arises from their unique molecular structure and electronic properties. The fluorescence properties of proteins are highly sensitive to their local environment, which makes fluorescence a powerful tool for studying protein structure, conformational changes, and interactions with other molecules.

1.4.2 State-of-the-Art of UV Auto-fluorescence Spectroscopy

Since the late twentieth century, ultraviolet (UV) absorption spectroscopy has been extensively used to understand protein behaviour by monitoring UV absorption and emission spectra that change based on the protein environment and protein structures.WETLAUFER 1963 Following the field of UV autofluorescence spectroscopy, which was mostly based on ensemble measurement using spectrophotometry, Seeger's group in year 2006 Q. LI et SEEGER 2006 published results on single-molecule label-free detection of freely diffusing protein β -galactosidase using one-photon UV excitation, this work was a follow-up of an interesting article published by the same group in 2004 on one-photon excitation imaging of label-free single molecule of 2,2-dimethyl-p-quaterphenyl (a UV dye).

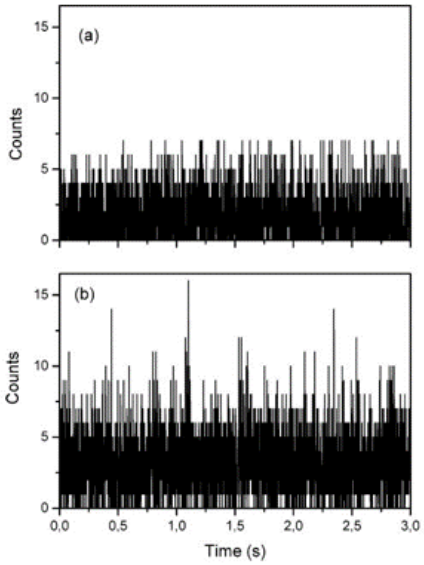

FIGURE 1.9 – Fluorescence time trace is taken by UV confocal setup (a)buffer background signal (b)Single diffusing molecule of label-free protein. Results were produced from Q. LI et SEEGER 2006

figure 1.9 shows the results of Seeger's work. This work was the first single-molecule UV detection of a label-free protein, setting the stage for single-molecule UV spectroscopy on labelled proteins. In Figure 1.9, it can be seen that the signal is very low compared to the buffer background, and for single-molecule studies, the protein is diluted to pM, which is not physiologically favourable concentration.
Similar feats were achieved by T.Basche in 2002 (LIPPITZ, ERKER et al. 2002)where researchers were able to detect 24-meric hemocyanin (148 Trp residues) using two-photon excitation* (TPE). The results shown in the work explain the advantages and disadvantages of the two-photon excitation and suggest that "*This result implies that TPE fluorescence imaging of single Trps will be extremely hard, if not impossible, to achieve.*" This conclusion supports that Trp, which is key to label-free protein spectroscopy, has weak emission, which leads to challenges in achieving single molecule single emitter resolution. It should be noted that the TPE technique discussed above also successfully targeted imaging of label-free protein avidin (340 trp residues) immobilized on a silica sphere. TPE-based spectroscopy was further implemented by SAHOO, BALAJI et al. 2008 to study protein aggregation. They were able to study the aggregate(10^5 molecules) of barstar (3 trp residue) with the TPE FCS technique; the authors however concluded that the TPE technique is less sensitive than the one-photon excitation.
Later in 2019 BARULIN, J. CLAUDE et al. 2019 implemented UV photo stabilization technique and nanophotonic technique to increase the sensitivity of single molecule label-free sensing of protein using its intrinsic emission. The authors successfully detected β-galactosidase (156 Trp residues) and streptavidin(24 Trp residues) reaching state-of-the-art on UV Autofluorescence spectroscopy. However, the authors highligh-

ted further study is needed to reach the fundamental sensitivity of the single molecule single emitter.
Thus, in the literature, it was evident that label-free UV autofluorescence spectroscopy has great potential, but the low signal-to-background ratio was the limiting factor. It is also preferable to use one-photon excitation over two-photon excitation to achieve better sensitivity, but it is worth noting that using TPE does not require custom optics and is less photo-corrosive compared to one-photon excitation. The one-photon UV excitation has an adverse effect on the photostability of proteins limiting the sensitivity of the spectroscopic technique; in the next section, we will see how to tackle these problems.

1.4.3 Limitation of UV auto-fluorescence spectroscopy and microscopy

Although UV autofluorescence spectroscopy and microscopy offer unique advantages, they also come with certain limitations and disadvantages.

Auto-fluorescence Background Noise : One of the main challenges in UV autofluorescence techniques is the presence of background fluorescence from unwanted sources. This background noise can interfere with the signal from the target molecules, making it difficult to discern the specific fluorescence of interest.

Photobleaching : Another limitation is photobleaching, where fluorescent molecules lose their ability to fluoresce as a result of prolonged exposure to the excitation light source. Photobleaching can cause a decrease in signal intensity over time and may lead to inaccurate measurements.

Phototoxicity : UV light can potentially cause damage to biological samples, a phenomenon known as phototoxicity. This is particularly relevant in live cell imaging, where UV exposure can cause cell damage or death. This phenomenon is more pertinent in UV microscopy, whereas for UV spectroscopy overall

Limited Penetration Depth : UV light has a limited penetration depth in biological tissues, which restricts the imaging depth of UV autofluorescence microscopy. This is a significant limitation when imaging thicker tissues or whole organisms.

Non-Availability of UV-grade optics : The use of UV spectroscopy to study single molecules is a relatively new area of research, making it difficult to find microscope and UV-grade optical components. In particular, the availability of a UV objective, which is essential for microscopy, is especially challenging. The UV objectives that are available have low transmission in the deep UV (266nm) range or, if the transmission is acceptable, the numerical aperture is low.

The complexity of Fluorescence Spectra : The interpretation of fluorescence spectra can be complex because of the overlapping emission spectra of different molecules. This requires sophisticated data analysis methods to deconvolve the spectra and identify the contribution of individual fluorophores.

Despite these limitations, UV auto-fluorescence spectroscopy and microscopy remain invaluable tools in various research and clinical fields. Continued advancements in technology and methodology are expected to mitigate some of these

limitations, further expanding the potential applications of these techniques. In this thesis, we will discuss and deal with the problems mentioned above and show how we can mitigate them and make the UV spectroscopy technique a prominent and effective technique.

1.5 Methods used in UV Auto-fluorescence spectroscopy

1.5.1 Fluorescence Correlation Spectroscopy

Fluorescence correlation spectroscopy (FCS) is a powerful and versatile technique that measures fluctuations in fluorescence intensity to extract information about the dynamical processes that occur within a small volume. PRAMANIK et WIDENGREN 2006These processes can include diffusion, chemical reactions, and conformational changes, among others.FELEKYAN, KALININ et al. 2012 FCS has proven to be an invaluable tool in many research fields, such as physics, chemistry, and biology.KALISZEWSKI, SHI et al. 2018

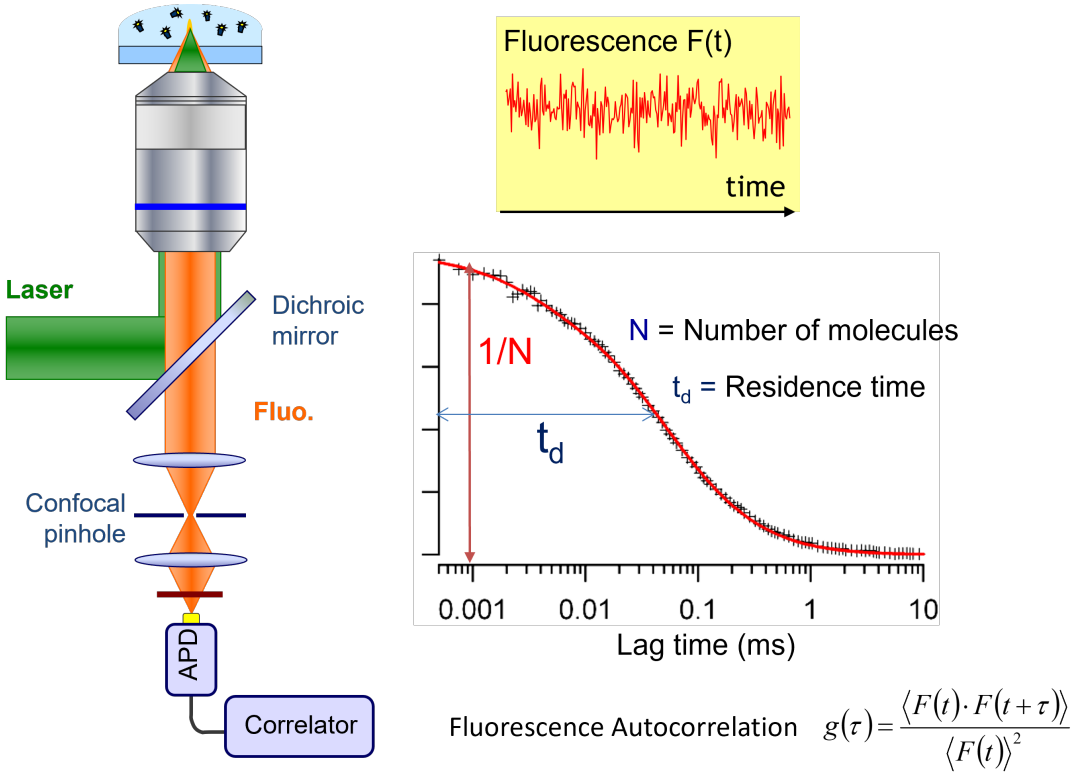

FIGURE 1.10 – Schematics of FCS system

The basic principle of FCS involves the illumination of a small volume of a sample and the detection of the fluctuations in fluorescence intensity that occur as

fluorescent molecules move in and out of the volume as shown in figure 1.10. These fluctuations are analysed to produce an autocorrelation function (ACF), which provides information on the dynamical processes that occur in the sample. FCS allows for the determination of diffusion coefficients of fluorescently labelled molecules or label-free fluorescent molecules, enabling the analysis of molecular mobility and interactions with cellular structures. By monitoring changes in the autocorrelation function, FCS can characterise binding and unbinding events between fluorescently labelled molecules and their binding partners. FCS can be used to estimate the concentration of fluorescent molecules in the observation volume, making it useful for studying cellular environments. In the study of protein folding, FCS has been utilised to investigate the oligomeric state of proteins during the folding process and to measure refolding rates GEORGESCAULD, POPOVA et al. 2014. For example, FCS and dual colour fluorescence cross-correlation spectroscopy (dcFCCS) were used to study the oligomeric state of the DapA protein during refolding and to measure the refolding rates.PADILLA-PARRA, AUDUGÉ et al. 2011

The exceptional sensitivity of FCS allows for the detection of single molecules in complex mixtures. This sensitivity has important implications in protein detection, where the identification and quantification of specific proteins from a complex biological matrix is crucial. When specific fluorescent tags are introduced, FCS enables the detection of individual molecular species amidst an assortment of biological molecules, providing high specificity in protein detection.

The application of FCS extends beyond protein detection. It has been used to study the structure and dynamics of polymer systems WÖLL 2014, diffusion and transport in lipid membranes RIES, PETRÁEK et al. 2010, dynamics of nucleic acid hairpin conformational fluctuations ORDEN et JUNG 2008, as well as molecular interactions between different species SCHWILLE et HAUSTEIN 2001. FCS can also be combined with other techniques, such as fluorescence lifetime imaging microscopy (FLIM) to analyse the behaviour of nanotherapeutics in cellsPANEK, KOZIOLOVÁ et al. 2016. One of the main advantages of FCS is its ability to probe dynamics on a wide range of timescales, from microseconds to seconds. This makes it a versatile tool for studying various processes in different fields. Furthermore, the use of nanophotonic FCS can be performed under physiological conditions, making it highly relevant for biological studies. WINKLER, REGMI et al. 2018, P. ZHU et CRAIGHEAD 2012
We will use FCS as a tool to study the single-molecule biophysics of label-free proteins throughout this thesis. The equation and analysis of the FCS curve and fit parameters are elaborated in detail in each result section in subsequent chapters.

1.5.2 TCSPC system

In this research, we will use the lifetime of protein fluorescence as a way to gain insight into proteins. To do this, we have incorporated a Time-Correlated Single Photon Counting (TCSPC) system from Picoquant into our optical setup, which already has a picosecond pulse laser unit. The module we are using is the Picoharp 300. This is connected to a PC via a USB port, and for data acquisition, we are using Sympho

Time64 software. This software allows us to observe the fluorescence counts on the PMT, and to perform more advanced measurements such as FLIM, FCS and lifetime histograms. The usual working of a TCSPC system is explained in the following figure.

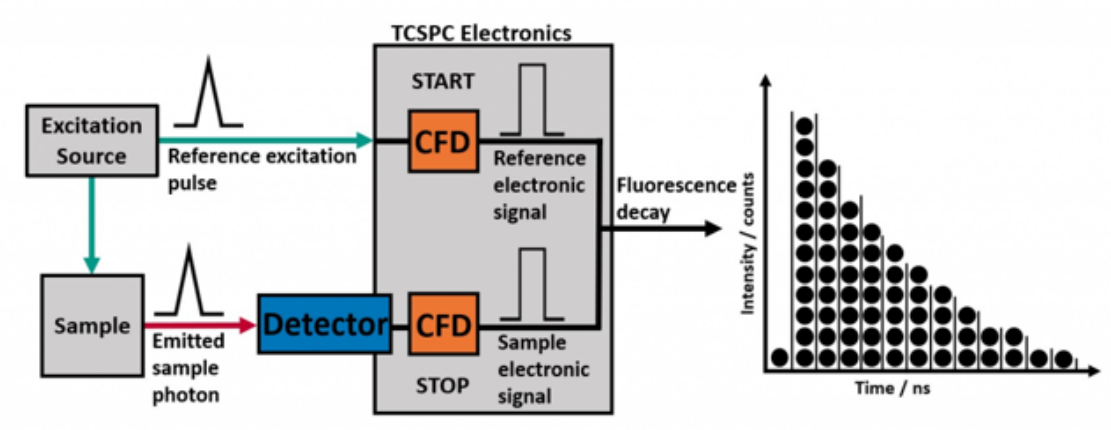

FIGURE 1.11 – Schematics of TCSPC system for calculating lifetime histograms. produced from website *TCSPC - What is Time-Correlated Single Photon Counting?* s. d.

A Time-Correlated Single Photon Counting (TCSPC) system is a sophisticated technique used in various fields, particularly in fluorescence spectroscopy and imaging, to measure the arrival time of single photons emitted by a sample. The primary purpose of TCSPC is to gather information about the lifetime and dynamics of fluorescent molecules or other light-emitting processes.

The fundamental principle of TCSPC is based on measuring the time delay between an excitation pulse and the detection of a single emitted photon. The process can be broken down into the following key steps :

Excitation Pulse : The TCSPC system starts by emitting a short and intense excitation pulse of light onto the sample. This pulse serves to excite the fluorescent molecules within the sample.

Emission and Detection : After the sample is excited, some of the fluorescent molecules undergo relaxation and emit photons of light. These emitted photons are typically of lower energy (longer wavelength) than the excitation pulse. A specialized detector within the TCSPC system then detects these individual emitted photons.

Photon-to-Electronic Pulse Conversion : When a photon is detected, the TCSPC system converts the photon's optical signal into an electronic pulse. This electronic pulse is generated with a precise and well-defined timing resolution.

Arrival Time Measurement : The TCSPC electronics are designed to measure the precise time at which the electronic pulse arrives. This time interval is known as the "time-of-flight" or "time delay" between the excitation and the detection of the emitted photon.

Time-Stamping : The measured time delay is recorded as a data point in the TCSPC histogram. The histogram essentially represents the distribution of photon

arrival times over a period of time, creating a detailed map of the emission kinetics of the sample.

Repeat and Accumulate : The TCSPC process is typically repeated numerous times, with each emitted photon's arrival time noted and added to the histogram. This repetition and accumulation allow for a more statistically significant analysis and results in a higher signal-to-noise ratio.

The resulting TCSPC histogram reveals important information about the fluorescent properties of the sample. In particular, this study provides insights into the lifetimes of the excited states of fluorescent molecules, molecular interactions, and other dynamic processes.

1.5.3 Experimental Setup

We operate a custom-built confocal microscope with a LOMO 58x, 0.8 NA, water immersion objective as shown in fig 1.12Experiments on p-terphenyl use a 266nm picosecond laser (Picoquant LDH-P-FA-266, 70ps pulse duration, 80MHz repetition rate) with 80µW average power, while experiments on proteins use a 295nm picosecond laser (Picoquant VisUV-295-590, 70ps pulse duration, 80MHz repetition rate). The 295nm wavelength selectively excites tryptophan residues, as tyrosine and phenylalanine have negligible absorption above 290nm. Both laser beams are spatially filtered to ensure a Gaussian profile filling the objective back aperture, they pass through a short-pass filter (Semrock FF01-311/SP-25) and are reflected by a dichroic mirror (Semrock FF310-Di01-25-D). The sample with protein solution is positioned at the laser focus with a 3-axis piezoelectric stage (Physik Instrumente P-517.3CD). We use the microscope LED illumination to localize the nanophotonic structures on quartz coverslips.

The fluorescence light is collected back by the microscope objective and separated from the laser light by the dichroic mirror and two emission filters (Semrock FF01-300/LP-25 and Semrock FF01-375/110-25). The spectral range for fluorescence detection goes from 310 to 410nmIn a particular instance, which will be discussed in the following chapter, an additional stack emission filter (FF01-334/40-25) is placed on the collection path to select fluorescence photons in the 310-360 nm range. Confocal detection is performed using a 200mm focal length doublet lens (Thorlabs ACA254-200-UV) and an 80m pinhole. Single-photon counting uses a photomultiplier tube (Picoquant PMA 175) connected to a photon counting module (Picoquant Picoharp 300 with time-tagged time-resolved mode). The amount of time spent integrating typically ranges from two to three minutes, although this can differ depending on the experiment.

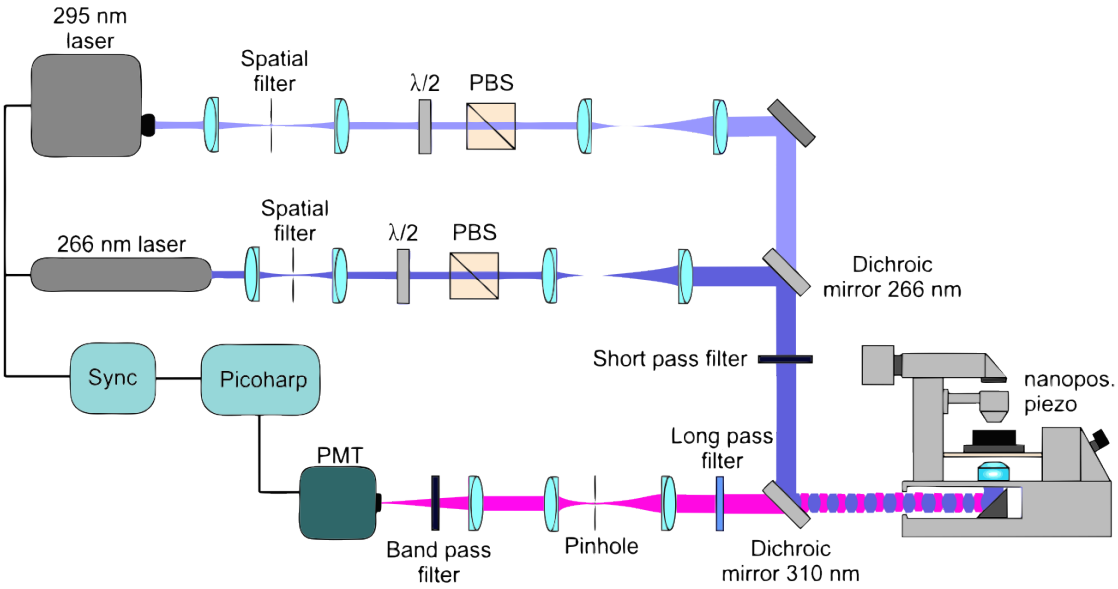

FIGURE 1.12 – Schematics of custom build UV confocal setup

Our former colleague constructed the setup as part of their PhD research.Aleksandr BARULIN 2020 I then made some modifications to it while I was working on my PhD dissertation.

1.6 UV Auto-fluorescence stabilization using chemical agents

The emission of ultraviolet (UV) light from proteins follows the same principle as that of any other organic dye. This emission can be conceptualized as a three-level system with different rate constants and states. The interaction of the emitter with its environment can lead to the formation of nonradiative channels, such as triplet and radical states, which can reduce the fluorescence emission from proteins. These pathways are also responsible for the saturation and photobleaching of the emitters.

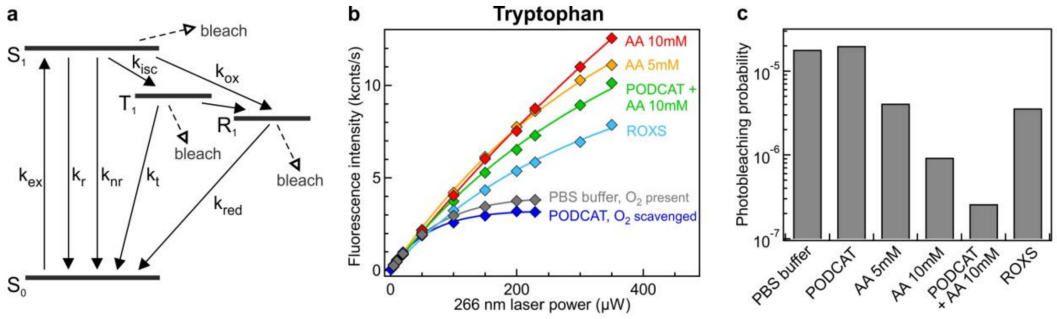

FIGURE 1.13 – Fluorescence antifading agents to improve the photostability of pure tryptophan. (a) Electronic state model describing tryptophan fluorescence with the ground and excited states S0 and S1, the triplet state T1, the radical state R1, and the different rate constants ki. (b) Fluorescence intensity detected for 1 μM solution of tryptophan dissolved in different buffers as a function of the UV laser power. The markers are experimental data points, and the lines are numerical fits. AA stands for ascorbic acid, PODCAT for pyranose oxidase catalase oxygen scavenging system, and ROXS for reducing and oxidizing system (GODCAT with 10 mM AA and 1 mM methyl viologen). The background intensity detected for oxygen scavengers and the different agents was subtracted for each curve. (c) Tryptophan photobleaching probability, pb, deduced from the fits in panel b for the different antifading conditions.reproduced from BARULIN et WENGER 2020

In order to raise the total emission, we must suppress the radical and triplet states, which form a non-radiative pathway for the de-excitation of energized states. The triplet state is a high-energy molecular state that possesses two unpaired electrons with parallel spins. Triplet states are notorious for their longer lifetimes, often leading to a phenomenon known as intersystem crossing (ISC), which causes a transition from the singlet excited state to the triplet state. This can subsequently result in phosphorescence, a slower form of emission, or nonradiative decay, which can lower the efficiency of fluorescence.WIDENGREN, RIGLER et al. 1994 HA et TINNEFELD 2012b Molecular oxygen is a common quencher that is used to deactivate triplet states due to its own triplet ground state. It can readily accept energy from the triplet excited state of the fluorophore, leading to the formation of singlet oxygen.WINTERBOURN 2012 Oxygen in the system is the source of radical oxygen species which can lead to radical oxidative states, which are further promoted when the solution is exposed to the UV laser. On the other hand, radical states are often quenched using radical scavengers, such as butylated hydroxytoluene (BHT), vitamin E, and other antioxidants. These compounds react readily with the radical states, stabilizing them and preventing them from interfering with the fluorescence emission.LOBO, A. PATIL et al. 2010
To quench both states, a combination of antioxidants and oxygen scavengers must be used to enhance overall emission, as seen in Figure 1.13. Different buffer solutions can be used to reduce the photobleaching probability. However, adding extra chemistry into the buffer can increase the background signal, which can reduce the sensitivity

of FCS. To overcome this, other methods must be explored to increase the saturation limits. It is important to note that different proteins may require different buffers to achieve maximum emission. Thus, it is essential to optimize the buffer for the protein before experiments to improve the photostability of proteins. Our group conducted an in-depth study on UV photostability previouslyAleksandr BARULIN et Jérôme WENGER 2020a, and we will use that information and implement it in our study in this thesis and further investigate how to improve the photostability of different proteins.

1.7 Nanophotonics can enhance UV Auto-fluorescence

Nanophotonics, also sometimes known as nano-optics, is a branch of science that studies the behavior of light and its interaction with matter at the nanometer scale, usually within the sub-wavelength range NOVOTNY et HECHT 2006. This is an exciting and rapidly developing field that blends optics and nanotechnology principles and enables unprecedented control of light at the nanoscale. Nanoplasmonics is a subset of nanophotonics technology where plasmons are used to change the emission of emitters near them at the nanoscale, for example, using SPP (surface plasmon polariton) on bulk surfaces or LSPR (local surface plasmon resonance) on metallic nanoparticles.GIANNINI, FERNÁNDEZ-DOMÍNGUEZ et al. 2011a Nanophotonics and its subset of nanoplasmonics are widely used to increase emitter emission rates, ranging from semiconductor quantum dotsGROSS, HAMM et al. 2018 to organic moleculesJuanjuan WANG, JIA et al. 2018 and biomolecules such as proteins Aleksandr BARULIN, ROY, Jean-Benoît CLAUDE et al. 2021, due to their ability to store light in as small a volume as possible and for as long as possible (PELTON 2015).

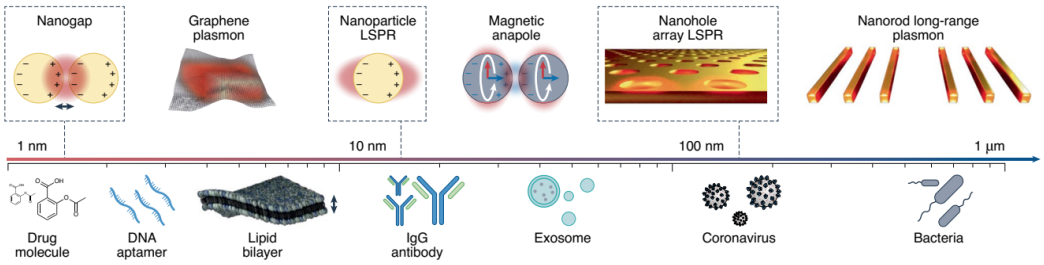

FIGURE 1.14 – Size comparison between common biological analytes and the decay length of the evanescent field in various nanophotonic structures. LSPR, localized surface plasmon resonance.Reproduced fromALTUG, OH et al. 2022. In this thesis we will be focusing on the left end of images i.e analyte size less than 10 nm and using LSPR

Here we can introduce the term needed to understand the figure of merits of

Nanophotonics in enhancing emission. The term is the Purcell factor; it was coined by Purcell in 1946 when he suggested that nuclear magnetic transition rates can be modified by placing it inside a cavity.PURCELL 1946 Thus, the ratio of modified emission rates to free-space emission rates of the emitter is termed the Purcell factor given in the following equation.AGIO et CANO 2013 PELTON 2015

$$F_p = \frac{3Q\lambda^3}{4\pi^2 V_0} \tag{1.2}$$

where λ is the wavelength associated with transition, Q is the quality factor of the cavity and V_0 is the volume of the cavity. To increase the Purcell factor, for a given wavelength, we can use low-loss photonic cavities S NODA 2007 KRASNOK, MIROSHNICHENKO et al. 2012 with a high Q factor but a larger mode volume, or we can use plasmonic cavities, which are known to have a very low mode volume in the range of $10^{-6}(\lambda/n)^3$ (possible for gap plasmon antennas)KINKHABWALA, Z. YU et al. 2009. The equation above is a general expression for a cavity whose fundamental mode coincides with the emitter's transition wavelength, the dipole is aligned with the polarization of the cavity mode, and the emitter has a very narrow line width.PELTON 2015 To further understand quantitatively how nanophotonics affect emission rates and enhance the overall signal from the emitter let us see the equation of Fluorescence enhancement

$$\eta_F = \kappa * \eta_{exc} * \frac{\Gamma^*_{rad}}{\Gamma_{rad}} * \frac{1}{1-\phi_0+\phi_0(\Gamma^*_{rad}+\Gamma^*_{loss})/\Gamma_{rad}} \tag{1.3}$$

where 'η_F' is fluorescence enhancement, κ is collection gain, η_{exc} is excitation gain, and Γ^*_{rad} is modified radiative rates, Γ_{rad} is free-space radiative emission rate, ϕ_0 is initial quantum yield of the emitter and Γ^*_{loss} is non-radiative rates which accounts for the rate constant for losses due to plasmonic quenching. In the previous section, we have seen that using nanophotonics-nanoplasmonics we can modify the light-matter interaction thus to enhance the fluorescence emission of the molecules; we need to use nanophotonic tools to increase the terms η_{exc} ,κ and $\frac{\Gamma^*_{rad}}{\Gamma_{rad}} * \frac{1}{1-\phi_0+\phi_0(\Gamma^*_{rad}+\Gamma^*_{loss})/\Gamma_{rad}}$ (the Purcell factor) given in the above equation.

Let us see the first term, that is, excitation gain η_{exc} its ratio of the electric field intensity inside the nanophotonic-nanoplasmonic cavity to the electric field intensity in free space. In free space, the size mismatch between the emitter (few nm) and the wavelength light (few 100s of nm) leads to ineffective excitation of the emitter and, by reciprocity theorem, to ineffective outcoupling of radiation in the far fieldJérôme WENGER 2019. Thus, we need a device to squeeze light down to the nanometre scale for better light-matter interaction. Such devices that can convert propagating optical radiation in free space to localised energy and vice versa are called optical antennas as shown in fig1.15 NOVOTNY et VAN HULST 2011 . The antenna can be dielectric basedKRASNOK, MIROSHNICHENKO et al. 2012 using dielectric gap antennas made from siliconREGMI, BERTHELOT et al. 2016a or low-loss gallium phosphideSHIMA, SUGIMOTO et al. 2023 , antennas with higher enhancement factors are more com-

monly metallic in nature where the plasmon generated by LSPR or SPR squeezes light millions of times smaller than the diffraction volume leading to a few-order high excitation enhancement GIANNINI, FERNÁNDEZ-DOMÍNGUEZ et al. 2011b. M. MAYER et H. HAFNER 2011 , PUNJ, MIVELLE, VAN ZANTEN et al. 2013

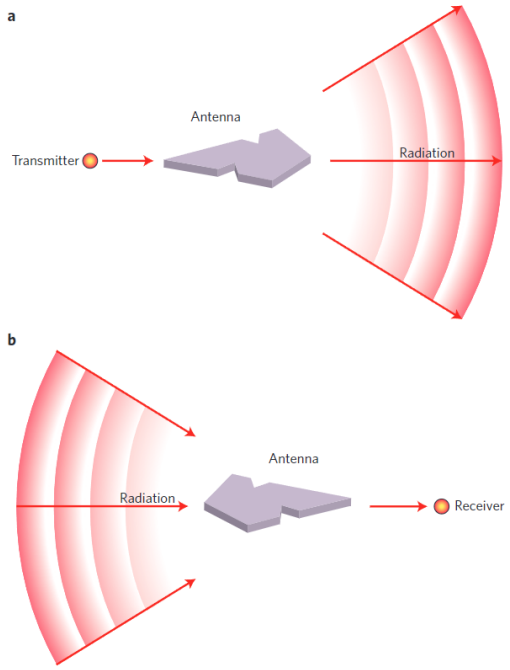

FIGURE 1.15 – The concept of optical antenna. reproduced from NOVOTNY et VAN HULST 2011

Another important factor in the fluorescence enhancement equation is κ which is collection gain. In general, the gain of the collection is the measure of how effectively the emitted light from the analyte molecule is collected by the objective of the microscope. The emitter source can be thought of as a point source that emits light at a wide range of angles (isotropic emission). A high numerical aperture (NA) objective can be used to collect a wide range of emission angles, except for light above the critical angle.RUCKSTUHL, ENDERLEIN et al. 2000 As seen in figure1.15 antenna outcouples the light from the source to far-field effectively which means it's possible to use optical antennas to control the far-field emission pattern and make the emission directive. Such techniques to make emission more directive are well known in the microwave, where antennas like Yagi Uda, bull's eye, and horn antennas are extensively used. In addition to plasmonic nanoantennas, other types of antennas have also been explored to control the directionality of the emission. For example, leaky-wave antennas (LWAs) have been investigated for their ability to produce narrow-beam radiation with steering capabilityKUZNETCOV, COMITE et al. 2023 HUMMADI et FYATH 2015. These antennas use guided modes and leaky modes to dominate the far-field emission pattern and govern the direction of the main lobe emissionFARHEEN, LEUTERITZ

et al. 2021. However, when discussing nanophotonics and light-matter interactions, the light wavelength that is most commonly used falls in the visible range because of many reasons, such as the availability of low-loss plasmonic material, the wide range of uses of visible plasmonics-photonics, and the feasibility of the fabrication technique. It is clear that plasmonic nanoantennas are essential for increasing the signal through excitation gain, collection gain, and alteration of the Purcell factor, which affects the radiative rates of emitters. The antennas discussed earlier in this section were mainly designed for the visible range, using materials such as gold and silver, which are well-known plasmonic materials. Research on plasmonic antennas for UV is limited to some simulation work or proof-of-concept studies on UV Raman or UV enhancement of fluorescent dyes. Exploring the use of antennas to amplify UV signals from proteins or biomolecules has yet to be done. The difficulty lies in the accuracy of nanofabrication needed for nanostructures used in the ultraviolet (UV) spectrum, as the size of nanostructures is smaller than those used in the visible range. Additionally, the selection of material is critical, as gold and silver are not suitable for UV plasmonics due to their higher losses and interband transitions. We will analyze these elements in the following sections.

1.7.1 The material used in UV Nanophotonics

The Drude's model suggests that each metal has a plasma frequency, which determines the spectrum of the plasmonic response for different materials. Metal particles for which plasma frequency lies higher than 3 ev can have LSPR and SPR in UV regime. There are 12 such materials ranging from aluminum (Al), gallium (Ga), indium (In), rhodium (Rh), ruthenium (Ru), tungsten (W), titanium (Ti), chromium (Cr) palladium (Pd), copper (Cu), platinum (Pt), and magnesium (Mg).J. M. SANZ, D. ORTIZ et al. 2013a . Apart from these some studied have also shown plasmonic behaviour in metals like Sn, Tl, Pb, and BiMCMAHON, SCHATZ et al. 2013 . The location of SPR of different metals is depicted in 1.16.The figure shows faraday number for different metals, its dimensionless quantity representing 'Fa' (enhancement factor)LALISSE, TESSIER et al. 2015.

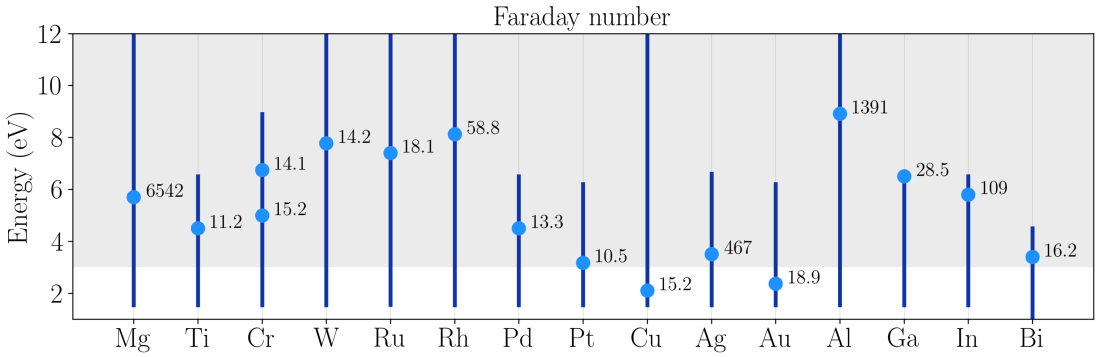

FIGURE 1.16 – Comparison of performance of different UV plasmonic material. blue dot is plasma frequency and numbers are faraday numbers(plasmonic enhancement indicators). reproduced GUTIÉRREZ, OSA et al. 2018

Although there is a range of materials that can be used for UV, however not all of them are applicable for biosensing and have a strong plasmonic response in UV. As seen in figure 1.16 Based on Rh, Ga, Al, Mg and Ag are the most widely studied UV plasmonic materials. Their behaviour and physical properties have been extensively examined in several reviews, such as .Juan M. SANZ, Dolores ORTIZ et al. 2014 J. M. SANZ, D. ORTIZ et al. 2013b GUTIÉRREZ, LOSURDO, GONZÁLEZ et al. 2020 MCMAHON, SCHATZ et al. 2013

We can see in the figure 1.17, in the UV range plasmonic response of different materials, the top four being Al, Mg, Rh and Ga. We will be focusing on only four of these metals moving forward in this discussion.

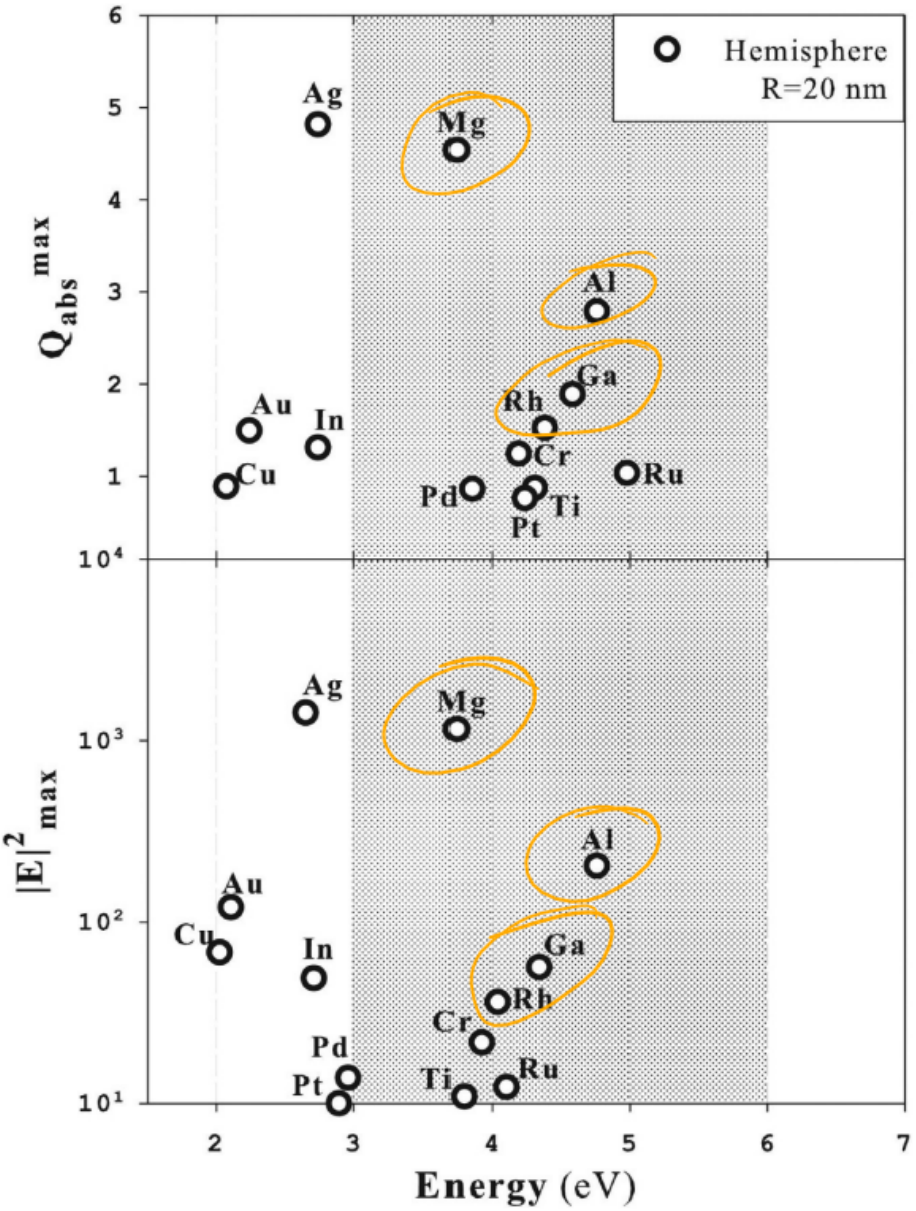

FIGURE 1.17 – Plasmonic response of different metals in UV. Top image highlights absorption cross-section maxima for different metal and bottom plots shows maximum intensity enhancement. The response is calculated for the 20 nm hemisphere on a substrate. Image is produced fromGUTIÉRREZ, LOSURDO, GONZÁLEZ et al. 2020

1.7.1.1 Gallium

Gallium with a Faraday number of 28.5 and plasma frequency in the range of 6-7 eV is a unique plasmonic material and is known for its low oxidation, chemically inert making it bio-compatible and also possesses a broad plasmonic response Y. YANG, AKOZBEK et al. 2014 ranging from visibleHORÁK, ČALKOVSKÝ et al. 2023 to UV

Y. YANG, CALLAHAN et al. 2013. One of the key features which make Ga NPs unique is the co-existence of the liquid-solid phase at room temperature, this makes it an ideal candidate for active UV plasmonicsROY et BOLSHAKOV 2020 and phase-change materialSOARES, JONSSON et al. 2007. Gallium nanoparticles are used for SERS P. C. WU, KHOURY et al. 2009 , to enhance photoluminescent XIANG, J. CHEN et al. 2019 fluorescence enhancement for biosensing LOSURDO, GUTIÉRREZ et al. 2021 there are many methods to prepare gallium nanoaparticles however two main techniques are Molecular Beam Epitaxy (MBE) and colloidal technique. MBE is used to grow NPs on the substrateP. C. WU, LOSURDO et al. 2009 GUTIÉRREZ, LOSURDO, GARCÍA-FERNÁNDEZ et al. 2019 LOSURDO, GUTIERREZ et al. 2018 the MBE technique used in mentioned papers, provide huge control on phase of Ga NPs, angstrom precision on NPs size as well as control over average plasmonic response which tuned by introducing ellipsometry in the MBE setup. However, for some other applications where NPs are needed in suspension colloidal technique is used MELÉNDREZ, CÁRDENAS et al. 2010 YAREMA, WÖRLE et al. 2014. Given the unique feature of low oxide formation. Vis-UV plasmonic response and resistance to corrosion from water pr hydroxyl ion makes Gallium a formidable UV plasmonic material. However, in comparison to Al, its weaker in plasmonic response and one major drawback of gallium as a plasmonic material for UV spectroscopy is photoluminescence from Gallium oxide which overlaps with fluorescence from aromatic amino acids. We will discuss the effect of gallium oxide in the upcoming chapter in context to Gallium ion-FIB which is used to fabricate nanostructure throughout this work.

1.7.1.2 Rhodium

Rhodium NPs have been introduced as a non-oxidising catalytic noble metal for ultraviolet plasmonics. A study by WATSON, X. ZHANG et al. 2015synthesized planar tripods of 8-nm Rh nanoparticles using a modified polyol reduction method. These nanoparticles exhibited a calculated local surface plasmon resonance near 330 nm. Rhodium nanoparticles are made mainly using colloidal techniques HUMPHREY, GRASS et al. 2007 techniquesWATSON, X. ZHANG et al. 2015.X. ZHANG, P. LI et al. 2016 Rhodium nanostructures with variable shapes are used for UV SERS like cubes REN, X. F. LIN et al. 2003 and nano-crescents KUMAR et SONI 2022 Rhodium Fa values are twice higher than gallium around 58 and its plasma frequency lies in deep UV around 8 eV, Rh Nps are usually oxide free, making them a good contender for UV plasmonics. Similarly to Ga, it is also chemically inert and biocompatible. It is worth noting that Rhodium is not as strong a plasmonic material as Mg or Al based on the Fa numbers; however, because of its resistance to UV photo-corrosion, it stands out as a UV plasmonic material. We will study the plasmonic property of Rh Nps in the coming chapters in detail.

1.7.1.3 Magnesium

Magnesium (Mg) has the highest Fa number of 3000+ and the plasma frequency lies close to 6eV, making it suitable for visible to UV plasmonics, thus it has gained significant attention as a potential plasmonic material in various fields.Y. WANG, E M PETERSON et al. 2017 BIGGINS, YAZDI et al. 2018 Mg nanoparticles (Mg NPs) have been shown to support localized surface plasmon resonances in the UV, visible and near-infrared parts of the electromagnetic spectrum RINGE 2020. This makes Mg a promising alternative to other plasmonic materials, such as aluminium (Al), with higher extinction efficiencies in the same wavelength rangeSTERL, STROHFELDT et al. 2015

The potential applications of Mg in plasmonics are diverse. For example, MgNPs have been used in tip-enhanced Raman spectroscopy (TERS) to examine the photocatalytic properties of MgNPs and their Au-modified bimetallic analogs S. J. PATIL, LOMONOSOV et al. 2023). Mg has also shown promise in improving fluorescence and surface Raman scattering for excitation wavelengths in the UV rangePONZELLINI, GIOVANNINI et al. 2019. Furthermore, Mg-based plasmonic structures have been explored for applications in catalysis, hydrogen storage, and solar-driven chemical transformations DOUGLAS-GALLARDO 2021 JOSHI, MIR et al. 2022 Magnesium nanoapertures and ZMWs were used to study P-terphenyl a UV dye using UV spectroscopy Y. WANG, JIAO et al. 2016JIAO, Y. WANG et al. 2015. Mg nanoapertures exhibit a lifetime reduction higher than that reported for the Al aperture. Even with all these features, Mg is not suitable for UV spectroscopy of biomolecules because of its reactivity toward the H_2 gas. Mg upon exposure to H_2 becomes MgH_2, which, as a dielectric material, does not support plasmonic resonances. Similarly, Mg reactivity towards water and oxygen poses limitations for its application as a biocompatible material for the plasmonic resonator

1.7.1.4 Aluminum

Of all plasmonic materials, aluminium is the best performing plasmonic materialKNIGHT, L. LIU et al. 2012 due to its high Fa numbers (1391) and very high plasma frequency (9eV) ; Apart from this factor, Al being an abundant metalPROUST, S. SCHUERMANS et al. 2013 and its compatibility with CMOS technology make it the most lucrative of all UV plasmonic materials. In the major part of this thesis, we will focus on Al as the main plasmonic material. Al Nps and AL plasmonics form the main part of the research on UV plasmonics as depicted in 1.18

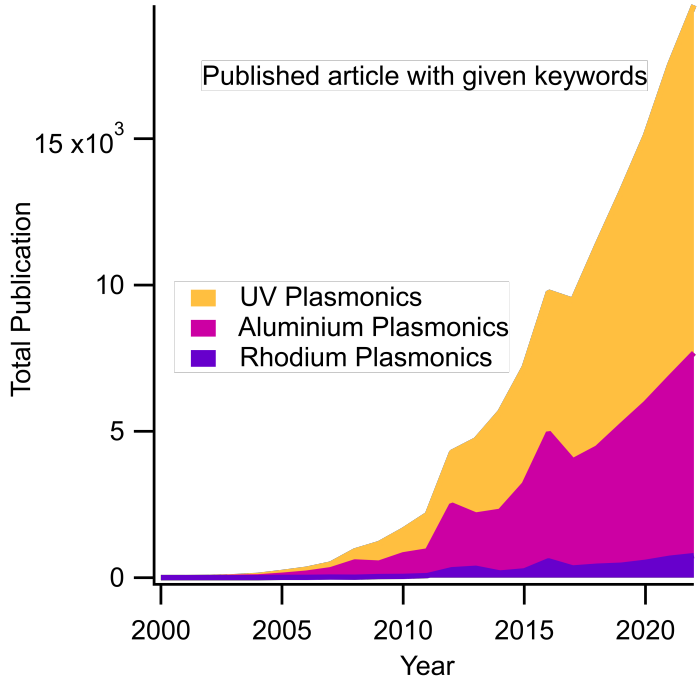

FIGURE 1.18 – Articles published with keywords "UV plasmonics", "Aluminium Plasmonics" and "Rhodium Plasmonics". The data is taken from the website Dimensions.ai

Fabrication of Al nanostructures As we saw in the previous section, all other metal nanoparticles were synthesized using the colloidal technique, and for thin film a vapor deposition process is used. In context to this thesis, we will discuss Al thin film fabrication and Al nanoparticle fabrication techniques.

Chemical vapour deposition (CVD) is a method in which a precursor gas reacts at the surface of a heated substrate to form a solid thin film. For Al thin films, common precursors include trimethylaluminium and aluminium chloride. CVD can produce high-quality films with excellent conformity, making it suitable for complex substrate shapes. However, the process often involves high temperatures and potentially toxic precursor gases. Furthermore, the resulting films can contain impurities from the precursor gas Luzhao SUN, YUAN et al. 2021.

Physical vapor deposition (PVD) is the most common method for the fabrication of Al thin films. It involves evaporating or sputtering the target material (Al) in a vacuum, where the vapor then condenses on a substrate to form a thin film. This method offers high purity and uniformity of the thin film, making it ideal for electronic applicationsX. SUN, AN et al. 2019 In this thesis, we employed electron beam evaporation (e-beam) (Buhler Syrus Pro 710) as a Physical Vapor Deposition (PVD) technique to deposit high-quality Aluminum (Al) thin films BUNSHAH et DESHPANDEY 1985. This method utilizes a concentrated beam of high-energy electrons to vaporize the source material (Al) in a vacuum environment. The evaporated atoms then travel and condense onto a substrate, forming a thin film. The process is rapid, with a deposition rate

of 10nm/s, resulting in a film with no alumina in the bulk that could significantly alter the plasmonic response. Note that a thin film of alumina is formed on the top of Al thin film once the Al film comes in contact with ambient conditions outside the PVD chamber. This extra layer provides some resistance to photo-corrosion and shifts the plasmonic response. The above techniques can be used to make Al thin film that acts like visible-UV reflectors, thus making a special class of nanostructure called ZMWsAleksandr BARULIN, Jean Benoît CLAUDE et al. 2019a BAIBAKOV, Aleksandr BARULIN, ROY, Jean-Benoît CLAUDE et al. 2020

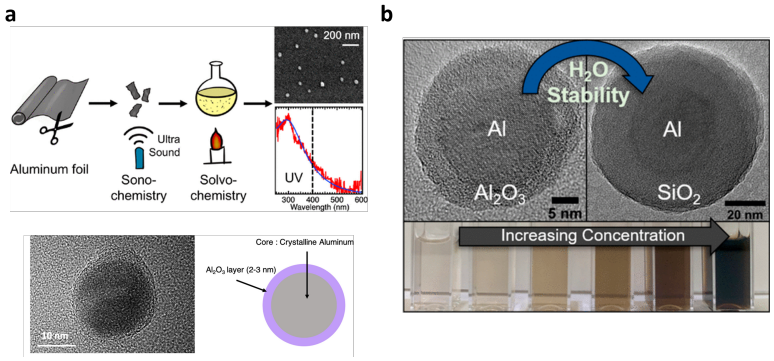

FIGURE 1.19 – a. Fabrication of Al Nps with Alumina coating CASTILLA, Silvère SCHUERMANS et al. 2022 (b) Al Nps with thick silica coating RENARD, TIAN et al. 2020produced from

For fabrication Al NPs group of researchers in UTT Troyes PROUST, S. SCHUERMANS et al. 2013CASTILLA, Silvère SCHUERMANS et al. 2022 describes the synthesis of Al NPs using a method that involves the reduction of aluminium ions in the presence of a stabilizing agent. The resulting Al NPs are found to be highly stable and exhibit excellent optical properties. This method combines sonochemistry and solvochemistry and is scalable to industrial uses. The resulting nanoparticles have a crystalline aluminium core of 10-100 nanometers in diameter, which is encased in a thin alumina shell, providing long-term stability in ethanol. . When dealing with biology, water with salt and a high pH is the preferred solution. In this environment, Alumina is not enough to prevent corrosion (we will discuss corrosion in detail in the upcoming section and chapter) of the Al NPs. To deal with H_2O instability group of Naomi Halas at Rice University developed a technique to make Al Nps with Silica coating RENARD, TIAN et al. 2020The method involves the use of trioctylphosphine as the solvent, which yields small, quasi-spherical Al NCs through the Ti(IV)-catalyzed decomposition of dimethylethylamine alane (DMEAA) at 60 °C. The resulting Al NPs have a plasmon resonance in the ultraviolet region of the spectrum and appear transparent, or slightly yellow, in the solution phase. The authors also developed a procedure for coating these Al NCs with a nanoscale SiO2 layer. This coating preserves their optical and photothermal properties and greatly enhances their stability in aqueous media from hours to weeks. The Al@SiO2 nanoparticles were then investigated for their use as broadband photothermal heaters of aqueous media. It must be noted that Al NPs

with thin Alumina are perfect for making plasmonic antennas however it is not stable in water and UV exposure whereas 10 nm silica coating on Al makes it robust for application in aqueous media but a 10 nm thick layer reduces the coupling of plasmon to the emitter or to another Al NPs thus reducing the effective plasmonic response. This opens up the scope for improvement in the fabrication of Al NPs suitable for plasmonics in biology.

UV photocorrosion and Aluminium In this section, we discuss the UV photocorrosion of Al especially the effect on the thin film of Al. When UV light is shined on water, depending on the intensity of UV light, the water breaks down into radicals and these radical species are very reactive and readily react with the metal in contact with the water media and lead to corrosion. BURLEIGH, RUHE et al. 2003 found that exposure to UV light caused photo-corrosion in several metals, including zinc, carbon steel, aluminium, copper, and silver.DENG, H. LIU et al. 2020studied the influence of UV light irradiation on the corrosion behaviour of electrodeposited Ni and Cu nanocrystalline foils in 3.5% NaCl solution. The authors used electrochemical methods, electron work function analysis, and characterization with atomic force microscopy and X-ray photoelectron spectroscopy to understand the corrosion behaviour of these metals. In reported studies UV exposure has changed the surface chemistry of the metals, but didn't results in increased corrosion for all metals, sometimes UV exposure has boosted the photo-corrosion resistance like in the case of nanocrystalline Cu foils DENG, H. LIU et al. 2020. Thus it is fair to say it's not a rule of thumb that UV always leads to metal corrosion, the reason behind this is the metal oxide layer formed on the metals. Different metal oxide layers react differently to UVCHANG et RAMANATHAN 2007.

Aluminium has amphoteric properties which allow it to react with acids and basic *Understanding Aluminum Corrosion* s. d. substances. Aluminium exhibits high reactivity and quickly reacts with water and/or air, resulting in the immediate formation of a thin layer of aluminium oxide (alumina) on its surface.The chemical reactions involved in the process are : Reaction of aluminum with oxygen :

$$4Al + 3O_2 - - > 2Al_2O_3 \tag{1.4}$$

Possible reactions of aluminum with water :

$$2Al + 6H_2O - - > 2Al(OH)_3 + 3H_2 \tag{1.5}$$

$$2Al + 4H_2O - - > 2AlO(OH) + 3H_2 \tag{1.6}$$

$$2Al + 3H_2O - - > Al_2O_3 + 3H_2 \tag{1.7}$$

This oxide layer acts as a protective barrier and reduces the metal sensibility to corrosion ANDRIEVSKII 2013 by reducing the vulnerability of the metal. However, oxygen

presence can speed up the corrosion process, especially in high concentrations and acidic solutions. Aluminium corrodes in aqueous solutions outside the pH range of 4-9 due to the solubility of its oxides in many acids and bases *Understanding Aluminum Corrosion* s. d. due to its corrosion in aqueous solutions outside the pH range. If the protective oxide film is damaged, it can normally regenerate in most environments. However, corrosion occurs when the film is removed or damaged under conditions that prevent self-repair J. LEE, SHIN et al. 2017.

$$Al + 3OH^{\bullet} - - > Al^{3+} + 3OH^{-} \tag{1.8}$$

The oxide formed on Al films is not uniform, particularly at the grain boundaries. Cracks in the oxide at these boundaries permit radicals created by the UV excitation of water molecules to penetrate and corrode the Al (as seen in the chemical reaction of 1.8). Although there is a range of radicals which are formed during the UV excitation of water molecules but $OH^{\bullet}$ is a major contributor to corrosion.

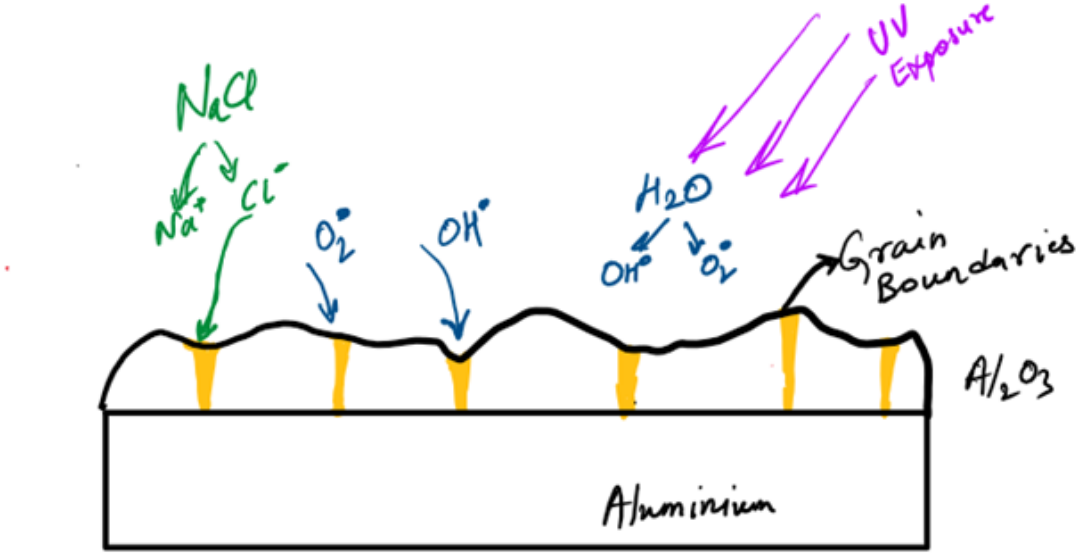

FIGURE 1.20 – Pictorial representation of diffusion of radical species into pits of Alumina layer and corroding Al thin films.

It is worth noting that UV excitation accelerates the corrosion process by generating excessive radicals. The same corrosion can occur on Al films exposed to ambient light and a pH7 solution containing a few mM of salts, although the time frame for this is days rather than seconds as with UV laser exposure.

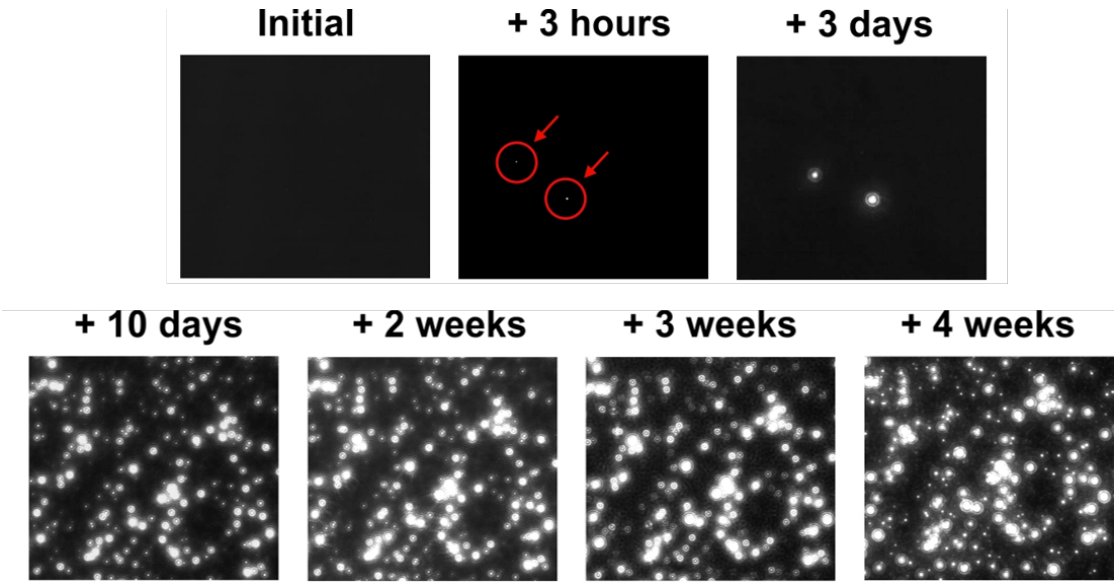

FIGURE 1.21 – Evolution of corrosion of Al thin film under ambient condition and mM salt and pH7 buffer solution. The bright spots are the corroded spots where Al is dissolved and light can transmit through the spot.Images taken with a brightfield transmission optical microscope with a 40x 0.65NA objective. Each image corresponds to a 120*100 μm^2 region.

Several studies have looked into ways to stop or reduce aluminium corrosion. Utilizing a buffer with a pH of 4, using heavy water instead of regular water or using alcohol solutionCASTILLA, Silvère SCHUERMANS et al. 2022, applying PVP coating on an Al thin filmAleksandr BARULIN, Jean-Benoît CLAUDE et al. 2019b, and the most effective is coating Al metal with a thin film of UV transparent oxidesROY, BADIE et al. 2021. We will discuss the last point in more detail in the following chapter and examine how different oxide layers influence the corrosion resistance of the Al layer.

1.7.2 Nano-fabrication of UV-plasmonic structure

Nano-fabrication techniques play a crucial role in the development of plasmonic structures for various applications. Several methods have been explored to fabricate these structures, each with its own advantages and limitations.In previous section we saw that nanoparticles for UV plasmonics were made mostly by chemical methods and in colloidal form, colloidal technique can be fast and suited for mass production however proper position of these NPs respective to each other at proper gap and orientation is key to getting plasmons excited. In this section we will discuss few most prominent techniques which can be used to do so, first is DNA-based plasmonic structure assembly, second we will see more intuitive and precise yet time-consuming Focused Ion beam milling technique which we used throughout this work and lastly self-assembly using capillary forces.

1.7.2.1 Focused Ion beam Milling

FIB milling operates by utilising a focused beam of ions, often gallium ions, to selectively remove material at the nanoscale level. The process involves scanning the ion beam across the target surface, where interactions between the ions and the target material lead to sputtering, i.e., ejection of atoms or clusters, thus creating a desired pattern. The resolution in FIB milling depends on factors such as the size of the beam spot, the current of the beam, the dwell time and the overlap between passes. With advanced FIB systems, features down to 5 nm can be achieved, although the resolution is more commonly in the tens of nanometersMENARD et RAMSEY 2011. For instance, Vogel et al. fabricated gold nanostructures with the smallest feature size of about 30 nm using FIB milling, suitable for plasmonic applicationsKOLLMANN, PIAO et al. 2014.

Although FIB milling is renowned for its high resolution and precision, several drawbacks must be acknowledged. A significant issue is the implantation of gallium ions into the material, which can alter the properties of the material and potentially affect its performance, especially in plasmonic applications where the optical properties are crucial.J. MAO, Y. WANG et al. 2018ROY, Jean Benoît CLAUDE et al. 2023

Finally, FIB milling is a relatively slow process, making it less suitable for large-scale fabrication. This limitation is a significant factor in the high cost associated with this technique, limiting its application primarily to prototyping and research settings.HORÁK, BUKVIŠOVÁ et al. 2018.

Despite these drawbacks, FIB milling remains a valuable tool in the arsenal of nanofabrication techniques, especially for applications where high precision and flexibility in pattern design are required.TSENG 2005 Research into methods of mitigating ion damage and redeposition could further enhance the potential of FIB milling for the fabrication of plasmonic nanostructures.

1.7.2.2 Plasmonic nanoantennas using DNA Origami template

Among the diverse fabrication methods for optical antennas, DNA origami has emerged as a promising and versatile technique due to its ability to create complex and precisely tailored nanostructures.Swarup DEY, FAN et al. 2021

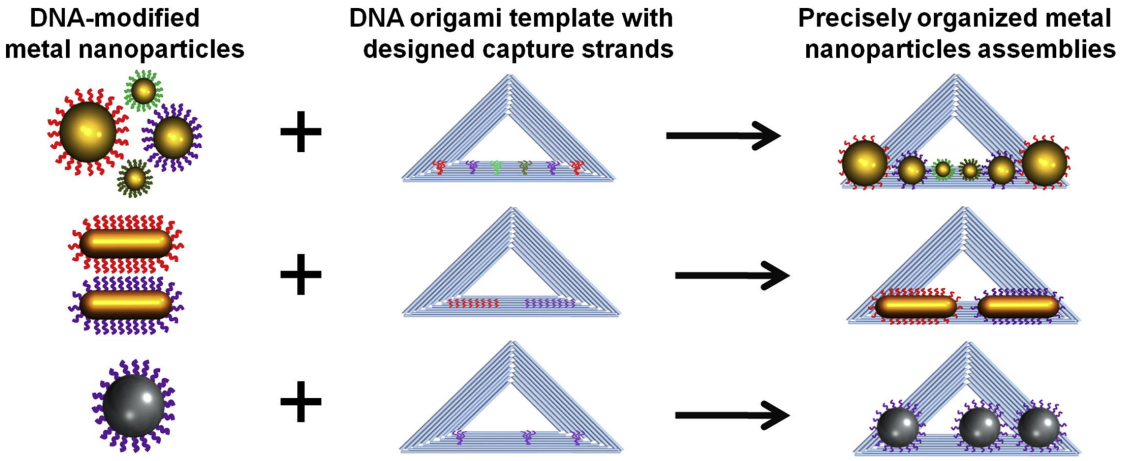

FIGURE 1.22 – Schematics of nanostructure fabrication using DNA origami templates. reproduced fromSwarup DEY, FAN et al. 2021

DNA origami is a revolutionary bottom-up nanofabrication approach developed by Paul W.K. Rothemund in 2006ROTHEMUND 2006. The technique utilises the programmability and self-assembly properties of DNA molecules to create a wide array of nanoscale shapes with exceptional precision. DNA origami involves folding a long single-stranded DNA scaffold using numerous short oligonucleotide staple strands to hold the desired shape together. By designing the sequence of these staple strands, researchers can fabricate various nanostructuresTROFYMCHUK, KOŁATAJ, GLEMBOCKYTE, F. ZHU, Guillermo P ACUNA et al. 2023, including optical antennas that can have an enhancement of 5000 timesPUCHKOVA, VIETZ et al. 2015a, a gap size of less than 5 nm can be achieved, leading to a strong coupling regime in plasmonic antennas HEINTZ, MARKEŠEVIĆ et al. 2021 DNA origami can be used to align antennas in a specific orientation and thus control the emission pattern YEŞILYURT et J.-S. HUANG 2021 SANZ-PAZ, F. ZHU et al. 2023 While DNA origami shows promise for optical antenna fabrication, there are several challenges that need to be addressed. One major concern is the stability of DNA structures under different environmental conditions, especially when integrated into real-world applicationsL. LI, NIE et al. 2023. Another challenge is the scalability and cost-effectiveness of the fabrication process. As the complexity of the designed structures increases, there is a need for precise and efficient assembly methodsKUZYK, JUNGMANN et al. 2018.Advancements in automated synthesis and assembly techniques can potentially overcome these limitations and allow large-scale production.

1.7.2.3 Plasmonic nanostructures using Capillary-Assisted Particle Assembly

CAPA is a versatile nanofabrication technique that enables the directed assembly of nanoparticles into well-defined structures through capillary forces. The process involves depositing a suspension of nanoparticles onto a substrate and then allowing the liquid to evaporate, leading to self-organization and assembly driven

by capillary flowMALAQUIN, KRAUS et al. 2007. The spatial confinement of the particles during evaporation, often achieved by using patterned templates or surface treatments, determines the final arrangement and morphology of the plasmonic nanostructures.FLAURAUD, MASTRANGELI et al. 2017

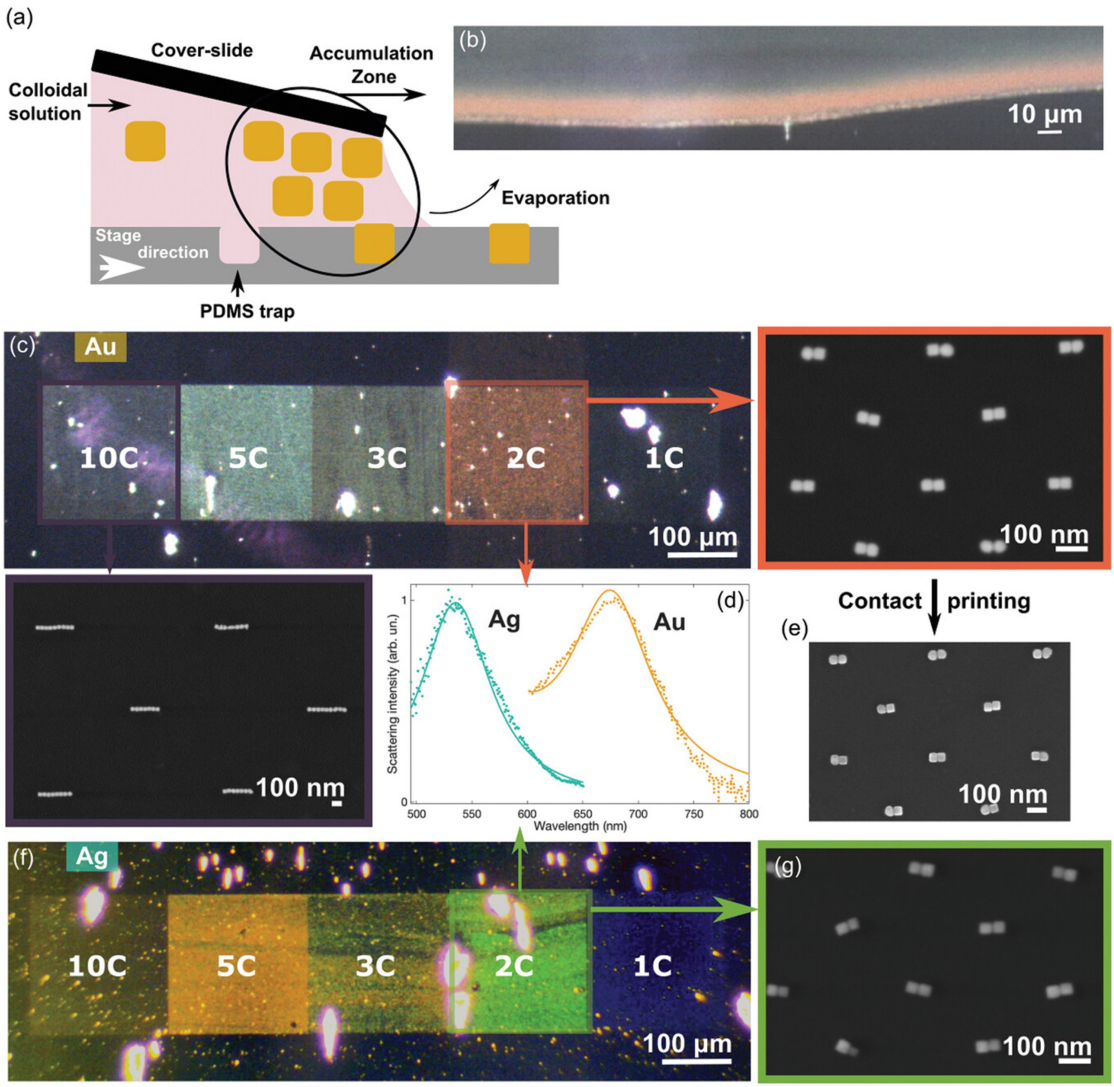

FIGURE 1.23 – Schematic representation of capillary assembly working principle. b) Optical image of self-limited and crystalline AZ obtained at 1 m·s1 and 45°C using gold colloidal solutions c) Optical image showing high yield Au nanocube assembly in the five dense arrays and SEM images of dimers (2C) and 10C arrays. d) Optical spectra of Ag and Au dimer arrays and the respective Lorentzian fit. e) Dimer array deposited from PDMS to silicon by contact printing. f) Optical image showing high-yield Ag nanocube assembly in the five dense arrays. g) SEM characterization of the dimer array (Ag) adapted from CAPITAINE, FAJRI et al. 2023

Advantages of CAPA for Plasmonic Nanostructures : Scalability and Through-

put : CAPA is amenable to large-scale production of plasmonic nanostructures. The process is relatively simple, cost-effective, and compatible with high-throughput manufacturing techniques, making it attractive for industrial applications.FLAURAUD, MASTRANGELI et al. 2017

Tunable Plasmonic Properties : By controlling the assembly parameters, such as particle size, shape, and interparticle distance, the plasmonic properties of the nanostructures can be tailored to meet specific application requirements. This tunability is highly advantageous for various sensing and imaging applications.LAO, Yuanyuan ZHENG et al. 2020

Multifunctional Nanostructures : CAPA allows the integration of different types of nanoparticles or the combination of nanoparticles with other functional materials, enabling the creation of multifunctional plasmonic nanostructures with enhanced capabilities.

While CAPA holds great potential for plasmonic nanostructure fabrication, several challenges remain to be addressed.CAPITAINE, FAJRI et al. 2023

Control and uniformity : Achieving precise control over particle assembly and ensuring uniformity across large areas is critical for practical applications. Improvements in process control and optimization of assembly parameters are needed to improve reproducibility.CAPITAINE, BOCHET-MODARESIALAM et al. 2023

Integration with Other Techniques : Combining CAPA with other nanofabrication techniques, such as lithography or self-assembly, can further extend its capabilities and enable the creation of complex plasmonic architectures.

Stability and Durability : The long-term stability and durability of CAPA-assembled plasmonic nanostructures need to be carefully evaluated, especially when they are used in harsh environments or integrated into functional devices.

1.8 Conclusion

Single-molecule biophysics is essential for comprehending biomolecules and their potential for use in medicine and early disease detection. Fluorescence-based single-molecule spectroscopy is a widely used technique, but it has drawbacks due to the labelling of analyte molecules. This can be avoided by using non-fluorescent, label-free techniques such as Raman or iScat however, these lack the advantage that fluorescent techniques can provide. Therefore, there is a need for a label-free fluorescent technique that has the same contrast as fluorescence spectroscopy. UV autofluorescence spectroscopy is the answer, as it uses amino acids found in 90% of human proteins as a source of intrinsic fluorescence or autofluorescence. This autofluorescence technique is effective but weak, so nanophotonics is needed to boost the signal. UV nanophotonics is an emerging field and much development is needed to effectively enhance UV autofluorescence.The main obstacles to overcome are low autofluorescence signal emission, resulting in a low Signal-to-Background ratio, the photostability of proteins under UV light, the development of nanophotonics for UV with materials resistant to UV corrosion, and the ability to study proteins at

concentrations of hundreds of μM with single-molecule sensitivity.

2 UV Autofluorescence Spectroscopy with Zero-Mode Waveguides

Connected Publications

Mikhail BAIBAKOV, Aleksandr BARULIN, Prithu ROY, Jean-Benoît CLAUDE et al. « Zero-mode waveguides can be made better : fluorescence enhancement with rectangular aluminum nanoapertures from the visible to the deep ultraviolet ». In : *Nanoscale Advances* 2.9 (2020), p. 4153-4160. ISSN : 2516-0230. DOI : 10.1039/d0na00366b

Prithu ROY, Clémence BADIE et al. « Preventing Corrosion of Aluminum Metal with Nanometer-Thick Films of Al2O3 Capped with TiO2 for Ultraviolet Plasmonics ». In : *ACS Applied Nano Materials* 4.7 (juin 2021), p. 7199-7205. DOI : 10.1021/acsanm.1c01160

Aleksandr BARULIN, Prithu ROY, Jean-Benoît CLAUDE et al. « Purcell radiative rate enhancement of label-free proteins with ultraviolet aluminum plasmonics ». In : *Journal of Physics D : Applied Physics* 54.42 (oct. 2021), p. 425101. ISSN : 0022-3727. DOI : 10.1088/1361-6463/ac1627. URL : https://iopscience.iop.org/article/10.1088/1361-6463/ac1627

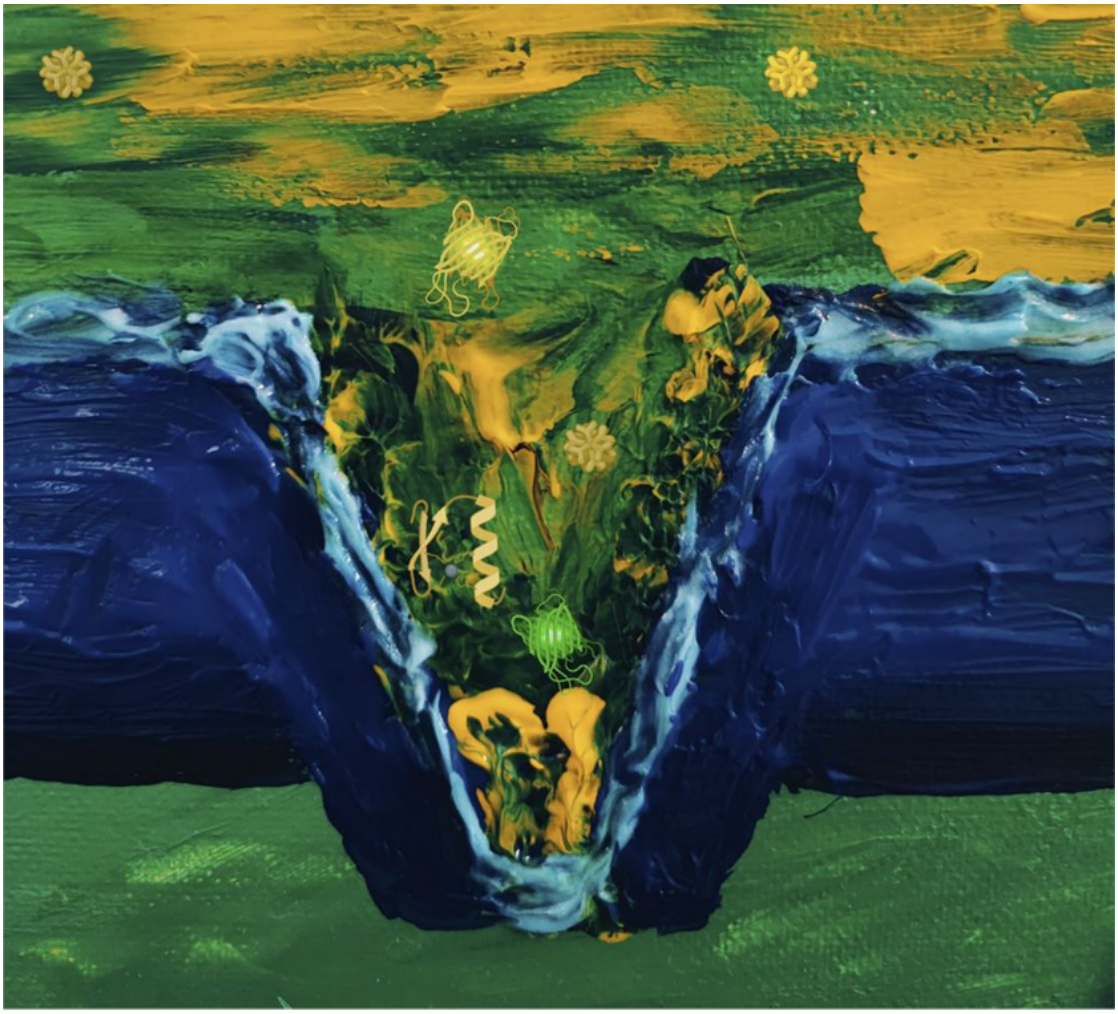

FIGURE 2.1 – Oil paint impressionism of ZMWs

Summary

2.1 Introduction to Zero Mode Waveguide

Zero-mode waveguides (ZMWs) are optical nanostructures that confine fluorescent excitation within subdiffraction volumes, enabling single-molecule analysis at high concentrations P. ZHU et CRAIGHEAD 2012 SHON et COHEN 2012. The name "zero-mode" refers to the fact that the waveguide mode has a very small mode volume, or to say it attenuates all the propagating waves and we get an evanescent wave confined close to the bottom of the ZMWs.AL MASUD, W. E. MARTIN et al. 2020 The history of ZMWs dates back to the 1940s when Hans Bethe studied the idealized case of a sub-wavelength hole in a perfectly conducting metal sheet of zero thickness and showed how the waves are attenuated at the entrance of ZMWs BETHE 1944. We can also consider that Edward Synge's concept of near-field imaging in 1928 might provided a foundation for the ZMWs. It was further developed by the biotech company Pacific Biosciences (PacBio), ZMWs have been instrumental in their Single Molecule, Real-Time (SMRT) sequencing technology.
To understand the physics behind ZMWs, we define the cutoff wavelength, which is denoted as λ_c, for a given aperture size, and can be computed using waveguide theory. The formula is λ_c= 1.7d, where 'd' represents the diameter of the aperture. When the excited wavelength exceeds λ_c, light does not travel through the structure; instead, it generates an evanescent wave at the entrance of the aperture. Thus the size of ZMWs varies from 200-300nm in the Visible-IR spectrum to 40-50 nm in DUV. The characteristic evanescent decay constant, denoted as Λ, can be calculated using the well-established formulaLEVENE, J. KORLACH et al. 2003

$$\frac{1}{\Lambda} = 2\sqrt{\frac{1}{\lambda_c^2} - \frac{1}{\lambda_M^2}} \tag{2.1}$$

In this equation, λ_M refers to the wavelength of the incident light in the medium that fills the zero-mode waveguide (ZMW). ZMWs are also called Nanoaperture or Nanometer-scale apertureJonas KORLACH et TURNER 2013, due to their physical appearance and Zero-mode waveguide is a name suiting the optical property.
Traditional single-molecule optical spectroscopy is typically defined by observation volumes that are restrained by the diffraction limit of light, which is approximately 1 femtoliter (10^-15 litres). This constrains the maximum concentration level at which distinct fluorescent molecules can be identified within a range of picomolar to nanomolar. However, the majority of physiological processes, enzymatic reactions, and ligand interactions take place at elevated concentrations of at least one participating biomolecule.HOLZMEISTER, Guillermo P. ACUNA et al. 2014 Zero-mode waveguides (ZMWs) are unique nanostructures that significantly decrease the effective optical

observation volume beyond the diffraction limit, thus allowing the use of higher concentrations of molecules.Jonas KORLACH et TURNER 2013LEVENE, J. KORLACH et al. 2003

ZMWs are the important building block of this thesis and further work will be built by adding and exploiting features to ZMWs, thus I dedicate this chapter to understanding the ZMWs and how they are key to UV Auto-fluorescence spectroscopy and single molecule sensitivity in fluorescence spectroscopy in general. ZMWs have been used in a variety of applications, including single-molecule experiments. DE TORRES, GHENUCHE et al. 2015a P. ZHU et CRAIGHEAD 2012, photonic crystal waveguides H. MAO, Jiqing WANG et al. 2010, Förster Resonance Energy Transfer (FRET) measurementsSRINIVASAN, RICHARDS et al. 2012 BAIBAKOV, PATRA et al. 2019a, and quantum entanglement studies JIN, Lei SUN et al. 2013. One of the advantages of ZMWs is their ability to enable single-molecule experiments at high concentrations LEVENE, J. KORLACH et al. 2003. However, free diffusion out of the waveguide limits observations of untethered molecules to microseconds. ZMWs have also been used for fluorescence correlation spectroscopy at micromolar dye concentrations LIAO, GALAJDA et al. 2008

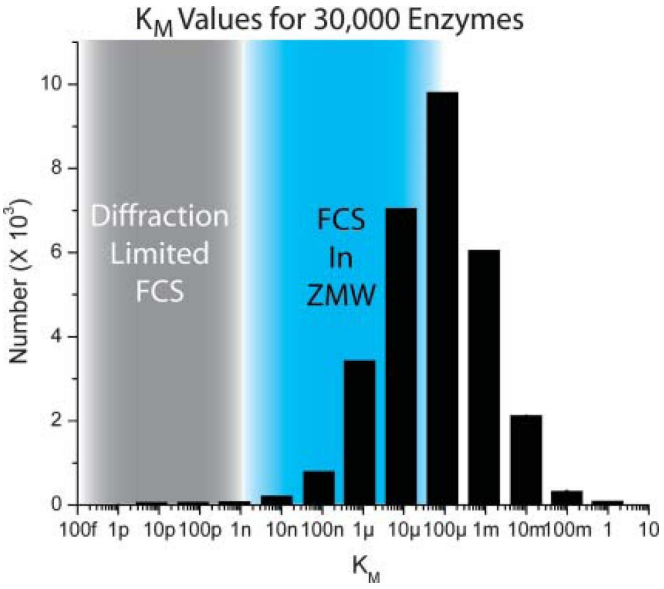

FIGURE 2.2 – Histogram of K_M values for 30,000 enzymes taken from the Brenda Database. The effective concentration ranges for diffraction-limited and zero-mode waveguide FCS are shown in grey and blue, respectively. Kinetics for the vast majority of enzymes are out of reach for diffraction-limited FCS. Reproduced fromK T SAMIEE, FOQUET et al. s. d.

The low mode volume has enabled Fluorescence correlation spectroscopy of biomolecules at very high concentrations ranging inμM compared to pM concentration in confocal. This helped in probing the kinetics of different enzymes which was previously not possible with confocal spectroscopy as shown in figure2.2

The ZMWs have been shown to be capable of providing a high degree of entanglement between the QDs and the single photons, with a fidelity of up to 0.99. Investigations into the use of plasmonic waveguides with near-zero mode indices for quantum entanglement have been conducted.JIN, Lei SUN et al. 2013. The sinusoidal phase variation of the propagating surface plasmon mode in the waveguide is a key factor in achieving this entangled state.
They have also been used to investigate adiabatic waveguide modes and the conditions under which single mode and zero birefringence operation are possible. As technology continues to advance, ZMWs are likely to play an increasingly important role in a wide range of scientific fields. In this chapter, we will explore ZMWs, with a brief literature review and then focus on how we implement these structures for UV Auto-fluorescence spectroscopy. We will discuss the variation of ZMWs we implemented'ROY, BADIE et al. 2021 and explore how ZMWs modify the emitter properties like radiative rate and saturation power curveAleksandr BARULIN, ROY, Jean-Benoît CLAUDE et al. 2021 etc.

2.2 Design and Fabrication of Zero-Mode Waveguides

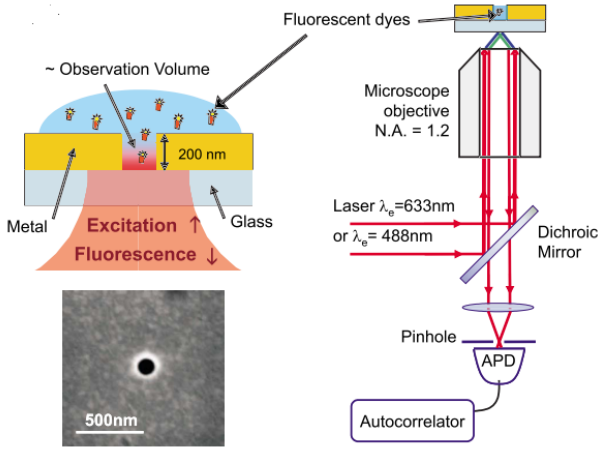

FIGURE 2.3 – Schematics of ZMWs used with Visible excitation for FCS experiments produced fromGÉRARD, Jérôme WENGER et al. 2008

Zero-Mode Waveguides are quite simple yet elegant structures. It is a single nanoaperture milled in opaque (for a given wavelength of light) metal films with sub-wavelength diameters. In some cases, we can use multiple layers using different metals to make ZMWsAL MASUD, W. E. MARTIN et al. 2020.They fabricated ZMWs composed of aluminium and gold individually and also in mixtures of three different ratios. The ZMWs are usually single nanostructures however in recent work researchers were

able to exploit new features by coupling different ZMWs. The material used for making ZMWs and its size depends on the excitation wavelength, for example for visible wavelengths, GoldM. WU, W. LIU et al. 2019 and Aluminium PUNJ, GHENUCHE et al. 2014aI. RICHARDS, LUONG et al. 2012 sometimes metals like palladium KLUGHAMMER et DEKKER 2021are used as an opaque material in which ZMWs-nano apertures are milled. Apart from metals in some cases, it is possible to use high-refractive-index dielectric materials like Si_3N LARKIN, Mathieu FOQUET et al. 2014which is well-known and commercially available. Si_3N nanoapertures arrays are used in multiple biophysical experiments DANELON, PEREZ et al. 2005. The size of ZMWs usually ranges from 100-200 nm in the case of visible wavelengths. Apart from the visible range of green and red, ZMWs have been used in NIR as well as UV regime. For NIR wavelengths ZMWs are mostly used for optical trapping and tweezer applicationsGORDON 2019.

2.2.1 Numerical Simulation of Zero-mode Waveguides

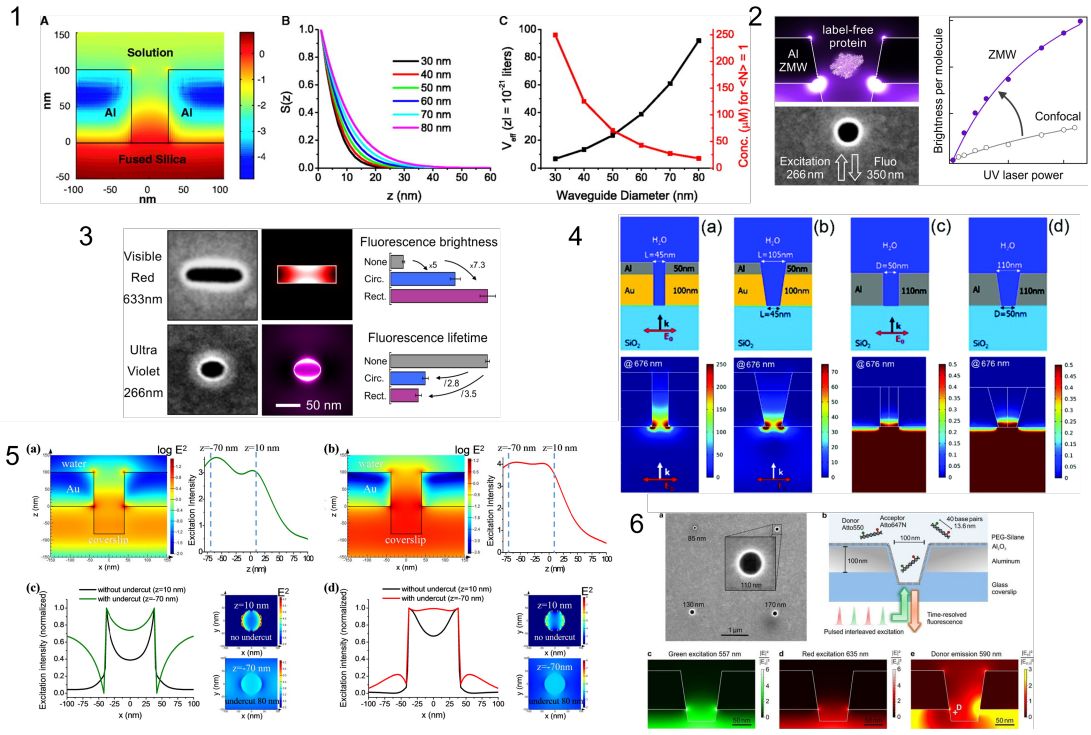

FIGURE 2.4 – The figure presents examples of different ZMWs and electric field intensity patterns inside them. Figures are reproduced from different work (1)LEVENE, J. KORLACH et al. 2003(2)Aleksandr BARULIN, Jean Benoît CLAUDE et al. 2019b(3)BAIBAKOV, Aleksandr BARULIN, ROY, Jean-Benoît CLAUDE et al. 2020(4)PONZELLINI, ZAMBRANA-PUYALTO et al. 2018(5)M. WU, W. LIU et al. 2019(6)BAIBAKOV, PATRA et al. 2019b. As we can see they all share a common trait irrespective of different material and excitation wavelengths i.e field confined at the bottom of the aperture.

Zero-mode Waveguides (ZMWs) or Nanoapertures(note : we will be using either of the names, interchangeably throughout the thesis) as the name suggest waveguides which do not allow any modes to pass through i.e due to the size of the aperture which is smaller than $\lambda/4$, the electric field attenuates inside the ZMW giving it ultra-small mode volume. From the different optical simulation performed in literature and in our studies there are two key feature we can see, first the field is concentrated at the bottom of hole and do not propagate and second in case of ZMWs made of metals we can see a surface plasmon at the metal-dielectric interface. ZMWs are made of different materials (Si_3N, Au or Al) with different excitation wavelengths or applications however the basic working principle remains the same and field distribution inside is qualitatively the same. In some particular cases to increase the number of molecules in the detection volume we increase the size of nanoapertures close to λ Aleksandr BARULIN, ROY, J.-B. B. CLAUDE et al. 2022 increasing size changes the field pattern inside the ZMWs as shown in figure2.5. However, for diameters greater than 100 nm, the nano-aperture enables light propagation, resulting in an increase in signal enhancement at around 200 nm, which corresponds to the first fundamental waveguide mode of the nano-aperture. Thus based on the application we can choose what size of nanohole we want. For example, if we want to functionalize the nanoholes and want to see single-molecule events using bigger nanoholes is more appropriate because the larger area it will give more binding sites on the other hand if we want to do titration or study single-molecule activity at a higher concentration it will be better to use 65 nm holes which provide higher enhancement and smaller detection volume.

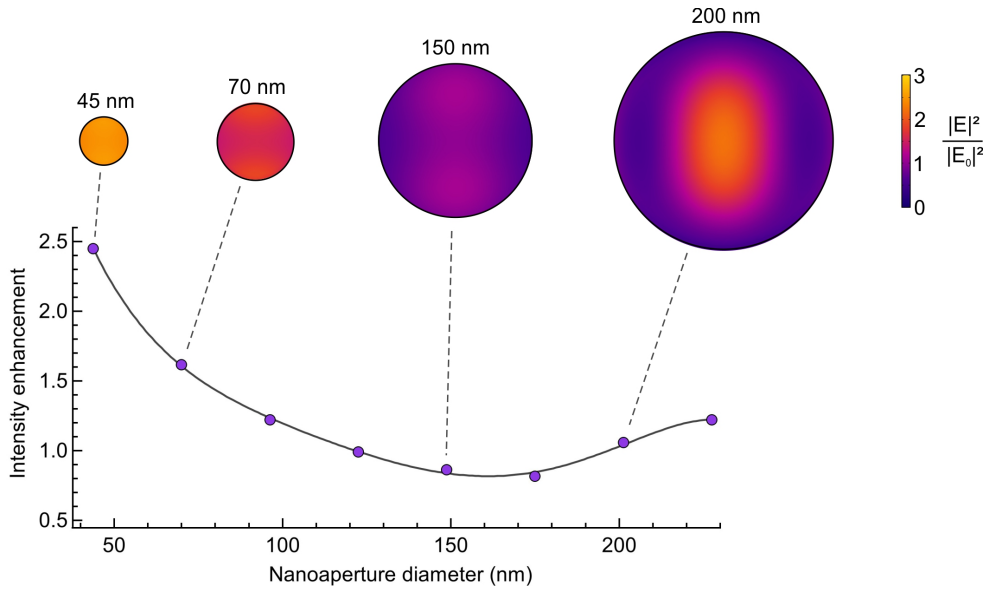

FIGURE 2.5 – Numerical simulation of different sizes of Nanoholes for plane wave UV excitation at λ=295 nm. The colour map shows the intensity of light inside the holes 10 nm above the interface of hole-substrate

2.2.2 Fabrication of Zero-Mode Waveguide

There are multiple ways of fabricating ZMWs, however, there are three techniques most used in literature, namely Focused Ion Beam MillingRIGNEAULT, CAPOULADE et al. 2005,Jérôme WENGER, GÉRARD et al. 2008Mathieu FOQUET, Kevan T. SAMIEE et al. 2008, Colloidal Lithography and Electron beam lithography. Every method of fabrication possesses its own strengths and weaknesses, as elucidated by GU, W. ZHANG et al. 2018.

FIB-based ZMWs fabrication : The fabrication step is simple and it requires the deposition of metal on a silica or glass substrate and then the Focused Ion Beam (FIB) technique which uses accelerated ions to carve out ZMWs in metal thin-films which are a few 100 nm thick. The FIB employed for milling exhibits remarkably high lateral resolution in contrast to optical lithography approaches (which rely on either light or colloids), thereby enabling superior control over the structuresNÜESCH, IVANOVIĆ et al. 2022KLUGHAMMER et DEKKER 2021. Furthermore, the fabrication process is instantaneous, obviating the need for curing or removing excess materialPREISS, MERLE et al. 2021. Nevertheless, observed that the ions emitted by the FIB like Gallium might taint the surface, although no mention of this concern has been encountered in other literature for the visible regimes for UV Gallium implants from FIB has been a major source of unwanted backgroundROY, Jean-Benoît CLAUDE et al. 2023. Apart from Gallium based, the Gold ionMESSINA, SRIJANTO et al. 2022 or Helium ion-basedC. ZHANG, J. LI et al. 2020 ZMWs fabrication is also used.

Colloidal Lithography : In scenarios where multiple waveguides are required simultaneously, Colloidal Lithography (CL) emerges as an intriguing technique, as it allows for the simultaneous creation of numerous waveguides.

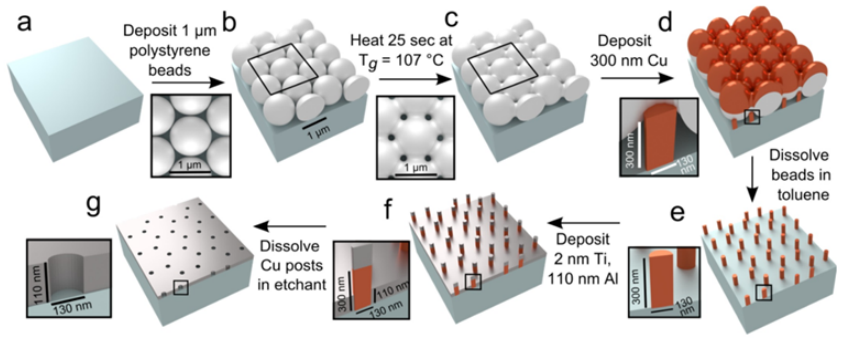

FIGURE 2.6 – Schematic of aluminium ZMW fabrication. The starting material is a glass microscope coverslip. Steps in fabrication and listed and explained in the main text. Black boxes represent expanded insets. Tg is the glass transition temperature of the polystyrene microspheres. Reproduced from JAMIOLKOWSKI, K. Y. CHEN et al. 2019

However, the overall procedure is more intricate and time-consuming. For instance, the CL process necessitates the utilization of multilayer precursors with rinsing and drying between the application of each layer, incorporation of the colloids (polystyrene balls in this case), and a final step to prevent colloidal aggregation before

curing. This procedure merely results in the template, with the actual deposition of metal and subsequent removal of the balls requiring a distinct process altogether. Nonetheless, upon completion, a collection of uniformly sized holes can be anticipated. The size of these holes is determined by the dimensions of the colloids, which serves as a limiting factor in this technique. Moreover, the spacing between the holes tends to be somewhat random. In contrast, the FIB enables precise control over both the size and spacing of the holes. **Electron Beam Lithography (EBL)** Electron beam lithography (EBL) is a powerful nanofabrication technique used for creating structures with dimensions on the order of nanometers S. GANGNAIK, M. GEORGIEV et al. 2017. It involves using a focused beam of electrons to selectively expose a resist material, resulting in the desired patternALTISSIMO 2010. EBL offers high resolution and precise control over the pattern shape and size, making it a preferred choice for fabricating nano-electronic devices and other applications requiring critical dimensions below 10 to 20 nmS. GANGNAIK, M. GEORGIEV et al. 2017. The EBL technique provides ways to fabricate ZMWs in large arrays suited for optical devices or microfluidic chipsW. E. MARTIN, GE et al. 2017. It is to note that ZMWs made by EBL might performed worse than the ZMWs made by FIB due to leftover resists or metal films however this is never been properly benchmarked.

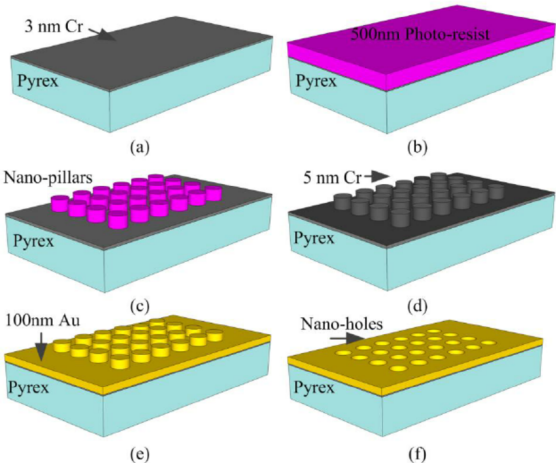

FIGURE 2.7 – Electron beam lithography (EBL) for fabrication of Gold nano-hole arrays reproduced from NAJIMINAINI, VASEFI et al. 2011

Apart from the technique mentioned above DUV-EUV lithography technique can be used for commercial grade and scale development of ZMWs. The DUV-EUV lithography could compensate demerits of discussed fabrication method.Mathieu FOQUET, Kevan T. SAMIEE et al. 2008

Technique	Pros	Cons
Optical Lithography	Cost-effective, high-throughput, scalability	Limited by diffraction limit, larger feature size
Electron Beam Lithography	High resolution, precise control	Time-consuming, expensive
Nanoimprint Lithography	High resolution, potential low-cost	Challenges in mold fabrication, template lifetime
Focused Ion Beam Milling	High lateral resolution, precise control, instant fabrication	Potential surface contamination
Colloidal Lithography	Simultaneous creation of multiple waveguides	Complicated and time-consuming process

FIGURE 2.8 – Pros and Cons of different fabrication techniques used to make ZMWs

.

Due to the meticulous control and flexibility needed for optimizing experimental waveguide sizes, FIB milling was chosen as the fabrication technique for this ZMW performance study.

2.3 Variations of ZMWs

Since its invention a few decades ago, ZMWs have been subjected to many modifications as per the demands of particular applications which ranged from FCS, to FRET In figure 2.9 we can see a few prominent modifications implemented on ZMWs targeting specific applications including a resonant antenna in ZMWs to enhance the signal, the varying shape of ZMWs to incorporate nanopores to do protein sequencing and lastly, modification to take make them stable and biocompatible for UV Autofluorescence spectroscopy. Since it is pertinent to this thesis we discuss in detail Antenna-in-box and oxide protect ZMWs. BAIBAKOV, Aleksandr BARULIN, ROY, Jean-Benoît CLAUDE et al. 2020 has developed rectangular nanoaperture ZMWs which provide better performance than circular ZMWs. The gold rectangular nanoaperture, due to its material and shape, has polarization-dependent properties that are distinct from those of circular waveguides. This can be used to advantage for chiral sensing within Zero-Mode Waveguides (ZMWs).CUI, X. YANG et al. s. d.

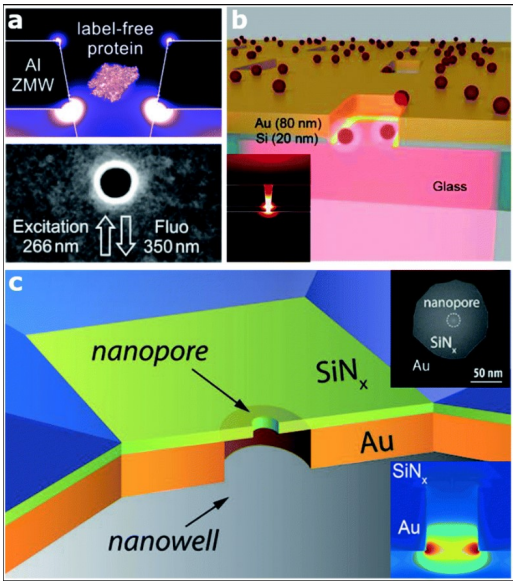

FIGURE 2.9 – Various architectures of the zero-mode waveguide (ZMW) plasmonic nanoapertures. (a) Deep ultraviolet plasmonic enhancement of single protein autofluorescence in an Al ZMW. This figure has been reproduced fromAleksandr BARULIN, Jean Benoît CLAUDE et al. 2019a. (b) A hybrid Au–Si zero mode waveguide for enhanced single molecule detection. This figure has been reproduced from ASSAD, GILBOA et al. 2017 . (c) Enhanced single molecule fluorescence detection with a plasmonic nanowell–nanopore device architecture made of a nano-well fabricated in a gold film (orange) with a nanopore drilled in a freestanding Si3N4 membrane (light green). This figure has been reproduced from ZAMBRANA-PUYALTO, PONZELLINI et al. 2019

.

2.3.1 Antenna in-box

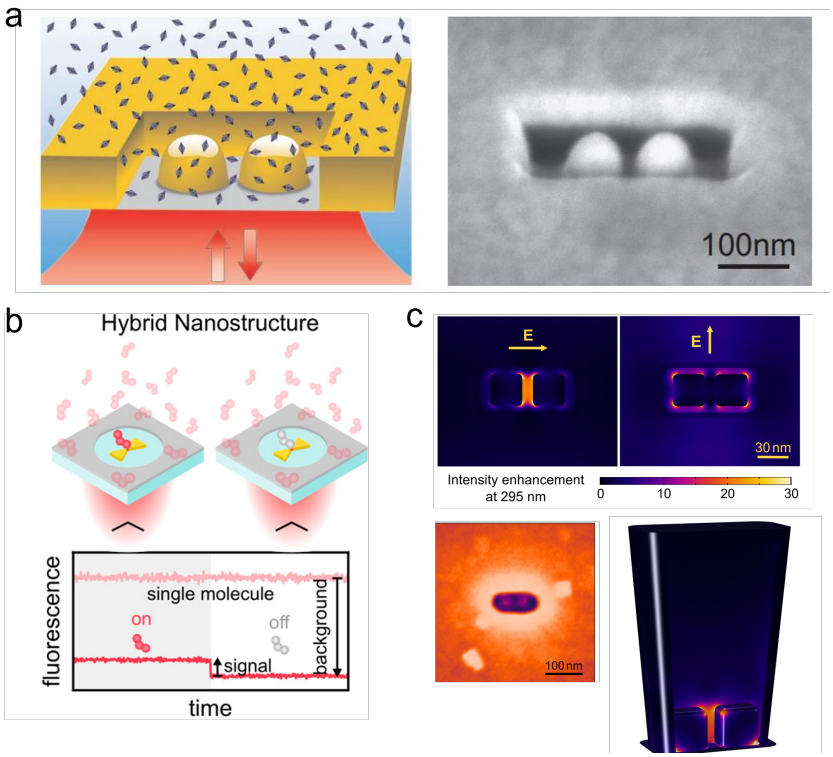

FIGURE 2.10 – Different Antenna-in-box configuration (a) using Gold dimer antenna in the box reproduced fromPUNJ, MIVELLE, MOPARTHI et al. 2013a (b) A hybrid antenna with ZMWs and bowtie optical antenna KAAN HERKERT, ROMINA BERMEO ALVARO et al. 2023 (c) Rhodium cube dimer in Al ZMWs, this structure will be discussed in a subsequent chapter

.

The 'antenna-in-box' (AiB) concept, a relatively novel notion within the realm of optical biosensing, has made significant strides over the past few years. Central to this idea is the use of resonant plasmonic nanostructures embedded in zero-mode waveguides that combine the enhancement of the fluorescent signal of the plasmonic nanostructure and the background screening of ZMWs, providing fluorescence enhancement up to 1,100-fold and microsecond transit times at micromolar sample concentrationsPUNJ, MIVELLE, MOPARTHI et al. 2013a. The resonant plasmonic nanostructures aid in the confinement of light down to nanoscale volumes, thus overcoming limitations of traditional diffraction-limited optics that restrict detection volumes to the femtolitre range. These, increased confinement has been found to enhance fluorescence brightness and offer high single-molecule sensitivity at micromolar sample concentrations, thereby optimizing single-molecule fluorescence studies at physiologically relevant concentrations. The Zero-mode Waveguide not only provide screening but also couples with the dimer antenna electrically as well as

magnetically thus affecting the response of the dimer antenna. As a recent example, the AiB device involves placing gold nanoantennas in a gold aperture, which results in high single-molecule detection sensitivity at high fluorophore concentrations KAAN HERKERT, ROMINA BERMEO ALVARO et al. 2023. The AiB platform can be optimized for single-molecule fluorescence studies at physiologically relevant concentrations, and it has been used to study various biomolecules PUNJ, MIVELLE, MOPARTHI et al. 2013a. One of the main features of the AiB device is the ability to create a high electric field in its gap region G. A. HASSAN et J. u. HASSAN 2019. The sensitivity of the device to the index changes of the environment and substrate has also been investigated in detail FISCHER et O. J. F. MARTIN 2008. The device has been used in biosensing applications with a broad description using different types of data KAUSAR, REZA et al. 2015. The use of AiB devices for the detection of non-fluorescent biomolecules has also been reported Yang CHEN, Yuhang CHEN et al. 2017. The device's ability to produce an electromagnetic hot spot has led to its application in surface-enhanced spectroscopy as well as nonlinear optics Yang CHEN, Yuhang CHEN et al. 2017. Despite the promising results from the use of AiB devices in biosensing, there are some challenges that need to be addressed. One of the main concerns is the toxic effects of nanoparticles(like Ag when used as Antenna material) on biomolecules or in some cases the stability of nanoparticles in aqueous solution and under laser excitation. For example, Al nanoparticles are used for UV resonance antenna but in aqueous solution with salt or Acidic pH are Al AiBs are not stable. Thus material used for antenna in box could be one of the limitations.

2.3.2 Oxide protected ZMWs

In the above-mentioned modifications of ZMWs, there was something common i.e. the excitation wavelength was either visible or longer wavelengths. However when subjected to UV light the metal used for making ZMWs : Aluminium corrodes and it's fast, in just a few seconds the Al thin film around ZMWs can just disappear(2.11), rendering ZMWs inoperative. We have discussed Al corrosion in detail in the previous chapter, where we saw Al react with radicals generated in media with UV exposure. To protect this researchers have covered ZMWs will polymer to provide insulation Aleksandr BARULIN, Jean-Benoît CLAUDE et al. 2019b however these polymers didn't protect the ZMWs at pH-7 so in this work, we will implement oxide-protected ZMWs. We will discuss in detail this in the next section dedicated to photocorrosion.

2.4 Photocorrosion of Zero-mode Waveguides in UV

When working in the UV range, the choice of metals for plasmonics needs to be reconsidered. Traditional metals like gold and silver suffer from interband transitions and significant losses below 400 nm. Hence, aluminium is currently the preferred material for UV plasmonics. It has relatively low losses, is cost-effective, and is compatible

with CMOS technology. Aluminum's plasmonic optical response is also advantageous as it covers a wide spectral range from deep UV to infrared, allowing for multicolour applications in spectroscopy, fluorescence sensing, light harvesting, and optical colour filters.

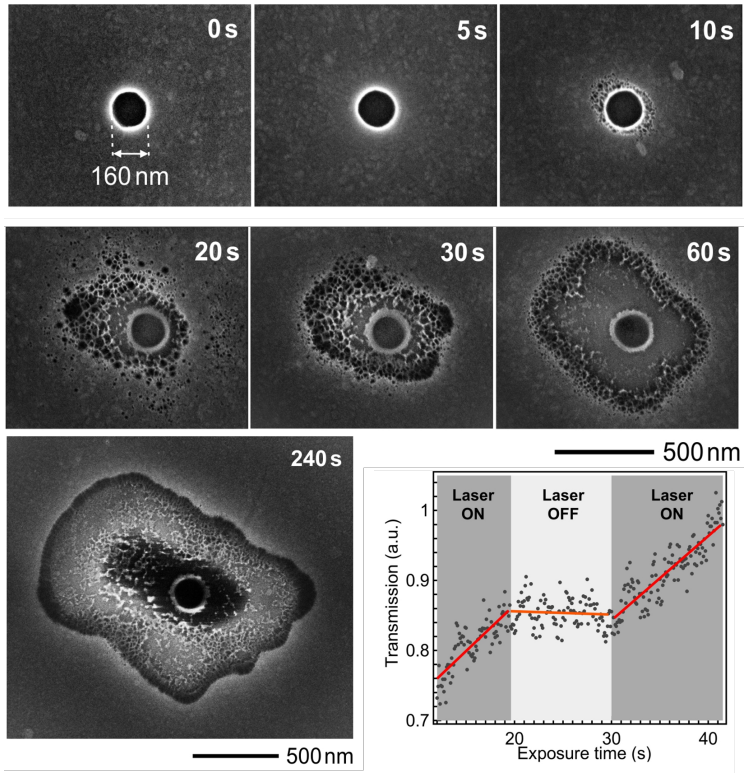

FIGURE 2.11 – Evolution of ZMWs under UV exposure and aqueous media. Aleksandr BARULIN, Jean-Benoît CLAUDE et al. 2019a

However, aluminium has a significant drawback related to its limited stability in the presence of water. Bulk aluminium is highly reactive and dissolves rapidly upon contact with water. Although the naturally occurring alumina layer on the surface provides partial protection against water corrosion, it tends to develop cracks at the junctions between metal grains, leading to pitting corrosion. As a result, the long-term durability of aluminium-based devices is limited by corrosion, particularly at the nanoscale where the large surface area amplifies the effect. The situation worsens in UV plasmonics due to the accelerated corrosion process induced by UV light. UV illumination has two main effects : first, it promotes the growth of aluminium oxide while increasing the porosity and presence of cracks where pitting corrosion can occur; second, it triggers the formation of radicals in water, further accelerating the dissolution of alumina and aluminium. To evaluate photocorrosion resistance, we define the damage threshold power (P_{th}) as the maximum laser power that maintains stable transmission for at least 90 seconds. Powers exceeding P_{th} result in aperture corrosion within less than 90 seconds, leading to a rapid increase in the transmission signal. We employ this benchmark to assess the impact of oxide materials deposited

via ALD and PECVD on the top of Al layer, as well as other experimental parameters. Several approaches have been investigated to protect aluminium against corrosion, such as passivating the surface with polyvinyl phosphonic acid and polydopamine layers. However, using organic molecules for UV plasmonics is limited due to direct photodamage caused by UV light and the generation of reactive radicals. Alternatively, atomic layer deposition (ALD) and plasma-enhanced chemical vapour deposition (PECVD) of thin inert metal oxide layers offer effective strategies for corrosion protection. These methods allow for the deposition of dense oxide layers with controlled nanometer thickness and conformal coating at the nanoscale. Commonly used oxide materials for corrosion protection include alumina (Al2O3), titania (TiO2), and hafnia (HfO2), which have been extensively tested for flat metal surfaces. However, their performance in the specific context of UV plasmonics, considering UV irradiation and the presence of photogenerated radical species, has not been investigated yet while also considering the constraints of nanoscale features required for plasmonic nanodevices. In this section we will discuss the technique, we implemented in our work to make Al ZMWs stable against photo-corrosion induced by radicals generated by UV, aqueous media and salt. The developed technique will be used throughout the work to make ZMWs more robust and bio-compatible.

2.4.1 Effect of different Metal-Oxide coating on Photocorrosion of Al

We evaluate the corrosion resistance of a single nanoaperture (65 nm diameter) in a 100 nm thick aluminium layer, representing a generic platform for UV aluminium plasmonics. The nanoaperture is filled with a water solution (with 100mM NaCl) and subjected to an increasing power-focused UV laser spot. Simultaneously, we monitor the transmission through the nanoaperture, which is highly sensitive to aperture diameter changes, allowing real-time in situ monitoring of photocorrosion evolution.

In the absence of an additional protective layer, the nanoaperture corrodes rapidly, even at a low UV power of 10 μW, within a few tens of seconds. The aluminium surrounding the aperture dissolves, resulting in the formation of a porous region at the boundary of the intact aluminium film. However, when a 5 nm Al2O3 layer followed by a 5 nm TiO2 capping layer is deposited using ALD, the nanoaperture withstands a laser fluence 10 times higher for an extended duration. This highlights the importance of appropriate photocorrosion protection through nanometer-thick metal oxide films on the aluminium nanostructure. Additionally, our observations indicate the absence of direct laser-induced photodamage, with the photodamage threshold estimated to occur at an average power of 150 μW for our pulsed laser at 266 nm.

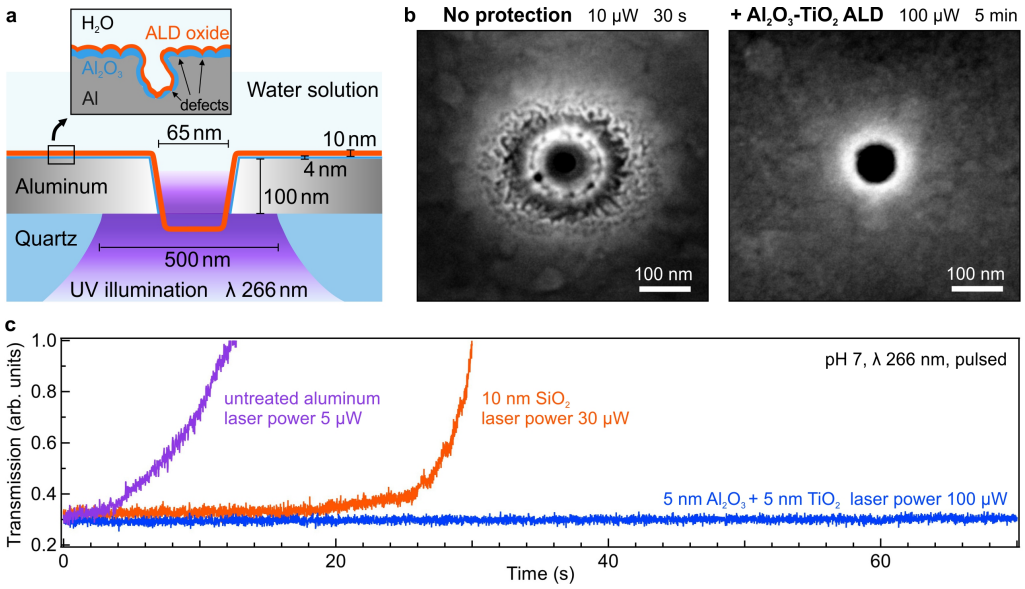

FIGURE 2.12 – (a) The single aperture of 65 nm diameter milled in a 100 nm thick aluminium film. The aperture is illuminated by a focused ultraviolet laser beam, and a water solution fills the aperture and the upper medium. The natural aluminium oxide (alumina) layer covers the aluminium bulk, but this layer is not fully dense or homogeneous on the surface, leaving defect sites for aluminium corrosion. The nanometer-thick extra oxide layer efficiently protects the aluminium surface. (b) Example of scanning electron microscopy images of a single aperture without and with a protective ALD layer (here 5 nm of Al2O3 followed by 5 nm of TiO2 as capping). In the absence of protection, corrosion is clearly visible around the central aperture. (c) Transmitted intensity time trace for different nanoaperture samples and UV laser power. The stability of the time trace indicates corrosion resistance.

All aluminium nanoapertures undergo the same treatment and possess a typical 3-4 nm natural aluminium oxide layer. For a fair comparison, we maintain a constant 10 nm thickness across all experiments, as thicknesses above 15 nm compromise plasmonic applications' nanoscale features and proximity to the metal film. A 5 nm thickness provides insufficient photocorrosion protection, necessitating the selection of a 10 nm thickness as a trade-off between corrosion protection and plasmonic performance. The presence of a 10 nm protective layer has minimal impact on plasmonic performance, reducing the fluorescence enhancement factor by less than 10% compared to an unprotected aluminium nanoaperture.

While all additional layers exhibit improved photocorrosion resistance compared to raw aluminium, there are notable distinctions among the materials. Among the tested oxides (Al2O3, TiO2, HfO2, and SiO2), the 10 nm Al2O3 layer offers the least improvement due to cracks, porosity, and limited resistance to water dissolution. SiO2, TiO2, and HfO2 provide better protection with higher threshold powers. The combination of a 5 nm Al2O3 layer followed by a 5 nm TiO2 capping layer yields the best overall protection, limited only by direct laser damage to the aluminium struc-

ture at 150 µW. The preference for Al2O3 with a TiO2 capping aligns with previous findings indicating their effectiveness in protecting copper against water corrosion. Surprisingly, the combination of a 5 nm Al2O3 layer with a 5 nm HfO2 layer does not significantly enhance corrosion resistance, despite the individual performance of the 10 nm HfO2 layer. This could be attributed to the limited 5 nm thickness and residual porosity of the HfO2 layer, which may not fully protect against pitting corrosion in the Al2O3 layer cracks.

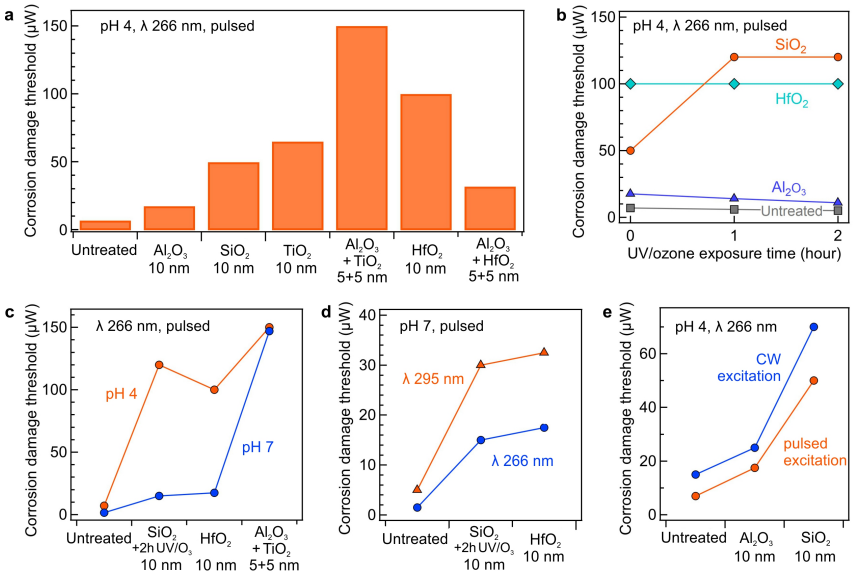

FIGURE 2.13 – Corrosion protection strategies and influence of experimental parameters. Throughout this figure, the upper line indicates the pH, laser wavelength and laser operation mode (pulsed or continuous). (a) Threshold power leading to corrosion in 90 s as a function of different oxides deposited on top of the aluminium surface. Al2O3, TiO2 and HfO2 were deposited by ALD while SiO2 was deposited by PECVD. (b) Influence of supplementary UV/ozone exposure on different samples.It shows UV exposure consolidates Silica layer (c) Influence of the solution pH, a more acidic pH enables better corrosion protection. The Al2O3+TiO2 case is limited by the available laser power here and the occurrence of direct laser-induced damage. (d) Influence of the laser wavelength. (e) Influence of the illumination mode : pulsed or continuous (CW).

In fig2.13 b we see that UV exposure consolidates Silica layer, it is due to intreaction of dangling silica bonds on the film of silica and ozone generated in UV-Ozone chamber. This effect was not seen in any other oxides. We also observe that corrosion resistance is slightly better for CW laser than for pulse excitation. This is likely due to the reduced generation of radical species, which are responsible for corrosion. We believe that two-photon processes are partly responsible for the generation of reactive species when UV light is shone on a water-salt solution. Since it is known that pulse excitation tends to facilitate two-photon absorption, it can be inferred that pulse exci-

tation leads to more corrosion than CW laser. We utilize the photo corrosion strategy illustrated in Figure 2.13 to enhance the detection of label-free streptavidin proteins, as shown in Figure 2.14. We employ single aluminium nanoapertures in conjunction with a UV confocal optical microscope for their detection. However, without an additional protective layer, the UV photo corrosion of aluminium imposes a severe limitation on the maximum usable power, restricting it to only a few microwatts. To avoid damaging the nanoaperture, we set the maximum power to 5 µW with a 295 nm laser (Figure 2.13d). Under these conditions, fluorescence correlation spectroscopy (FCS) can still be recorded, but the resulting curve is highly noisy, rendering it unreliable to extract FCS parameters such as protein count, brightness, or diffusion time (Figure 2.14b,c). At higher powers, when no protective measures are implemented, the nanoaperture rapidly deteriorates, as depicted in Figure 2.12c, rendering the experiment infeasible.

By introducing a 10 nm SiO2 layer with UV/ozone treatment, the corrosion resistance of the aluminium sample is significantly improved. Consequently, the laser power can be increased to 20 µW without observing any photo corrosion (Figure 2.14a). This higher excitation power leads to increased fluorescence brightness, thereby directly enhancing the quality of the FCS data and reducing noise levels (Figure 2.14b,c). These findings demonstrate that the corrosion protection strategies derived from Figure 2.13 enable the detection of label-free proteins using aluminium plasmonic nanostructures in the UV range. Given the necessity of aluminium for UV plasmonics and the ubiquity of water in biochemistry and molecular biology applications, corrosion protection will be essential for numerous other applications as well.

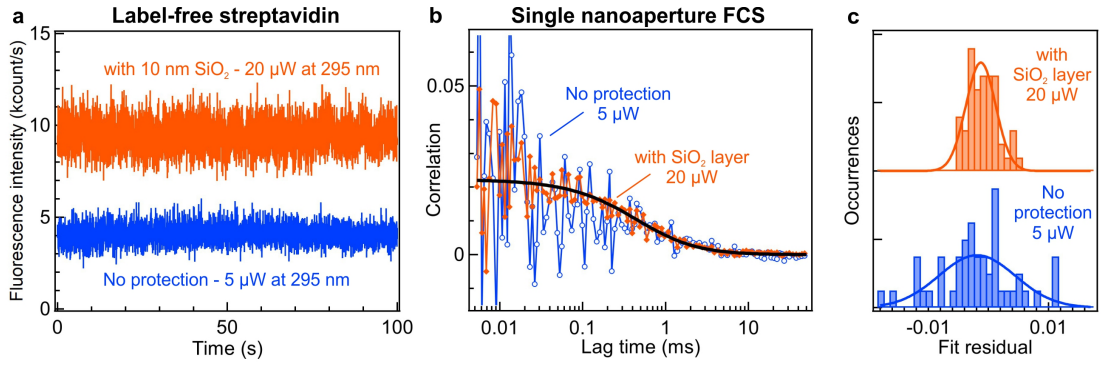

FIGURE 2.14 – Application of the corrosion protection of single aluminium nanoapertures for the ultraviolet autofluorescence detection of label-free streptavidin proteins. (a) Ultraviolet (310-410 nm) autofluorescence time traces for a single 65 nm diameter aperture filled with a 10 µM solution of streptavidin at pH 7. The fluorescence stems from the 24 tryptophan amino acid residues present in each streptavidin tetramer. (b) Temporal correlation of the time traces in (a), the thick black line is a numerical fit. Thanks to the higher 20 µW excitation power enabled by the extra SiO2 protection layer, the noise is significantly reduced. Fitting the FCS data yields Nmol = 26 ± 2 at 5 µW and Nmol = 25 ± 1 at 20 µW. The diffusion times are respectively 630 ± 100 µs at 5 µW and 670 ± 50 µs at 20 µW. The diffusion values are relative to confocal. (c) Histogram of the fit residuals in (b) for the two excitation powers, the curves are vertically offset for clarity.

The protective strategies implemented through ALD for UV plasmonics can also be beneficial for safeguarding aluminium structures in the presence of corrosive buffer solutions. In biophysical studies involving protein unfolding, guanidinium chloride (GdmCl) is commonly used as a denaturant at high molar concentrations. However, due to its high chloride ion content, GdmCl is highly corrosive to aluminium. In this study, we examine the effectiveness of various ALD layers in shielding the aluminium surface against long-term corrosion caused by GdmCl.

To evaluate the corrosion protection capabilities, we immerse the samples in a de-ionized water solution containing 6 M of GdmCl and 500 mM of NaCl at pH 7. These concentrations represent the upper range typically used for protein and peptide denaturation. In the absence of any corrosion protection, the aluminium film begins to corrode within a few hours and sustains significant damage after 5 days of immersion (Fig.2.15). However, by employing combined layers of 5 nm Al2O3 + 5 nm TiO2 or 5 nm Al2O3 + 5 nm HfO2, the corrosion resistance is notably improved, allowing for up to 3 weeks of immersion in the GdmCl solution. Furthermore, these combined layers exhibit significantly fewer defects compared to the layer containing only SiO2. These results highlight another advantage of ALD in protecting the aluminium from corrosion and facilitating biophysical studies in demanding environments with high chloride concentrations in the range of several moles.

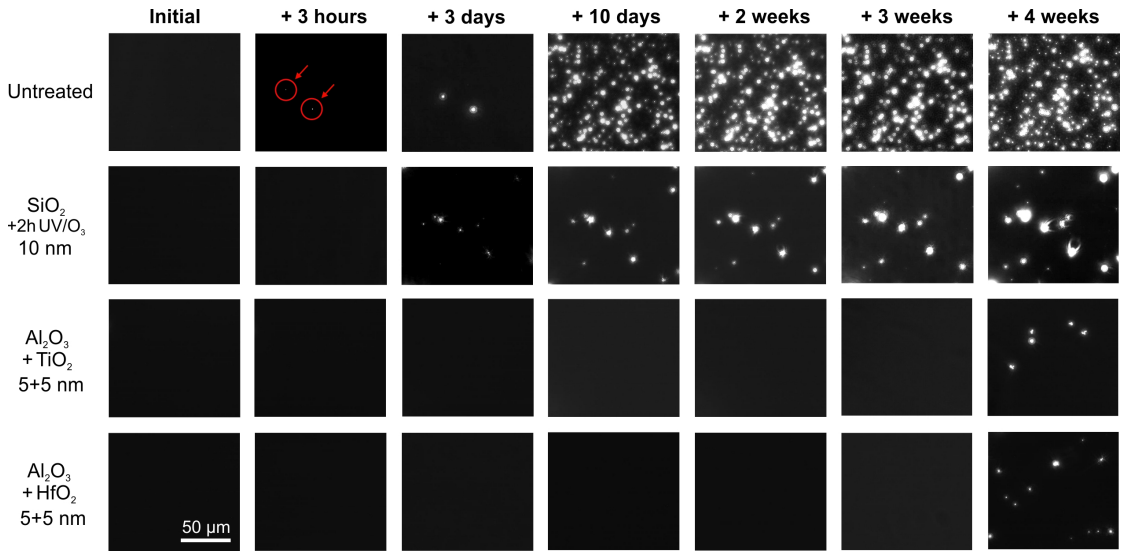

FIGURE 2.15 – Transmission of optical microscope images of the aluminium film during several days of immersion into a water solution containing 6 M of guanidinium chloride (GdmCl) and 500 mM of sodium chloride (NaCl) at pH 7. Fiducials located outside the camera field of view were used to image the same zone throughout the experiments

2.5 Enhancing UV signal with Zero-mode waveguide

In this section, we will discuss instances from literature where a Zero-mode waveguide is used for sensing UV-excited fluorescence from proteins and dyes.

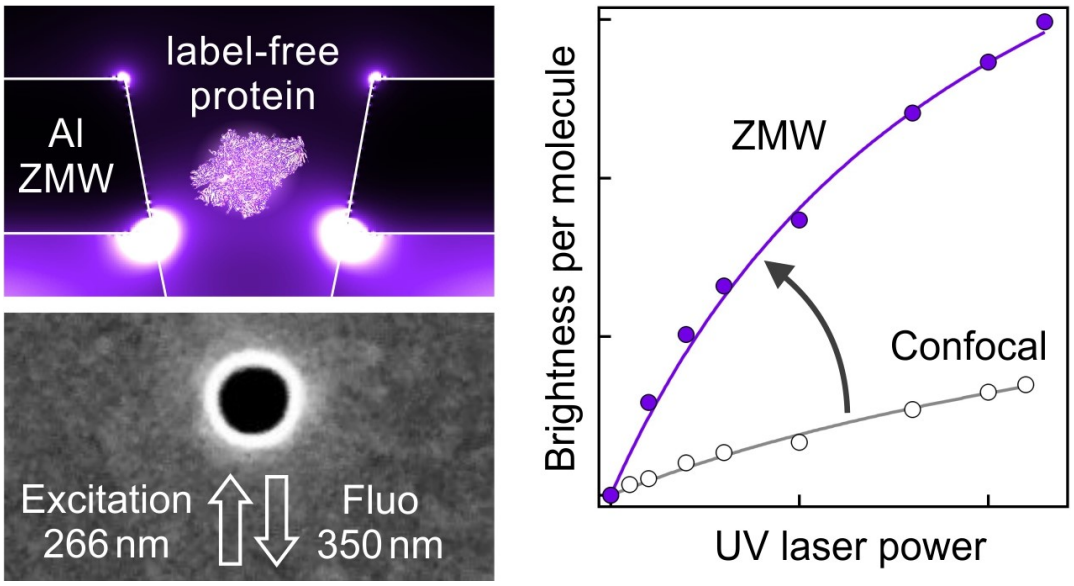

FIGURE 2.16 – Zero Mode Waveguides in Deep UV using Aluminium at 266 nm Excitation to enhance the signal from tryptophan-carrying proteins. Reproduced from Aleksandr BARULIN, Jean Benoît CLAUDE et al. 2019a

2.5.1 High Quantum yield dyes

To characterize the performance of ZMWs p-terphenyl which is photostable and has a high quantum yield. The performance of ZMWs is studied as shown in figure2.17 Aleksandr BARULIN, Jean Benoît CLAUDE et al. 2019a J.-Y. LEE, CHENG et al. 2021 and Xiaojin JIAO, Eric M. PETERSON et al. 2014 In fig2.17 authors studied different diameters of ZMWs and showed that due to increasing the diameter total signal increases (a), which is due to an increase in the number of molecules inside the ZMWs (d). The diffusion time also changes with the diameter of the Nanholes and varies linearly with diameter. The lifetime reduction shown by the nanoaperture infers that LDOS is modified inside the antenna which changes the decay rate constants. In fig2.17 g we see that fluorescence enhancement peaks at values close to cut-off wavelength. Small diameters do not permit light to pass through and interact with the analytes, and larger wavelengths lead to a decrease in the plasmonic response as the lifetime reduction and excitation gain (h) decrease with increasing diameter (f).

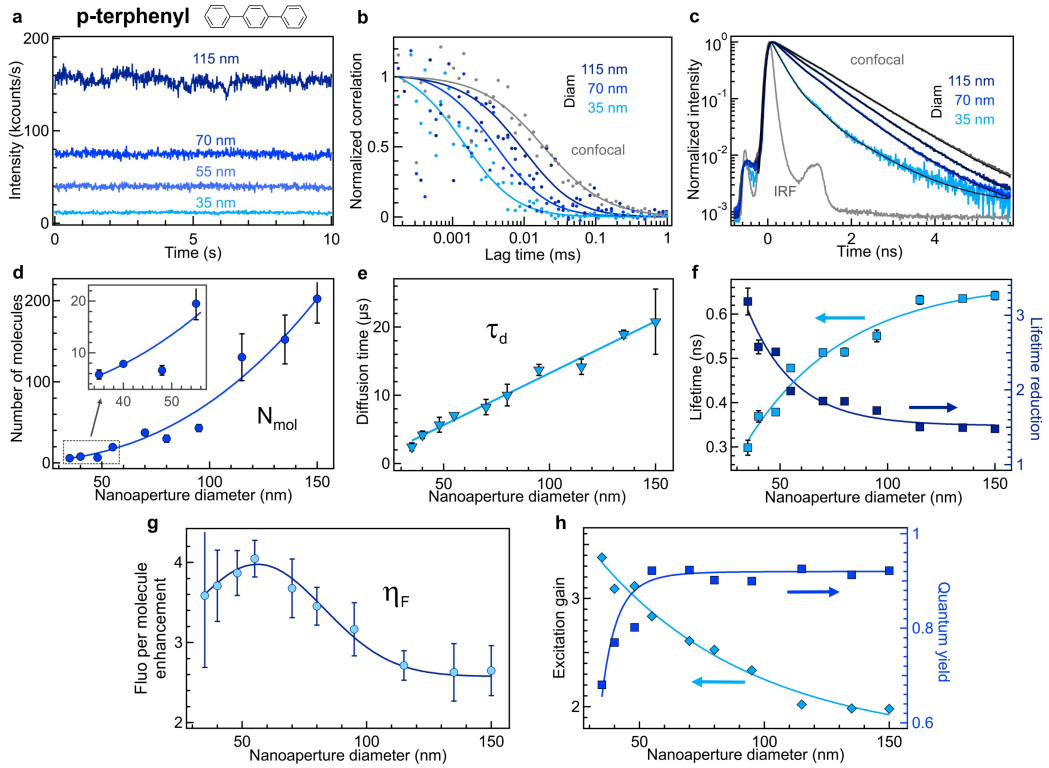

FIGURE 2.17 – Characterization of aluminium ZMWs performance in the UV. (a) p-terphenyl fluorescence intensity time traces were recorded on ZMWs with different diameters. The p-terphenyl concentration is constant at 10 µM for all the experiments shown here. (b) Normalized FCS correlation functions show a reduction of the diffusion time as the ZMW diameter is decreased. (c) Normalized fluorescence lifetime decay traces for the confocal reference and ZMWs of decreasing diameters. The black lines are numerical fits, and IRF indicates the instrument response function. (d) A number of p-terphenyl molecules in the ZMW detection volume and (e) average diffusion time deduced from the FCS fits as a function of the ZMW diameter. (f) p-terphenyl fluorescence lifetime measured from the decay in (c) and corresponding lifetime reduction as compared to the confocal reference. (g) Fluorescence brightness per molecule enhancement as a function of the ZMW diameter. (h) Quantum yield and excitation gain in ZMWs were deduced from the lifetime reduction in (f) and the fluorescence enhancement in (g) with respect to the diameter. Throughout (d-h) the lines are guided to the eyes.Aleksandr BARULIN, Jean Benoît CLAUDE et al. 2019a

Similar features of ZMWs arrays made in Al film were shown by Xiaojin JIAO, Eric M. PETERSON et al. 2014 where Al ZMWs show lifetime reduction for p-Terphenyl. The fig 2.18 shows linear dependences of lifetime reduction however in fig 2.17 f we see the decaying curve, this difference is due to the lower range of diameter studied in fig 2.18 in comparison to study in the figure above.

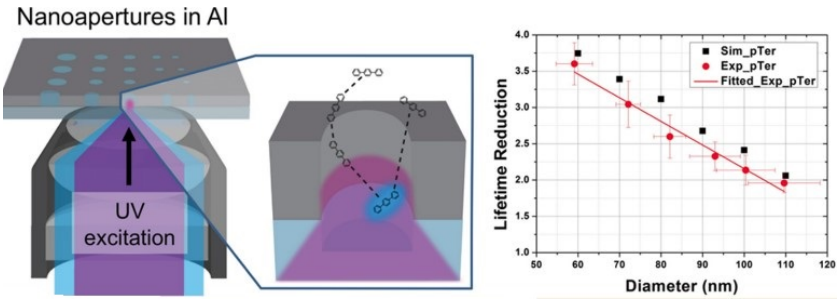

FIGURE 2.18 – Modification of lifetime of p-Terphenyl inside ZMWs. Reproduced fromXiaojin JIAO, Eric M. PETERSON et al. 2014

2.5.2 Proteins with Tryptophan

In literature, some tryptophan-carrying proteins were explored, like β-galactosidase Aleksandr BARULIN, Jean Benoît CLAUDE et al. 2019a , streptavidinAleksandr BARULIN, ROY, Jean-Benoît CLAUDE et al. 2021. It is worth noting that β-galactosidase is quite a large protein with 156 Trp residues, however, the detected intensity per protein is almost an order less than expected, owing to internal quenching and screening of Trp residues. Thus ZMWs played a major role in detection with single molecule sensitivity by screening the background as shown in figure2.19(a,b,c). It is further possible to detect smaller proteins like streptavidin with 24 Trp residues using ZMWs see fig2.19(d,e,f) however signal per molecule is less, in subsequent chapters we will see how we can modify the ZMWs platform to detect the smaller proteins down to single emitter -single molecule levelROY, Jean-Benoît CLAUDE et al. 2023
In the figure below authors were able to study label-free proteins and do FCS at μM with single-molecule resolution for bigger proteins like β-galactosidase. However, reaching single molecule sensitivity is not possible for proteins smaller and dimmer like streptavidin.

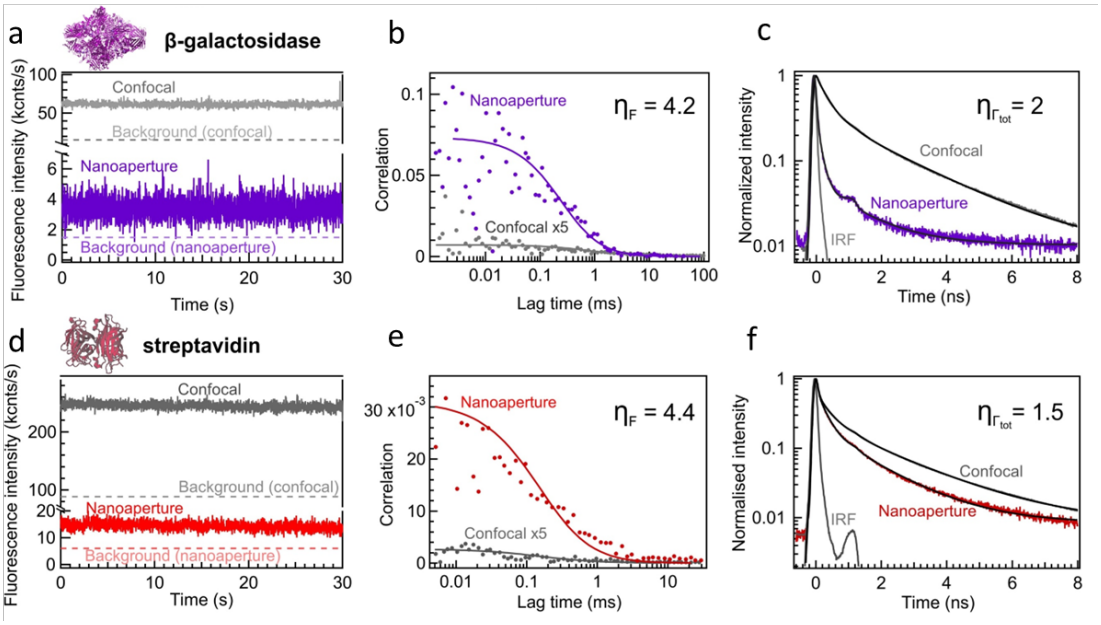

FIGURE 2.19 – Experimental characterization of intrinsic protein fluorescence and total decay rate in the Al ZMW of 65 nm diameter. (a) Fluorescence intensity time traces with background level values, (b) FCS correlation functions, and (c) fluorescence lifetime decay of β-galactosidase protein for the confocal reference and the ZMW. β-galactosidase concentration in the aqueous buffer is 0.5 M in the free solution and 1.7 M concentration in the ZMW. (d) Fluorescence intensity time traces with background level values, (e) FCS correlation functions, and (i) fluorescence lifetime decay of streptavidin protein for the confocal reference and the ZMW. Streptavidin concentration in the aqueous buffer is diluted to 1.5 M in the free solution and 6 M concentration in the ZMW. The dashed lines in panels (a,d) correspond to the fluorescence intensity of the solution in the absence of the analyzed UV molecules for the confocal reference and in the ZMW. The values of fluorescence enhancement corresponding to each UV emitting molecule are shown in panels (b,e), while the gains of total decay rate are indicated in panels (c,f). IRF denotes the instrument response function of the experimental setup

2.6 The Purcell factor of Proteins in Zero-Mode Waveguide

In this section, we will explore how the optical property of the emitter is manipulated inside the ZMWs. We will use experimental results from FCS and lifetime histogram and explain the method of how the signal from the emitter is enhanced by ZMWs

Figure 2.20a-c illustrates the modification of protein UV emission in the presence of Al nanoapertures and introduces relevant notations. In a homogeneous solution, the protein's total decay rate constant (Γ^0_{tot}) is the sum of the radiative rate constant (Γ^0_{rad})

and the internal non-radiative decay rate constant (Γ^0_{nr}). Protein UV autofluorescence typically exhibits a high internal non-radiative rate (Γ^0_{nr}) surpassing the radiative rate (Γ^0_{rad}), resulting in a quantum yield () ranging from 1% to 10% depending on the protein of interest. The plasmonic nanoaperture alters the local density of optical states (LDOS) [4,20], accelerating the relaxation rate from the excited state to the ground state. This leads to an enhanced radiative rate (Γ^*_{rad}), quantified by the Purcell factor ($\eta\Gamma_{rad}$) as the ratio of the radiative decay rate with the plasmonic nanostructure to the decay rate without it. Quenching losses into the metal introduces an additional energy transfer pathway with a rate constant (Γ^*_{loss}). Thus, the total decay rate constant becomes $\Gamma^*_{tot} = \Gamma^*_{rad} + \Gamma^0_{nr} + \Gamma^*_{loss}$ (assuming the internal conversion rate Γ^0_{nr} remains unaffected by the photonic environment, while losses introduced by the environment are accounted for by Γ^*_{loss}).

Our aim is to experimentally measure these decay rate constants for two different proteins (-galactosidase and streptavidin) to quantify the impact of a plasmonic nanoaperture on LDOS and investigate the potential demonstration of Purcell enhancement in label-free proteins. Additionally, we compare our results with p-quaterphenyl, a well-established fluorescent dye with a high quantum yield in the UV range. While a single fluorescent dye can be approximated as a point electromagnetic dipole whose radiation is influenced by LDOS, extending LDOS enhancement and the Purcell effect to protein UV autofluorescence is more complex due to the presence of multiple tryptophan emitters within each protein, closely packed at a nanometer distance and surrounded by other amino acids that act as fluorescence quenchers through electron or proton transferYu CHEN et BARKLEY 1998
Fluorescence decay histograms provide information for determining the average fluorescence lifetime τ, which is the inverse of the total decay rate constant($\Gamma_{tot} = 1/\tau$). The presence of the nanoaperture reduces the fluorescence lifetime, indicating an enhancement of the total decay rate ($\eta\Gamma_{tot} = \Gamma^*_{tot}/\Gamma^0_{tot}$). For p-quaterphenyl, the fluorescence lifetime decreases from 0.76 ns to 0.3 ns with the nanoaperture, resulting in a total decay rate enhancement of $\eta\Gamma_{tot} = 2.5 \pm 0.2$. Similarly, the fluorescence lifetimes of proteins (β-galactosidase and streptavidin) are also shortened with the nanoaperture, exhibiting accelerations of $\eta\Gamma_{tot} = 2.0 \pm 0.3$ and 1.5 ± 0.2, respectively. However, the reduction in autofluorescence lifetime for proteins alone does not confirm radiative rate enhancement since quenching losses to the metal (Γ^*_{loss}) contribute to the observed increase in total decay rate. To distinguish the modification of the radiative rate from the total decay rate, further analysis of fluorescence brightness enhancement is conducted.

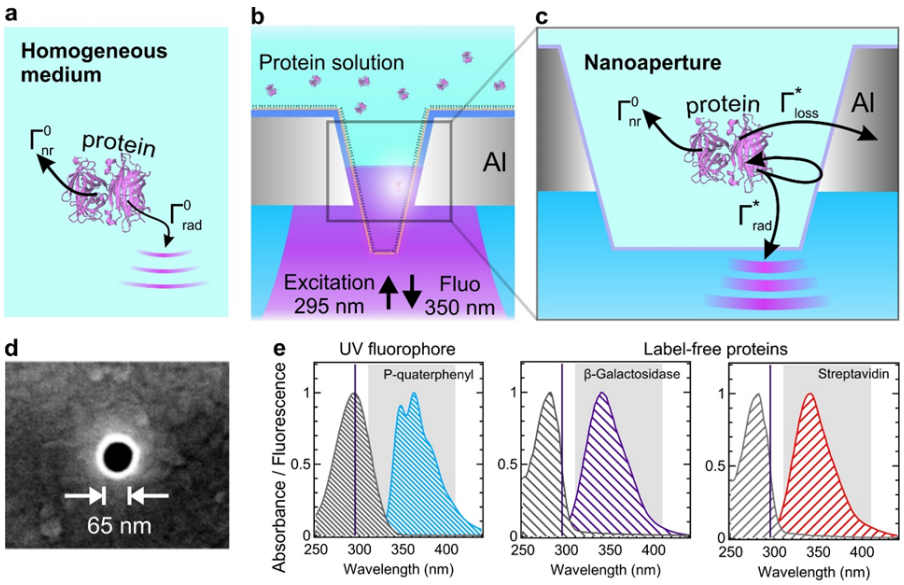

FIGURE 2.20 – Aluminium nanoaperture to enhance the radiative rate of label-free proteins in the UV. (a) Notations describing the decay pathways of protein excited in the homogeneous space (free solution). (b) Schematic view of the experiment in the presence of Al nanoapertures. (c) Notations describing the protein decay pathways modified in the presence of nanoapertures. (d) Scanning electron microscope image of a 65 nm diameter nanoaperture. (e) Normalized absorbance and fluorescence spectra of the UV dye p-quaterphenyl and two proteins -galactosidase and streptavidin. The violet vertical lines correspond to the excitation wavelength of 295 nm, while the shaded regions show the wavelength range used for fluorescence detection.Aleksandr BARULIN, ROY, Jean Benôit CLAUDE et al. 2021

The net fluorescence enhancement (η_F) near the nanoaperture depends on three factors : excitation intensity increase, quantum yield (ϕ), and collection efficiency. It can be expressed as $\eta_F = \frac{\eta_{coll} * \eta_{exc} * \eta_{\Gamma_{rad}}}{\eta_{\Gamma_{tot}}}$, where$\eta_{coll}$ represents the gain in collection efficiency, η_{exc} corresponds to the enhancement of local excitation intensity, and $\eta_{\Gamma_{rad}}/\eta_{\Gamma_{tot}}$ relates to the gain in quantum yield. The experimental measurements in Figure 2.19provide values for η_F and $\eta_{\Gamma_{tot}}$ as shown in fig2.21. To extract the enhancement of the radiative decay rate enhancement ($\eta_{\Gamma_{rad}}$or the Purcell factor), we utilize two additional pieces of information. Firstly, the antenna reciprocity theorem states that the excitation intensity gain (η_{exc}) is the product of the collection efficiency gain (η_{coll}) and the radiative rate gain ($\eta_{\Gamma_{rad}}$). Second, we set the collection efficiency gain (η_{coll}) to 1.44 for the 65-nm nanoaperture based on previous descriptions of the directionality of the bare aluminum nanoapertures. Consequently, the radiative rate enhancement is given by $\eta_{\Gamma_{rad}} = \sqrt{(\eta_F \eta_{\Gamma_{tot}})}/1.44$. This expression is used for all three fluorescent samples (proteins and p-quaterphenyl). Moreover, with the knowledge of all rate enhancements, the reference fluorescence quantum yield in the confocal case enables the computation of various decay rate constants contributing to the fluorescence process in both the confocal and nanoaperture scenarios. The figure 2.21

summarizes the main findings and assess the fluorescent enhancement of ZMWs as a product of excitation gain, collection gain and quantum yield gain.

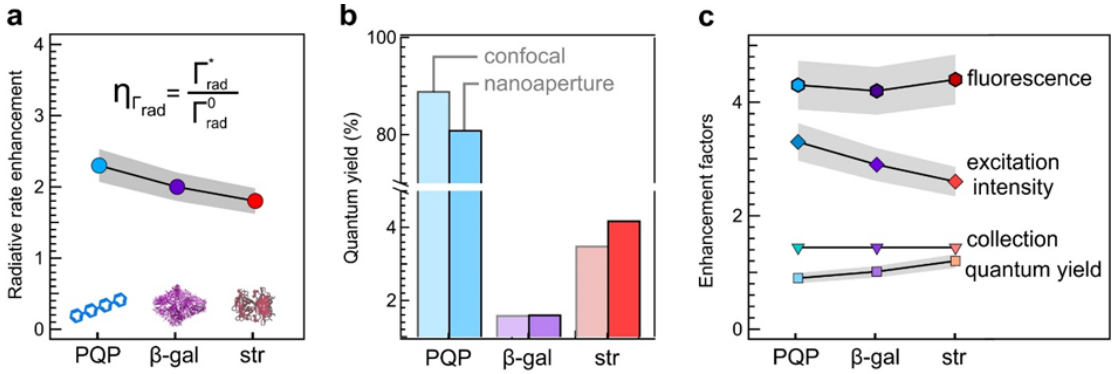

FIGURE 2.21 – Enhancement of the different decay rate constants and comparison between label-free proteins and p-quaterphenyl (PQP). (a) Radiative rate enhancement (Purcell factor). (b) Average quantum yield of UV fluorescent molecules. The data for the confocal reference is displayed in pastel colours, while the brighter colours represent the nanoaperture. (c) Excitation intensity gain, collection efficiency gain, quantum yield gain, and net fluorescence enhancement. The grey-shaded areas represent the error bars.

2.7 Conclusion

In conclusion, zero-mode waveguides (ZMWs) are a major innovation in the fields of biotechnology, nanophotonics, and molecular biology. As we have seen in this chapter, their ability to confine light within zeptoliter volumes, far below the diffraction limit, enables single-molecule sensitivity and high temporal resolution, providing unprecedented opportunities to observe biological phenomena at the individual molecule level. The key features of plasmonic ZMWs are plasmonic enhancement, background screening, and low detection volume. There are multiple variations of ZMWs that can be used for biophysical research. The simplicity of the design makes it a mass-produced technique for applications based on visible light, especially DNA sequencing. Furthermore, the potential of ZMWs extends beyond sequencing. As we have discussed, they have been instrumental in studying the dynamics of smaller proteins tagged with fluorophore or label-free. However, despite these significant advancements, the full potential of ZMWs is yet to be realized. The UV ZMWs add a new regime that connects label-free sensing of proteins under physiological and biologically relevant conditions. The study of ZMWs for application in UV autofluorescence spectroscopy is still in its nascent stage; we saw some work done in the literature on the spectroscopy of UV dyes and tryptophan-carrying proteins; however, it is limited to larger proteins. Throughout this thesis, we will discuss and implement methods to enhance the performance of ZMWs and make them biocompatible and stable to

photocorrosion. Through continued research and development, ZMWs are poised to push the boundaries of what we can achieve in the realm of nanoscale science.

3 Enhancing Collection Efficiency Using Optical Horn Antenna

Connected Publications

Aleksandr BARULIN, Prithu ROY, Jean-Benoît Benoît CLAUDE et al. « Ultraviolet optical horn antennas for label-free detection of single proteins ». In : *Nature Communications* 13.1 (déc. 2022), p. 1842. URL : https://www.nature.com/articles/s41467-022-29546-4

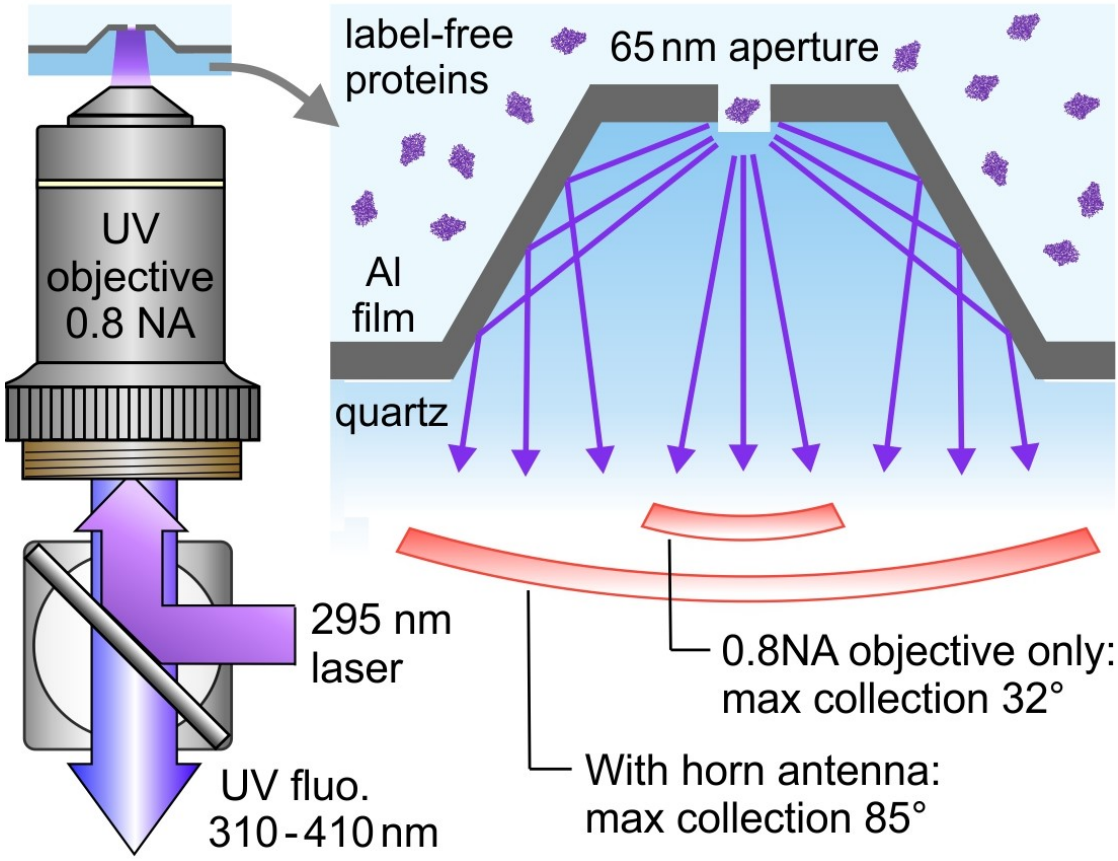

(a) Figure A

FIGURE 3.1 – Horn Antenna

Summary

3.1 Introduction

In the previous chapters, we learned that UV-excited autofluorescence is crucial for studying proteins without labeling. We also saw that Zero-Mode Waveguides (ZMW) offer a much smaller volume than the diffraction limit, allowing us to observe single molecules even at high physiological concentrations(a few μM). However, the increase in protein signal is only around 300-400% for circular ZMWs (Aleksandr BARULIN, Jean Benoît CLAUDE et al. 2019a) and slightly higher for rectangular ZMWs(BAIBAKOV, Aleksandr BARULIN, ROY, Jean-Benoît CLAUDE et al. 2020). Consequently, ZMWs are sufficient for larger proteins such as β -Galactosidase, which have hundreds of tryptophans and a comparatively strong signal. However, smaller proteins with only a few tryptophans, such as streptavidin, LicT, and thermonuclease, can produce a signal as low as 5-10 photons per second confocal at saturation power. In such cases, a 3 to 4 times enhancement of ZMWs is inadequate for conducting FCS or any advanced study of protein dynamics. Therefore, new nanotechnology tools need to be developed to intensify the emission from single proteins.
Optical antennas(NOVOTNY et VAN HULST 2011) offer a way to control and intensify the emission of single quantum emitters, similar to radio-frequency antennas. Although intense fluorescence enhancement factors have been achieved with dyes that absorb strongly in the visible range, most optical antenna designs are unsuitable for UV protein detection due to the losses in UV , challenging nanofabrication, or requirement for solid-state integration. Therefore, alternative designs must be developed to offer a highly efficient platform that meets the needs of high photon count rates, microsecond time resolution, background-free operation, and full compatibility with the UV detection of proteins.
To understand the scope of discussion more deeply, let us revisit the equation of

fluorescence enhancement

$$\eta_F = \kappa * \eta_{exc} * \frac{\Gamma^*_{rad}}{\Gamma_{rad}} * \frac{1}{1-\phi_0+\phi_0(\Gamma^*_{rad}+\Gamma^*_{loss})/\Gamma_{rad}} \tag{3.1}$$

here we will focus on 'κ' only which is the collection gain and other factors are the same as defined so far in the previous chapter. The equation illustrates that there is a direct and positive relationship between fluorescence enhancement and collection efficiency. As a result, to maximize the overall fluorescence, one approach is to improve the collection efficiency, which entails effectively capturing the emitted light. This can be achieved by directing all emitted light from the proteins toward the objective.
One of the main limiting factors in ZMW is that within the ZMW, close to a planar dielectric interface, a significant portion of the light emitted from a single dipole is emitted at high angles above 65 °. As depicted in figure 3.2, this phenomenon is known as supercritical or forbidden light. RUCKSTUHL, ENDERLEIN et al. 2000
When using microscopes that operate in the visible spectral range, objectives with a numerical aperture of 1.4 or greater are used to optimize the collection of fluorescence from individual molecules. However, when working with UV light, the selection of microscope objectives is restricted, and available UV objectives often have a numerical aperture of less than 0.8. This corresponds to a maximum collection angle of 33 ° in the quartz substrate, which has a refractive index of 1.48. It is crucial to collect UV light emitted at high angles to maximize the autofluorescence signal and allow for the detection of single, label-free proteins. Thus we need to find a way to manipulate the light at a higher emission angle and collect it in the objective.

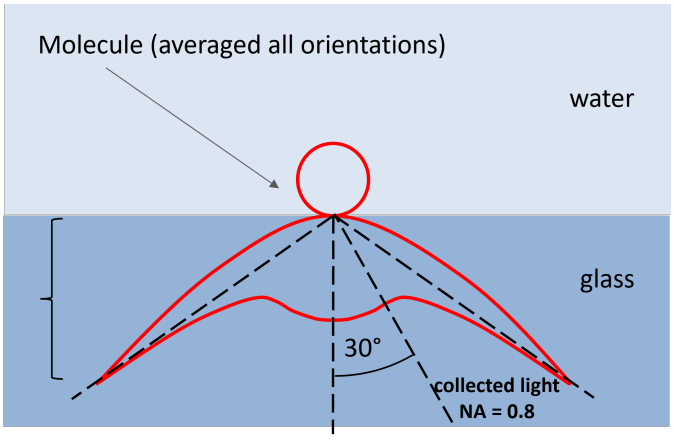

FIGURE 3.2 – The Radiation pattern of molecules near glass-water interface showing the fraction of light which is collected by microscope objectives

We embarked on a quest to find a directive antenna that would be appropriate for our research. Our exploration led us to the field of radio waves, where a significant amount of research has been conducted on various types of direct-antennas. Among the directive antennas commonly used for radio wave applications are Yagi-

Uda antennas, log-periodic antennas that are similar to bull's-eye antennas (a term frequently used in the optical antenna community), and conical antennas. Each of these antennas has distinct design characteristics and meritorious directivity figures. In our particular situation, the conical antenna proved to be a good fit for our optical setup and the ZMW geometry. Refer to figure 3.3

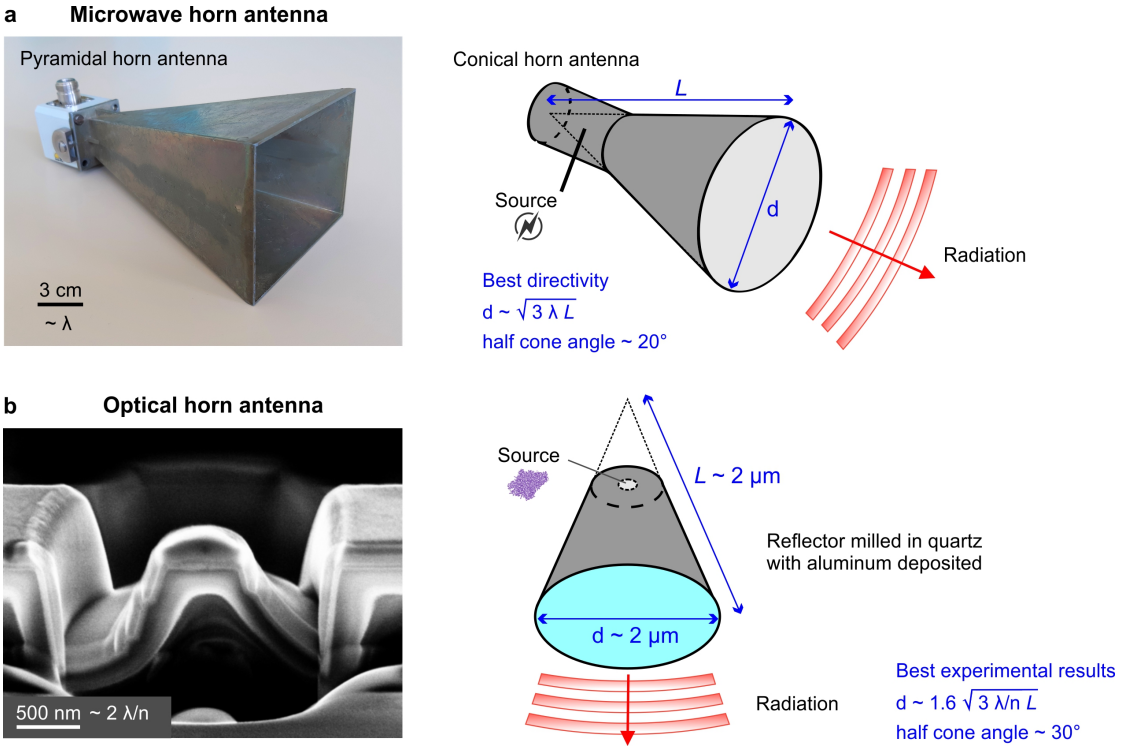

(a) Figure A

FIGURE 3.3 – Microwaves analogous of designed optical antenna

Our platform, which utilizes an optical horn antenna, specifically addresses the challenges associated with detecting single proteins using UV light without the need for labels. The platform incorporates a reflective unit and a nanoaperture (shown in Fig.3.4) and is analogous to a microwave horn antenna as depicted in Fig.3.3 The 65-nm diameter central nanoaperture focuses the light within an attoliter detection volume, allowing for the isolation and enhancement of the autofluorescence of a single protein. Meanwhile, the reflective conical unit, which is covered with a 100-nm thick layer of aluminium, directs the autofluorescence light toward the microscope objective. Unlike Yagi Uda or Bull's Eyes resonant designs, the conical horn has a broad bandwidth, covering the entire range of 300-400 nm, regardless of resonance or interference effects. The detection volume provided by the 65 nm central aperture is three orders of magnitude smaller than that of a diffraction-limited confocal microscope, allowing for single-molecule detection at micromolar physiological concentrations without the need for subnanomolar dilutions, as is necessary for conventional confocal microscopy.

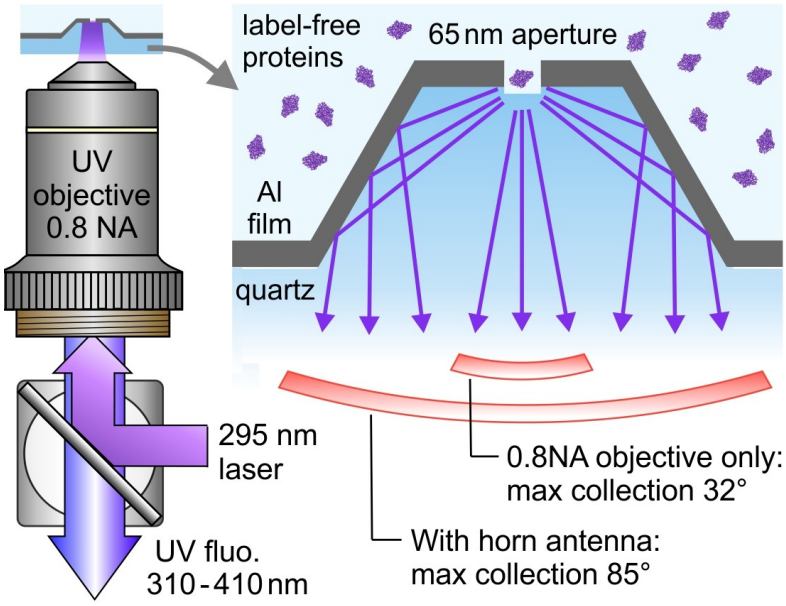

FIGURE 3.4 – Conceptual schematics of Horn antenna

3.2 Numerical Simulations to Optimize Horn Antenna

Once we agreed that a horn-shaped antenna could solve our directivity problem, optimizing the structure became crucial. The height and base diameter of the cones were important parameters to consider, and we needed to flatten the tops of the cones for a specific reason. Typically, conical structures have sharp, pointed tops, but in our case, we needed to create a hole in the top of the cone and deposit metal on it. On the basis of our experience with metal deposition, sharp corners can lead to nonuniform metal deposition, resulting in cracks in the film and lower reflectivity, ultimately impacting the performance of the metal-reflective coating. Our primary focus was on optimizing the base diameter and height of the cones, as shown in Figure 3.3, where we depict the analogy of an optical horn antenna to the microwave antenna, for the optimum directivity of a horn antenna in the UV spectrum, the relation of base diameter and height is given as $d = 1.6\sqrt{3\lambda/nL}$. By fixing the length of the horn antenna and varying the diameter of the cone, we could change the angle of the cone, which was our target optimization parameter in the future. In other words, changing the cone angle allowed us to control how effectively the light emitted by molecules in the hole would be directed toward the objective of the microscope. We will see two kinds of simulation, first, the collection part where we see how does horn antenna manipulates the electric field emanating out of the source(point dipole), and secondly, the excitation part where we will excite cones with a Gaussian beam and see the light propagation.

3.2.1 Numerical simulation of Horn Antenna : Collection Part

In this section, we will see how the horn antenna platform compares with ZMW and a simple air-glass interface in the collection regime where the source is a point dipole. We started the simulation from the basic step which is a dipole near the water-glass interface figure 3.5 (a)and as discussed in the previous section (depicted in Fig 3.2) the emission of dipole (averaged over x and y polarization) is quite isotropic or, to say, emits in a large angle which is not captured by objectives with low NA. Further, we model the same dipole in a cylindrical hole which provides a minute directivity to emission, but a major part of emission still remains at larger angles. We also modeled the horn antenna with holes for different cone angles ranging from 15 ° to 55 °.

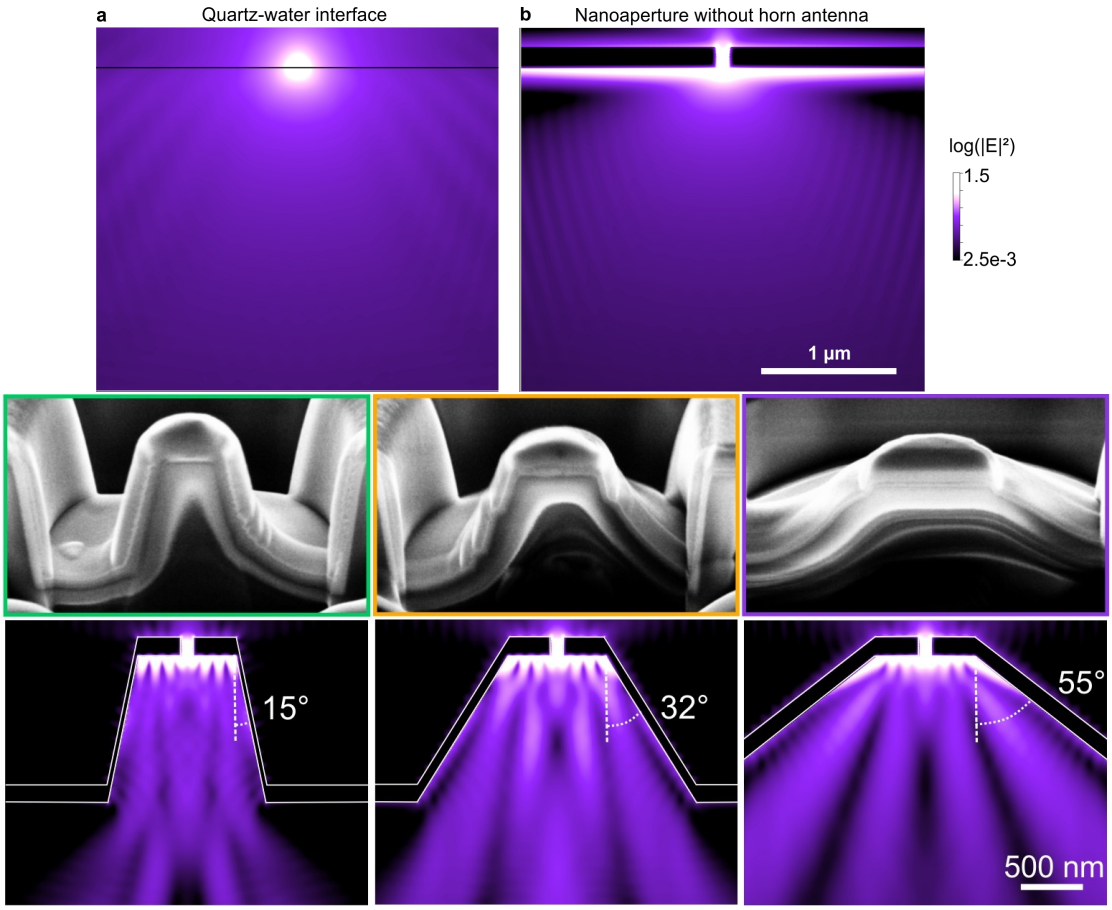

FIGURE 3.5 – Finite difference time domain (FDTD) simulation of the emission pattern of a dipole located 10 nm above the quartz interface for different cases emitting at 350 nm.The contributions from horizontal and vertical dipole orientations are averaged.

Intuitively the smaller angles did not direct the light effectively as smaller angles created multiple reflections on the wall of cones and the signal came out diverging from the cone as seen in the field pattern of the antenna in figure 3.5 (c). On the other hand, wider angles could not effectively direct light in the objective, thus emission

still reaches the objective at a higher angle. Thus, we found that the effective angle at which the fluorescence angle is optimum is 35°. We believe that this optimum angle at which fluorescence will be collected efficiently could depend on the NA of the objective.To see the difference in the far-field pattern of the glass-water interface and the optimum horn antenna we plot the far-field radiation plot as depicted in the plot shown in Figure3.6. There are two key parameters to see first, the front-to-back ratio of intensity. In the case of the horn antenna ratio of radiation downward(toward the objective) to the upward direction is larger than in the water-glass case thus more light comes toward the objective in the case of the horn antenna. Second is the angle of emission in the downward direction, for cones are very narrow, and the beam width is roughly 3 times narrower than a water-glass case, thus more light can be collected by objectives with lower NAs as the emission is at smaller angles.

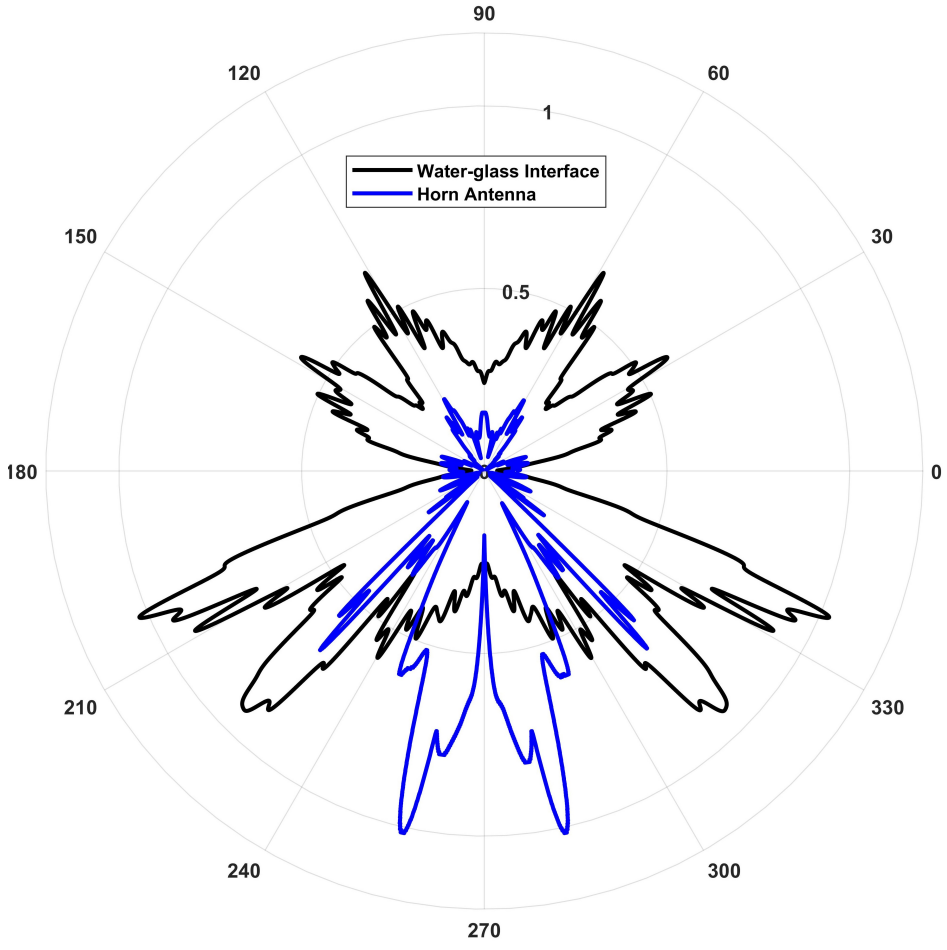

FIGURE 3.6 – Normalized Polar radiation pattern of water-glass interface and Horn antenna with 32° cone angle.

3.2.2 Numerical simulation of Horn Antenna : Excitation part

We used COMSOL Multiphysics for the simulation in this section. To understand how the horn antenna will behave in an experiment on UV excitation, we took our best performing horn antenna with a cone angle of 32° and illuminated it with the Gaussian beam (the waist is 300 nm). The parameters of the Gaussian beam of the laser were the same as measured in our experimental setup. As we can see from the field intensity plot in Fig. 3.7 for two different wavelengths, the cone acts as a nice reflector and only allows light to pass through the nanoaperture, thus keeping the key concept of nanoaperture i.e. only evanescent wave exists in the hole in very small volume (attoliters). We can see some Surface Plasmon Polariton (SPP) near the edge of the holes and the top(at the quartz-metal interface) of the cones. Another aspect is that if the cone base diameter is comparable to the size of the Gaussian beam waist, then we could see some excitation enhancement due to the focusing of light by the cone. However, this is not the case for Deep-UV where the FWHM of the beam from the 0.8 NA objective was around 300 nm, which is almost an order of magnitude smaller than the diameter of the cone, which is around 2 μm.
To give a perspective, such a structure can be used to focus light on the nanoaperture if we are using wide-field illumination, so that the spot size is comparable to the diameters of cones.ROY et BOLSHAKOV 2021a

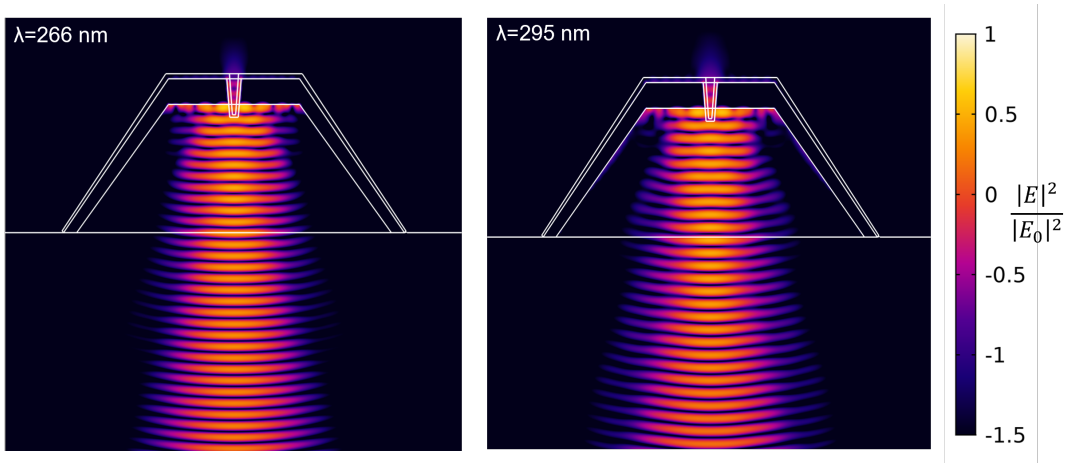

FIGURE 3.7 – Numerical simulation of Near-field of cone excited by the gaussian beam. The color map shows the intensity of light in log scale

Earlier, we discussed that there are two main components of the horn antenna platform : the micro-reflector cones and the nano-aperture, latter is the focus of this paragraph. Figure 2.5 in chapter2 illustrated the variation of field intensity over the diameter of nanoholes. To obtain more accurate values, we measured the field values on a plane 10 nm above to eliminate any erroneous values resulting from meshing at the sharp edges of the nano-holes (it's an intrinsic problem of numerical simulation). For our experiment, we utilized 65 nm nanoholes coated with a few nm of silica to protect against UV corrosion. It is noteworthy that nano-apertures with diameters

smaller than 100 nm are classified as "Zero Mode Waveguide" ZMW since they are small and attenuate light passing through them.

Thus, we can see that the horn antenna platform gives us a few choices based on what parameter we choose. In our case, we focused on higher directivity and smaller volumes, so we used large horn reflectors and smaller nanoapertures. We can have other combinations like reflectors comparable to the size of λ and smaller or larger apertures, etc. Therefore, it can be said that the horn antenna platform has quite a good potential to become a versatile tool for single-molecule biophysics.

3.3 Design and Fabrication of Horn Antennas

3.3.1 FIB-based Fabrication Techniques

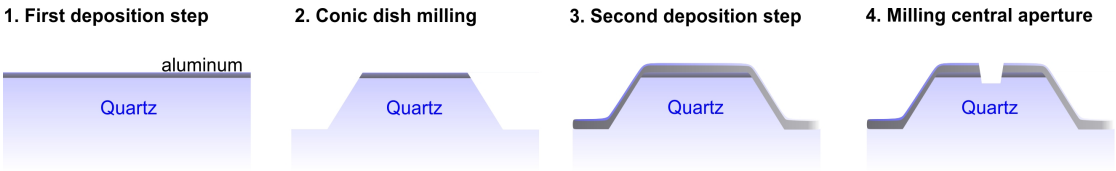

FIGURE 3.8 – Fabrication protocol of the horn antenna platform

The process of creating the device shown in Figure 1.3 comprises several steps. Initially, a thin layer (50-100 nm) of Al is deposited onto a quartz surface to enable electrical conductivity for use with a gallium ion-based Focused Ion Beam Milling (FIB) setup. Using FIB, the cone-shaped micrometer structure with a flat-topped structure known as the horn antenna is milled as illustrated in the image. Subsequently, a 100 nm layer of aluminum is deposited to enhance the horn antenna walls' UV reflectivity. Finally, a nanoaperture measuring 65-200 nm in diameter is carved in the center of the top plateau of the horn antenna using FIB.
The substrates are clean NEGS1 quartz microscope coverslips of 150 µm thickness (Neyco). Aluminum layers are deposited by electron beam evaporation (Bühler Syrus Pro 710) at a 10 nm/s rate at a chamber pressure of 10-6 mbar. FIB milling is performed using a gallium-based system (FEI dual beam DB235 Strata) with 30 kV acceleration voltage and 300 pA current to mill the horn antenna and 10 pA current to mill the central nanoaperture. All nanoapertures have a 50 nm deep undercut into the quartz substrate to maximize signal enhancement. A 10 nm thick SiO2 layer was deposited by plasma-enhanced chemical vapor protection (PECVD, PlasmaPro NGP80 from Oxford Instruments) to protect the aluminum surface against corrosion.

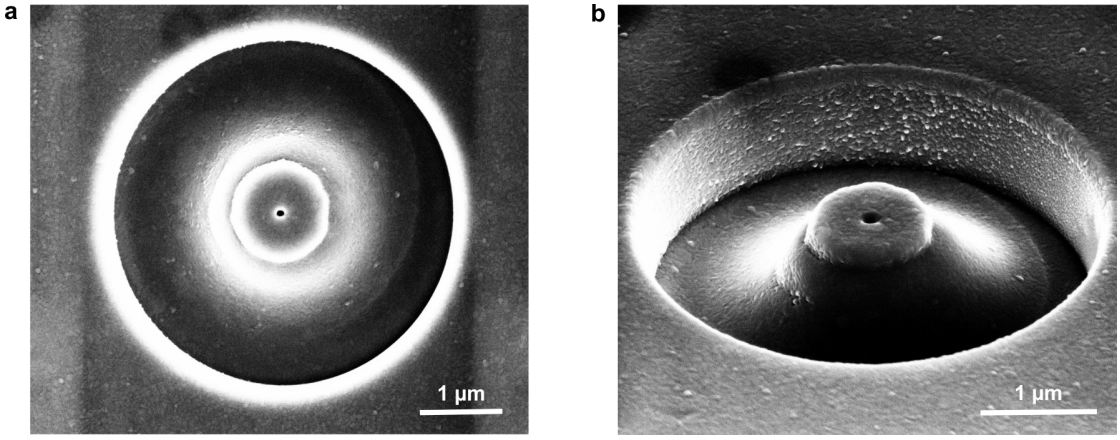

FIGURE 3.9 – SEM image of horn antenna with 32°(a)top view and (b)tilt view

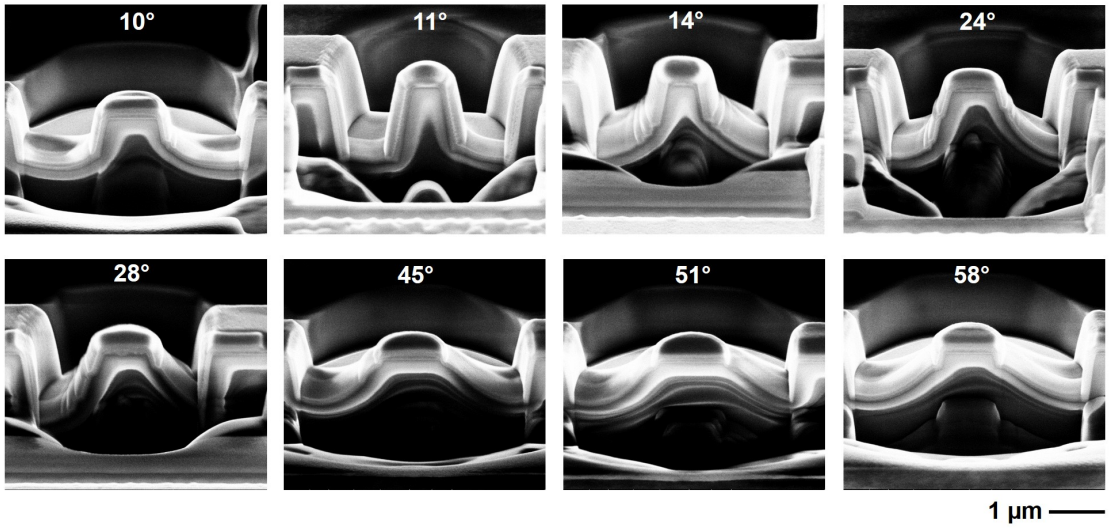

FIGURE 3.10 – SEM images of different horn antennas with increasing cone angles as indicated in each picture. The sample is tilted by 52° and a FIB cross section is performed to enable viewing the geometry of the device. The central nanoaperture has not been milled on these samples. We have checked five different independent samples leading to similar images.

3.3.2 Alternative Fabrication Techniques

Although the previous section's method is the most reliable and consistent approach for creating UV horn antennas, it has some drawbacks. For instance, the process involves numerous steps of FIB and metal deposition, which can be time-consuming and may lead to sample contamination during transfer between setups. Moreover, our research and the existing literature suggest that the gallium ions used for FIB can introduce a background signal when excited by a UV source because of

the implantation of Gallium atoms into the sample's aluminum surface layers and grain boundaries. The amount of gallium implantation is directly proportional to the dose of Ga ion during FIB as well as the milling time; given that the cone structure is a couple of microns in size, this step adds a substantial amount of gallium ion, which translates to the background in experiments. It is worth noting that we took extra measures to remove this background problem during experiments, which we will see in the following chapter. An alternate way will be to use Xenon-ion-based FIB as discussed in the work of ZHONG, WADE et al. 2021 which is inherently better than gallium-based FIB in terms of ion implantation, as the latter is inherently inert.
We tried various methods of producing cones, each with its own advantages and drawbacks. One of the techniques we tried involved using self-assembly with SiO_2 beads to create cone-like structures. The process involved depositing small Silica beads of 1-2 µm in size on a quartz coverslip and then coating them with Al metal to form a reflector layer for UV light. The plan was then to drill holes into this structure. However, this method encountered several technical issues. Due to the curvature of the spheres, the Al film did not cover the areas of the spheres in contact with the surface, which can be seen in figure 3.11 in tilt as well as in top view, resulting in light leakage and excessive transmission through the cones. As a result, this technique was not suitable for our purpose of directing light into a UV objective.

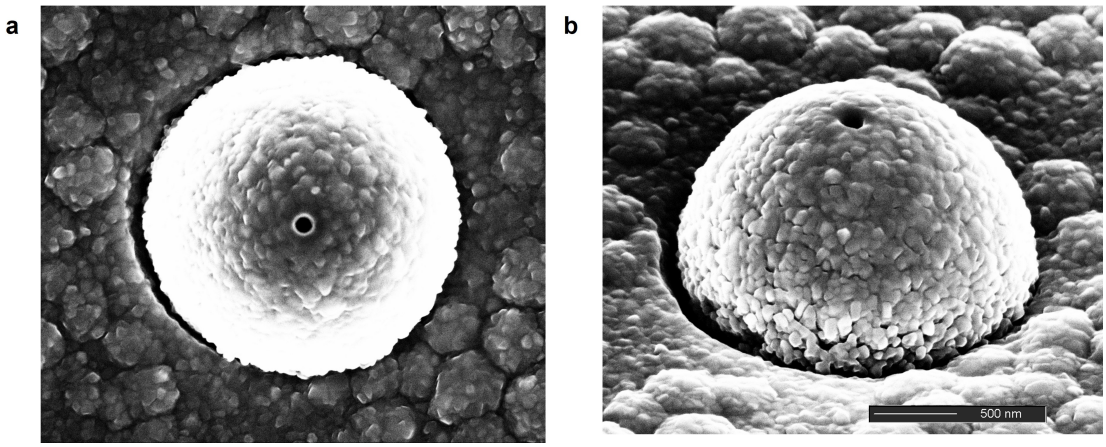

FIGURE 3.11 – SEM image of Silica bead (a)Top View and (b)Tilted View. It is coated with Al and ZMW milled in it.

In an alternative method, we investigated approaches to simplify the two-step process of Al deposition in a single step. We deposited carbon on the surface, which acts as conducting material for FIB, thus facilitating the creation of cones, followed by chemical etching and plasma cleaning to eliminate the carbon. Subsequently, the process would continue with Al deposition and hole milling, as usual. However, this technique has its own limitations, as traces of carbon remain on the sample even after thorough cleaning, causing photoluminescence during experiments. The strong signal from these nano-micro structures was enough to overshadow the valuable signal from proteins, leading us to abandon this fabrication method for now.

3.4 Optical Characterization of Horn antenna

3.4.1 p-Terphenyl FCS for Cone angle optimization

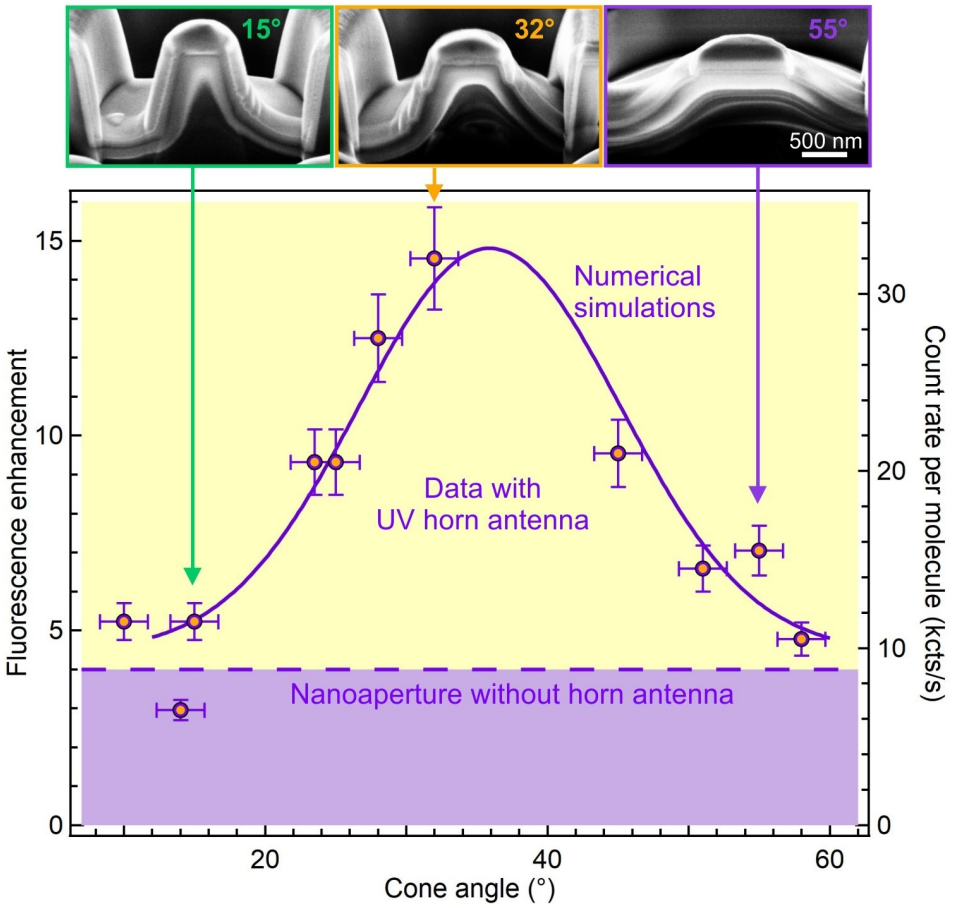

FIGURE 3.12 – Fluorescence enhancement of the brightness per molecule as a function of the horn antenna cone angle. The right axis shows the corresponding count rate per molecule at 80 µW of the 266 nm laser. The level achieved with a nanoaperture without any horn antenna is indicated by the dashed horizontal line. The solid line shows the numerical simulation results that account for the collection efficiency gain into the 0.8 NA microscope objective. The SEM images in the inset show the antenna geometry after a cross-section has been cut by the focused ion beam. Data are presented as mean values +/- one standard deviation determined from a pool of at least 3 different samples.

The performance of the horn antenna is evaluated using p-terphenyl, a UV fluorescent dye with a 93% quantum yield (Figure 3.12). The antenna's collection efficiency is determined by the angle of the conical reflector. As shown in the previous section, Horn antennas with various cone angles ranging from 10 to 55° have been fabricated to study how this angle changes the overall collection gain of the fluorescence signal.

The raw fluorescence time trace reveals a 4-fold larger signal with a 32° horn compared to the bare nanoaperture, indicating an improved collection efficiency by the same ratio (Figure3.13 a). Fluorescence correlation spectroscopy (FCS) analysis measures the fluorescence brightness per molecule, from which the fluorescence enhancement is computed and compared with the confocal reference. The enhancement factor depends on the cone angle, with an optimum of around 35°.

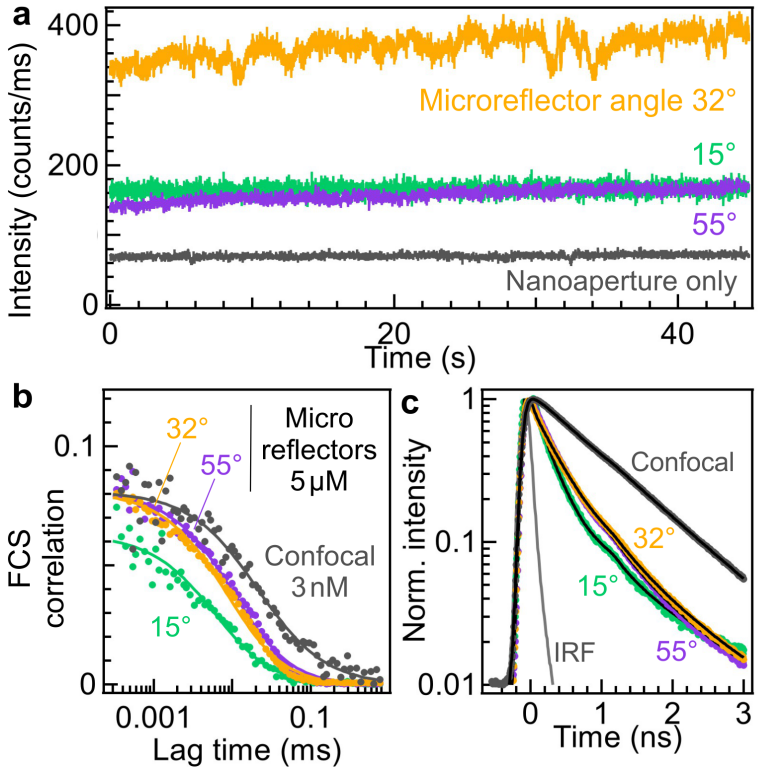

FIGURE 3.13 – (a)Fluorescence intensity time traces recorded on a 5 µM solution of p-terphenyl using horn antennas of different cone angles. (b) FCS correlation functions corresponding to the traces shown in (a) ; the case for the isolated nanoaperture is equivalent to the horn antennas with cone angles 32 and 55° (c) Normalized fluorescence lifetime decay traces were acquired simultaneously from the data in (a,b). IRF indicates the instrument response function. Black lines are numerical fits.

While a single nanoaperture improves the p-terphenyl brightness by a factor of 4, the horn reflector increases it to 15. These values are lower than previous reports using gold antennas TROFYMCHUK, KOŁATAJ, GLEMBOCKYTE, F. ZHU, P. ACUNA et al. 2023THACKER, HERRMANN et al. 2014PUNJ, MIVELLE, MOPARTHI et al. 2013b PUCHKOVA, VIETZ et al. 2015ain the red part of the spectrum, but this can be explained by the ultraviolet range and the simple non-resonant design of the horn antenna. The primary goal is not to compete with plasmonics in the visible world, but rather to enable the detection of single proteins by UV autofluorescence above background noise. The collection efficiency gain has been numerically simulated using the finite-

difference time domain (FDTD). The simulation results align well with the trend of the experimental data, which confirms the dependence on the cone angle. Fluorescence lifetime measurements in Figure3.13, shows that the p-terphenyl fluorescence lifetime is reduced by a factor of 3 in the antennas compared to the confocal reference. This lifetime reduction is independent of the cone angle and is similar to the lifetime reduction found for the single aperture without the conical reflector. This suggests that the fluorescence lifetime of the emitter (and hence the local density of the optical states) is mainly determined by the diameter of the apertureAleksandr BARULIN, ROY, Jean-Benoît CLAUDE et al. 2021. With a similar local density of optical states between the nanostructured samples, it can be concluded that the supplementary gain brought about by the optimized horn antenna is directly related to the increase in directivity compared to the bare nanoaperture. This confirms the idea of the conical reflector as a collection unit to steer the emitted light toward the objective of the microscope. Based on the gain relative to the bare nanoaperture, the maximum collection angle is estimated to be around 85° for our best system with a 32° cone angle. Our nanophotonic platform collects the fluorescence light emitted at high angles, even beyond the supercritical angle. As shown in Figure3.12, the presence of the horn reflector improves the collection efficiency, but the fluorescence excitation and emission enhancements occurring in the nanoaperture are not affected. We independently confirm the fluorescence enhancement by quantifying the noise reduction in the correlation data in figure 3.14. The high brightness observed with the optimized horn antenna directly improves the FCS signal-to-noise ratio, allowing for a reduction in the experiment integration time compared to the confocal reference while maintaining the same accuracy. All fit parameters are shown in Tables 3.1 and 3.2

	F(kHz)	B(kHz)	N_{mol}	$\tau_d(\mu s)$	CRM(kHz)	Enhancement
confocal	27.3	0	12.3	21.1	2.2	-
Single Aperture	62.1	3.8	6.6	15.5	8.8	4
Horn antenna 32°	347.9	32	9.9	13.8	31.9	14.5
Horn antenna 15°	145	32	9.7	9.2	11.7	5.3
Horn antenna 55°	146.9	32	7.3	16.6	15.7	7.1

TABLEAU 3.1 – The FCS data shown in Figure 3.13(a,b)are fitted with parameters. In the case of p-terphenyl, no rapid blinking contribution is observed, therefore, we set η_T and τ_T to zero. The shape parameter κ is set to 8 for the confocal case, based on the calibration of the microscope point spread function (PSF), while for the aperture and horn antennas, we use κ=1, which is consistent with our previous work using nanoapertures and fluorescent dyes in the visible spectral range. The fluorescence count rate per molecule (average brightness per emitter) is represented by CRM = (F-B)/Nmol. The translational diffusion time reduction for nanoapertures in the visible spectral range was similar to that observed for the diffraction-limited confocal reference.

	τ_1	τ_2	τ_3	I_1	I_2	I_3	Lifetime reduction
confocal	-	0.95	-	-	-	-	-
Single Aperture	0.01	0.32	0.95	0.23	0.47	0.3	3
Horn antenna 32°	0.01	0.34	0.95	0.24	0.35	0.41	2.8
Horn antenna 15°	0.01	0.25	0.95	0.31	0.4	0.29	3.8
Horn antenna 55°	0.01	0.35	0.95	0.19	0.49	0.32	2.7

TABLEAU 3.2 – Fit parameters for the fluorescence lifetime data displayed in Figure 3.13 The lifetimes are expressed in ns, the intensities are normalized so that their sum equals 1. All horn antennas and the single aperture share similar lifetime reductions. The horn antenna essentially affects the fluorescence collection, the local density of optical states is determined by the central 65 nm diameter aperture which remains constant among the different nanostructures. The lifetime reduction is calculated as 0.95 ns/τ_2

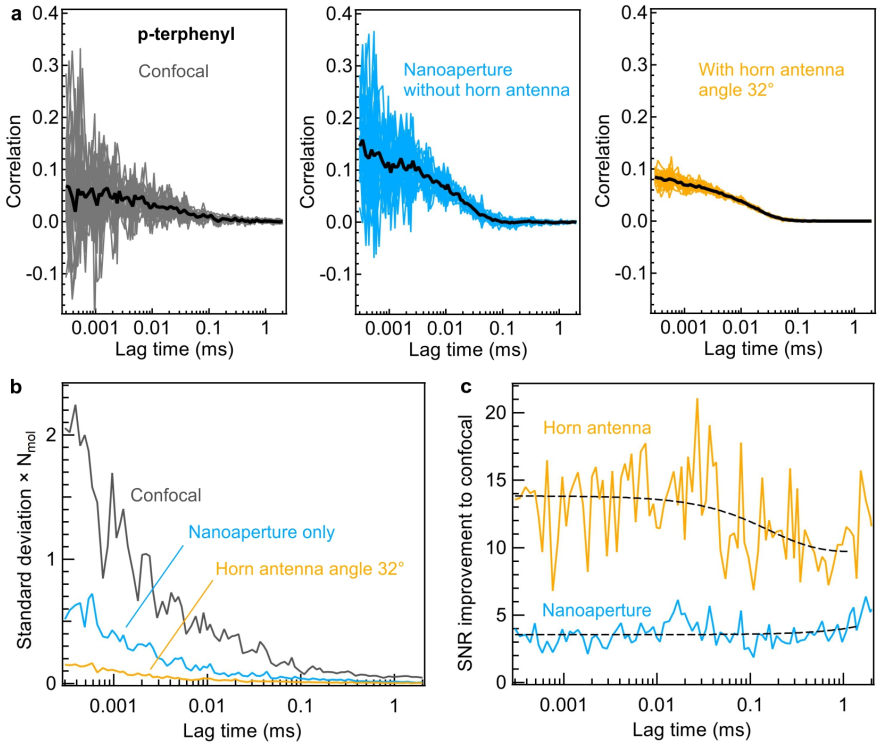

FIGURE 3.14 – High fluorescence brightness per molecule improves the signal-to-noise ratio in FCS. (a) Raw FCS correlation functions of p-terphenyl for the confocal reference, the single 65 nm nanoaperture, and the horn antenna. The concentration for the confocal data shown here is reduced by 1000x. (b) The standard deviation of the FCS trace is deduced from the spread of the experimental data points in (a),(c) The normalized standard deviation in (b) is used to compute the signal-to-noise ratio (SNR) improvement as compared to the confocal case.

Improving the signal-to-noise ratio in FCS is possible through higher fluorescence brightness per molecule. In Figure 3.14, raw FCS correlation functions of p-Terphenyl are shown for the confocal reference, the single 65 nm nanoaperture, and the horn antenna. Each graph displays a combination of 20 individual FCS curves recorded with a 1-second integration time. The spread of these 1-second FCS traces represents the statistical noise of the experimental data, while the thick black trace indicates the average data with a 20-second integration time. The horn antenna produces higher brightness, resulting in reduced noise around the average value without any post-treatment analysis. The concentration for the confocal data shown here is reduced by 1000x. In Figure 3.14, the standard deviation of the FCS trace is obtained by calculating the standard deviation among the set of FCS curves recorded with a 1 second integration time for each lag time. The standard deviation is then normalized by the number of molecules Nmol deduced from the FCS fit to obtain a concentration-independent quantity representing the noise in an FCS acquisition. These data quantify the noise reduction seen in Figure 1 and allow a direct comparison of the different cases. In figure 3.14, the normalized standard deviation is used to calculate the improvement of the signal-to-noise ratio (SNR) compared to the confocal case. It is important to note that the noise in FCS is linearly dependent on the fluorescence brightness per molecule. This approach is based only on statistical analysis and no numerical fit is performed. This data set independently confirms the fluorescence enhancement of the brightness per molecule deduced using the FCS fitting in Figure 3.12.

3.5 Detecting single proteins with Horn Antenna

3.5.1 Single diffusing molecules

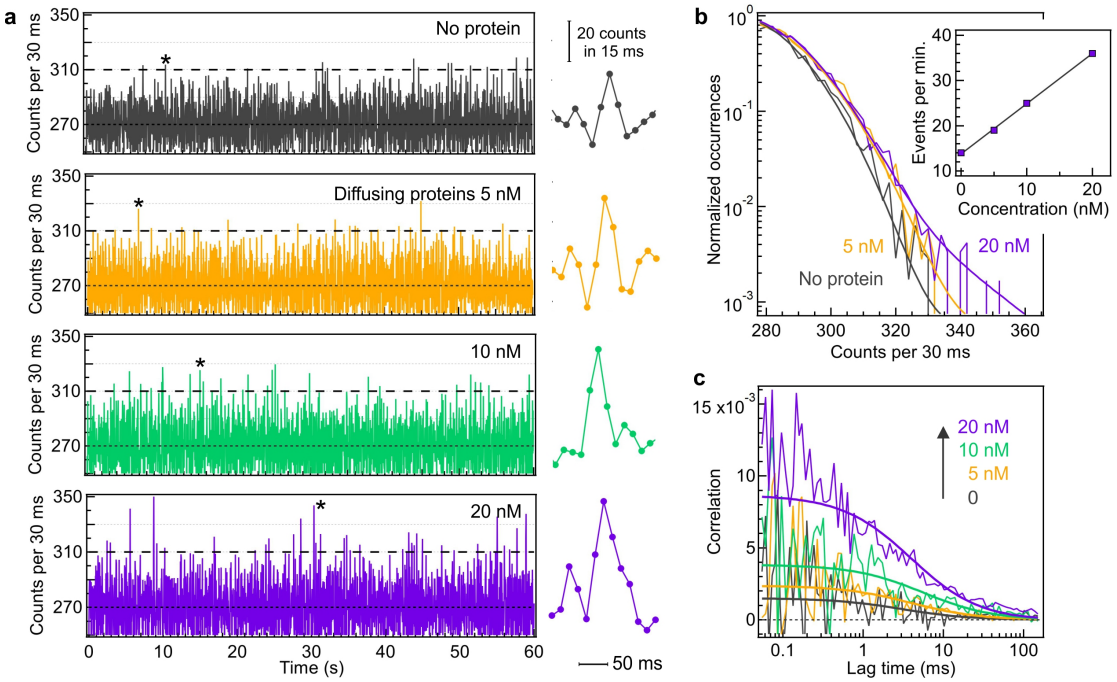

FIGURE 3.15 – Label-free detection of single diffusing proteins across the UV horn antenna. 55 % sucrose was added to the buffer to slow protein diffusion by 30× and ease observing the autofluorescence bursts. The thick lines are numerical fits

To show the single-molecule sensitivity of our Horn Antenna platform, we conducted experiments with diffusing -galactosidase-streptavidin proteins at very low concentrations, ensuring that the average number of proteins in the detection volume was significantly below 1 (as depicted in Figure 3.15). In these experiments, we employed a 200 nm diameter nanoaperture to increase the residency time of proteins inside the horn antenna. For the highest concentration of 20 nM, the average number of proteins inside the 200 nm nanoaperture was calculated to be 0.12, which aligns well with the regime required to observe fluorescence bursts from single molecules. To ensure that proteins stay within the nanoaperture volume for a long enough time, we added 55% sucrose to the buffer solution, thus increasing the viscosity. Without sucrose, the diffusion time of proteins across the nanoaperture would be below 1 ms, which is insufficient to record enough photons to clearly detect the UV autofluorescence bursts from a single protein. However, the presence of impurities in sucrose leads to higher background noise levels, which limits the maximum amount of sucrose that can be used. We found that a 55% w/w sucrose mixture is a good compromise between increased viscosity and a tolerable noise level. Figure 3.15a displays autofluorescence time traces recorded with increasing protein concentra-

tions, where the number of events exceeding the threshold of 310 counts per 30 ms bin time (corresponding to 2.5× the standard deviation of the background noise, dashed horizontal line in Fig. 3.15a) increases with protein concentration. The photon count histograms confirm an increasing difference with the background level as the protein concentration increases. The respective maxima show that the brightness for diffusing molecules is about 600 counts per second, consistent with an independent FCS calibration at the micromolar concentration. To confirm that the bursts seen on the autofluorescence traces stem from the proteins and are not just random noise, we compute the temporal correlations of the traces in Fig. 3a and obtain the FCS correlograms in Fig. 3c. The FCS amplitude increases with concentration because of the dominant presence of the background noise at low concentrations. The positive correlation amplitude and the 5 ms diffusion time (due to the presence of sucrose) indicate that the bursts seen in Fig. 3a stem from single -galactosidase-streptavidin proteins. Overall, the results demonstrate the ability of the UV horn antenna to detect and resolve autofluorescence bursts from diffusing single-label-free proteins.

3.5.2 Other applications of Horn-antenna

Apart from the work discussed earlier, the Horn antenna is a versatile platform and can be used to study other dynamic processes in UV as well as in the visible spectrum. In this section, we will see some of those examples. The first one is where the author studied the denaturation of β-galactosidase by changing the concentration of Urea and performing multiple sets of FCS measurements, as depicted in Fig. 3.16. The Horn antenna's high collection efficiency leads to higher CRM and SNR which helps in the precise calculation of hydrodynamic radius and evolution of the number of molecules wrt to urea concentration.

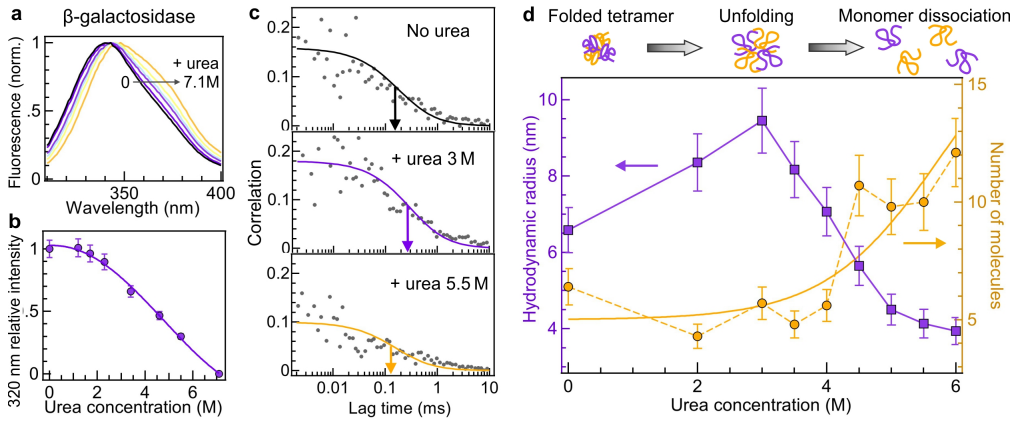

FIGURE 3.16 – Studying denaturation of β-galactosidase with Urea with single molecular resolution. Image is taken from Aleksandr BARULIN, ROY, J.-B. B. CLAUDE et al. 2022

In another study done on dyes in the visible regime as shown in Fig. 3.17, we could see that by tweaking the size of the horn antenna we can use it for red and green

laser excitation. The horn antenna outperforms the ZMW and the authors were able to perform high temporally resolved spectroscopy in a single molecule regime. In figure 3.17 a–c) Fluorescence time traces for the confocal reference showing typical bursts from diffusing single molecules with a binning time of 100 µs (a,b) and 10 µs (c). d–f) Same as (a)–(c) for the horn antenna. Alexa 647 concentrations are chosen to have a comparable average number of molecules detected by FCS in both configurations. The laser power is 200 µW. g) Histograms of the total number of photons per burst. The integration time in the confocal reference is 20 min while for the horn antenna, it is 30 s. h) Number of detected bursts per second as a function of the detection threshold for the configurations corresponding to (a) and (d). For further read refer TIWARI, ROY et al. 2023a

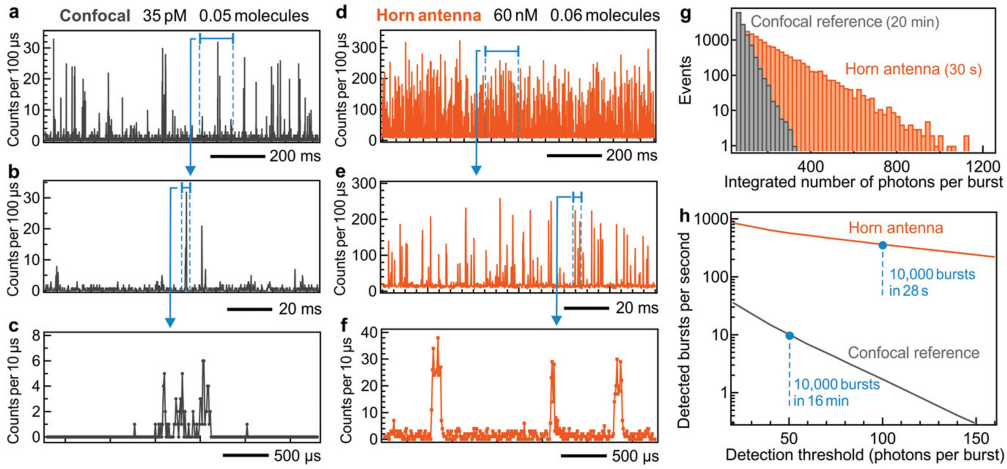

FIGURE 3.17 – Watching single molecule of Alexa 647 excited 633 nm bursts at 10 µs resolution thanks to the high fluorescence brightness from horn antennas.Image taken from TIWARI, ROY et al. 2023a

3.6 Conclusions

In this chapter, we saw that incorporating a reflector structure with ZMW can enhance the signal and keep the ingenious and simple features of ZMWs as well. The Horn antenna platform thus simultaneously provides plasmonic fluorescence enhancement, enhances fluorescence collection efficiency, attoliter volume, and strong background screening, giving an unprecedented protein autofluorescence signal for studying the dynamic process of protein without labeling. The Horn antenna is robust enough for protein spectroscopy measurements, as it can be used with slightly acidic to neutral solutions (pH-4 to pH-7) and salts thanks to its protective coating SiO_2 . With the help of the given configuration of the horn antenna, we were able to study proteins as small as Streptavidin (16kDa) with 24 tryptophan with single-molecule resolution; however, to reach the full potential of autofluorescence spectroscopy we need to reach a single protein with a single emitter (tryptophan). As we know, irrespective of advantages and usefulness, every technology has its own shortcomings

and limitations. The horn antenna platform is no different, the horn antenna has an intrinsically higher background signal (signal collected from cones when excited by a laser with buffer solution but no protein) than nanoaperture. The source of the background signal is mostly gallium ions embedded in a cone structure that originates in the fabrication stage; we will see a detailed analysis of the source of background in the subsequent chapter. Apart from the background signal, we believe we can use alternative techniques to make the horn antenna, as a multistage process makes the fabrication of the horn antenna time-consuming. In the next chapter, we will see how we can modify the experiment setup and use the high enhancement gain of cones to further enhance the SNR and reach the Uno-emitter-Uno-molecule level.

4 Reaching Ultimate Sensitivity down to a Single tryptophan level

Related Articles

Prithu ROY, Jean-Benoît CLAUDE et al. « Ultraviolet Nanophotonics Enables Autofluorescence Correlation Spectroscopy on Label-Free Proteins with a Single Tryptophan ». In : *Nano Letters* 23.2 (jan. 2023), p. 497-504. DOI : 10.1021/acs.nanolett.2c03797

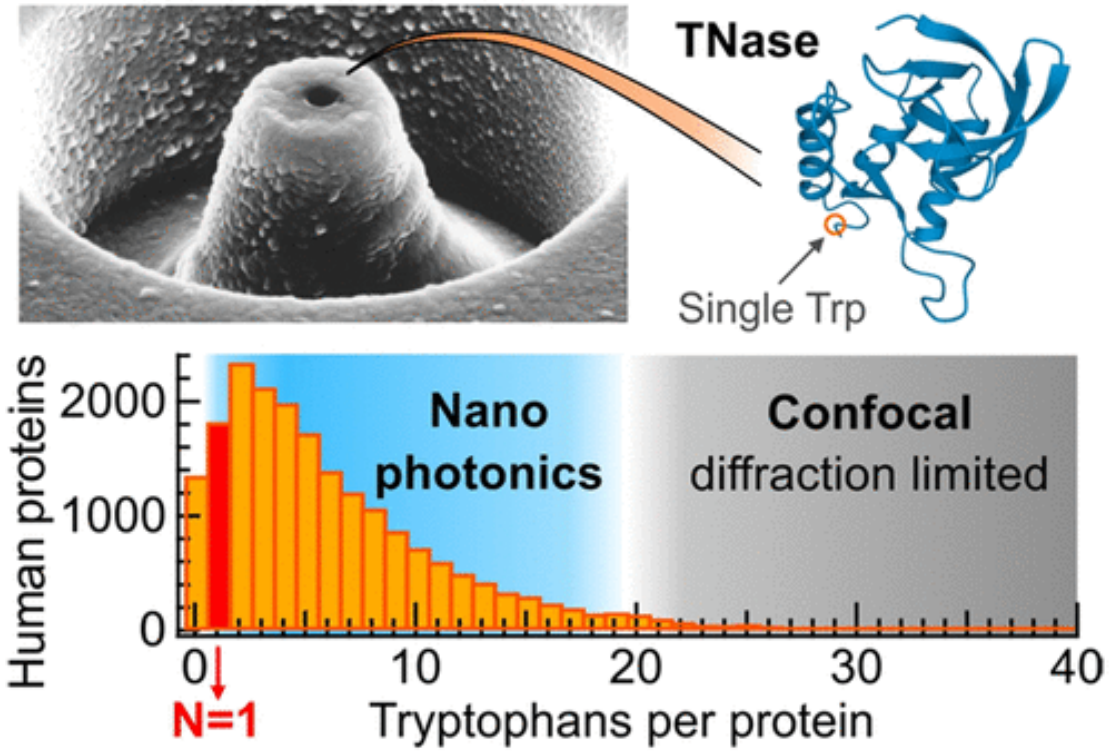

FIGURE 4.1 – Reaching single Trp sensitivity

Summary

4.1 Introduction

In previous chapters, we discussed how tryptophan, found in proteins, can be used for the analysis of label-free proteins. The primary challenge was the weak signal from proteins, which limited previous research on UV (auto)fluorescence correlation spectroscopy (UV-FCS) to large proteins with numerous tryptophan residues, such as -galactosidase (156 Trps), hemocyanin (148 Trps), phosphofructokinase oligomers (340 Trps), and protein amyloid fibrils (>500 Trps). Our horn antenna structure aims to address this problem and enhanced the signal 15 times giving us an unprecedentedly high signal from label-free Proteins. To date, the smallest proteins detected using UV-FCS are penicillin amidase (29 Trps) and streptavidin (24 Trps).

Unfortunately, tryptophan is one of the least abundant amino acids in eukaryotic proteins, which means that most proteins contain only a few Trp residues. An analysis of more than 20,000 human proteins in the UniProt database revealed that an average human protein contains around 7 Trp residues, and half of the proteins have between 1 and 5 Trp (Figure5.39). A mere 4%of human proteins contain more than 20 Trp residues. This indicates that to fully harness the potential of UV autofluorescence detection and examine a wide range of label-free proteins, UV-FCS sensitivity must be enhanced over an order of magnitude to reach the single tryptophan level.

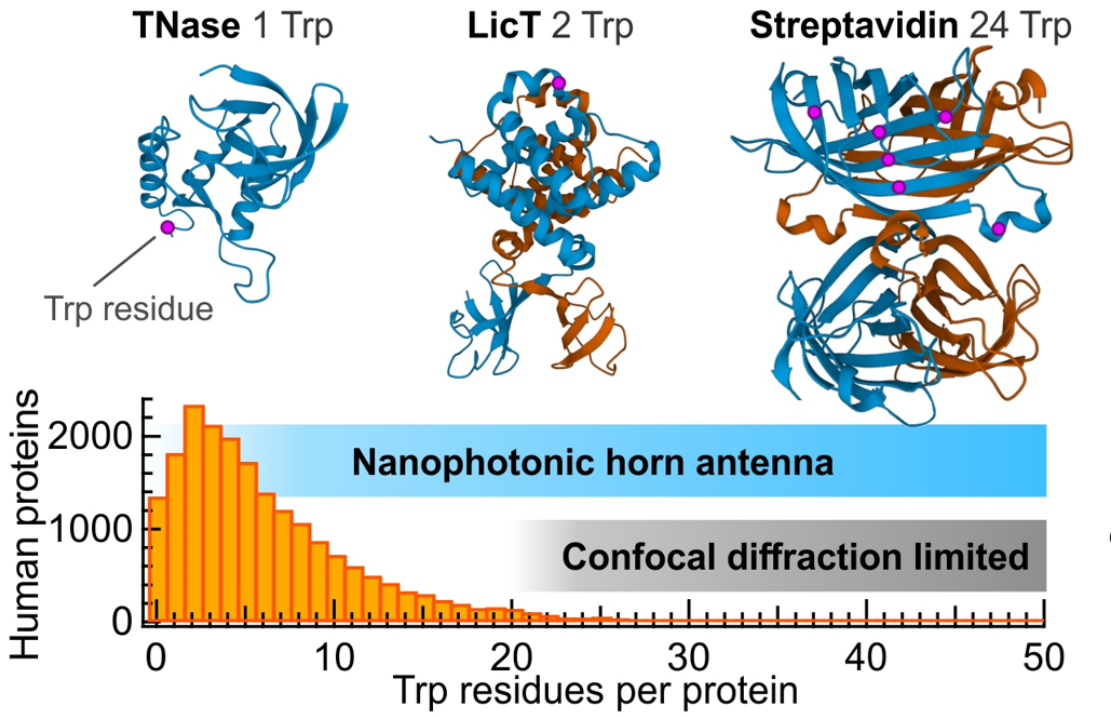

FIGURE 4.2 – Histograms of the number of tryptophan residues per protein extracted from a UniProt database of 20 399 reviewed human protein entries The top images show the 3D structures of the proteins used in this work, made using Mol* viewer, with tryptophan residues highlighted by magenta dots on selected monomers

To understand the motivation behind this chapter, we must first examine the fundamentals of detecting or sensing a signal. In order to sense or detect a signal, it is crucial to distinguish the important signal from other non-important or background signals received by the receiver. The way to improve this distinguishability is by increasing the signal strength and/or reducing the background signal.

In this chapter, we will tackle the challenge of enhancing sensitivity and demonstrate ultraviolet fluorescence correlation spectroscopy (UV-FCS) on label-free proteins containing a single tryptophan (Trp) residue. This is made possible through a combination of (i) a nanophotonic ultraviolet (UV) antenna (Horn Antenna) that boosts the signal, as discussed in the previous chapter, (ii) a detailed analysis to minimize background intensity, and (iii) the use of chemical photostabilizing agents to prevent fluorescence saturation. Our findings offer insight into how to expand plasmonics into the UV regimeZHAO, Z. LIN et al. 2021aKNIGHT, L. LIU et al. 2012TANABE, TANAKA et al. 2017 and further advance label-free single-molecule spectroscopy.

Previous studies using UV aluminum nanophotonics were limited to proteins with a large number of Trp residues, such as -galactosidase (156 Trp) and streptavidin (24 Trp). In this work, we have improved the sensitivity by more than an order of magnitude, down to the single tryptophan level. This significant achievement allows the UV-FCS technique to be applied to a vast array of proteins containing only a few Trp residues (Figure5.39).

4.2 Feasibility of FCS

The scientific community discusses enhancement and sensitivity in spectroscopy methods in general as a key figure of merit; in our previous chapters, we also emphasized enhancement factors and sensitivity. Typically, enhancement should be maximized, ranging from a two- to a three-fold increase in the UV spectrum and even higher in the visible spectrum. To accomplish this, additional components must be included in our spectroscopy methods, such as optical antennas
This raises the question of how much enhancement is sufficient and what level of sensitivity is required to efficiently analyze all target analytes with our chosen technique. The purpose of this section is to examine the feasibility of Fluorescence Correlation Spectroscopy for protein autofluorescence and determine the key changes we can make to attain the single Trp sensitivity

4.2.1 Numerical Simulation of FCS in different scenarios

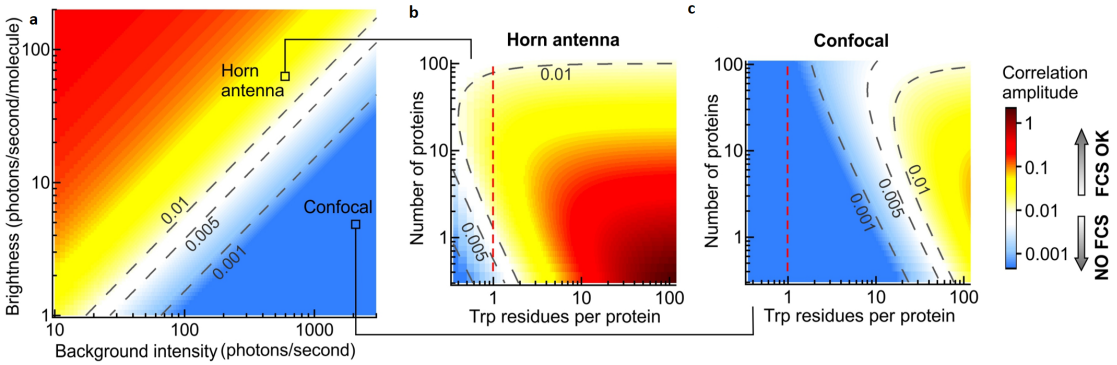

FIGURE 4.3 – (a) Calculation of the FCS correlation amplitude G(0) as a function of the background intensity B and the fluorescence brightness per molecule CRM. A constant number of N=5 proteins was assumed, each protein carrying a single tryptophan. All 2D maps in (a-c) share the same color scale. The lines at 0.001, 0.005 and 0.01 indicate the boundary threshold for possible FCS detection. Correlation amplitudes above 0.01 can be easily detected, while values below 0.001 are highly challenging, if not impossible to detect. (b,c) Calculations of the correlation amplitude for the horn antenna and the confocal case as a function of the number of tryptophan residues per protein and the number of diffusing proteins in the detection volume. The values for the background intensity and the fluorescence brightness per tryptophan residue are indicated by the markers in (a) and correspond to typical values in our experiments

To estimate the feasibility of the UV-FCS detection of proteins with a single tryptophan, we numerically compute the evolution of the FCS correlation amplitude G(0)

$$F = B + N * CRM \tag{4.1}$$

$$G(0) = (1 - \frac{B}{F})^2 \frac{1}{N} \tag{4.2}$$

as a function of the background intensity B, F the fluorescence brightness, CRM (Count Rate per Molecule) , the number of molecules N, and the number of Trp residues per protein (Fig. 4.3 Fig4.4). The ranges of values are taken to reproduce our experiments. We can see from the equation 4.2 that for a given number of molecules, the correlation amplitude quickly drops when the signal to background $\frac{N*CRM}{B}$ decreases due to the quadratic exponent in the$(1 - B/(B + N * CRM))^2$ term. We indicate on Fig4.3different minimum thresholds for possible FCS detection corresponding to the contours where G(0) amounts to 0.001, 0.005 or 0.01. Since there is no general consensus in FCS on defining this minimum threshold,ELSON 2013we decide to show three different values. FCS amplitudes above 0.01 should be easily detectable across various systems, while values below 0.001 pose significant challenges due to their proximity to electronic noise levels and residual background correlations. The results presented in Fig. 4.3(a) demonstrate that maximizing the signal-to-background ratio $\frac{N*CRM}{B}$ is essential to ensure the feasibility of UV-FCS experiments. We used typical values of UV autofluorescence brightness and background intensity, representative of our experiments, to calculate the predicted correlation amplitudes for the horn antenna (Fig. 4.3b) and the confocal setup (Fig. 4.3c). These calculations were based on the number of tryptophan residues per protein, assuming, for simplicity, that all Trp residues contribute equally to the autofluorescence signal. For the horn antenna, we found detectable correlation amplitudes above 0.01 for a single tryptophan, as long as the number of proteins in the detection volume ranged from 2 to 60 (Fig. 4.3b). This indicates that UV-FCS on a single tryptophan protein is feasible with the horn antenna. However, for the confocal reference, a single tryptophan consistently produces correlation amplitudes below 0.001 (Fig. 4.3b). In this case, increasing the number of proteins in the detection volume does not compensate for the lower signal-to-background ratio. For a realistic confocal UV-FCS experiment, the protein must have at least 20 Trp residues.
The (Fig. 4.3b) shows that even with the brightness enhancement brought about by the horn antenna, UV-FCS on a single Trp protein would be nearly impossible if the background intensity exceeds 2,000 counts/s.Reducing the background intensity is crucial for improving the sensitivity of UV-FCS.

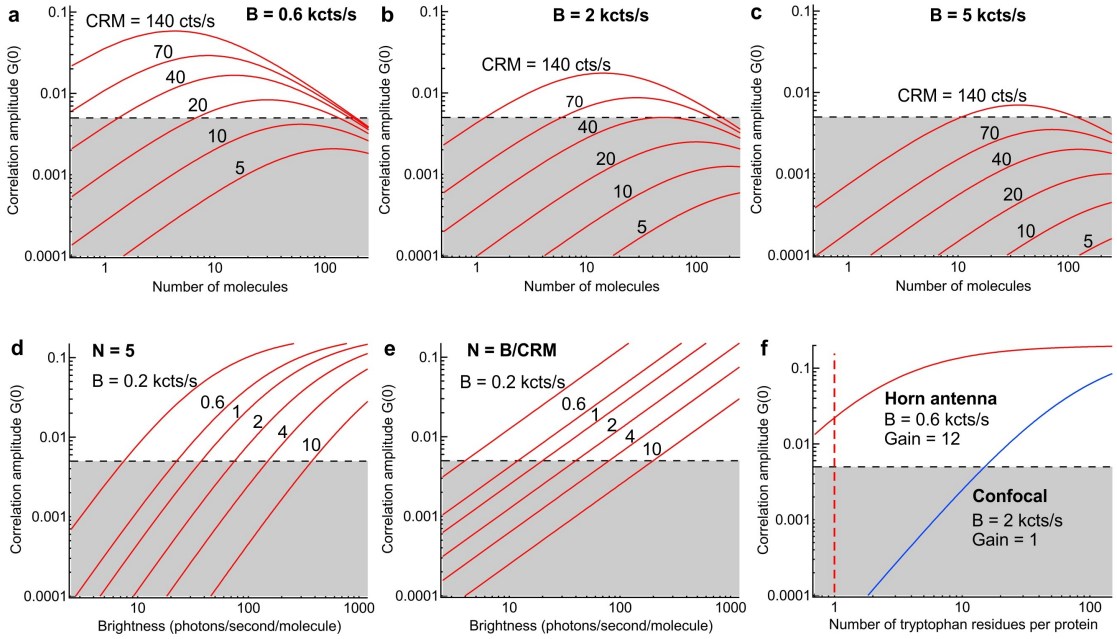

FIGURE 4.4 – Calculations results show that the background intensity plays a major role in determining the feasibility of UV-FCS experiments on label-free proteins.(a-c) Correlation amplitude as a function of the number of detected molecules N for different values of the fluorescence brightness per molecule CRM and background intensity B (as indicated on the graphs, these values are typical for the experiments performed here). The shaded area indicates correlation amplitudes below 0.005 which are highly challenging to detect with FCS due to the residual background correlation and the electronic noise.. (d) Correlation amplitude as a function of the CRM for different values of background B. For simplicity, the number of molecules is fixed to N=5. (e) Maximum $G_{max}(0)$ value at the optimum number of molecules $N = \frac{B}{CRM}$ corresponding to the highest correlation amplitude achievable for a given (B, CRM) set of values. (f)) Simulated correlation amplitudes as a function of the number of tryptophan residues for the cases corresponding to the horn antenna (red trace) and the confocal reference (blue).

To understand how the background plays a crucial role in deciding the feasibility of FCS for a given protein in UV we analyze some examples given In figure 4.4 and see how the evolution of background set limits to sensitivity of the FCS experiment.
The FCS correlation amplitude is given as equation 4.2 In equation 4.1'F' is the total detected intensity in presence of the fluorescent molecules. CRM denotes the average fluorescence brightness per molecule (count rate per molecule). In the simulation, we define the threshold of G(0) = 0.005 as a minimum amplitude for possible detection. This definition is an arbitrary choice, as discussed in the previous section any value in the range of 0.001-0.01 would be realistic. As a consequence of the low signal-to-background ratio, the G(0) dependence with N is more complex than just the classical

$\frac{1}{N}$ rule. For low N values, the background term is given by

$$(1-\frac{B}{F})^2 = (1-\frac{B}{B+N*CRM})^2 \tag{4.3}$$

thus it plays a major role and the correlation amplitude increases when the number of molecules grows. For large N values, the background term is not so influential, and we retrieve the $\frac{1}{N}$ dependence leading to a decrease of G(0) when N grows. It can be shown that the correlation amplitude G(0) reaches its maximum when the number of molecules amounts to $N = \frac{B}{CRM}$. In that case, the maximum amplitude is $G_{max}(0) = \frac{CRM}{4B}$. The calculations result throughout4.4 (a-e) show that the background intensity plays a major role in determining the feasibility of an FCS experiment at a given brightness CRM. For the range of brightness between 10 and 100 counts/s/molecule typically achievable in our experiments, the background intensity must remain below 2-3 kcts/s to yield a detectable FCS correlation. In Figure4.4(f) The total number of proteins is set to N=5 and we assume a constant brightness of 5 counts per second for each tryptophan residue, which is typical for our UV microscope. We also assume a gain of 12 brought by the presence of the horn antenna, which enhances the tryptophan brightness to 12*5 = 60 counts per second. The graph in (f) shows that the detection of a protein with a single tryptophan is feasible with the horn antenna, while for the confocal case, at least 20 tryptophan residues per protein are needed to yield a detectable FCS correlation amplitude.

4.2.2 Evolution of Signal-to-Noise Ratio of FCS in presence of Background

In this section, we delve into mathematics to derive the formulae for signal-to-noise ratio equation in the presence of a background signal. The signal-to-noise ratio SNR in an FCS experiment is commonly defined by $SNR = \frac{G(0)}{\sigma(G(0))}$ where$\sigma(G(0))$ is the standard deviation of the correlation amplitude G(0). Following Koppel's seminal work about statistical accuracy in FCS,D. E. KOPPEL 1974 the SNR is generally derived from Eq. (40) in D. KOPPEL 1974 as $SNR = CRM\sqrt{(T_{tot}\Delta\tau}$, where CRM denotes the fluorescence brightness (detected photons per second and per molecule), T_{tot} the total integration time and$\Delta\tau$ the minimum lag time defining the time interval for computing the correlation. Note that Koppel's Eq. (40) contains a denominator taking the form $(1+4CRM\Delta\tau+2CRM^2\Delta\tau\tau_d)^{1/2}$ where τ_d is the diffusion time. However, in practice, the correction introduced by this denominator is small and can generally be neglected. Note also that an extra term $1/\sqrt{(1+1/N)}$ can be introduced to account for a possible low average number of molecules in the detection volume 14 (Koppel's formula assumes $N1$).] It is important to stress that the generally used formula$SNR = CRM\sqrt{(T_{tot}\Delta\tau)}$ does not consider the presence of background.D. KOPPEL 1974In the presence of an extra background intensity B (counts per second) on the detector, the SNR expression must be modified. Combining Koppel's Eq.(40), FLAURAUD, REGMI, WINKLER et al. 2017a and ORTEGA ARROYO, COLE et al. 2016a in ref D. KOPPEL 1974

and using our notations, the signal-to-noise ratio in FCS in presence of background can be expressed as :

$$SNR = \frac{(CRM(SBR/(1+SBR))\sqrt{(T_{tot}\Delta\tau)})}{(1+4CRM\Delta\tau\frac{SBR}{1+SBR}+2CRM^2(\frac{SBR}{1+SBR})^2\Delta\tau_d)^{1/2}} \tag{4.4}$$

In the presence of background, this equation includes an additional term$(SBR/(1+SBR))$ where $SBR = (N*CRM)/B$ is the signal-to-background ratio. In practice, the denominator in above Eq. can often be neglected so that the simplified expression for the SNR with background becomes

$$SNR = CRM\frac{SBR}{1+SBR}\sqrt{(T_{tot}\Delta\tau)} = CRM(1-B/(B+N*CRM))\sqrt{(T_{tot}\Delta\tau)} \tag{4.5}$$

For large signal-to-background ratios, one retrieves Koppel's established formula, while for very low SBR values, signal-to-background becomes a linear prefactor that reduces the SNR. In our UV-FCS experiments with the horn antennas, our typical values are CRM = 70cts/s, B = 600 cts/s, N = 3 to 14 molecules,T_{tot} = 90 s,$\Delta\tau$= 10 µs. This gives signal-to-background ratios between 0.35 and 1.6, and signal-to-noise ratios between 0.5 and 1.3. In the confocal case, using CRM = 8 cts/s, B = 2000cts/s, N = 10 molecules, T_{tot} = 90 s $\Delta\tau$= 10μs, the signal to background becomes 0.04 and the signal to noise is less than 0.01, preventing any possible experiment. Increasing the integration time to 1 hour and the minimum lag time to 100 μs, improves the SNR to 0.18, yet this low value shows that any confocal UV-FCS experiment on a single Trp protein would remain a highly challenging task. Lastly, we point out that maximizing the SNR should not be the only consideration. As Koppel already pointed out, another constraint is that G(0) must remain much greater than the residual background correlation amplitude ρ_B : "If this is not much greater than [ρ_B], the experiment is in trouble" (D. E. KOPPEL 1974 page 1944). In our antenna experiments, we have ρ_B=0.01, while our different signal correlation amplitudes range from 0.022 to 0.04 (Fig. 4.14-4.13), satisfying the condition $G(0) > \rho_B$.

The SNR formula can be used to predict the feasibility of a UV-FCS experiment and provide guidelines to establish the experimental conditions. Taking into account the case of free tryptophan molecules in solution (quantum yield 12%, expected brightness in the antenna 30 counts/s), the small molecular mass of 0.2 kDa implies a diffusion time below 10 µs imposing to set$\Delta\tau$ in the microsecond range. Under current conditions with 20 molecules in the antenna, the predicted SNR for free tryptophan is 0.2, which remains too low to yield relevant FCS data. However, if with further work the background can be further reduced to 200 counts/s, and if the diffusion can be slowed down without introducing some photopolymerization artifacts, then UV-FCS on free tryptophans would become within the experimental range.

4.3 Understanding the Background Signal

In the previous section, it was established that the key to achieving single-molecule, single-emitter sensitivity was established in reducing the background signal. Therefore, to eliminate the background signal, it is crucial to identify and characterize the sources of background in our measurements, examining both their spectral and temporal responses.

4.3.1 Source of background signal

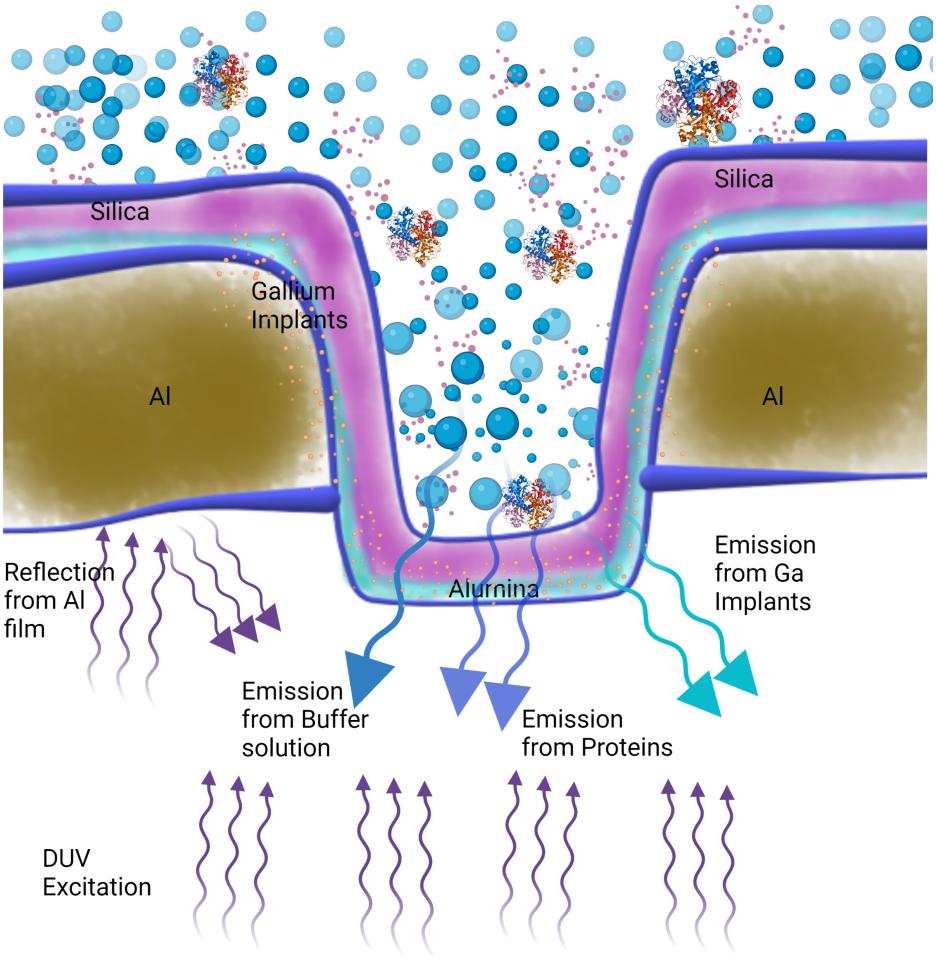

FIGURE 4.5 – Schematics of Source of signal inside ZMWs

In Fig4.5 we can see a schematic of nanoholes with different features and analyte solution (buffer+ protein). When excited by UV light there are multiple sources of emitted light that can be collected, first, the reflection from the $Al - SiO_2$ layer is more or less constant for different samples and scales with the power of the laser source. To some extent, this background signal is filtered out by a high-pass filter in the collection

path before the detectors. The filters attenuate signals lower than 310 nm. The second source is emission from the buffer solution; as we know Deep-UV can make most organic compounds fluoresce, and thus the buffer is also a source of background (unnecessary signal).

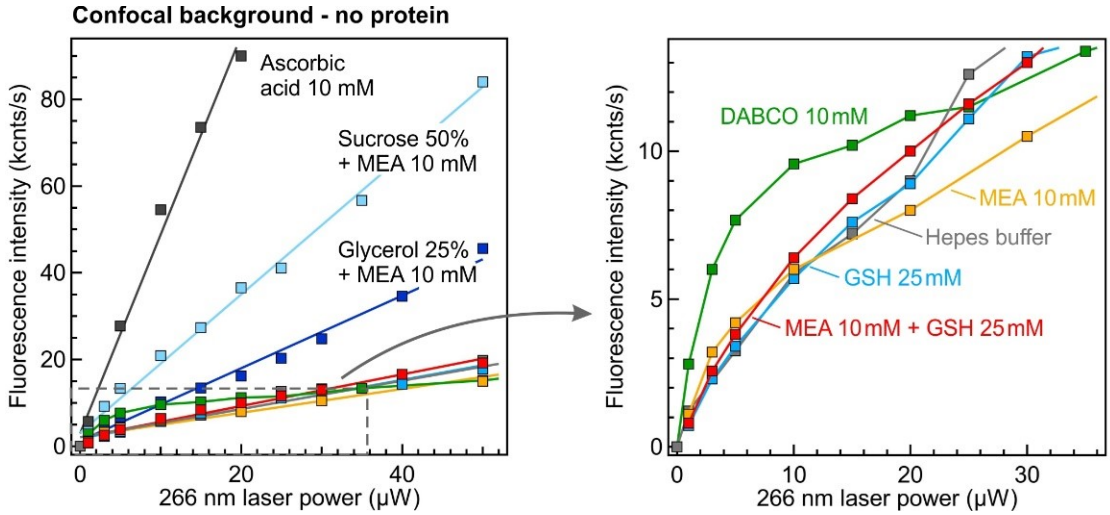

FIGURE 4.6 – Background intensity for the confocal microscope (without horn antenna).

In our previous work as well as in the literature, ascorbic acid is frequently used as an antioxidant; however, Ascorbic acid produces a high background intensity and is discarded as a reducing agent. MEA and GSH do not show a significantly higher background intensity than the normal buffer. The impurities present in sucrose and glycerol contribute significantly to the increase in background; therefore, we have discarded their use to increase the viscosity of the buffer. An alternative solution to increase buffer viscosity is the use of PEG400MONGIN, GOLDEN et al. 2016, which gives lower background photoluminescence in UV compared to sucrose or glycerol. We will discuss the merits of PEG400 in more detail in subsequent chapters. Its worth noting that the effective volume of nanoholes is in Femto to Atto liters so the total contribution of buffer to the overall background in the nanohole exists but is not the most significant one. The third and most worrisome(significant) source of background is gallium implants in the nanohole (mostly the implants in the base of nanoholes are significant). The gallium implants occur because of the use of the gallium-ion beam milling technique used to mill the nanostructure. These gallium implants infused with Alumina and Al form different kinds of alloys which are luminescent on UV excitation. To add to the misery, these gallium implants have an emission band that overlaps with the emission of tryptophan or tyrosine amino acids. Let us dive in to explore a detailed analysis of these background sources

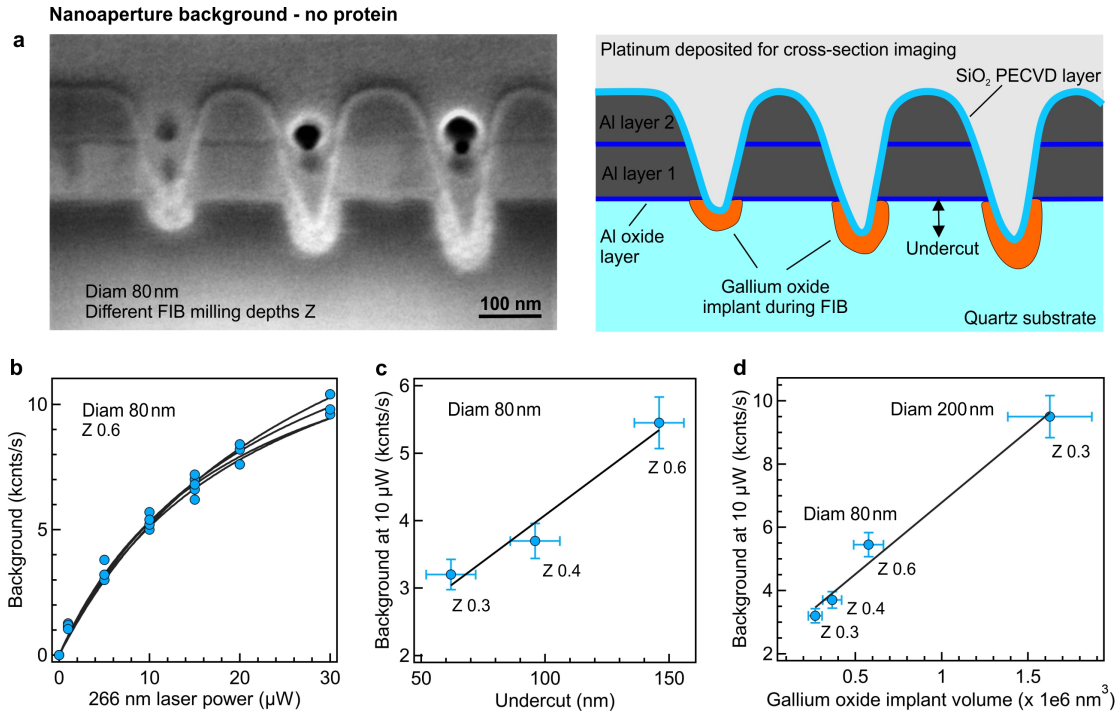

FIGURE 4.7 – (a). Cross-cut scanning electron microscope(SEM) image of nanoapertures milled with different depths Z. The sample was filled with platinum for better side view imaging, cut by FIB up to half of the aperture, and tilted 52 ° to enable a cross-cut view of the nanoaperture profile. The scheme on the right is a guide to understanding the SEM image. (b) Background intensity from a single nanoaperture as a function of the 266 nm laser power. (c) Evolution of the background intensity with the undercut depth for single apertures milled with different Z-parameter conditions (the Z-parameter is the input used by our FEI DB235 focused ion beam system). (d) Assuming a uniform thickness of 20 nm for the FIB gallium oxide implant, we compute the total volume of the gallium oxide implant and plot the background intensity as a function of this volume for 80 nm apertures and 200 nm apertures with different milling depths.

Figure 4.7 shows an SEM image of nanoapertures milled with different depths Z. Due to the FIB milling process, the region at the bottom of the nano aperture is enriched in gallium, forming different alloys with the quartz SiO2 substrate, notably the gallium oxide Ga2O3, which is UV photoluminescent. The middle aperture corresponds to the configuration used to mill the central aperture of the horn antenna in this work, using a 60 nm deep undercut into the quartz substrate to maximize signal enhancement. The aperture on the left is not fully milled, leading to a degradation of the signal. The background intensity from a single nanoaperture varies nonlinearly and seems to saturate as a function of the 266 nm laser power, shown in fig4.7 b . The different data points correspond to different nanoapertures milled with the same conditions. The black lines are numerical fits using a fluorescence saturation model $A * P_{laser}/(1 + P_{laser}/P_{sat})$. The saturation indicates that the background is mostly

photoluminescence, as scattering and back reflection scale linearly with the excitation power. The linear relationship between the total intensity of the background and the volume of the gallium implanted region confirms that gallium implantation during FIB is the main source of background in our system. We have tried to further reduce this background by annealing at 400 ° C or photobleaching with prolonged illumination with UV light, but both were unsuccessful.

4.3.2 Reduction of Background using filters

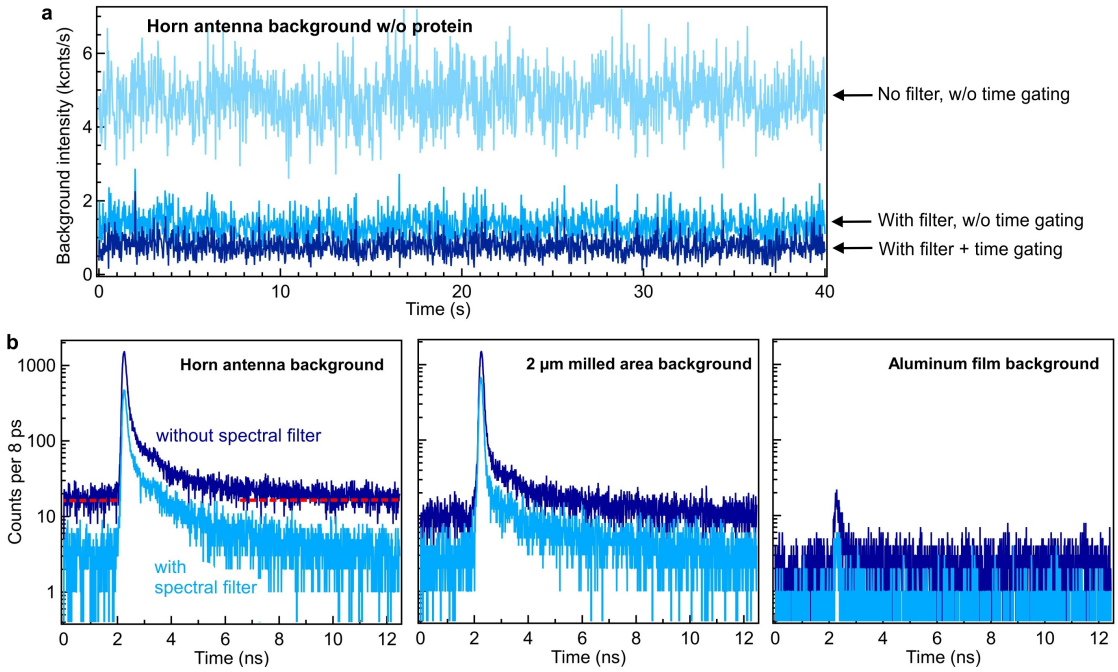

FIGURE 4.8 – (a) Background intensity was recorded on a single horn antenna with 10 µW average excitation power with and without spectral filtering and time gating. (b) Time-resolved TCSPC photon arrival time histograms respective to the 80 MHz synchronization signal from the pulsed laser. All histograms are sampled into 8 ps time bins and are integrated over the same 20 s duration so that the intensities on the left axis can be directly compared across the different curves. Dark blue traces correspond to the background without any spectral filter while light blue traces are with the 310-360 nm bandpass filter.

As visible in figure4.8 the background intensity of the horn antenna differs significantly from that recorded on the plain aluminum film, indicating that back-reflection from the laser and residual luminescence from the quartz substrate and aluminum layer are not the main sources of background. Instead, the background of the horn antenna closely mirrors the background observed at the center of a 2 µm diameter aperture, where only photoluminescent gallium oxide implanted during FIB

remains and no aluminum is illuminated. Pure heavy water was used to minimize the background of the solution in this experiment.

Without the spectral filter, the horn antenna background TCSPC histogram displays a baseline of approximately 15 counts per 8 ps binning, which corresponds to an average intensity of 1.2 kcnts/s. This baseline represents a photoluminescence with a lifetime much longer than the 12.5 ns period of the laser pulses, causing the photoluminescence photons' arrival time to appear uncorrelated with the laser pulses synchronization signal. The spectral filter significantly reduces this baseline, suggesting that most of the baseline photoluminescence occurs outside the 310-360 nm region, as anticipated for gallium oxide photoluminescence. A similar baseline is also observed in the 2 µm wide FIB-treated area where the aluminum layer has been completely removed and gallium oxide has been implanted.

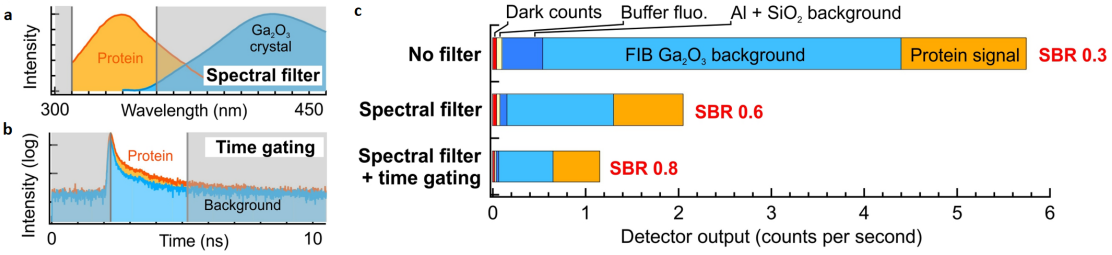

FIGURE 4.9 – Strategies to improve the signal-to-background ratio (SBR) by spectral filtering and time gating. The protein data correspond to 8 µM TNase solution in the horn antenna (6 proteins in the detection volume). The gallium oxide photoluminescence spectra is taken from BINET et GOURIER 1998. (c) Experimental background intensity and total signal (8 µM TNase solution) in the horn antenna upon spectral filtering and time gating

As discussed earlier and seen in Experiments performed on different samples milled by focused ion beam (FIB) that the implantation of gallium oxide resulting from the FIB process is the major source of background in the horn antenna. Gallium oxide is luminescent when excited in the UV. This background contribution can be controlled by FIB while selecting the proper milling depth. Moreover, the gallium oxide luminescence spectrum is shifted toward 400 nm and can be partially separated from the protein autofluorescence spectra with the 310-360 nm bandpass filter (Fig4.9 a). The gallium oxide photoluminescence contains a long lifetime component, significantly longer than the 12.5 ns laser repetition period . Temporal gating to select the photon arrival time in a 3 ns window immediately after the excitation pulse further reduces the background intensity without losing too much of the protein signal (Fig. 4.9 b). The 3 ns window is chosen to correspond to approximately 3× the tryptophan fluorescence lifetime for the different proteins used here in the horn antenna. Altogether, the combination of spectral filtering with temporal gating reduces the background intensity by 7× and improves the signal-to-background ratio by 2.7× (Fig. 4.9c) opening the possibility for single Trp detection

4.4 Experimental result on protein

So far, we have discussed ways to enhance the signal and reduce the background signals, thus boosting the SNR ratio. In this section, we will put that work into practice and show how effective the technique was in detecting proteins with single tryptophan at single-molecule levels.

4.4.1 Optimization of buffer for Proteins

Prior to beginning our journey of protein detection with our optimized setup, we had to address the buffer used to stabilize the protein. The buffers that were already known and used in literature were effective in preserving the proteins under UV exposure; however, the buffer fluorescence in UV and their reaction catalyzed by UV light limit our sensitivity. As illustrated in Figure 4.6, some popular buffers such as ascorbic acid contribute significantly to the background, which we were trying to avoid. Additionally, we found that the extensively used buffer combination of GODCAT (glucose oxidase and catalase enzymes) with glucose not only gave a high background signal but also polymerized under UV light, thus affecting the overall experiment. The polymerized product could sometimes block the nanoaperture and reduce the signal collected. We needed to investigate different combinations of buffers that have low background levels, but still do the job. We must consider what the buffer is expected to do, which is stabilize proteins in UV, prevent aggregation during storage, and most importantly, reduce the radical state. To understand why the right choice of buffer is so important, we must look at the equation of fluorescence enhancement (Equation 5.1). We need to focus on the term Γ^*_{loss}, which encompasses the effect of non-radiative rates Γ_{nr}. In simpler terms, the higher the Γ_{nr}, the lower the brightness we can achieve. Reactive oxygen species (ROS) are one of the many components that can increase Γ_{nr}, leading to loss in the system. Due to the finite lifetime of the fluorecent emitter the fluoresence brightness per molecules does not increase linearly with excitation power but rather saturates to certian value. To understand this phenomenon, let us see the equation of excited state S_1 in the Jablonski diagram in figure4.10(e). The model is well defined in literature ENDERLEIN et ZANDER 2003

$$S_{1eq} = N_{tot} \frac{\frac{\Gamma_{ex}}{\Gamma_0}}{1 + \frac{\Gamma_{ex}}{\Gamma_0}(1 + \frac{\Gamma_{isc}}{\Gamma_t} + \frac{\Gamma_{ox}}{\Gamma_{red}})} \tag{4.6}$$

where N_{tot} is the total molecule in the detection volume,Γ_{exc} is the excitation rate constant, Γ_0 is the deexcitation rate constant,Γ_{isc} is the intersystem crossing rate constant, Γ_{ox} is the photooxidation rate constant and Γ_{red} is the reduction rate constant. In our case, radical state buildup and intersystem constant have an order smaller rate constant and are thus ignored in the further calculation for simplicity.

The saturation for emitter occur when

$$\Gamma_{sat} = \Gamma_{exc} = \frac{\Gamma_0}{(1 + \frac{\Gamma_{isc}}{\Gamma_t} + \frac{\Gamma_{ox}}{\Gamma_{red}})} \tag{4.7}$$

All of this to say that the Γ_{ox} and Γ_{red} affect the saturation rate constant and the maximum fluorescence emitted from the protein at the saturation power. Therefore, to get the photon from the protein molecule, we need to increase Γ_{red} and/or decrease Γ_{ox}. To understand how to achieve this feat, we need to understand the source of the radical state. The radical states are due to the contribution of ROS.

From the above discussion, it seems apparent that we needed a buffer with low background fluorescence and the capability to neutralize the ROS in the system. In the figure4.10(a) The total fluorescence intensity gathered from the confocal volume, as a function of the 266 nm laser power, was studied for an 8 µM TNase solution with different chemical agents (MEA mercapto ethylamine or cysteamine; GSH glutathione; AA ascorbic acid; DABCO 1,4-diazabicyclo[2.2.2]octane). The idea was to understand which buffer combination will give the highest signal at the saturation power. Oxygen plays a major role in reducing triplet buildupAleksandr BARULIN et Jérôme WENGER 2020b, however, the chemical technique implemented earlier in our group and literature to remove oxygen using oxygen scavenger leads to undesirable background correlation thus we use simple oxygen removal via degassing with argon (detailed in the method section). In the case of TNase removal of oxygen did not significantly alter TNase results, so we let the oxygen dissolved in the buffer solution remain unchanged for TNase experiments. In figure4.10 (b, c) the TNase fluorescence intensity evolution was analyzed for various GSH concentrations along with the associated fluorescence lifetime decays to understand the evolution of photochemistry of the proteins. The GSH concentrations in the 5-25 mM range moderately enhance signal intensity by increasing quantum yield, fluorescence lifetime, and excitation power leading to saturation. This suggests a reduction in nonradiative decay rate and radical state buildup. However, higher GSH concentrations result in a signal decrease, possibly due to GSH-TNase complex formation and/or tryptophan singlet excited state quenching by concentrated GSH. We also found that adding a combination of MEA-GSH was more effective than using a high concentration of either of them. The GSH and MEA are well-documented antioxidants and are used for ROS neutralization. They are known as singlet oxygen-radical hydroxyl scavengers (CAMPOS, J. LIU et al. 2011). The mechanism involved is well studied in WINTERBOURN 2012 TOWNSEND, TEW et al. 2003NAUSER, KOPPENOL et al. 2005(we will explore this phenomenon in subsequent chapter)

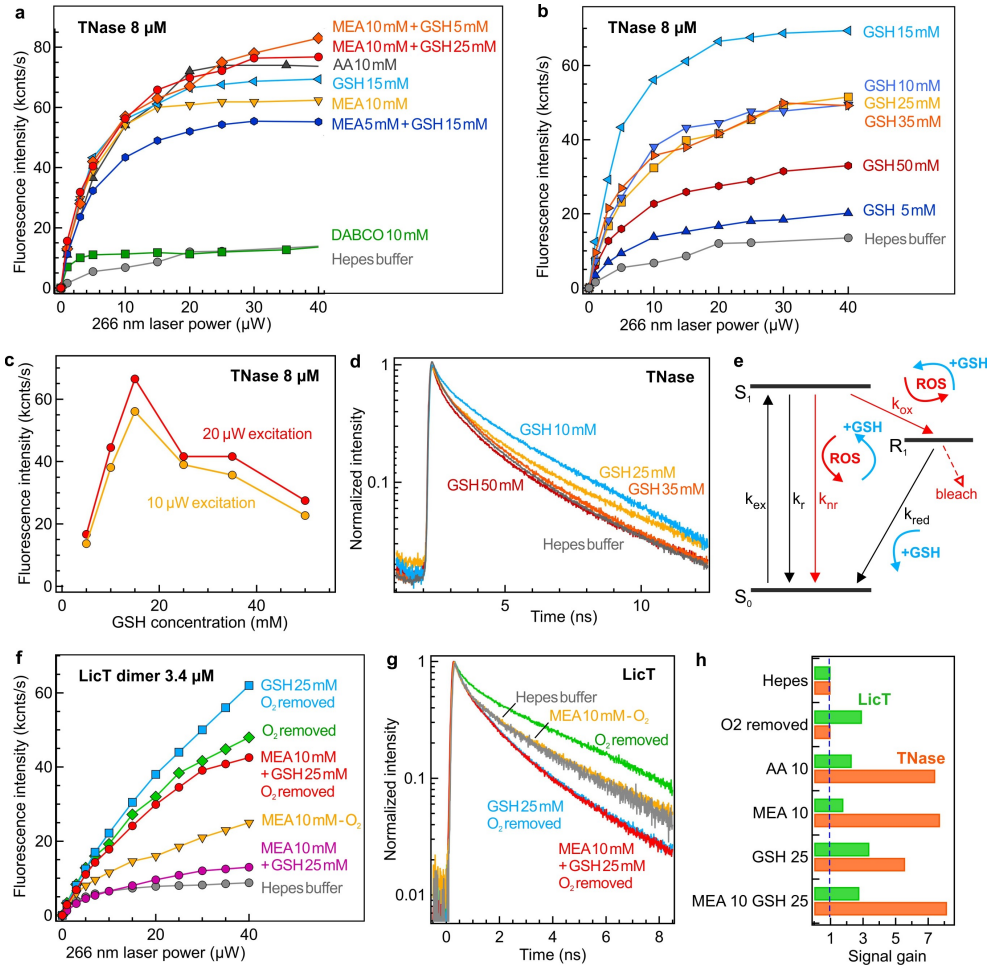

FIGURE 4.10 – (a) Total fluorescence intensity collected from the confocal volume as a function of the 266 nm laser power for a 8 µM TNase solution in presence of different chemical agents. (b,c,d) Evolution of the TNase fluorescence intensity for different GSH concentrations and the associated fluorescence lifetime decay.(e) Simplified Jablonski diagram of the ground state S0, the singlet excited state S1 and the radical state R1 (the triplet state is omitted for simplicity,(f,g) Evolution of the fluorescence intensity for different GSH concentrations and the associated fluorescence lifetime decays for LicT proteins.. (h) Signal gain at 10 µW power for TNase and LicT in presence of different antifading compositions as compared to the hepes buffer reference

In figure4.10(e) A simplified Jablonski diagram depicts the ground state S0, the singlet excited state S1, and the radical state R1 with different rate constants. The Reactive oxygen species (ROS) production through UV illumination (TERESA, PETERSEN et al. 2012 Aleksandr BARULIN et Jérôme WENGER 2020b)promotes nonradiative decay and oxidation rates. Adding antioxidants like GSH or MEA neutralizes ROS's negative effects and may encourage reduction from R1 to S0. However, GSH concentrations above 25 mM tend to increase nonradiative decay Γ_{nr} and quench fluorescence. A similar analysis was performed for LicT proteins as in figure4.10 (a, d). Here, oxygen

removal using argon degassing proved beneficial, enhancing signal linearity and delaying saturation onset. Oxygen removal also tends to increase fluorescence lifetime and promote quantum yield. However, the addition of reductants (MEA, GSH) further reduces fluorescence lifetime without significantly altering the total detected intensity. The Signal gain at 10 µW power for TNase and LicT was examined in the presence of different antifading compositions compared to the hepes buffer reference. For LicT, oxygen was removed by argon degassing, while for TNase, oxygen dissolved in the buffer was maintained, as it did not significantly impact results.
Finally, for FCS experiments with horn antennas, we used 10 mM MEA and 25 mM GSH with and without oxygen for TNase and LicT, respectively. Our data reveals that moderate MEA and GSH concentrations (5-25 mM range) improve autofluorescence intensity linearity with excitation power and increase autofluorescence intensity and lifetime. These characteristics correspond to a reduction in nonradiative decay rate and radical state buildup, which we associate with ROS neutralization by antioxidants. We also found that the oxygen scavenger system GODCAT generated too high a background for our objectives and was susceptible to photopolymerization issues in the nanoaperture.

4.4.2 Detection of proteins with Single tryptophan

In this work, three different proteins are investigated : thermonuclease staphylococcal nuclease (TNase) from Staphylococcus aureus, transcription antiterminator protein (LicT) from Bacillus subtilis, and streptavidin from Streptomyces avidinii (Strep). TNase is a monomer that contains a single Trp residue, LicT is a homodimer with a total of 2 Trps on the protein dimer, and streptavidin is a homotetramer with a total of 24 Trps. TNase was selected because its single Trp residue was theoretically predicted CALLIS et T. LIU 2004 to have a quantum yield of 28%in good agreement with ensemble spectroscopy measurements. TNase is also widely studied as a model system in protein chemistry.COTTON, HAZEN et al. 1979,NAKANO et FINK 1990. LicT was selected for its UV signal being comparable to TNase and its availability in purified form labeled with Cy3B to serve as a control using visible fluorescence spectroscopyCLERTE, DECLERCK et al. 2013AIT-BARA, CLERTÉ et al. 2017. Streptavidin was selected due to its higher number of Trp, large availability, moderate mass, and good water solubility. The experimental results presented in Figure 4.11 aimed to achieve greater sensitivity in UV fluorescence correlation spectroscopy (UV-FCS) down to the single tryptophan level.

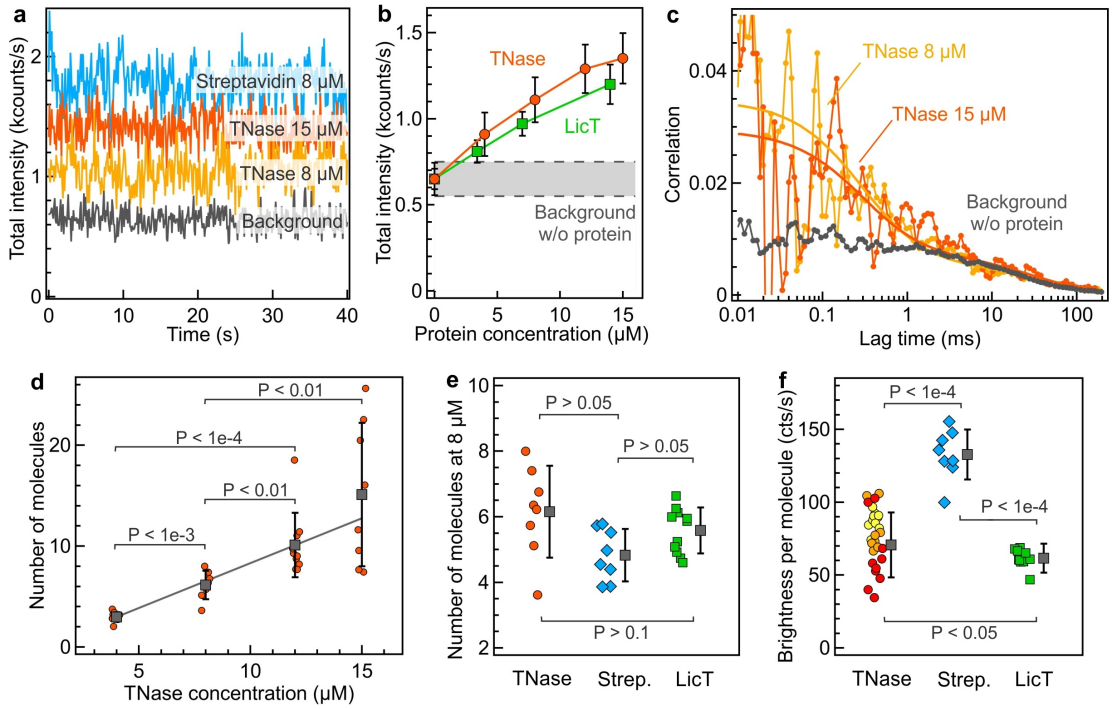

FIGURE 4.11 – Label-free UV-FCS on proteins with a single tryptophan residue enabled by UV horn antennas. (a) Fluorescence time traces and background intensity after spectral filtering and time gating for a single UV horn antenna with different proteins and different concentrations. (b) Fluorescence intensity increase with the protein concentration. The shaded area indicates the background level ± 2 times the standard deviation of the background intensity. (c) FCS correlation traces were recorded with the horn antenna for two TNase concentrations. The background correlation is shown in gray, it corresponds to the FCS correlation obtained in the same experimental conditions in the absence of a protein target. (d) The number of TNase proteins determined by FCS in the horn antenna as a function of the TNase concentration. Statistical T-tests have been performed to compare the distributions in (d-f), and the resulting p-values are written on the graphs for each pair of distributions. In (d-f), color markers represent individual measurements, gray squares represent the average ± one standard deviation. (e) Comparison between the numbers of proteins detected by FCS for three different proteins at the same 8 µM concentration. (f) Fluorescence brightness per molecule CRM determined by FCS for the different proteins.

The linear dependence of total intensity on TNase and LicT protein concentrations (Fig 4.11a,b) confirms the sensitivity of our experiments to the autofluorescence signal of proteins, even those with only one or two Trp residues. The number of detected proteins N and their autofluorescence brightness CRM were extracted by computing and fitting the UV-FCS signal (Fig. 4.11c, 4.144.14), using methods described in the literature. Even in the absence of any protein sample, residual background correlation(gray trace in Fig. 4.11c) was detected from the horn antenna filled with buffer solution(note : this background correlation rising from our optimized buffer is

comparatively weaker than the likes of GODCAT or Ascorbic acids which is quite extensively used in literature) . This background correlation appeared on all our traces with a long characteristic time above 50 ms and an amplitude below 0.01 (Fig. 4.13-4.14), indicating a possible origin related to remaining mechanical vibrations or electric noise on our microscope. However, the significant difference in characteristic correlation time between this background and protein diffusion time enables clear separation of their contributions in the FCS signal, allowing recovery of the contribution from the diffusing proteins. Additionally, the correlation amplitude related to the protein was always at least twice as large as the residual background correlation. As seen in results of fig 5.26In the absence of spectral filtering and time gating, the correlation amplitude found with the TNase protein fell to 0.002 and was no longer distinguishable from the background. The results for both TNase and LicT were consistent with numerical calculations where the experimentally determined parameters for the background intensity B and the autofluorescence brightness CRM were used to predict the observed correlation amplitudes in accordance with our model (Fig.4.15).

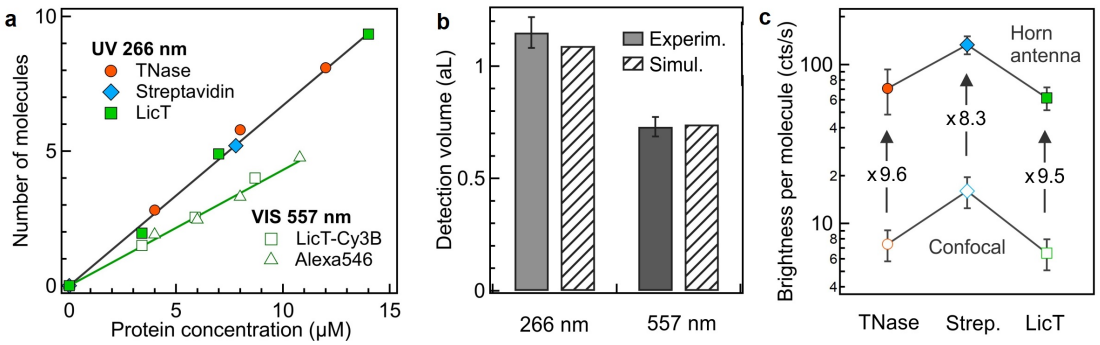

FIGURE 4.12 – (a) The average number of molecules measured by FCS in the horn antenna as a function of the concentration for the three different proteins in the UV (color markers, the black line is a fit). Empty markers show the numbers of molecules determined by FCS using Alexa 546 and Cy3B fluorescent dyes at 557 nm excitation. The slope of the lines is proportional to the detection volume, which is shown in (b) for both UV (266 nm) and visible (557 nm) laser excitation. Numerical simulations of the detection volume (patterned area) confirm the FCS results. (c) Fluorescence brightness per protein in the horn antenna as compared to the confocal reference for the three different proteins. The data points for the horn antenna correspond to the average CRM determined by FCS. To determine the number of molecules for the confocal data, we assume a 1.8 fL confocal volume on our UV microscope.

We further explored the data and check the robustness and correctness with a well-known statistical model, the Figure 4.11 d-f presents a comparison of the statistical distributions of UV fluorescence correlation spectroscopy (UV-FCS) results for different proteins and horn antennas. It was observed that the number of TNase molecules detected through UV-FCS had a linear relationship with protein concentration (Fig. 4.11d). Additionally, statistical T-tests were performed to confirm the

differences between data distributions. However, when probing similar concentrations of different proteins, the T-tests showed p-values above 0.05, indicating that the number of molecules could not be clearly distinguished (Fig.4.11 e). The brightness of fluorescence was found to be different between TNase, streptavidin, and LicT (Fig. 4.11f). Nonetheless, the UV autofluorescence brightness did not scale linearly with the number of Trp residues due to the presence of nearby amino acids that could quench Trp emission by charge or energy transfer. The experimental results were in good agreement with the estimated brightness for streptavidin, which was 1.9 ± 0.7 times higher than that of TNase. No sign of photobleaching was observed during the experiments.

The UV-FCS average number of molecules is plotted in Fig. 4.12a as a function of the protein concentration for the different proteins used in this work. We find that the different datasets follow the same line whose slope is proportional to the size of the detection volume. Experimentally, we determine a detection volume of 1.15 ± 0.07 attoliter($10^{-18}L$), in good agreement with the numerical simulations (fig 4.16). To further validate the UV-FCS data, the same 80 nm apertures in aluminum are probed with visible fluorescent dyes and 557 nm laser excitation.BAIBAKOV, PATRA et al. 2019b We use a Cy3B label on LicT protein and the free fluorescent dye Alexa Fluor 546 to perform visible FCS experiments recording the number of fluorescent molecules as a function of the concentration (raw FCS data are shown in Fig. 4.17). The data for both LicT-Cy3B and Alexa Fluor 546 follow the same linear relationship with the concentration defining a similar detection volume inside the aperture (Fig. 4.12a). Because of the longer illumination wavelength (557 instead of 266 nm), the penetration depth inside the nanoaperture is different and hence the size of the detection volume is different between the UV and the visible experiments. This difference can be accounted for by the numerical simulations (Fig. 4.12b 4.17), providing a supplementary control of the experimental results.

We compare the brightness between the three different proteins using the horn antenna and the confocal reference (the brightness for the confocal case is estimated from the measured concentration and the 1.8 fL value of the confocal volume). The horn antenna improves the brightness by about 9× for all the different proteins (Fig. 4.12c). As the horn antenna is a weakly resonant structure (as compared to a dimer nanogap antennaPUCHKOVA, VIETZ et al. 2015bFLAURAUD, REGMI, WINKLER et al. 2017a, its gain is essentially brought by the local excitation intensity increase and the improved collection efficiency.Aleksandr BARULIN, ROY, J.-B. B. CLAUDE et al. 2022 The quantum yield enhancement plays a minor role here,Aleksandr BARULIN, ROY, Jean Benôit CLAUDE et al. 2021 so similar net fluorescence enhancement is expected despite proteins with different Trp quantum yields are used. The 9× enhancement stands also in good agreement with our calibration using the UV fluorescent dye p-terphenyl. We have performed FCS on different horn antennae for the sake of reproducibility and consistency. For a given horn antenna angle and hole size, the horn antennas are quite robust and results are fairly reproducible. We have presented some FCS curves and analysis parameters for different proteins in fig4.13-4.14

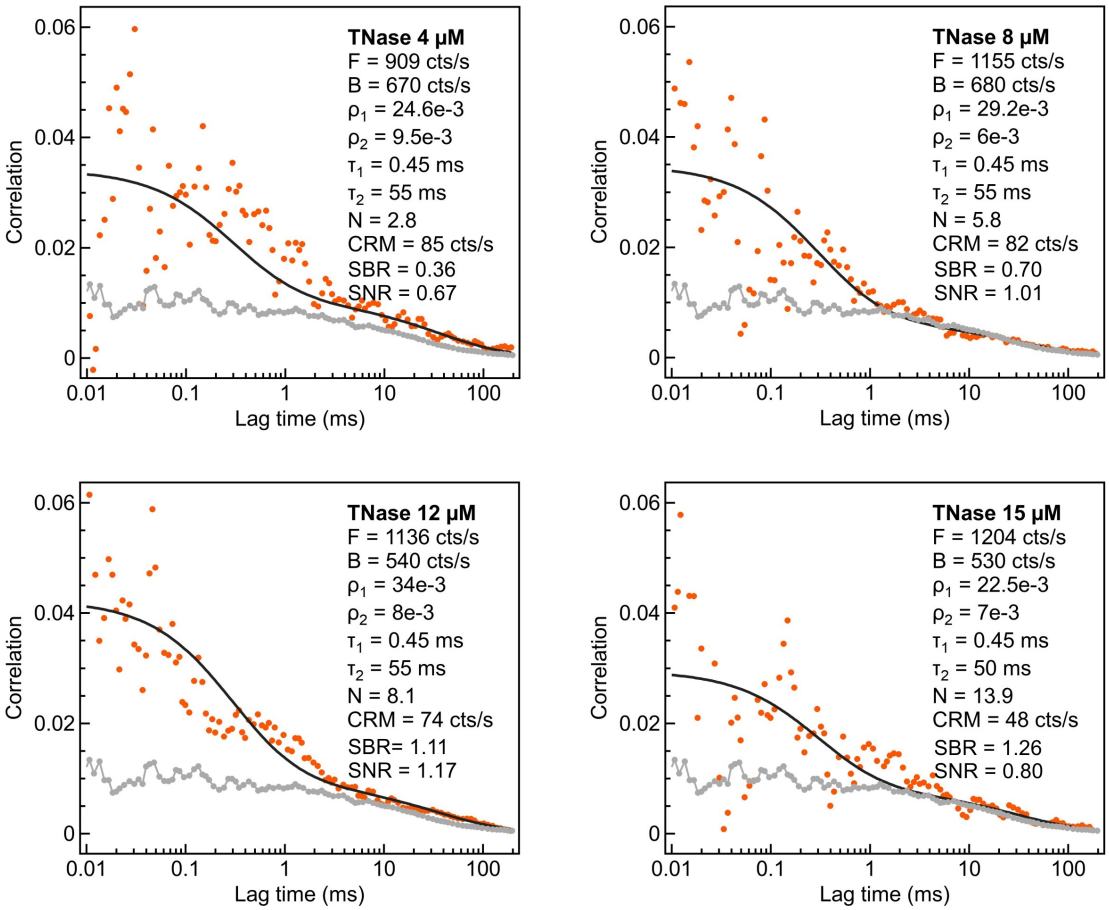

FIGURE 4.13 – FCS correlation functions for different TNase concentrations in the horn antenna (orange dots) and their numerical fits (black line) with spectral filtering and time gating. The fit parameters are indicated for each case. We also indicate the values for the signal to background (SBR) and the signal to noise (SNR). For definitions of these quantities, see section 14 page S16 of this document. The gray data trace is the residual background correlation recorded in the absence of proteins.

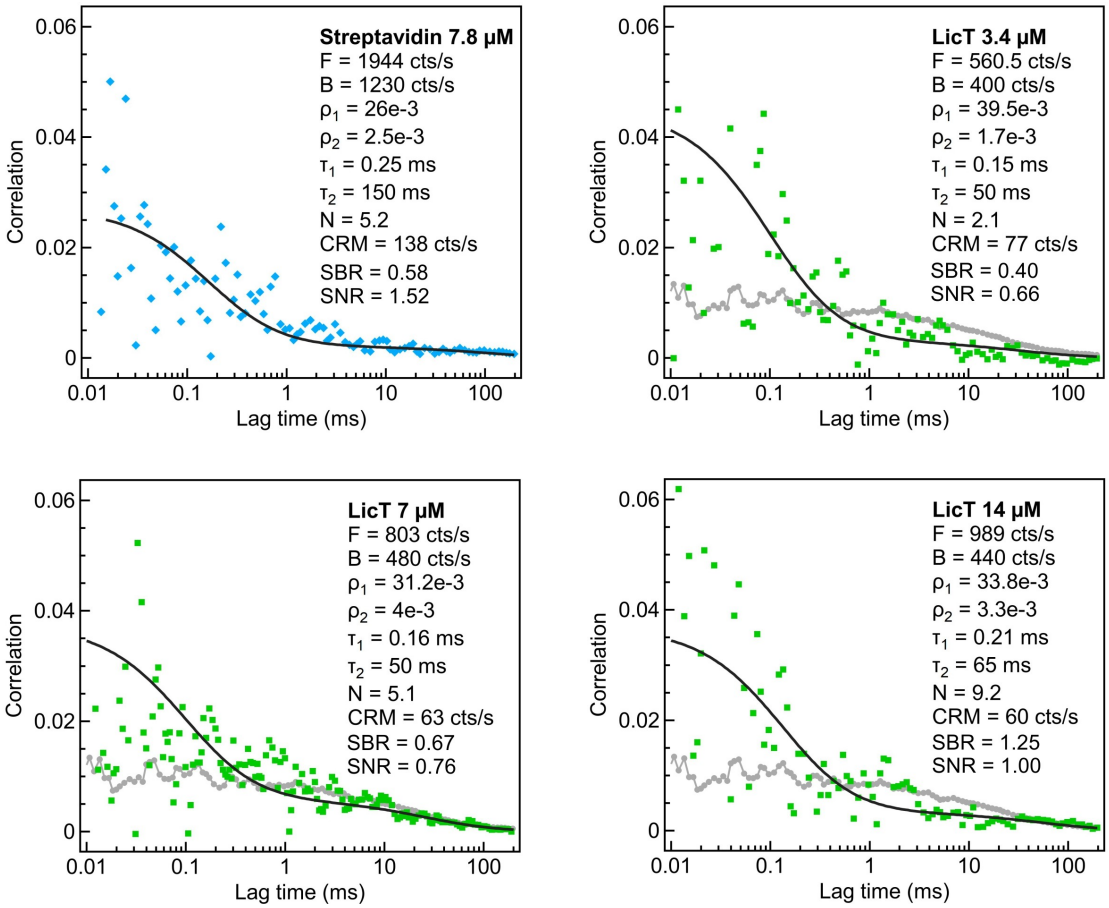

FIGURE 4.14 – FCS correlation functions for streptavidin and LicT in the horn antenna (blue and green markers) and their numerical fits (black line) with spectral filtering and time gating. The fit parameters are indicated for each case as well as the corresponding signal-to-background (SBR) and signal-to-noise (SNR). The gray data trace is the residual background correlation recorded in the absence of proteins.

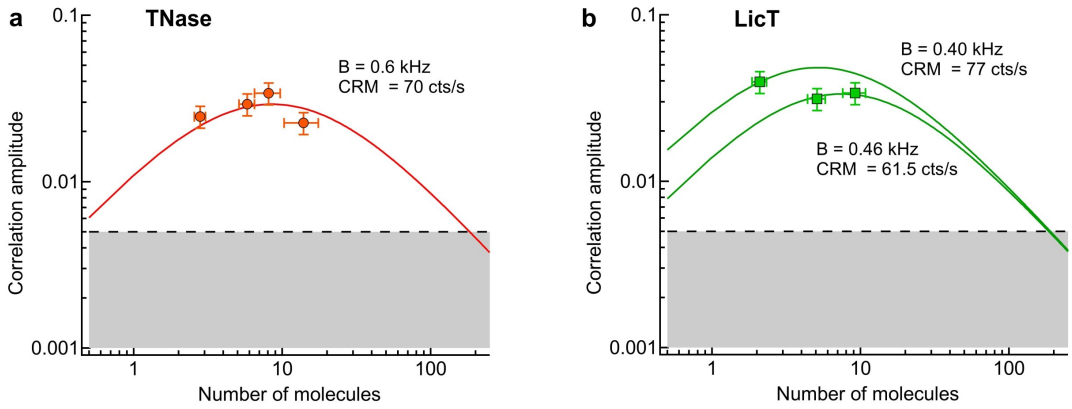

FIGURE 4.15 – Comparison of the experimental correlation amplitudes for the first speciesρ_1 (markers, corresponding to proteins contribution separated from background) with the theoretical predictions (lines) for TNase (a) and LicT (b). For LicT, we used a specially selected sample with low background (presumably because of a slightly reduced milling depth during the FIB process, the background values were recorded for each structure). Two lines are shown for LicT corresponding to slightly different parameters for the background intensity B and the fluorescence brightness CRM. The dispersion remains within the uncertainty margins on our experimental data. The shaded region corresponds to the detection limit. The higher concentration leds to lower CRM and and lower concentration led to low correlation in both cases correlation-fit was not clear thus we did not include too low or too high concentration points in graph

If we compare the best results found for the horn antenna (single Trp brightness 70 cts/s, background 600 cts/s) and the confocal setup (single Trp 8 cts/s, background 2000 cts/s), our combined solution improves the signal-to-background ratio by 30×. The 1000× lower detection volume with the antenna efficiently eliminates the background intensity stemming from the solution (Fig.4.10), yet at the expense of a supplementary background from the antenna luminescence (Fig. 4.9c). As we saw in the previous section, in the presence of background, the signal-to-noise ratio (SNR) for determining $G(0)$ is given by the following equation :$SNR = CRM\left(\frac{SBR}{1+SBR}\right)\sqrt{T_{tot}\Delta\tau}$The SNR provides a figure of merit to compare between experiments and discuss the feasibility of an FCS experiment. For the horn antennas and proteins used here, the SNR ranges from 0.7 to 1.5 (figure 4.13,4.14) while for the confocal configuration, even with one hour of integration time, the SNR remains below 0.2.

The nanophotonic antenna is essential for UV-FCS on proteins with a small amount of Trp residues. The FCS diffusion time affects the selection of the temporal width $\Delta\tau$, which must be much shorter than the FCS diffusion time. The detection of slower diffusing species allows for a longer counting interval $\Delta\tau$, which increases the signal-to-noise ratio and partially offsets the lower autofluorescence brightness.

4.4.3 Method

4.4.3.1 Protein sample preparation

Thermonuclease staphylococcal nuclease from Staphylococcus aureus and streptavidin from Streptomyces avidinii are purchased from Sigma-Aldrich. The transcription antiterminator protein LicT from Bacillus subtilis is provided by Emmanuel Margeat, Nathalie Declerck and Caroline Clerté (CBS Montpellier, France). The proteins are dissolved in a Hepes buffer (25mM Hepes, 300mM NaCl, 0.1v/v% Tween20, 1mM DTT, and 1mM EDTA 1mM at pH 6.9). The protein solutions are centrifuged for 12 min at 142,000 g using an air centrifuge (Airfuge 20 psi) and the supernatants are stored in small aliquots at -20°C. Concentrations are evaluated using a spectrofluorometer (Tecan Spark 10 M,) using extinction coefficients derived from the protein sequence and summarized in ROY, Jean-Benoît CLAUDE et al. 2023. 10 mM of mercapto ethylamine MEA and 25 mM of glutathione GSH (both from Sigma Aldrich) is added to the buffer just before the experiments to improve photostability and neutralize reactive oxygen species. Oxygen removal by degassing did not significantly modify the autofluorescence signal of TNase. Therefore, we decided to not undertake any special action to remove the oxygen dissolved in the buffer solution for the TNase and streptavidin experiments. For LicT experiments, the oxygen dissolved in the solution is removed by bubbling the buffer with argon for at least 5 minutes, as it has a significant impact on the LicT autofluorescence signal. The solution was then quickly placed on the UV microscope and the chamber is filled with argon and covered with a coverslip to prevent oxygen from entering the solution. The LicT autofluorescence remained stable for about one hour, with no sign of oxygen rediffusion during this period.

4.4.3.2 Fluorescence correlation spectroscopy fitting model

The fluorescence time traces data are analyzed with Symphotime 64 (Picoquant) and Igor Pro 7 (Wavemetrics). For time-gating, only the photons within a 3 ns window after the fluorescence peak are selected for analysis. The rationale behind this choice is that for an exponential decay of characteristic time τ, 95% of the signal is collected within a time window of width 3τ. We thus consider a time window corresponding to 3× the fluorescence lifetime (which is about 1 ns for tryptophan in the horn antenna for the different proteins tested here) in order to provide a good trade-off between signal collection and noise rejection. The FCS correlations are computed using Symphotime 64 and fitted with a two-species model :21

$$G(\tau) = \rho_1(1+\frac{\tau}{\tau_1})^{-1}(1+\frac{1}{\kappa^2}\frac{\tau}{\tau_1})^{-0.5} + \rho_2(1+\frac{\tau}{\tau_2})^{-1}(1+\frac{1}{\kappa^2}\frac{\tau}{\tau_2})^{-0.5} \tag{4.8}$$

where ρ_i and τ_i are the amplitude and diffusion time of each species and is the aspect ratio of the axial to transversal dimensions of the detection volume (set to = 1 for the horn antenna following our previous works BARULIN, J. CLAUDE et al. 2019. The rationale behind this two-species model is that the first fast-diffusing species account for the protein while the second slow-diffusing species corresponds to the

residual background. In the absence of any protein sample (using only the same buffer solution), a correlation is still observed from the background with an amplitude below 0.01 and a characteristic time of 50 ms . The origin of this background correlation remains unclear, the 50 ms time (20 Hz) suggests some remaining mechanical vibration or electric noise on our microscope. As the diffusion times of the proteins are below 500 µs, the background contribution (ρ_2, τ_2)can be readily separated on the FCS data. All the fit results are detailed in 4.13 and 4.14.From the correlation amplitude ρ_1, the total fluorescence intensity F and the background intensity B, we compute the background-corrected number of proteins 21 as $N = \frac{(1-B/F)^2}{\rho_1}$ and the fluorescence brightness per protein as $CRM = \frac{(F-B)}{N}$ 16. As we consider lag times longer than 10 µs for the UV-FCS analysis, the afterpulsing from the photomultiplier and the repetition rate of the laser is not a problem.

4.4.3.3 Numerical Simulation to calculate detection Volume

We use the wave optics module of COMSOL Multiphysics 5.5 to simulate the propagation of light inside an 80 nm diameter nanoaperture. The excitation is a plane wave with 266 or 557 nm. The vertical profile of the nanoaperture takes into account the tapering due to FIB milling and the 12 nm thick silica layer deposited by PECVD. To mimic our experiments, light is incoming from the bottom of the aperture where the diameter is the smallest. The inside volume of the aperture and the upper medium are set to a refractive index of water. A tetrahedral mesh is used with mesh size ranging from 0.3 nm to 10 nm. Scattering boundary conditions were used to suppress reflections from the domain boundaries. Figure 4.16 show the simulation results for the two excitation wavelengths. The decay profile of the excitation intensity along the vertical center axis of the aperture is also represented. The light with the longer 557 nm wavelength has a shorter penetration inside the sub-wavelength aperture, explaining why the detection volume is smaller with 557 nm as compared to 266 nm excitation (4.12a,b). To compute the FCS detection volume at each wavelength, we take into account the undercut into the quartz substrates, which add a constant volume of 0.45 aL for both wavelengths. Then we sum the volume from the undercut to the volume from the aperture, assuming for simplicity a monoexponential decay inside the aperture with a characteristic decay length 27 nm at = 557 nm and 35 nm at = 266 nm. For UV illumination, a cavity-like mode is excited, which shifts the attenuation decay by an extra 50 nm inside the aperture. With these values, we obtain a detection volume of 1.1 aL at 266 nm and 0.7 aL at 557 nm, in very good agreement with the experimental volumes (Fig. 4.12b) determined from the slope of the linear fits in Fig. 4.12a

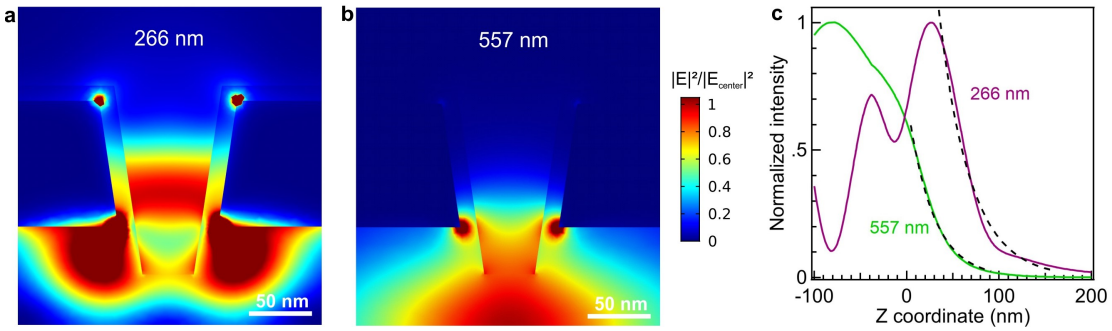

FIGURE 4.16 – Normalized intensity profiles at two different wavelengths 266 nm (a) and 557 nm (b) computed for an 80 nm diameter aperture milled in aluminum and covered by a 12 nm thick silica layer aiming at reproducing the experimental FIB-milled configuration. The peak enhancement value along the vertical center axis is 4.6 for 266 nm and 3.7 for 557 nm. (c) Comparison of the normalized decay profiles of the excitation intensities along the vertical center axis of the aperture. The origin (Z=0) is taken at the bottom quartz-aluminum interface. Monoexponential fits of the evanescently decaying sections are shown in black dashed lines.

4.4.3.4 Control Experiments on Labelled Proteins

To validate the UV FCS experiments, we conducted FCS measurements using Alexa 546 and Cy3B fluorescent dyes on a visible fluorescence microscope. The detailed experimental setup is described in BAIBAKOV, PATRA et al. 2019b, and it features a 557 nm laser that is focused by a 1.2NA water immersion objective, and confocal detection in the range of 570-620 nm is achieved by an avalanche photodiode. We used 80 nm apertures that were milled under similar conditions as the devices used for the UV experiments. Therefore, the number of detected molecules and the size of the detection volume can be compared while taking into account the difference in the illumination wavelength. Figure 4.17 displays FCS correlation functions recorded at various Alexa Fluor 546 concentrations. The FCS correlation data were fitted using a three-dimensional Brownian diffusion model with an additional blinking term.PRAMANIK et WIDENGREN 2006

$$G(\tau) = \frac{1}{N}[1 + \frac{T}{1-T}exp(-\frac{\tau}{\tau_d})](1 + \frac{\tau}{\tau_d})^{-1}(1 + \frac{1}{\kappa^2}\frac{\tau}{\tau_d}) \tag{4.9}$$

Where N is the total number of molecules, T is the fraction of dyes in the dark state, $_T$ is the dark state blinking time, $_d$ is the mean diffusion time, and is the aspect ratio of the axial to transversal dimensions of the nanohole volume. Although the ZMW geometry does not meet the assumption of free 3D diffusion, the above model equation has been empirically found to describe well the FCS data inside ZMWs using an aspect ratio set to = 1, as previously reported (BAIBAKOV, PATRA et al. 2019b, POPOV, GÉRARD et al. 2008). The contribution of the dark state remains quite small and is only required to account for fast dynamics below 10 µs. Due to the larger statistical noise, this type of fluctuation is currently not detectable in the UV.

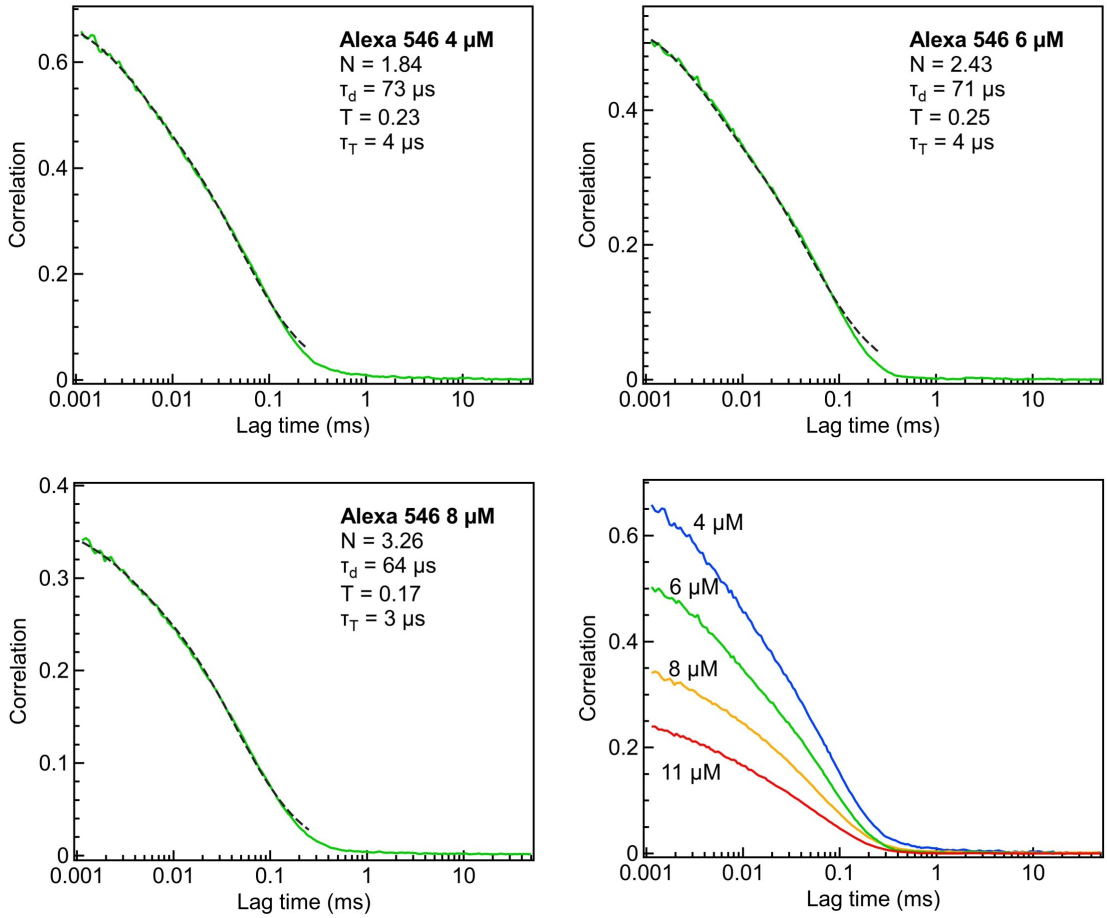

FIGURE 4.17 – FCS correlation (green) and numerical fits (black dashed lines). The fit parameters are indicated for each panel. The 80 nm ZMW is milled with identical parameters as the one used for the UV experiments.

4.5 Conclusion

In Figure 5.26, we present an overview of the entire chapter, illustrating a comprehensive setup where horn antennas serve as amplifiers for UV auto-fluorescence. This process amplifies the signal by orders of magnitude, and then we direct the collected signal through an objective and mirrors to spectral and temporal filters, improving the signal-to-background ratio. The experimental FCS results displayed in Figure 5.26 clearly demonstrate the effectiveness of the technique described in this section, turning an experiment previously deemed unfeasible into a viable one.

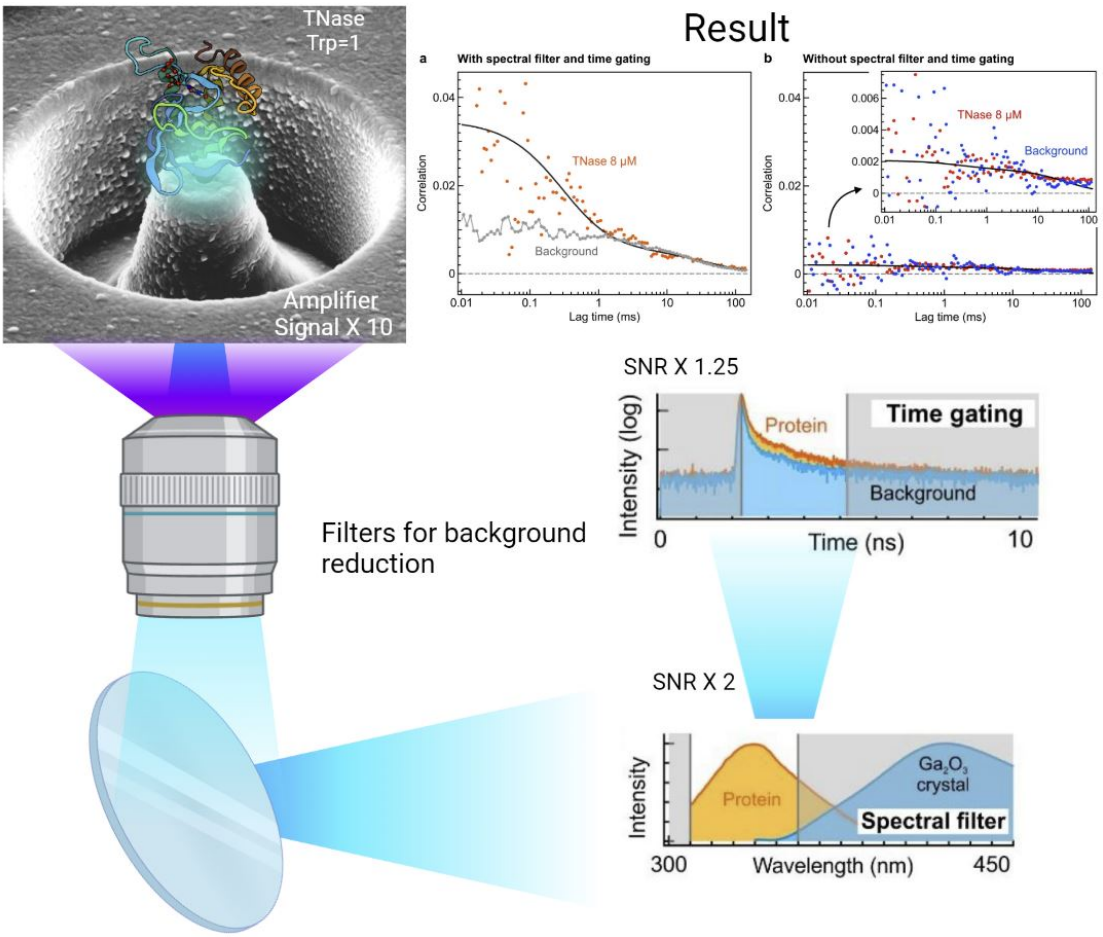

FIGURE 4.18 – Horn antenna, spectral filter, and time gating to reach ultimate sensitivity of UV autofluorescence spectroscopy on label-free proteins

When we compare the FCS correlation of a horn antenna with and without spectral filtering and time gating, the correlation amplitude without these features is significantly lower due to the higher background level. This makes the correlation indistinguishable from the background correlation. From the calculations, for a background intensity of 4.4 kcnts/s, 5 proteins, and a brightness of 70 cnts/s, the estimated G(0) amplitude is about 0.001, which is in good agreement with the experimental results. The FCS of TNase at the single-molecule level with a single emitter is now distinguishable from the background correlation and strong enough to obtain valuable information such as diffusion constants and hydrodynamic radius. In the end, I would like to add that as most proteins bear only a few tryptophan residues, being able to detect a single tryptophan (instead of several tens) is a major breakthrough opening the possibility to apply the UV-FCS technique to a huge library of label-free proteins. This challenging task requires careful optimization of the signal-to-background ratio combining approaches to maximize the signal (optical horn antenna, antioxidants) and reduce the background intensity (FIB milling depth, spectral filtering, time gating, buffer composition). Our calculations provide useful guidelines to predict the feasi-

bility of the experiments based on the correlation amplitude and the signal-to-noise ratio.

Altogether, the data presented in Fig. 4.11 demonstrate that a protein bearing a single Trp residue can be detected using UV-FCS. We envision that the methods developed here to optimize the UV autofluorescence signal-to-background ratio will be useful to a wide range of future studies on label-free single protein spectroscopy,ARROYO et KUKURA 2016ADHIKARI et ORRIT 2022as well as the advancement of plasmonics into the UV range.ZHAO, Z. LIN et al. 2021aKNIGHT, KING et al. 2014 JHA, AHMED et al. 2012b. UV-FCS can provide information about local concentration, diffusion properties, and autofluorescence brightness per molecule to shine new light on protein interaction dynamics with ligands or other molecular partners.HAUSTEIN et SCHWILLE 2003RIES et SCHWILLE 201246–48 While in scattering microscopy the interference signal scales with the 3rd power of the nanoparticle diameter,ARROYO et KUKURA 2016,ŠPAČKOVÁ, KLEIN MOBERG et al. 2022 ORTEGA ARROYO, COLE et al. 2016bUV-FCS is less sensitive to the protein size, relying more upon its tryptophan content. The TNase proteins detected here have a molecular weight lesser than 20 kDa, opening the possibility to detect label-free proteins with molecular weights in the single-digit kDa range. As a supplementary advantage of the technique, the detection volume is in the attoliter range, three orders of magnitude below that of a diffraction-limited confocal microscope, so that single molecule detection and UV-FCS can operate at micromolar concentrations.LEVENE, J. KORLACH et al. 2003PUNJ, GHENUCHE et al. 2014b. Being able to work at high concentrations with single-molecule resolution and/or FCS is essential to study a broad range of enzymatic reactions, protein-protein, and protein-DNA/RNA interactions with Michaelis constants or dissociation constants in the micromolar range.HOLZMEISTER, Guillermo P. ACUNA et al. 2014

5 Enhancing Auto-fluorescence of Proteins with Self-Assembled Deep UV Dimer Antenna

Related Articles

Prithu Roy,et.al "Ultraviolet Resonant Nanogap Antennas with Rhodium Nanocube Dimers for Enhancing Protein Intrinsic Autofluorescence" (Minor Revision submitted, ACS Nano, Aug,2023)

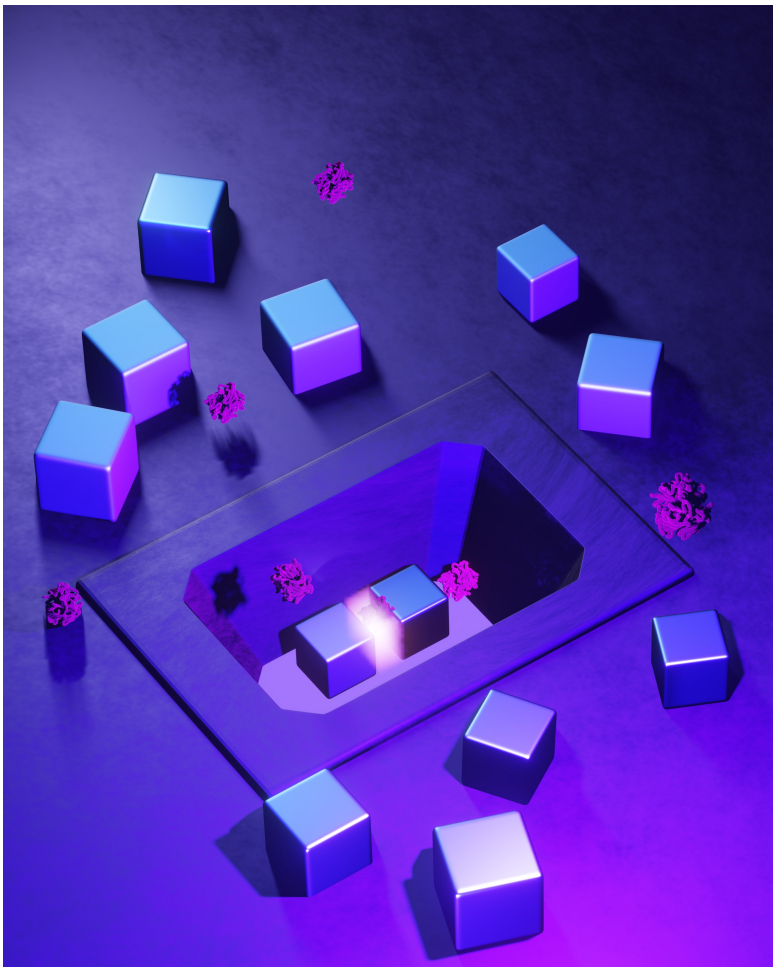

FIGURE 5.1 – Rh Cube dimer antenna in Nano-Aperture.

Summary

5.1 Introduction

In the previous chapter, we saw that using the Horn antenna and SBR (signal to background ratio) enhancement, we could reach a single-Tryptophan-single-Protein sensitivity level. The feat was achieved by enhancing the collection gain with the horn antenna, optimizing the chemistry to reduce the buildup of radical states, and then further decreasing the background signal, thus boosting the SNR-SBR. If we look again at the equation of the fluorescence enhancement :

$$\eta_F = \kappa * \eta_{exc} * \frac{\Gamma^*_{rad}}{\Gamma_{rad}} * \frac{1}{1-\phi_0+\phi_0(\Gamma^*_{rad}+\Gamma^*_{loss})/\Gamma_{rad}} \tag{5.1}$$

So far we have tried to enhance the signal by increasing κ, (the collection enhancement), increasing Γ^*_{rad} (radiative rates), and to some extent increasing η_{exc} (excitation gain) by plasmon created at the base of nano-aperture. The η_{exc} factor as reported in our previous workAleksandr BARULIN, Jean Benoît CLAUDE et al. 2019a is around 4-5 times. The objective of this chapter is to explore techniques for amplifying the excitation gain by at least two orders of magnitude in the UV regime, a capability that has already been achieved in the visible spectrum using resonant optical antennasBIAGIONI, J. S. HUANG et al. 2012.In our study till now, we have employed nonresonant nanostructures, such as the Zero-Mode waveguide (nano-aperture) and the Horn antenna (broad-band reflector), in our design modifications. Therefore, it is logical to investigate how we can harness the potential of resonant nanostructures to amplify the excitation signal by one or two orders of magnitude.
To understand how we can use the optical resonance structure to enhance the excitation signal we explore how molecules interact with light at the nanoscale and what are the limiting factors. The interaction between light and a single fluorescent molecule is fundamentally limited by the over 100-fold size mismatch between their respective wavelengths and dimensions,NOVOTNY 2007 leading to a weak net fluorescence signal per molecule in diffraction-limited microscopes. As a result, the sensitivity and temporal resolution of single-molecule fluorescence techniques, which are essential in modern biophysics and biochemistry, are also limited.ZIJLSTRA, ARMSTRONG et al. 2019 To overcome these limits, plasmonic optical nanoantennas have been introduced to manipulate light at the deep subwavelength scale and enhance the light-matter interactions.NOVOTNY 2012 Swayandipta DEY, DOLCI et al. 2023 A broad range of optical nanoantenna designs including bowtie,KINKHABWALA, Z. YU et al. 2009single nanorods,ZIJLSTRA, PAULO et al. 2012 DNA-origami dimers,TROFYMCHUK, KOŁATAJ, GLEMBOCKYTE, F. ZHU, Guillermo P. ACUNA et al. 2022THACKER, HERRMANN et al. 2014DNA-templated dimerGLEMBOCKYTE, GRABENHORST et al. 2021,ZHAO, Z. LIN et al. 2021b metasurface, or antenna-in-boxPUNJ, MIVELLE, MOPARTHI et al. 2013c has been demonstrated to significantly enhance the fluorescence brightness of single molecules, reaching impressive fluorescence enhancement factors above 1000-fold. By manipulating light at the nanoscale, the optical nanoantennas provide exquisite control over the radiation properties of a single quantum emitter, opening new possibilities to tune the directionality of the fluorescence lightMOROZOV, GAIO et al. 2018ROY et BOLSHAKOV 2021b achieve ultrafast photoemission,TIWARI, ROY et al. 2023b, PELLEGROTTI, Guillermo P. ACUNA et al. 2014reduce the photobleaching rate,DE TORRES, GHENUCHE et al. 2015b control the near-field dipole-dipole energy transfer, or trap single nano-objectsPANG et GORDON 2012JIANG, ROY, Jean Benoît CLAUDE et al. 2021 Previous research has demonstrated the enhancement of excitation gain by several orders of magnitude through the utilization of resonant optical antennas. NEVELS et ABBAS 2016XIN, NAMGUNG et al. 2018TROFYMCHUK, KOŁATAJ, GLEMBOCKYTE, F. ZHU, Guillermo P. ACUNA et al. 2022PUNJ, MIVELLE, MOPARTHI et al. 2013a.

However, the current demonstrations and operating range of nanoantennas remain largely limited to the visible and near-infrared regions. While this range is

well suited for organic fluorophores and quantum dots, extending it towards the ultraviolet (UV) region brings the key additional benefit of exploiting directly the auto-fluorescence of proteins without requiring any additional fluorescent label. Despite the growing interest in utilizing the UV range to enhance the light-matter interaction, there have been limited reports about UV resonant optical nanoantennas.ZHAO, Z. LIN et al. 2021b Earlier works concerned mostly aluminium nanoparticle arrays to enhance Raman scattering,JHA, AHMED et al. 2012a and fluorescenceRAY, SZMACINSKI et al. 2009 from dense molecular layers. Another important class of UV nanoantennas is subwavelength nanoapertures, Aleksandr BARULIN, Jean Benoît CLAUDE et al. 2019aBAIBAKOV, Aleksandr BARULIN, ROY, Jean Benoît CLAUDE et al. 2020which can be combined with a micro reflector to increase the collection efficiency.Aleksandr BARULIN, ROY, Jean Benoît CLAUDE et al. 2022 However, all these designs are only weakly resonant, and lack the strong field confinement achieved with gap surface plasmon resonances.NOVOTNY et HECHT 2006 Although numerical investigations have explored UV resonant nanoparticlesKUMAR et SONI 2022 and dimer gap antennasX. ZHANG, P. LI et al. 2016 to achieve higher local field enhancement, their experimental demonstrations have been limited so far to Raman scattering and near-field imaging. The major application in enhancing the autofluorescence of label-free proteins remains unexplored. Beyond the challenging difficulty of such experiments, another limiting factor is the poor stability of aluminium plasmonic structures in an aqueous environment,*Understanding Aluminum Corrosion* s. d., especially under UV illumination.ROY, BADIE et al. 2021 While coating with silica or other oxide materials can promote the Al corrosion stability, this comes at the expense of a 10 nm-thick supplementary layer which in turn enlarges the gap size and reduces the net enhancement in the antenna hotspot.

In this chapter, we will tap into resonance antenna-based enhancement of UV auto-fluorescence signal from protein. The scope of the chapter is to make a Deep-UV plasmonic antenna and push the limit of enhancement of auto-fluorescence signal, without losing the features of a Zero-mode waveguide (nano-aperture). Needless to say, the design has to be robust against corrosion and bio-compatible too.
The idea is to introduce a resonant antenna in the Zero-mode waveguide. Zero-mode waveguide has an evanescent mode at its bottom, we will couple this mode to the resonance mode of the antenna. We will use a plasmonic dimer-gap antenna which can provide very large field enhancement and confinement compared to signal plasmonic particles. This brings us to the discussion about the choice of metal for optical antenna, the usual metals like Au-Ag are no any more viable solutions as their LSPR (Localize Surface Plasmon Resonance) response lies in visible-near-UV. The metal most commonly used is Al, Ga, Rh in some cases Mg too Juan M. SANZ, Dolores ORTIZ et al. 2014ZHAO, Z. LIN et al. 2021a. We will use Rh cubes to design our dimer antenna as it is more stable than Al, and Mg and performs better as plasmonic material than Ga. Dimer antenna using Rhodium has been studied beforeM. WATSON, X. ZHANG et al. 2015ALCARAZ DE LA OSA, M. SANZ et al. 2015 for UV plasmonics for enhancing Resonance Raman signal. Different designs of Rh structure are explored for example recently KUMAR et SONI 2022 simulated a concave nanocube structure for UV plasmo-

nic showing superior performance than regular Rh nanocube, however, the fabrication of such design was not discussed or implemented. In other work, groups have studied tripod designALCARAZ DE LA OSA, M. SANZ et al. 2015, cylindrical-spherical dimers AHMADIVAND, SINHA et al. 2016. The resistance to corrosion from radicals generated during UV illumination and no oxide formation on the Rh cube qualifies it as the most optimum choice for high-enhancement UV plasmonic material. We also demonstrate in our simulations (in the method section) that the Rh dimer antenna is a better choice than the Al dimer antenna or other materials such as Au and Si, which are well-known for their use in the visible spectrum.

5.2 Design and Optical Simulation of Rh Dimer Antenna

The electric field distributions were computed using the wave optics module of COMSOL Multiphysics v5.5, relying on the finite element method. We used a user-defined mesh, for 2D model mesh size ranging from 0.01 nm near the metallic structure to 10 nm in the surrounding water media, for excitation wavelengths ranging from 220 to 500 nm. In the case of the 3D model, we relaxed the mesh to 1 nm (near metal) to 10 nm in the surrounding. We used tetrahedral geometry, as it adheres nicely to curved and sharp edges. The reflections from the boundaries were suppressed by using scattering boundary conditions. . The refractive index parameters were taken from predefined libraries of COMSOL Multiphysics. The refractive index of Rhodium was taken from Weaver et.al 1977, the data was available in the COMSOL material library. We used both 2D and 3D models for the numerical simulations. The 2D model was used for brute optimization of the antenna parameters, as the modeling was very computationally intensive. The optimized structure was then further studied with a 3D model. We modeled and simulated some designs for both 2D and 3D models to compare and validate 2D models. Given the symmetry of the antenna model, we saw that the enhancement values we got for 2D, and 3D were comparable. Thus, we resorted to 2D simulation to optimize the Rh nano-cube plasmonic response and to study the coupling of two Rh nano-cubes to form a gap-plasmon dimer antenna.

5.2.1 Nanorectangle Aperture

So far in our work, we have extensively used cylindrical nanoapertures (ZMW) because they are reproducible and robust in performance. However, in this chapter, we will be using rectangular-shaped nanoapertures because of the geometry of the rectangular nanoaperture. The final idea is to embed cubical rhodium nanostructures inside the nanoapertures to form a dimer-like structure. By keeping the width of the rectangular nanoaperture close to the size of the cube and the length a bit larger than twice the size of the rhodium cubes, we can selectively fill (via self-assembly) the rectangular nanoapertures with two Rh cubes separated by some small distance with a pre-selected orientation.

In the literature, a similar concept has been implied to make an array of nanorods inside a rectangular nano-aperture using capillary forces KUEMIN, STUTZ et al. 2011. It should be noted that we have seen in our previous work that rectangular nanoapertures can perform better than circular nanoapertures BAIBAKOV, Aleksandr BARULIN, ROY, Jean-Benoît CLAUDE et al. 2020. However, in this case, rectangular apertures are optimized to accumulate only two Rh cubes with the least gap, not for better enhancement, as discussed in our work BAIBAKOV, Aleksandr BARULIN, ROY, Jean-Benoît CLAUDE et al. 2020. The dimensions of the nanorectangles are 120x50 nm^2, which is a bit bigger compared to the optimum size of 70x30 nm^2.

We used gallium-ion-based FIB milling to make the rectangular nanoapertures. Details of the fabrication are given in the method section at the end of the chapter.

In this section, we will discuss the numerical simulation and design of rectangular apertures for two excitation wavelengths λ = 295 nm and 266 nm, which are pertinent for the experiments to be discussed in the subsequent section.

As we can see in the simulation design shown in Figure 5.2, we compensated for the fabrication constraints by keeping the edges a bit rounded and making the structure conical along the height. the field intensity map and enhancement of the electric field for different polarization are shown in Figs5.2 and 5.3

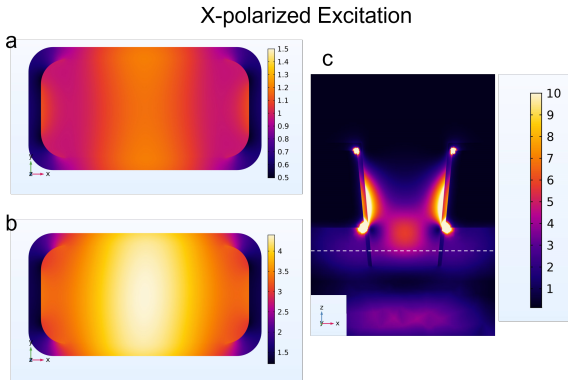

FIGURE 5.2 – The figure shows an Intensity enhancement plot for 120X50 nm^2rectangular nanoaperture. For excitation with X polarization, top view (a) λ=295 nm,(b) λ=266 nm and (c) side view forλ=266 nm. The white dotted line represents the plane where the top view was taken. It is worth noting that (c) high field enhancement occurs at the interface of metal and dielectric but it is embedded inside the Silica coating thus not accessible for proteins in solution. The field intensity enhancement presented in the top view depicts a value which closer to the experiments

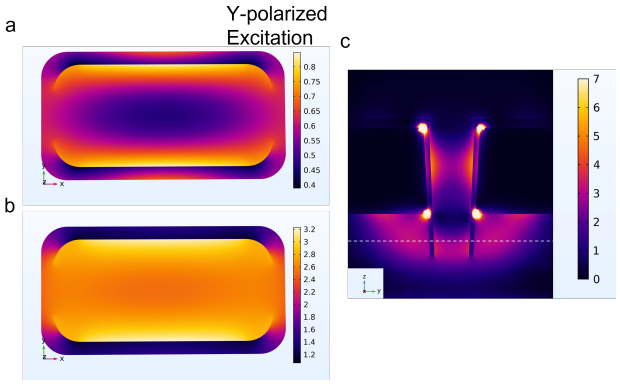

FIGURE 5.3 – Figure shows an intensity enhancement plot for 120X50 nm^2rectangular nanoaperture. For excitation with Y polarization, top view (a) λ=295 nm,(b) λ=266 nm and (c) side view forλ=266 nm. The white dotted line represents the plane where the top view was taken. It is worth noting that for (c) high field enhancement occurs at the interface of metal and dielectric but it is embedded inside the Silica coating thus not accessible for proteins in solution. The field intensity enhancement presented in the top view depicts a value which closer to the experiments

5.2.2 Rhodium Nanocube dimers

In this section, we discuss the second most important component of the antenna i.e. rhodium nanocubes. We have discussed many times in the previous sections emphasizing the plasmonic resonance of metal nanoparticles and their ability to focus the light at a nanometric scale. Thus, to harness this plasmonic response, we are using metallic cubes. The choice of material is guided not just by the wavelength of excited field but also by its material stability to corrosion as well as biocompatibility. The key advantages of rhodium in this context are (i) the precise control on the nanocube size and shape, allowing the plasmonic resonance to be tuned down into the UV region, (ii) the resistance to UV-induced photo-corrosion, largely outperforming aluminum BURLEIGH, RUHE et al. 2003ROY, BADIE et al. s. d. and (iii) the absence of a native oxide layerGUTIERREZ, Dolores ORTIZ et al. 2016 to maximize the enhancement of the nanogap accessible to protein molecules diffusing in the gap.
The plasmonic resonance of the metal nanostructure is a function of its size and environment. To achieve even higher enhancement we deploy a gap antenna which is a coupled metal nanostructure separated by distance 'd'<λ/10.NOVOTNY 2012. To optimize the antenna design, we vary the gap size, size of Rh cubes and calculate the enhancement factor inside the gap for different configurations. To obtain a precise enhancement value comparable to those obtained in experiments, we took care of the fabrication constraints in the simulations.

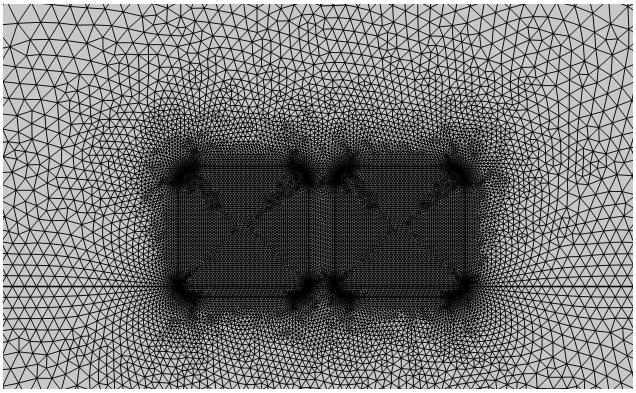

FIGURE 5.4 – User-defined Meshing is used for nanocubes ranging from 0.01 nm near the metallic structure to 10 nm. The edges of cubes are rounded with 5 nm curvature to avoid any artefact generated by the sharp edges of cubes

The figure 5.5 shows the simulation model and settings considered for the optimization of Rh dimer.

5.2.2.1 Optimizing Excitation gain of UV Dimer antenna

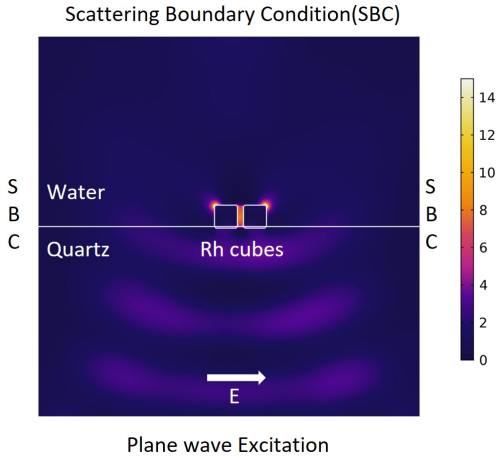

FIGURE 5.5 – Numerical simulations of the electric field intensity enhancement at 266 nm for a UV nanogap antenna made of two 30 nm rhodium cubes separated by a 10 nm gap. The arrows indicate the orientation of the incident electric field.

In fig5.6 The spectra of field enhancement within the dimer antenna's gap have been graphed for various changes in gap and cube size. It is important to note that there are two resonances observed : one at the range of 260-290 nm, which corresponds to the quadruple mode, and another near 350 nm, which corresponds to the dipole mode. The dipole mode resonance is particularly strong. The peak at 260-290 nm, which is shifted towards the blue, aligns with the excitation wavelength, while the peak

at 350 nm, which is shifted towards the red, aligns with the emission of tryptophan residues.Yu CHEN et BARKLEY 1998. From the spectra on fig5.6(b) we can see intensity enhancement increases with a decrease in the gap size,

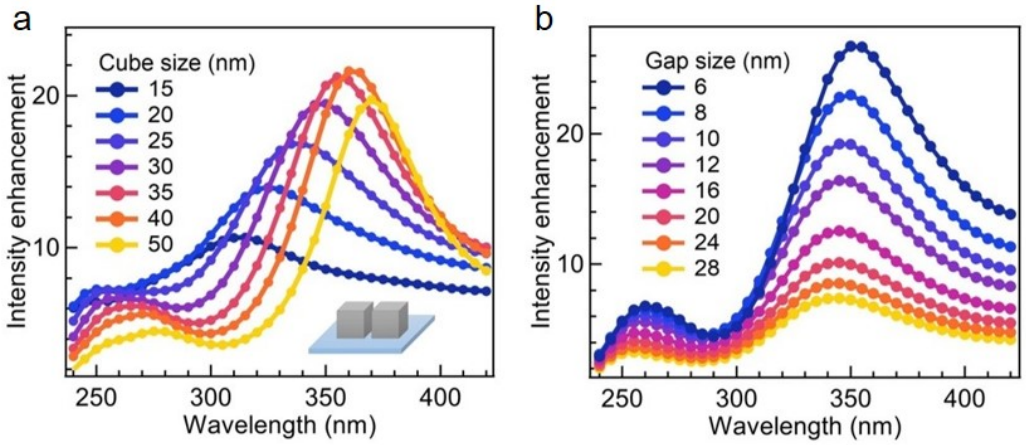

FIGURE 5.6 – Numerical simulations of the spectral dependence of the intensity enhancement in the centre of the nanogap antenna as a function of the rhodium nanocube size and gap size. For (a) the gap size is set at 10 nm, while for (b) the cube size is 30 nm. The enhancement value plotted in the spectrum is taken at the centre of the gap of the dimer

From the spectra fig5.6, we can see that increasing cube size for fixed gap size leads to a monotonous red shift in the spectrum however peak enhancement increases and then decreases exhibiting resonance-like features. The response of the dimer gap antenna is complex and depends on both gap and dimer cube size, to understand the response we have plotted a 2D colour map in fig5.7 for different gap sizes. The colour map gives a better understanding of enhancement, gap size and Rh cube size complex dependence and helps in achieving the optimum design parameters.

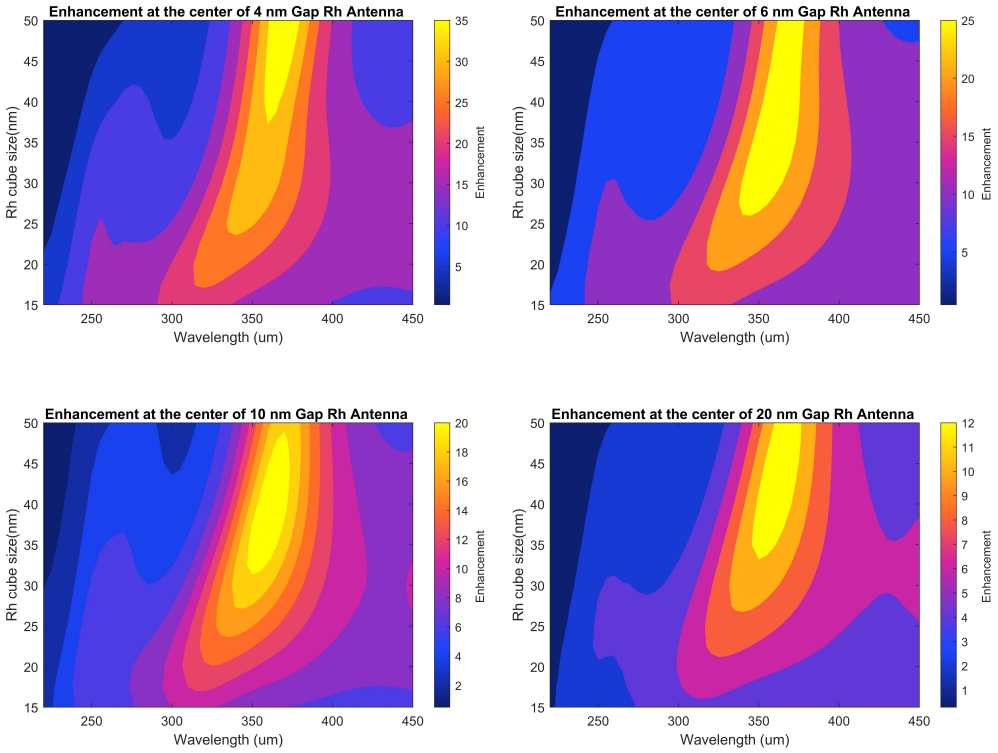

FIGURE 5.7 – A colour map of the electric field intensity enhancement at 266 nm for a UV nanogap antenna for different gap sizes.

5.2.2.2 Optimizing the Radiative rate enhancement of UV dimer antenna

We know that from 5.1, fluorescent enhancement not only depends on excitation gain but also radiative rate enhancement. Especially for metal nanostructures where losses are significant in comparison to all-dielectric antennasREGMI, BERTHELOT et al. 2016bKRASNOK, MIROSHNICHENKO et al. 2012. To calculate the radiative rate enhancements, we define two monitors surrounding the source dipole one a few wavelengths far from the dipole to calculate the radiative power and one only a few nanometers away from the source to calculate the total dissipated power. The antenna influence is determined by comparing it with a similar dipole source near a quartz substrate in a water medium in the absence of the rhodium nanocubes. The convergence is checked by generating the error over the iteration chart in-built in COMSOL. The decay rate enhancements are calculated for parallel and perpendicular dipole (with respect to gap plasmon mode)

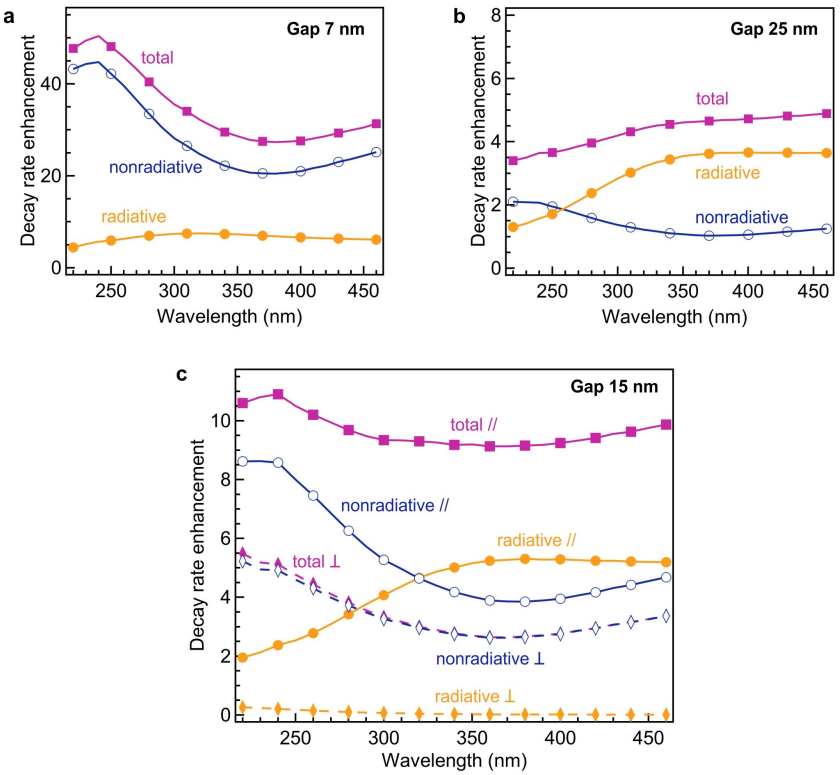

FIGURE 5.8 – Numerical simulations of the enhancement of the decay rate constants as a function of the emission wavelength for a perfect point dipole emitter with parallel orientation located in the centre of the nanogap. In (c), the enhancement factors for a dipole with perpendicular orientation are displayed with dashed lines and diamond markers. The rhodium cube size is constant at 30 nm. The gap size is 7 nm in (a), 25 nm in (b) and 15 nm in (c). All rates are normalized respective to the dipole radiative rate in free space

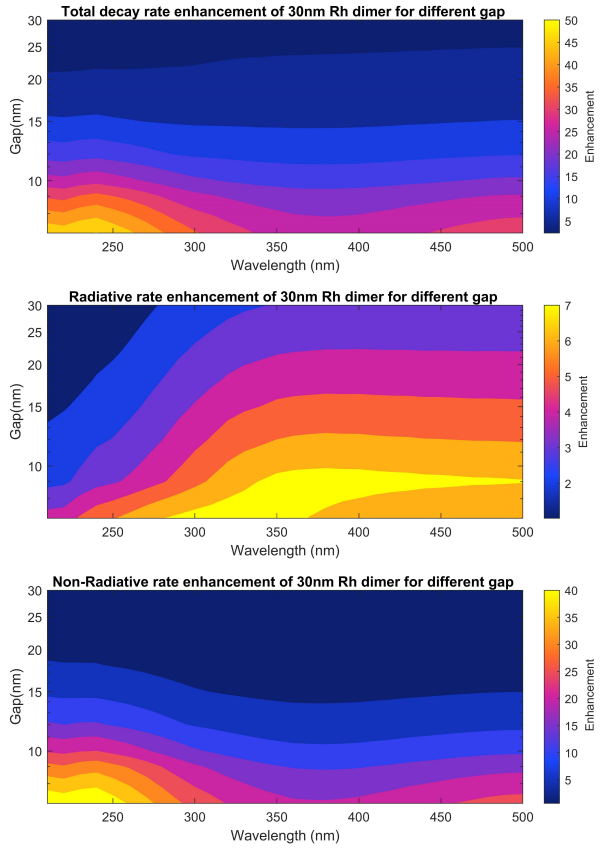

FIGURE 5.9 – (a) Numerical simulations of the total, radiative and non-radiative decay rate constant enhancement for a point dipole located in the centre of a rhodium dimer nanogap antenna oriented along the antenna's main axis as a function of the emission wavelength and the gap size. The cube size is constant at 30 nm. All rates are normalized to the dipole's radiative rate in free space. (b) Simulations of the antenna radiative efficiency (ratio of radiative rate to total decay rate) as a function of the emission wavelength and the gap size for a perfect point dipole emitter with parallel orientation located in the centre of the nanogap. The rhodium cube size is constant at 30 nm.

After all the simulations we can conclude that for the range of gap 7nm to 20 nm, the optimum cube size is 25-30 nm. We consider a range for gap size because we will implement self-assembly using capillary force, these fabrication techniques unlike Laser writing, Focused Ion Milling or EUV photo-lithography aren't very precise, nevertheless, the self-assembly technique using capillary force is faster and simpler to implement.

5.2.3 Simulation of Nanocube Dimer in Nanoaperture

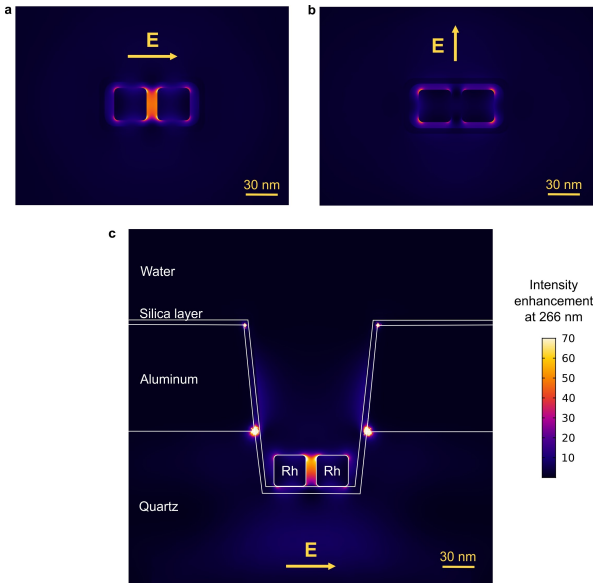

FIGURE 5.10 – Numerical simulations of the electric field intensity enhancement at 266 nm for a UV nanogap antenna made of two 30 nm rhodium cubes separated by a 10 nm gap inside a rectangular nanoaperture. The arrows indicate the orientation of the incident electric field. All the maps share the same colour scale.

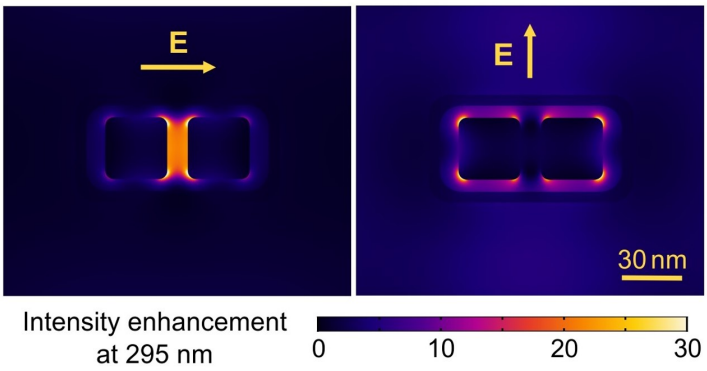

FIGURE 5.11 – Numerical simulations of the electric field intensity enhancement at 295 nm for a UV nanogap antenna made of two 30 nm rhodium cubes separated by a 10 nm gap inside a rectangular nanoaperture. The arrows indicate the orientation of the incident electric field. All the maps share the same colour scale.

To calculate the maximum fluorescence enhancement possible in numerical simulation (for dipole parallel to field) we use the following formulae

$$\eta_F = \frac{\eta_{exc} * \eta_{\Gamma rad}}{1 - \phi_0 + \phi_0(\frac{\eta_{\Gamma tot}}{\eta_{\Gamma rad}})} \tag{5.2}$$

where ϕ_0 is the intrinsic quantum yield of the emitter, η_{exc} is the excitation gain calculated at the centre of the gap antenna for λ=266nm and 295 nm. The radiative rate gain $\eta_{\Gamma rad}$ and total decay rate gain $\eta_{\Gamma tot}$ is calculated for λ=350 nm (at the emission peak of tryptophan). The spectra in figure5.12 shows how for different quantum yield emitter UV dimer antenna performance changes. It is a well-known fact about plasmonic systems that low quantum yield system is enhanced better than high quantum yield system SCHULLER, BARNARD et al. 2010which is also visible in the plot.

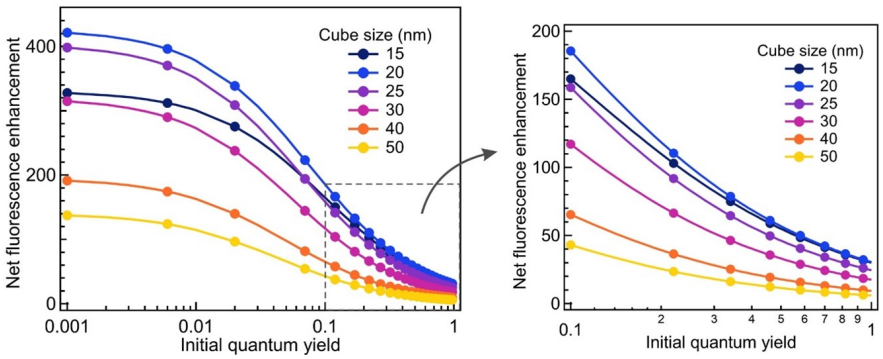

FIGURE 5.12 – Simulations of the maximum fluorescence brightness enhancement as a function of the initial quantum yield for a point dipole located in the centre of the nanogap with an orientation parallel to the dimer's main axis. The gap size is kept constant at 10 nm. The excitation wavelength is 295 nm and the emission is 350 nm. The right panel is a close-up view of the zone with quantum yields between 0.1 and 1

To calculate the efficiency of the antenna we used the following equation

$$\eta_{dimers} = \frac{\eta_{\Gamma rad}}{\eta_{\Gamma tot}} \tag{5.3}$$

We calculated the efficiency value at different wavelengths for different gap distances. The colour map is shown in fig5.13. As we can see the antenna has an efficiency of 350 nm which coincides with the emission peak of tryptophan. However, for lower gap size antenna efficiency falls, on the other hand, excitation gain rises exponentially when gap size reduces. Thus the efficiency of the antenna is an important figure of merit which encompasses the information about the loss in the system due to metal and plasmons.

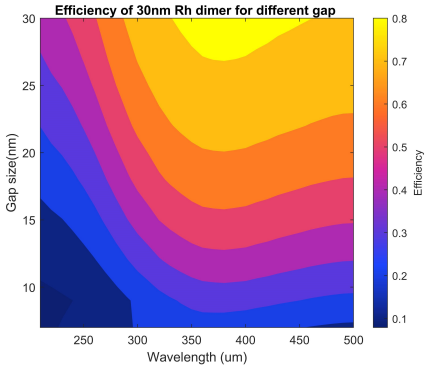

FIGURE 5.13 – Simulations of the antenna radiative efficiency (ratio of radiative rate to total decay rate) as a function of the emission wavelength and the gap size for a perfect point dipole emitter with parallel orientation located in the centre of the nanogap. The rhodium cube size is constant at 30 nm.

5.3 Fabrication of Dimer Optical Antenna

The antenna is self-assembly of two components, Rh nanocubes and silica-coated Al Nanoaperture. The fabrication of the antenna is a three-step process, fabrication of nanoaperture array with Gallium FIB, fabrication of precise Rh nanocubes in solution and then self-assembly of Rh nanocubes into Al-Nanoaperture using capillary force-assisted nanoparticle assembly.

5.3.1 Fabrication of Nanorectangular apertures

Arrays of 120*50 nm² rectangular nanoapertures and fiducial marks are milled by a focused ion beam (FIB) on a UV-transparent quartz coverslip substrate covered with a 100 nm thick aluminium layer. FIB milling is performed on the FEI DB235 Strata with 30 kV acceleration voltage and 10 pA gallium ion current. The aluminium nanoapertures are covered by a 10 nm-thick silica layer deposited with plasma-enhanced chemical vapour protection (Oxford Instruments PlasmaPro NGP80) in order to protect the aluminium layer against UV-induced photo corrosion.ROY, BADIE et al. 2021

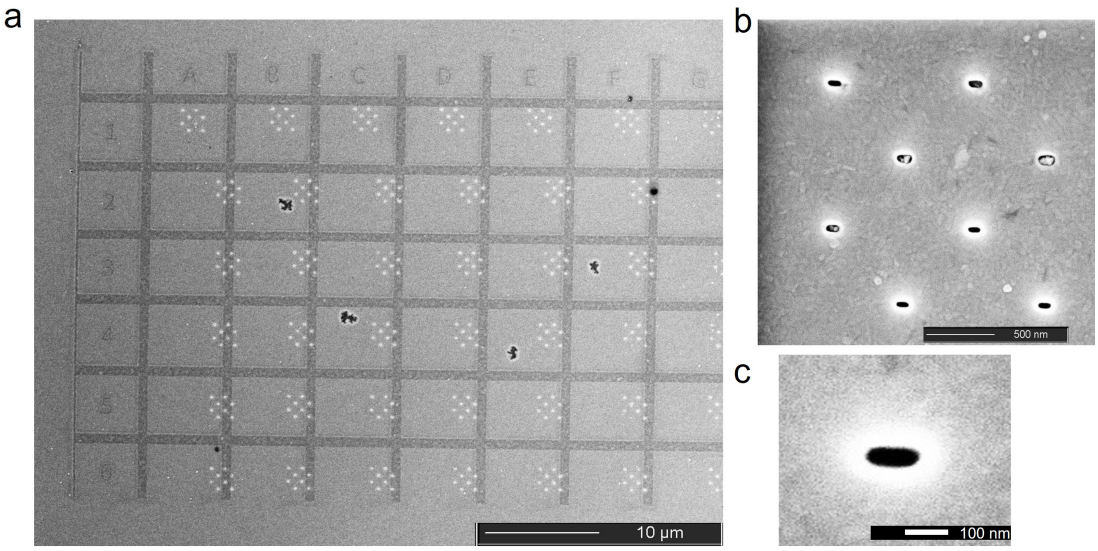

FIGURE 5.14 – SEM images of an (a)array of rectangular nanoapertures (b)small group of non-interacting nanoaperture(c)Empty nanoaperture

5.3.2 Fabrication of Rhodium nanocubes

Rhodium is a rare and expensive noble metal that has unique properties, such as high melting point, high corrosion resistance, and excellent catalytic activity. The fabrication of rhodium nanostructures has attracted significant attention due to their potential applications in various fields, including catalysis, electronics, and biomedicine. This section discusses the different fabrication techniques of rhodium nanostructures and compares their advantages and disadvantages. One of the most common methods for fabricating rhodium nanostructures is the solvo-thermal method.DUAN, N. YAN et al. 2014.Another technique for fabricating rhodium nanostructures is electroless platingMUENCH, NEETZEL et al. 2012 developed a versatile electroless plating procedure for fabricating porous rhodium nanotube catalysts. he electron beam lithography and electroplating techniques can produce rhodium nanostructures with high precision and reproducibility. However, the electron beam lithography and electroplating techniques are time-consuming and expensiveNG, SENIUTINAS et al. 2019. One of the most common methods for the synthesis of rhodium nanocubes is the seed-mediated growth method. HUMPHREY, GRASS et al. 2007first synthesized high-yield rhodium nanocubes and multi pods by reducing RhCl3 in the ethylene glycol-poly(vinylpyrrolidone) (PVP) system using the seed growth method by manipulating the temperature. The seed-mediated growth method is a simple and effective technique that can produce rhodium nanocubes with controlled size and shape.

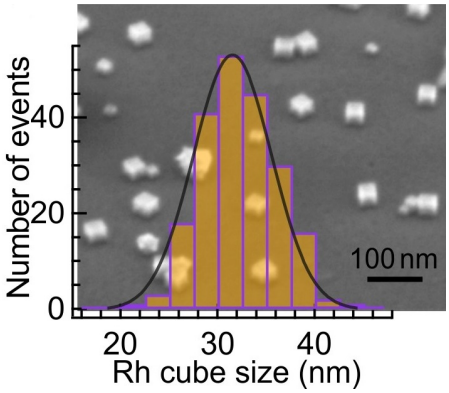

FIGURE 5.15 – Rh cubes on cover-slip and size distribution

The rhodium nanocubes were synthesized by our collaborators at Duke University (USA) using a seed-mediated method reported earlier.X. ZHANG, P. LI et al. 2016 First, the rhodium seeds solution was synthesized prepared : . 0.45 mmol KBr (ACROS, reagent ACS) was dissolved in 2 mL ethylene glycol (J.T. Baker, 99.0%) in a 20 mL scintillation vial. The vial was put in the oil bath for 40 min at 160°C. Susequestly, 0.045 mmol $RhCl_3$ůxH_2O (Aldrich, 98%) and 0.225 mmol PVP (Aldrich, MW=55000) were dissolved in 2 mL ethylene glycol separately. A two-channel syringe pump was used to pump these two solutions into the vial at a speed of 1 mL/h. The solution was aged for 10 min at 160°C before cooling to room temperature as the seed solution for another 10 min. Second, 0.4 mL of the prepared rhodium seeds solution from the first step was mixed with 1.6 mL ethylene glycol for a total of 2 mL solution in another 20 mL scintillation vial. The new vial was put in the oil bath for 40 min at 160°C. Two additional solutions produced by dissolving 0.045 mL $RhCl_3$ůxH_2O were dissolved in 2 mL ethylene glycol and . 0.225 mmol PVP (Aldrich, mw=55000) and plus 0.45 mmol KBr were also dissolved in another 2 mL ethylene glycol. These two solutions were also be pumped into the heated vial at a speed of 1 mL/h. After all, solutions were added, the mixture was cooled to room temperature and The rhodium nanocubes were collected after centrifuge and washing with water/acetone several times.

5.3.3 Self-assembly of Rh Dimer antenna inside Al Nanoapertures

Fabricating a precise nanostructure inside a nano-aperture is a cumbersome process, in literature, researchers have used photo-lithography for bigger nanostructuresJAMIOLKOWSKI, K. Y. CHEN et al. 2019 VALIEV et VALIEV 1992and for smaller nanostructure intensive use of FIB milling using gallium and or helium.PUNJ, MIVELLE, MOPARTHI et al. 2013a Fabricating nanostructures with colloidal techniques has paved the way for the industrial application of metal nanostructures however bottleneck lies in aligning these structures in an ordered manner on a surface or inside the nano aperture. One of the important techniques that can solve this problem is Capillary-Assisted Particle Assembly (CAPA),KUEMIN, STUTZ et al. 2011 this is a method for creating

nano- and micro-scale structures using the forces exerted by a liquid's capillary action. The approach often involves the self-assembly of particles under the influence of capillary forces during the evaporation of a liquid. The process can be summarized in the following stepsMALAQUIN, KRAUS et al. 2007
The simplified version of the process :

Particle Suspension : The process starts with a suspension of particles (such as nanoparticles or microparticles) in a liquid medium. The particles could be made of various materials like polymers, metals, or semiconductors, depending on the desired application.

Deposition : The suspension is then deposited onto a substrate. This could be done in various ways, such as by dip-coating, spin-coating, or simply by dropping the suspension onto the substrate.

Evaporation and Assembly : As the liquid medium evaporates, the particles are drawn together by capillary forces. This is because the liquid's surface tension changes as it evaporates, pulling the particles into close contact with each other. This can lead to the formation of organized structures such as layers or arrays of particles.

Final Structure : Once the liquid has completely evaporated, a solid structure remains, composed of the assembled particles. The final structure's properties (like its optical or electrical properties) depend on the particles used and their arrangement.

CAPA is a versatile method and has been used to create a wide variety of structures, from simple coatings to complex photonic crystals. It's also compatible with a wide range of materials and substrates, making it a valuable tool in fields like materials science, nanotechnology, and bioengineering. However, controlling the assembly process to achieve specific structures can be challenging and is a major focus of ongoing research in this area.FLAURAUD, MASTRANGELI et al. 2017

In our case, we have used a similar technique. For the deposition of rhodium nanocubes and their self-assembly into nanogap antennas, 2 mM sodium dodecyl sulfate (SDS) and 1% Tween20 are added to the 100 µL rhodium solution. This solution is then left for 15 minutes in an ultrasonic bath to ensure all nanoparticles are well dispersed. Droplets of 4 µL are then deposited on the aluminium nano rectangle sample and left to evaporate. Different movements of the droplet respective to the sample have been tried to benefit from capillary-assisted self-assembly, but the simple horizontal evaporation of the rhodium nanocube droplet gave the best results in our case. As we are illuminating from below the quartz substrate, the presence of extra nanoparticles on top of the aluminium film has no effect on our measurements. The nanoantennas are then imaged with a scanning electron microscope (electron beam of the FEI DB235 Strata). The position of the antennas containing two rhodium nanocubes is noted and used later to find the same antennas in the UV microscope. The rhodium antennas are remarkably stable, the sample can be rinsed and dried several times without disturbing the antenna geometry

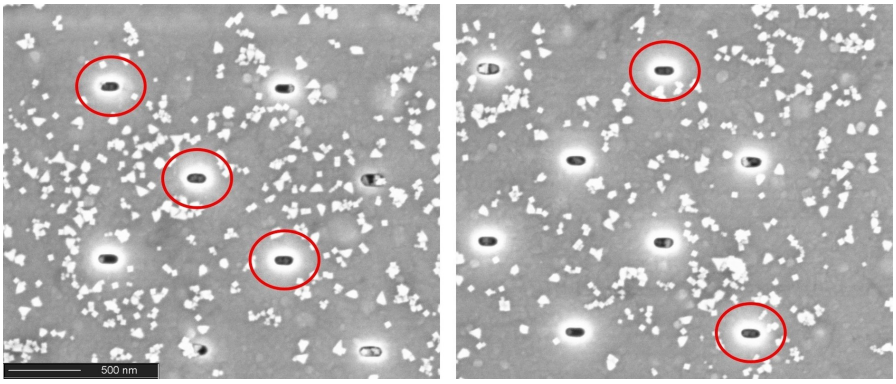

FIGURE 5.16 – SEM image of Array of 120X50 nm^2 after deposition and drying process of rhodium nanocubes. The nanoaperture with the nanocube is encircled. It is evident that not all the nanorectangles are filled with NPs, however, the fill factor is more than 50% and each antenna is robust enough for multiple measurements

In figure5.17 the volume in zeptoliter written in the bottom left of each image is deduced from the FCS measurement of the number of molecules inside the nanogap region and the known molecular concentration. The gap size in the bottom right is obtained from the SEM images as the difference between the total length of the rhodium dimer (measured along the main axis) minus the size of each rhodium nanocube (measured along the direction perpendicular to the main axis). For a correlation between the gap sizes deduced from FCS and SEM, please refer to Fig. 5.30. The nanoantennas are ranked from top left to bottom right as a function of the FCS volume. The alphanumeric code in the top left of each image is our internal reference of each antenna. As the nanocubes forming the antenna are positioned inside the rectangular aperture and are thus below the aluminum surface, they appear dimmer than the other rhodium nanocubes and triangular nanoparticles dispersed on top of the aluminum surface. It is worth mentioning that we had other configurations like monomers(we will elaborate some of the expt results for monomers in upcoming sections), trimers and tetramers but their optical performance was not reproducible and worse than the dimers so they are not considered in further studies.

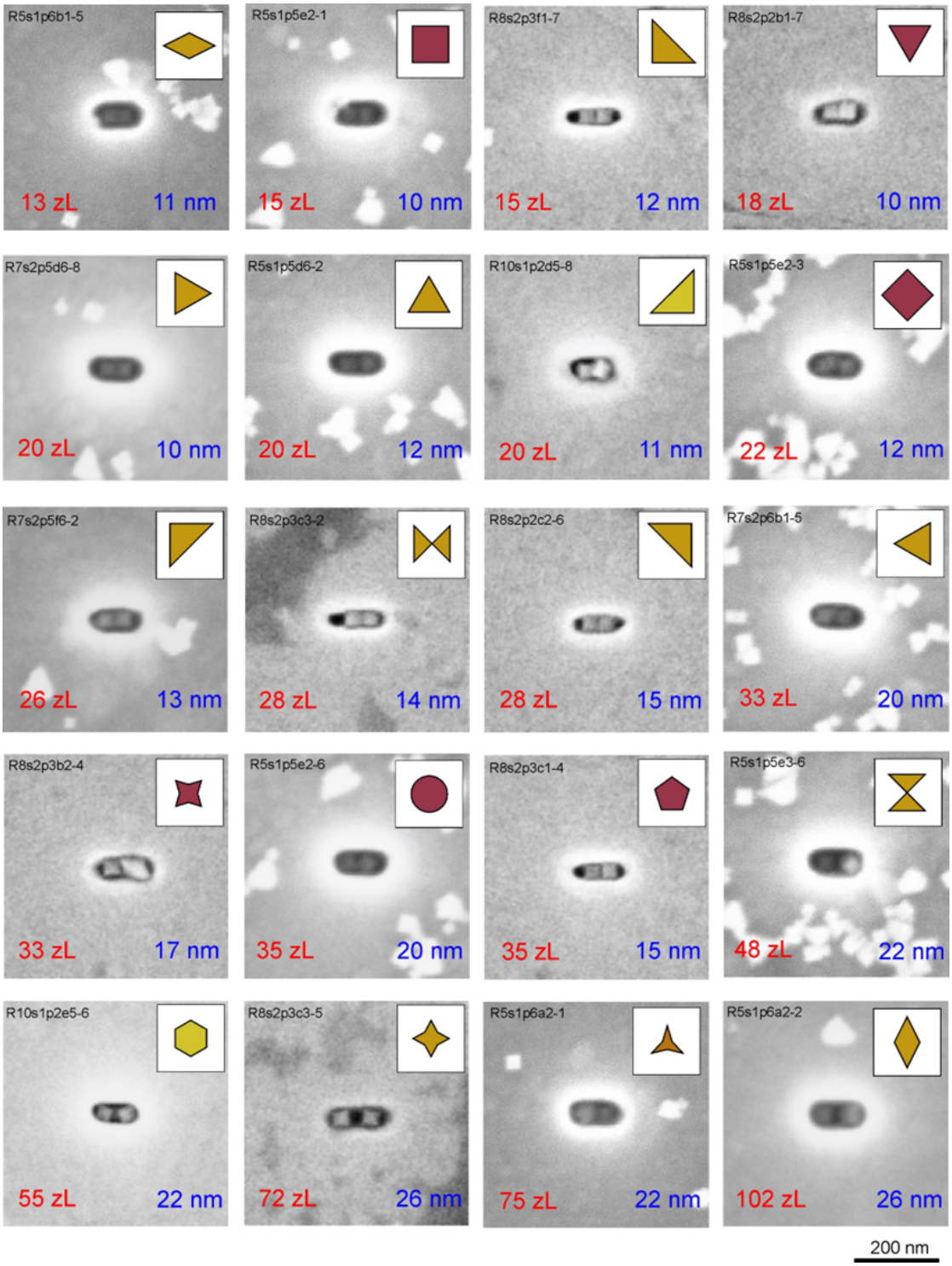

FIGURE 5.17 – Scanning electron microscopy images of the rhodium nanogap antennas used in the experiments corresponding to the data displayed in Fig. 5.23 5.20. The color symbol in the top right corner of each SEM image corresponds to the symbol used in Fig. 5.23 f 5.20 d-f so that a direct correlation between FCS results and the actual SEM images can be made.

5.4 Sensing with Rh Dimer in Nanoaperture antenna

We use fluorescence correlation spectroscopy (FCS) and time-correlated single photon counting (TCSPC) experiments to assess the optical performance of the nanoantennas and their ability to enhance the UV autofluorescence of diffusing label-free proteins. The comparison between experiments performed with the excitation laser polarization set parallel and perpendicular to the main antenna axis demonstrates the contribution of the nanogap enhancement. To test the fabricated and optimized Rh dimer in a nanoaperture antenna, we used a UV dye P-terphenyl with a high quantum yield. In addition, we will study proteins containing tryptophan and explore the rate constants of different analytes. We will study streptavidin with a quantum yield of 3.5% and 24 tryptophan and hemoglobin with a quantum yield of 0.5% and 6 tryptophan per protein. The autofluorescence emission spectra of all analytes are shown in fig5.18

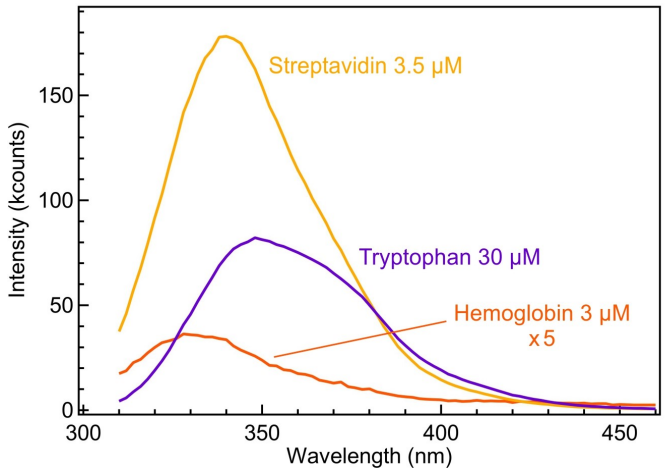

FIGURE 5.18 – Autofluorescence emission spectra of streptavidin and hemoglobin solutions were recorded along with a solution of tryptophan diluted in water to serve as a reference quantum yield. The spectra were recorded on a Tecan Spark 10M spectrofluorometer with 260-nm excitation and identical fluorescence detection conditions. The intensity for the hemoglobin spectrum has been multiplied 5 times to simplify viewing on the same graph. To estimate the average quantum yield of protein autofluorescence, we computed the ratios of the integrated fluorescence intensities over the 310-410 nm spectral region, normalized by the absorbance of the same solutions measured at 260 nm, and we used the calibrated 12% quantum yield of tryptophan in 100 mM water phosphate buffer solution R. F. CHEN 1972

We conducted an analysis with UV Rh dimer antenna using a 266nm pulse laser for P-terphenyl and a 295nm pulse laser for proteins such as streptavidin and hemoglobin. The experimental setup is illustrated in Figure5.19. The molecules of

the analyte move freely within the nanorectangle aperture, and the signal from it is amplified when it passes through the gap of the Rh dimer antenna.

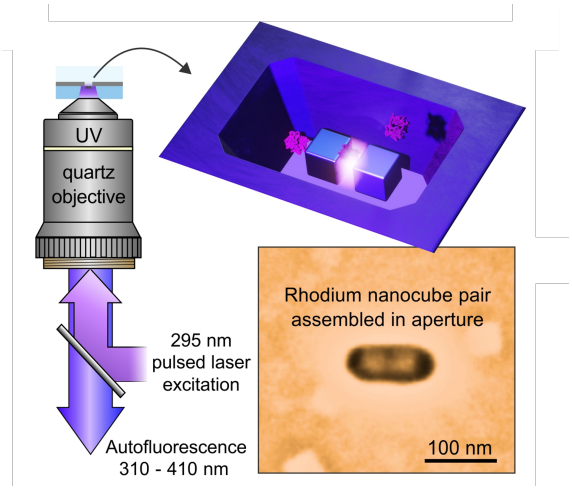

FIGURE 5.19 – Experiment scheme of the UV microscope with the rhodium nanogap antenna made from two nanocubes assembled into a rectangular aperture milled in an opaque aluminum film. The insert shows a scanning electron microscope (SEM) image of nanogap antenna made of two rhodium nanocubes inserted into a 120 x 50 nm² aperture milled in an aluminium layer.

5.4.1 Enhancing UV signal from p-terphenyl

P-terphenyl is a UV fluorescent dye with 93% quantum efficiencyAleksandr BARULIN, Jean Benoît CLAUDE et al. 2019c . In fig 5.20(a)we can see the characteristic polarization-dependent signature of the dimer gap antenna is observed for p-terphenyl. The time trace shows a higher signal for the case when polarization is parallel to the gap, parallel polarization excites gap antenna mode as discussed in 5.10. However to rely solely on the total intensity averaged across the entire antenna volume is inadequate for estimating the brightness enhancement per molecule. This is because the total intensity comprises the product of brightness and the number of molecules. To overcome this challenge, we employ FCS as a powerful technique to independently determine both the number of molecules contributing to the signal and their individual autofluorescence brightness per emitter. In addition, FCS is supplemented with time-correlated single photon counting (TCSPC) to estimate the fluorescence lifetime. To quantify the brightness enhancement with the nanoantenna, we use UV-FCS to measure the average number of molecules N^*present inside the nanogap and their autofluorescence brightness per molecule Q^* (see Methods). This technique is previously well estabilished PUNJ, REGMI et al. 2015 PUNJ, MIVELLE, MOPARTHI et al. 2013a The enhancement can be seen in the FCS traces where FCS amplitude is higher than in the case of parallel polarization in comparison to perpendicular. We also see a reduction in the lifetime of P-terphenyl for parallel polarization. All these features point toward the fact that gap antenna mode is excited and the

signal from P-terphenyl is enhanced by 20 times better than the previously achieved state-of-art enhancementAleksandr BARULIN, ROY, Jean Benoît CLAUDE et al. 2022

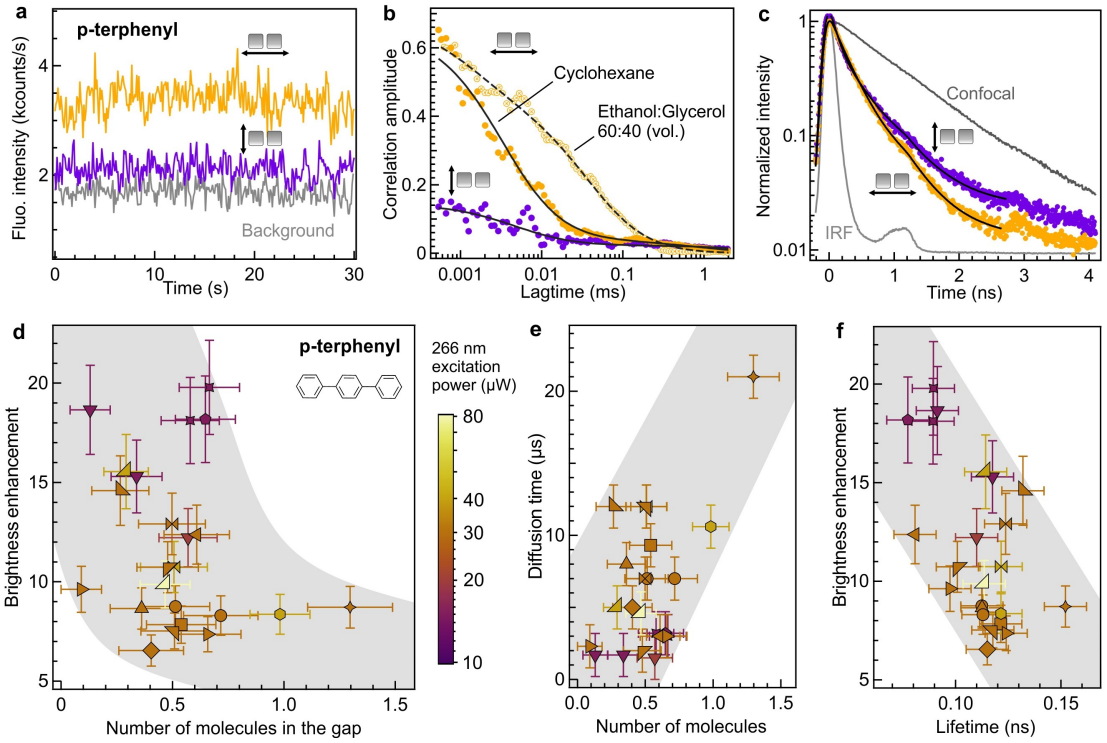

FIGURE 5.20 – UV fluorescence enhancement of p-terphenyl with rhodium nanogap antennas. (a) Fluorescence intensity time traces were recorded on a 10 µM solution of p-terphenyl in cyclohexane on a nanoantenna with the excitation polarization set parallel (yellow) or perpendicular (purple) to the main axis of the dimer antenna. The binning time is 100 ms. The gray trace shows the background intensity level in the absence of p-terphenyl. The 266 nm excitation power used here is 40 µW. (b) The FCS correlation functions correspond to the traces in (a) and when p-terphenyl molecules are diluted into a 60 :40 glycerol : ethanol mixture to increase the viscosity. Dots are experimental data, and lines are numerical fits. (c) Normalized time-resolved decay traces corresponding to the experimental data in (a) and the confocal reference (dark gray).The data in a-c correspond to the antenna reference number R10s1p2d5-8 for which a 11 nm gap size was inferred from the SEM image. (d) Scatter plot of the fluorescence brightness enhancement for p-terphenyl as a function of the number of molecules detected in the gap antenna. The various markers indicate different nanoantennas and the color codes for the excitation power. Among the different experiments, the number of molecules has been scaled to correspond to a 30 µM concentration of p-terphenyl. (e) Scatter plot of the FCS diffusion time as a function of the number of molecules detected in the nanogap. (f) Scatter plot of the fluorescence brightness enhancement as a function of the fluorescence lifetime. Throughout (d-f), the shaded areas are guides for the eyes

We further introduced glycerol in the system to slow down the molecules and thus extract more signals. When cyclohexane is replaced by a 60 :40 (v/v)glycerol : ethanol mixture, confocal experiments calibrate that the viscosity of the solution increases 12.5 times. Our nanoantenna data (Fig. 5.20 b) show a similar increase of 11.4 times the diffusion time, which we directly relate to the increase in the solution viscosity. We learned from the experiment that the gap size is in the range of zeptoliters, and the increase in viscosity increases the enhancement of CRM (count rate per molecule). Power has an inverse relation with enhancement, and an increase in excitation power leads to a lower enhancement, which can be explained by the fact that fluorescence emission from P-terphenyl saturates with an increase in power. This observation is not limited to P-terphenyl; rather, it is applicable to any emitter in the plasmonic cavity. For sake of better understanding the influence of gap size on enhancement experimentally, we plot a varitaion of enhancement wrt. to

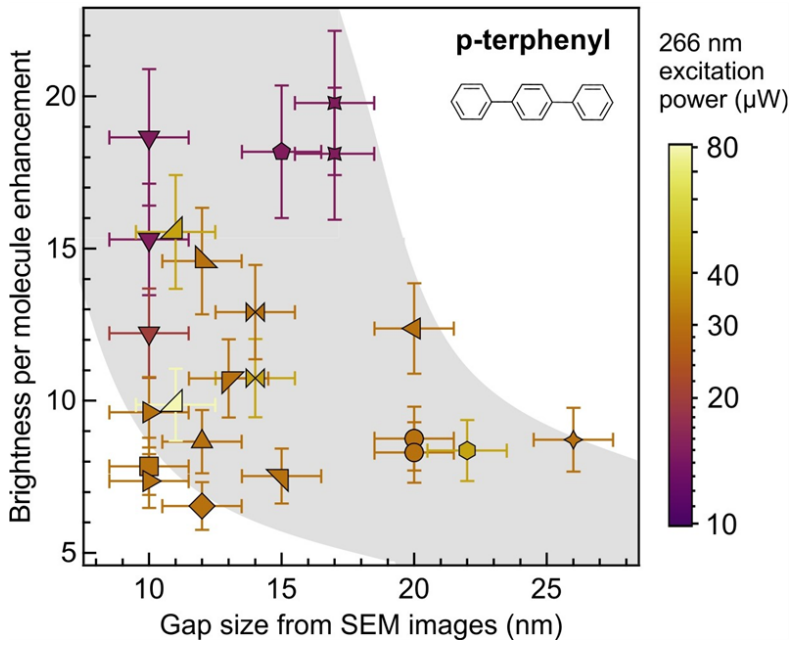

FIGURE 5.21 – Scatter plot of the fluorescence brightness enhancement p-terphenyl (b) as a function of the gap size deduced from the SEM images in Fig. S1. The enhancement values are the same as in Fig. 5.20 d, but the variable on the x axis is now the size of the gap deduced from the SEM images instead of the number of molecules in the nanogap measured with FCS. The different markers indicate the different nanoantennas (same code as in Fig. S1), and the color indicates the excitation power used. Shaded areas are guides to the eyes.

We performed a control FCS experiment with a single rhodium nanocube. The conditions are identical to those used for Fig. 5.20 for p-terphenyl dissolved in a glycerol :ethanol mixture (60 :40 volume ratio) to increase the viscosity, slow down the diffusion time and facilitate FCS measurement. The concentration is 10 µM, the 266 nm excitation power is 40 µW. In fig5.22 (a) FCS correlation functions. The average total

intensity F is 4570 counts/s, and the background intensity B is 1700 counts/s. From the FCS fit amplitude ρ_1 of 0.34, we deduce a number of molecules of $N = (1 - \frac{B}{F})^2 \frac{1}{\rho_1}$ of 1.2 molecules with a brightness $(F - B)/N$ of 2400 counts/s, which is enhanced by 5.2× above the reference 475 counts/s found for p-terphenyl in our confocal setup. In fig5.22 (b) Comparing the normalized time-resolved decay traces we slightly longer fluorescence lifetime is observed in the case of the single rhodium cube, which may be related to a reduced quenching rate with a single nanocube instead of two. A statistical T-test has been performed to compare the distributions of enhancement factor per emitter for monomer and dimer case; the resulting P-value is written in the graph of fig5.22 c. The p-value clearly indicate that null hypothesis is rejected.

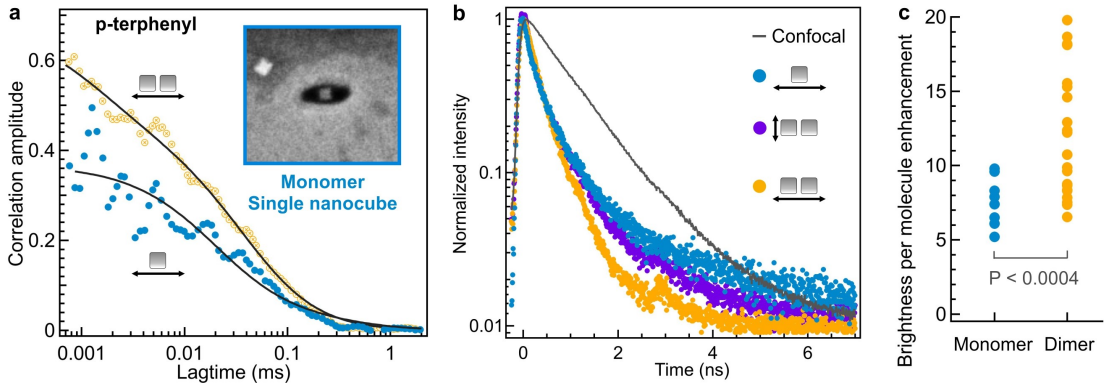

FIGURE 5.22 – Control FCS experiment with a single rhodium nanocube. (a) FCS correlation functions. (b) Comparison of the normalized time-resolved decay traces, superposing to the data in Fig. 5.20the result for the single rhodium nanocube. (c) Comparison of the fluorescence enhancement factors for the brightness per emitter for the single nanocube (monomer) and the dimer of nanocubes, both with parallel excitation.

5.4.2 Enhancing Auto-fluorescence of Proteins

5.4.2.1 Streptavidin

Figure 5.23 summarizes the results found with label-free streptavidin at 50 µM concentration. A higher intensity is obtained when the excitation polarization is set parallel to the gap (Fig. 5.23a). We have checked that the excitation and detection on our microscope are not polarization sensitive, so the polarization dependence can be directly linked with the enhanced autofluorescence signal stemming from the nanoantenna gap region. The FCS curve has a higher correlation amplitude with parallel excitation polarization (Fig. 5.23b, 5.28), while the autofluorescence lifetime is reduced when the excitation polarization is turned from perpendicular to parallel. The nanoantenna significantly reduces the autofluorescence lifetime from 1.5 ns for the confocal reference to 0.47 ns for the antenna with parallel orientation, demonstrating a higher local density of optical states (LDOS) in the nanoantenna hotspot. All these

raw observations highlight the contribution of the nanogap hotspot and its effect to enhance UV autofluorescence.
For the nanoantenna with parallel excitation, we find a brightness enhancement of 41± 5 fold for label-free streptavidin. This performance is clearly above the enhancement found with perpendicular orientation (6.7± 0.8) or the empty nanoaperture in the absence of rhodium antenna (7.3 ± 0.6,5.24). Importantly, the enhancement factor found with the nanoantenna and parallel polarization significantly outperforms the gain obtained earlier with nanoaperture-based designs (we obtained 4-fold enhancementAleksandr BARULIN, Jean Benoît CLAUDE et al. 2019a for a bare nanoaperture without microreflector and 15-fold with the so-called horn antennaAleksandr BARULIN, ROY, J.-B. B. CLAUDE et al. 2022 combining a nanoaperture and a microreflector). The observation of saturation of the autofluorescence brightness (Fig. 5.23e) is a supplementary control to show that the signal stems from protein autofluorescence and is not related to some laser backscattering or Raman scattering. Streptavidin autofluorescence brightness up to 1000 photons/s/molecule are reached, which is a key element in maximizing the signal-to-noise ratio in UV-FCS.

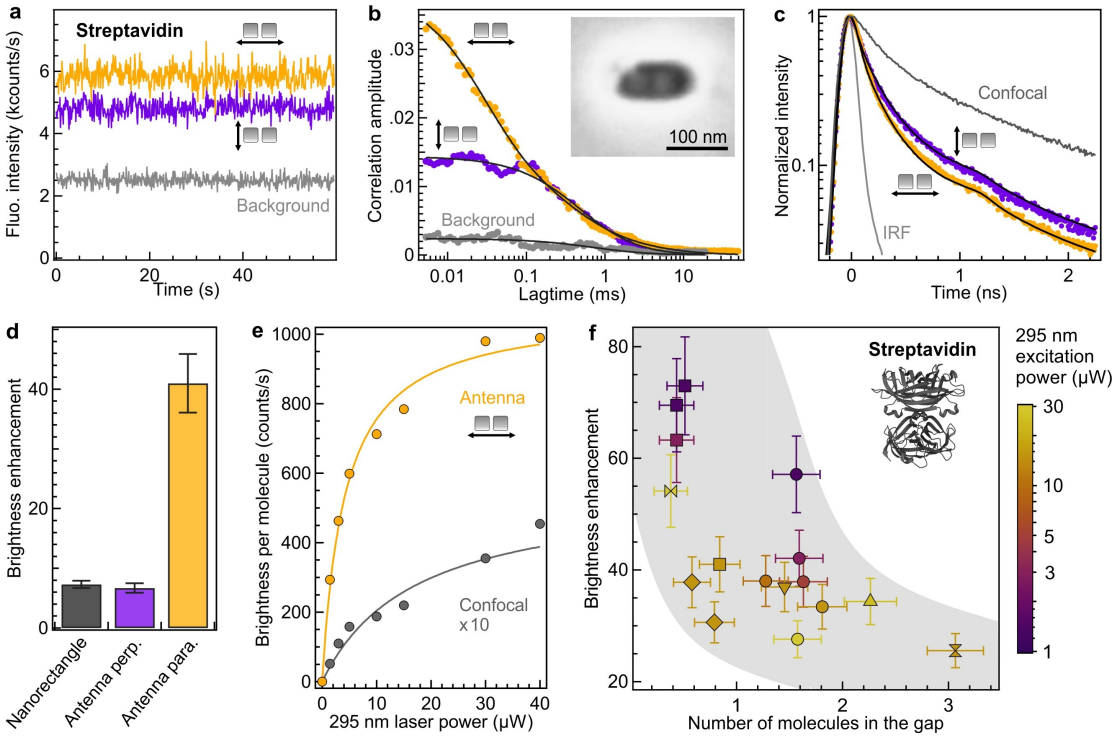

FIGURE 5.23 – UV autofluorescence from label-free streptavidin proteins enhanced with a nanogap antenna. (a) Autofluorescence intensity time traces (binning time 100 ms) for a rhodium nanogap antenna with the excitation polarization set parallel (yellow) or perpendicular (purple) to the dimer antenna's main axis. The antenna is covered with a 50 µM solution of diffusing label-free streptavidin proteins. The grey trace shows the background intensity level in the absence of the protein (the antenna is covered with the buffer solution). The 295 nm excitation power used here is 15 µW. (b) FCS correlation functions corresponding to the traces in (a). Dots are experimental data, lines are numerical fits. The insert SEM image shows the dimer antenna used for this experiment(the antenna reference is R5s1p5e2-1 with a gap size of 10 nm as measured by SEM) (c) Normalized time-resolved decay traces correspond to the experimental data in (a) and the confocal reference (dark grey). IRF stands for the instrument response function. (d) Comparison of the enhancement factors for the fluorescence brightness per molecule in the empty nano-rectangle (without rhodium nanocubes, see Fig.5.24) and the rhodium nanoantenna with parallel and perpendicular excitation polarizations. (e) Excitation power dependence of the brightness per molecule measured in the nanogap antenna (yellow markers) and in the confocal reference (grey). The line fit with a saturation model. (f) Scatter plot of the fluorescence brightness enhancement for streptavidin proteins as a function of the number of detected molecules in the gap antenna. Different markers indicate different nanogap antennas and the colour codes for the excitation power used. The shaded area is a guide to the eyes.

In the case of FIB PUNJ, MIVELLE, MOPARTHI et al. 2013a and electron-beam

lithography FLAURAUD, REGMI, M. WINKLER et al. 2017 there is an unavoidable variability in the size of the nanoantenna gap, which results in a dispersion of the nanoantenna's performance (comparison shown in method section). We evaluate this effect for our UV antennas, with Fig. 5.23f showing the brightness enhancement in relation to the number of gap molecules N^*. As previously observed for visible antennas and fluorescent dyes,PUNJ, MIVELLE, MOPARTHI et al. 2013a there is a relationship between the brightness enhancement and the number of molecules detected in the gap. Antennas with a smaller gap tend to yield a higher brightness enhancement and a lower number of molecules. We observe a similar pattern here for UV antennas and label-free proteins. With an average of 1.3± 0.7 molecules in the nanogap for a 50 µM concentration, the detection volume of the nanoantenna equates to 40 ± 20 zeptoliter (1 zL = 10^{-21} L = 1000 nm^3), which is 25000 times smaller than the femtoliter confocal detection volume. For reference, experiments with gold nanoantennas with 12 nm gaps resulted in detection volumes of 100 zL, while dimers of spherical 80 nm gold nanoparticles yielded volumes of 70 zL. To see evolution of enhancement with gap size in experiments for streptavidin, we did a correlative measurements and ploted enhancement versus gap size in following figure. The data point is same as fig5.23 f, but the x-axis is gap size which is calculated from FCS and correlative SEM images.

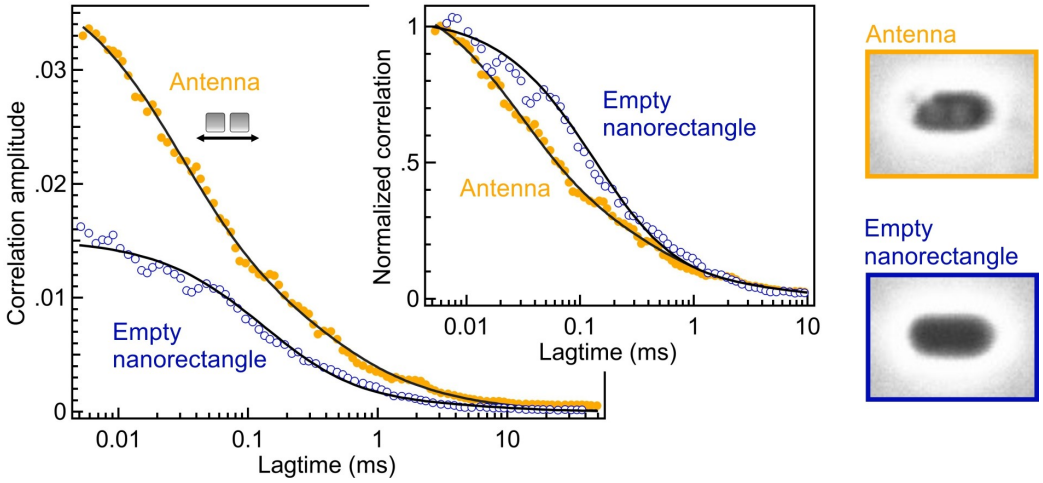

FIGURE 5.24 – Comparison between the FCS correlation functions obtained for a dimer nanoantenna and a rectangular nano-aperture without rhodium nanocubes. The conditions are identical to the ones used for Fig. 2 with streptavidin proteins. Dots are experimental data, lines are numerical fits. The inserted graph shows the amplitude-normalized FCS functions to highlight the shorter diffusion time in the case of the nanogap antenna

5.4.2.2 Hemoglobin

Hemoglobin is one of the important biological proteins which has 6 Trp residues. Our comparative spectroscopy experiments estimate the average quantum yield of haemoglobin to be around 0.5% . To give a context to this number, in confocal single

Hemoglobin molecule gives on average around 2-3 photons/sec. With the Rh nanocube dimer antenna, we could reach 250 counts/sec per molecule and were able to FCS measurement in fig 5.25 Hemoglobin molecules with single molecule sensitivity even with 50μM solution thanks to the zeptoliters detection volume of the antenna. This can open further opportunities to study the effect of oxygen or glucose on single molecules of haemoglobin without labelling.ORTAS, MAHOU et al. 2023

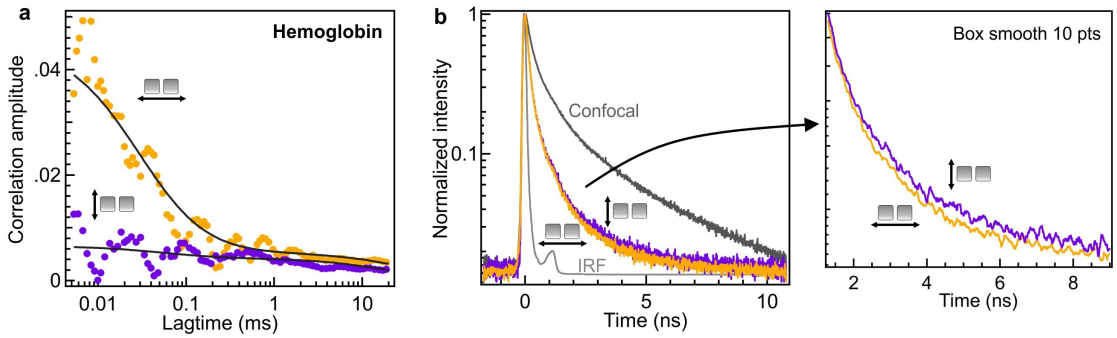

FIGURE 5.25 – FCS and TCSPC data for label-free haemoglobin in a nanogap antenna. (a) FCS correlation functions, dots are experimental data, and lines are numerical fits. The antenna is covered with a 50 µM solution of diffusing label-free Haemoglobin proteins. The 295 nm excitation power used here is 15 µW. (b) Normalized time-resolved decay traces corresponding to the data in (a) and to the confocal reference (dark grey). IRF stands for the instrument response function. The inserted graph on the right is a close-up view of the decays for excitation polarization set parallel and perpendicular to the dimer's main axis. The data have been smoothed with 10 points box averaging.

5.4.3 Discussion on Photokinetic Rates of Analytes

With the knowledge of the excitation intensity gain (Fig. 5.10) and the antenna's influence on the various photokinetic rates, we can infer the net fluorescence brightness enhancement as a function of the emitter's initial quantum yield and compare with our experimental results. Emitters with lower quantum yields give higher apparent brightness enhancement factors (Fig. 5.26d) as a maximum benefit can be taken from the nanoantenna's ability to enhance the radiative rate. We compare our experimental results with the numerical predictions in Fig. 5.26e. Within the experimental uncertainties, the enhancement values found for the different molecules agree well with the theoretical predictions, confirming the validity of our approach. Experimentally, the highest brightness enhancement at 120-fold is obtained with haemoglobin, which has the lowest 0.5% quantum yield in solution. The simulations predict even higher enhancement factors above 400-fold yet in the case of a dipolar source perfectly aligned with the nanoantenna (Fig5.12).

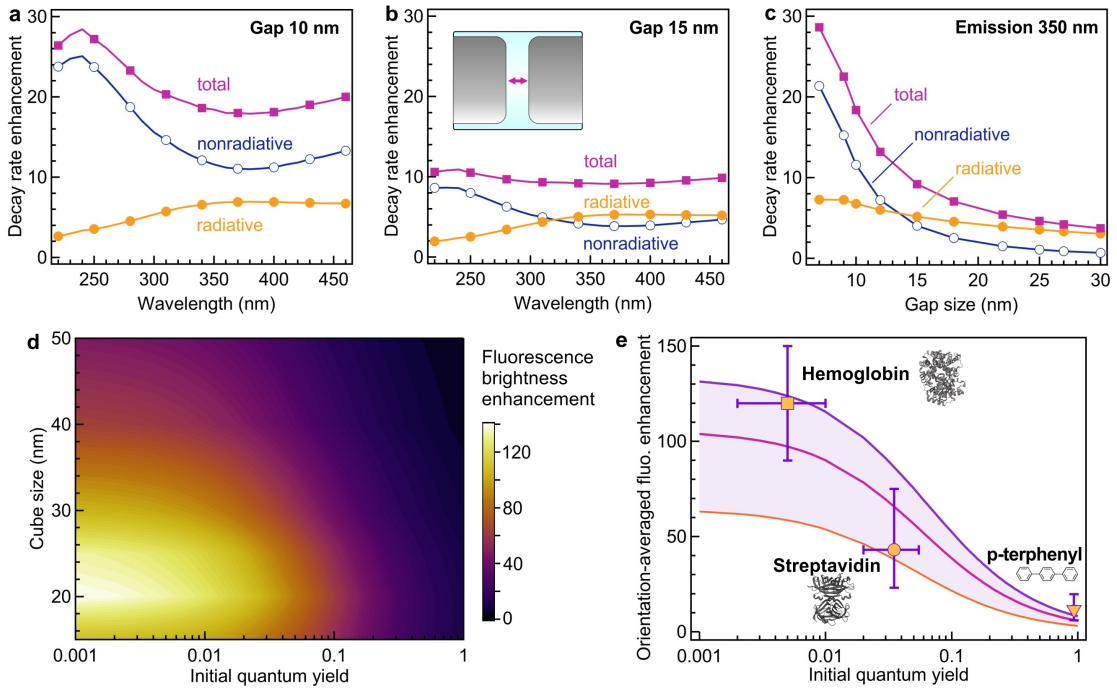

FIGURE 5.26 – Rhodium UV nanogap antennas to enhance the photokinetic rates. (a,b) Numerical simulations of the enhancement of the decay rate constants as a function of the emission wavelength for a perfect dipole emitter with parallel orientation located in the centre of the nanogap. The rhodium cube size is constant at 30 nm. The gap size is 10 nm in (a) and 15 nm in (b). All rates are normalized respective to the dipole radiative rate in free space. (c) Evolution of the decay rate enhancement factors as a function of the gap size, for an emission wavelength of 350 nm and a cube size of 30 nm. (d) Simulations of the fluorescence brightness enhancement as a function of the rhodium nanocube size and the emitter's initial quantum yield in free space. The gap size is kept constant at 10 nm. The excitation wavelength is 295 nm and the emission is 350 nm. The emission is averaged over the three orientation directions. (e) Comparison of the simulated (lines) and experimental (markers) fluorescence brightness enhancement factors as a function of the quantum yield in homogeneous solution for the different emitters used in this work. The emission is averaged over the three orientation directions. From top to bottom, the three lines represent rhodium cube sizes of 25, 30 and 40 nm respectively, with a gap size set to 10 nm. The protein structures in grey have been made using Mol* viewer.52

Combining all the experimental results on the brightness enhancement and the fluorescence lifetime reduction(equation discussed in Methods), we can compute back all the different decay rate constants in Figure '5.27.

	ϕ_0	τ_0	Γ^0_{tot}	Γ^0_{rad}	Γ^0_{nr}	η_F	τ^*	η_{exc}	$\eta_{\Gamma rad}$	Γ^*_{loss}	ϕ^*	η_ϕ
P-ter phenyl	0.93	1.00	1.00	0.93	0.07	16.1	0.11	12.4	8.6	1.5	0.84	0.9
Strep tavidin	0.035	1.50	0.67	0.02	0.64	65	0.47	14.4	10.0	1.3	0.11	3.1
Hemo globin	0.005	2.10	0.48	0.00	0.47	120	0.65	19.7	13.6	1.0	0.021	4.2

FIGURE 5.27 – Photokinetic rate parameters of different label-free proteins and p-Terphenyl. The decay rate constants are expressed in $(ns)^-1$, and the lifetimes are in ns.

For p-terphenyl, streptavidin and haemoglobin, and despite the large difference in their initial quantum yields, we find consistent excitation gains η_{exc}=15.5 ±3.8 and radiative gains $\eta_{\Gamma rad}$=10.8±2.6 in good agreement with numerical simulations considering the experimental values are orientation-averaged and position-averaged inside the nanogap. The loss decay rate constant into the metal is also a preserved feature among our different experiments, withΓ^*_{loss}=1.25±0.3 ns^-1. Compared with nanogap antennas in the red spectral range with comparable gap sizes, a loss decay rate constant of 0.5 ns^-1 can be found for gold,G. P. ACUNA, MÖLLER et al. 2012 while aluminium and silicon yield typically 2 ns^-1 and 4 ns^-1 respectivelyGHENUCHE, MIVELLE et al. 2015 The non-radiative losses associated with rhodium in the UV appear thus quite comparable to other materials in the visible range. Further discussion on lifetime analysis and photokinetic rates calculation is given in the subsequent Method section

5.5 Conclusion

Our study presents both experimental and numerical proof of the successful creation of rhodium nanogap antennas, which exhibit plasmonic resonances that extend well into the deep ultraviolet region. The design of our antenna capitalizes on the powerful combination of an intense electric field enhancement and the alteration of the photokinetic rate, resulting in a brightness enhancement factor of up to 120-fold. Additionally, it allows for detection volumes in the zeptoliter range and an autofluorescence lifetime under a nanosecond. The nanogap mode is crucial to this process, as demonstrated by polarization-dependent measurements and the observed interdependence of brightness, lifetime, and detection volume. Due to the intense nanogap enhancement, our antennas outperform previous devices based on nanoparticles or nanoapertures.

One of the key applications and motivations for UV plasmonics is the enhancement of autofluorescence in label-free proteins. We demonstrate this capability by successfully enhancing autofluorescence signals from streptavidin and haemoglobin proteins. Given that the autofluorescence quantum yield of tryptophan in most proteins is usually only a few percentages, there is a strong interest in using

UV nanoantennas to significantly boost the autofluorescence signal from single proteins, making it easily detectable. By utilizing UV-FCS experiments, we provide new opportunities for local measurements of concentration, mobility, brightness, and stoichiometry of label-free proteins.

In conclusion, our research expands the practical use of plasmonic nanoantennas into the deep UV range, paving the way for studying individual proteins in their native state under physiological concentrations. Looking forward, aluminium nanocubes and nanocrystals present intriguing possibilities for achieving lower losses than rhodium, provided their water corrosion issue can be addressed. Resonant UV nanoantennas also hold great potential for advancing several other plasmonic applications, such as resonant Raman spectroscopy, circular dichroism spectroscopy, photodetectors, and photocatalysis.

5.6 Method

5.6.1 FCS Analysis

The fluorescence time traces data are computed with Symphotime 64 (Picoquant) and fitted with Igor Pro 7 (Wavemetrics). The FCS analysis builds on our previous works on nanoantennas in the visible range.PUNJ, MIVELLE, MOPARTHI et al. 2013cFLAURAUD, REGMI, WINKLER et al. 2017bREGMI, BERTHELOT et al. 2016cFor the rhodium nanoantennas with parallel excitation, the FCS correlations are fitted with a three-species model :SOLTI, D. CHAPKIN et al. 2022

$$G(\tau) = \Sigma \rho_i (1 + \frac{\tau}{\tau_i})^{(-3/2)} \tag{5.4}$$

where ρ_i and τ_i are the amplitude and diffusion time of each species. Here for further simplification, we have assumed that the aspect ratio of the axial to transversal dimensions of the detection volume is equal to 1 following our previous works. The rationale behind these three species model is that the first fast-diffusing species accounts for the molecules inside the nanogap, the second intermediate diffusing species account for the molecules present inside the nanorectangle but diffusing away from the nanogap hotspot while the third slowly diffusing term is introduced to account for some residual correlation stemming from the background.ROY, Jean Benoît CLAUDE et al. 2023 For p-terphenyl, owing to the fast diffusion time and the high quantum yield of the dye, we find that a two-species model is sufficient to fit the FCS function. For the antennas with perpendicular excitation polarization, we always use only a two-species model as the nanogap contribution is absent in this case. Typical fit results are shown in the datasheet in Fig 5.28 for the three different target molecules probed here. Building on our earlier work on visible plasmonic antennas,PUNJ, MIVELLE, MOPARTHI et al. 2013dFLAURAUD, REGMI, WINKLER et al. 2017b1GHENUCHE, MIVELLE et al. 2015 we use the following notation in our analysis of antenna performance : the average number of molecules present inside the nanogap is

N^* with a brightness per molecule Q^*. The number of molecules diffusing outside the nanogap (but still contributing to the total detected fluorescence and hence to the FCS amplitude) is N^0 with a brightness per molecule Q^0. The total fluorescence intensity is F and B is the background intensity recorded on the same nanoantenna in the absence of the target protein. The general FCS formalism in the presence of multiple species can be inversed to express the number of molecules within the nanogap N^* and their brightness per molecule Q^* :

$$N^* = \frac{(F - B - N^0 Q^0)^2}{(F^2(\rho_1 + \rho_2) - N^0 (Q^0)^2)} \tag{5.5}$$

$$Q^* = \frac{(F^2(\rho_1 + \rho_2) - N^0 (Q^0)^2)}{(F - B - N^0 Q^0)} \tag{5.6}$$

For the values of the parameters $N^0$and Q^0 for the molecules diffusing outside the nanogap, we use the FCS measurements when the excitation polarization is set perpendicular to the dimer axis.

Protein	STREPTAVIDIN		P-TERPHENYL		HEMOGLOBIN	
Concentration	50 µM		10 µM		50 µM	
Power (µW)	15		40		15	
Exc. Polarization	Parallel	Perpendicular	Parallel	Perpendicular	Parallel	Perpendicular
F (counts/s)	5740	4860	3370	2100	4070	2970
B (counts/s)	2100	2100	1700	1450	2200	2200
ρ_1	0.0276	--	--	--	0.028	--
ρ_2	0.0093	0.0145	0.635	0.119	0.012	0.0024
ρ_3	0.0014	--	0.034	0.027	0.0053	0.0042
τ_1 (ms)	0.042	--	--	--	0.04	--
τ_2 (ms)	0.70	0.73	0.005	0.0066	0.07	0.08
τ_3 (ms)	8	--	1.4	4.6	49	30
G(0) = ρ_1 + ρ_2	0.0369	0.014	0.635	0.119	0.040	0.0024
N_0	22.2	--	0.8	--	28	--
Q_0 (counts/s)	124	--	807	--	27.5	--
N*	0.90	22.2	0.16	0.8	1.9	28
Q* (counts/s)	987	124	6530	807	583	27.5
Q_{ref} (counts/s)	22	22	475	475	3.5	3.5
Brightness enhancement	44.9	5.6	13.75	1.7	166	7.9

FIGURE 5.28 – Datasheet and fit parameters obtained for different proteins from Rh gap antenna.

5.6.2 Lifetime Analysis

The fluorescence decay histograms are computed and analyzed with Symphotime 64 (Picoquant). We use an iterative deconvolution fit taking into account the

measured instrument response function (IRF). The decay histograms in the nanoantenna are fitted with a three-component exponential model. To ease the comparison between the parallel and perpendicular polarizations, we use the same characteristic lifetimes for both polarizations and compute the intensity-averaged lifetime as the final readout. All the fit parameters are summarized in datasheet given in fig 5.29

Protein	STREPTAVIDIN		P-TERPHENYL		HEMOGLOBIN	
Exc. Polarization	Parallel	Perpendicular	Parallel	Perpendicular	Parallel	Perpendicular
τ_1 (ns)	0.025		0.025		0.025	
τ_2 (ns)	0.166		0.140		0.243	
τ_3 (ns)	0.860		0.450		1.740	
I_1 (%)	19.74	23.91	7.48	30.85	11.09	18.52
I_2 (%)	32.61	23.91	25.99	--	60.27	52.15
I_3 (%)	47.64	52.18	66.53	69.15	28.64	29.33
$\tau_{average\ intensity}$ (ns)	0.47	0.49	0.114	0.32	0.65	0.64

FIGURE 5.29 – Fitting parameters for the TCPSC data. For the average lifetime of p-terphenyl in a parallel case, we took only the first and second components into consideration to compute the intensity-averaged lifetime

To determine experimentally the influence of the rhodium nanoantenna on the photokinetic rates, we use the following approach and notations : for the confocal reference, the total decay rate constant $\Gamma^0_{tot} = \Gamma^0_{rad} + \Gamma^0_{nr}$ is the sum of the radiativeΓ^0_{rad} and nonradiative Γ^0_{nr}decay rate constants. It also amounts to the inverse of the fluorescence lifetime $1/\tau_0$. The quantum yield is$_0 = \Gamma^0_{rad}/\Gamma^0_{tot}$. The different values are summarized in fig5.27 for the various molecules used here. In the presence of the nanoantenna, the lifetime is shortened, and becomes$1/\tau^* = \Gamma^*_{rad} + \Gamma^0_{nr} + \Gamma^*_{loss}$. Here we consider that the radiative decay rate constant Γ^*_r is enhanced (Purcell effect), that the internal nonradiative decay rate constant Γ^0_{nr} is unaffected by the photonic environment and that an additional nonradiative decay channel Γ^*_{loss} is introduced to account for the extra losses into the free electron cloud in the metallic antenna.2,3 The fluorescence brightness enhancement η_F corresponds to the product of the gains in excitation intensity η_{exc}, quantum yield η, and collection efficiency η_{coll}.4 The quantum yield gain can be further written as the ratio between the gains in the radiative rate $\eta_{\Gamma rad}$ and the total decay rate $\eta_{\Gamma tot}$, so the fluorescence enhancement becomes $\eta_F = \eta_{exc} * \eta_{coll} * \eta_{\Gamma rad}/\eta_{\Gamma tot}$ (here $\eta_{\Gamma tot}$is also equivalent to the reduction in the fluorescence lifetime). With the 0.8 numerical aperture of our microscope objective, the laser beam can still be considered to be moderately focused (this numerical aperture corresponds to a maximum angle of 34ř in quartz). In this case, the reciprocity theorem states that the gain in excitation intensity amounts to the products of the gains in collection efficiency times the gain in radiative rate :$\eta_{exc} = \eta_{coll} * \eta_{\Gamma rad}$.5 We also use recent numerical simulations of the collection efficiency gain to estimate its value to$\eta_{coll} = 1.44$for all the different molecules here.6 From the measurements of

the brightness enhancementη_F together with the fluorescence lifetimes in confocal and in the nanoantenna and the knowledge of the quantum yield ϕ_0 in homogeneous solution, we can compute back all the different rate constants, including the losses to the metal Γ^*_{loss}. The main results are summarized in fig5.27. Interestingly, despite more than two orders of magnitude difference in the initial quantum yields of P-terphenyl, Streptavidin and Haemoglobin, we find consistent results in the excitation gain, radiative gain and loss decay rate, indicating a common electromagnetic origin for these effects. The orientation-averaged and position-averaged excitation gain $\eta_{exc} = 15.5 \pm 3.8$ appears in correct agreement with the numerical simulations, as well as the radiative gain $\eta_{\Gamma rad} = 10.8 \pm 2.6$. The loss rate constant $\Gamma^*_{loss} = 1.25 \pm 0.3 ns^-1$ appears to be preserved among our different experiments.

5.6.3 Correlation between FCS volume and gap size

The correlation between the gap size obtained from SEM images and the volume measured with FCS is demonstrated in Figure 5.30 (a) and (b) for a selection of antennas with the smallest gaps.

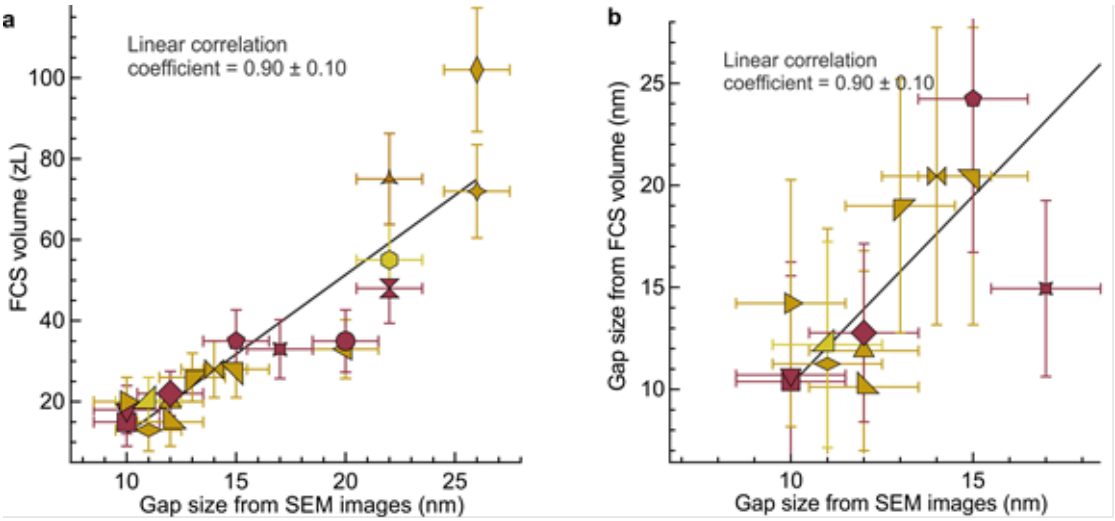

FIGURE 5.30 – Correlation between the gap size obtained from the SEM images with the volume measured with FCS (a) or the gap size deduced from the FCS volume (b) for a selection of the antennas with the smallest gaps

The SEM gap size is the same as the one indicated on Fig. . 5.17. It is obtained from the SEM images as the difference between the total length of the rhodium dimer (measured along the main axis) minus the size of each rhodium nanocube (measured along the direction perpendicular to the main axis). The FCS volume (a) is derived from the FCS measurement of the number of molecules inside the nanogap region and the known molecular concentration. To estimate the gap size from the FCS volume (vertical axis in b), we divide the FCS volume by the lateral area of the rhodium nanocube (square of the average nanocube size measured from the FCS images along

the perpendicular direction plus a constant 6 nm to account for the expansion of the detection volume beyond the geometrical limits of the nanocube). Linear fits and Pearson correlation coefficient are indicated on each graph. These results demonstrate the correlation between the FCS results and the SEM gap sizes.

5.6.4 Comparison of the enhancement factors with aluminum nanogap antennas

In first chapter we discussed different plasmonic material like Rh,Ga,Mg and Al. We showed that Al is one of the best material for UV plasmonics however corrosion remains key limitation so we opt to use Rh in this chapter, however its fair to compare Al (bare and oxide protected) dimer antenna with Rh dimer antenna. In this section we will discuss COMSOL simulation of Al dimer antenna (bare and oxide coated) in water and compare it with Rh antenna as shown in fig 5.31 . In (a) the gap is constant at 10 nm. Corrosion of aluminum in water environment is a major issue, especially under UV illumination thus we need an extra coating to protect Al. We introduced a 7 nm thick conformal silica layer surrounding the nanocube to simulate the influence of an extra corrosion protection layer. Based on the results in (a), we select a nanocube size of 35 nm for pure aluminum, and a 40 nm size in the presence of silica. In fig5.31 The decay rate enhancement of an Al dimer is better than that of a Rh dimer due to the fact that the imaginary part of the refractive index of Al material is lower than that of Rh, resulting in lower losses. However, when considering coated Al and Rh dimer antennas, they are on par with each other in terms of radiative rate enhancements. In comparison of the intensity enhancement for dimer antennas made of different materials, which are usually used for optical antennas (mostly in the visible regime), it can be concluded that Al (bare) is the best choice of material. However, due to corrosion, it needs to be coated with oxide, which reduces its performance lower than that of a Rh antenna. Lastly, a comparison of the net fluorescence brightness enhancement for three different materials as a function of the emitter's initial quantum yield in free space shows that Al (bare) is better than Rh, and Rh is better than Al (oxide coated) when it comes to dimer antenna performance.

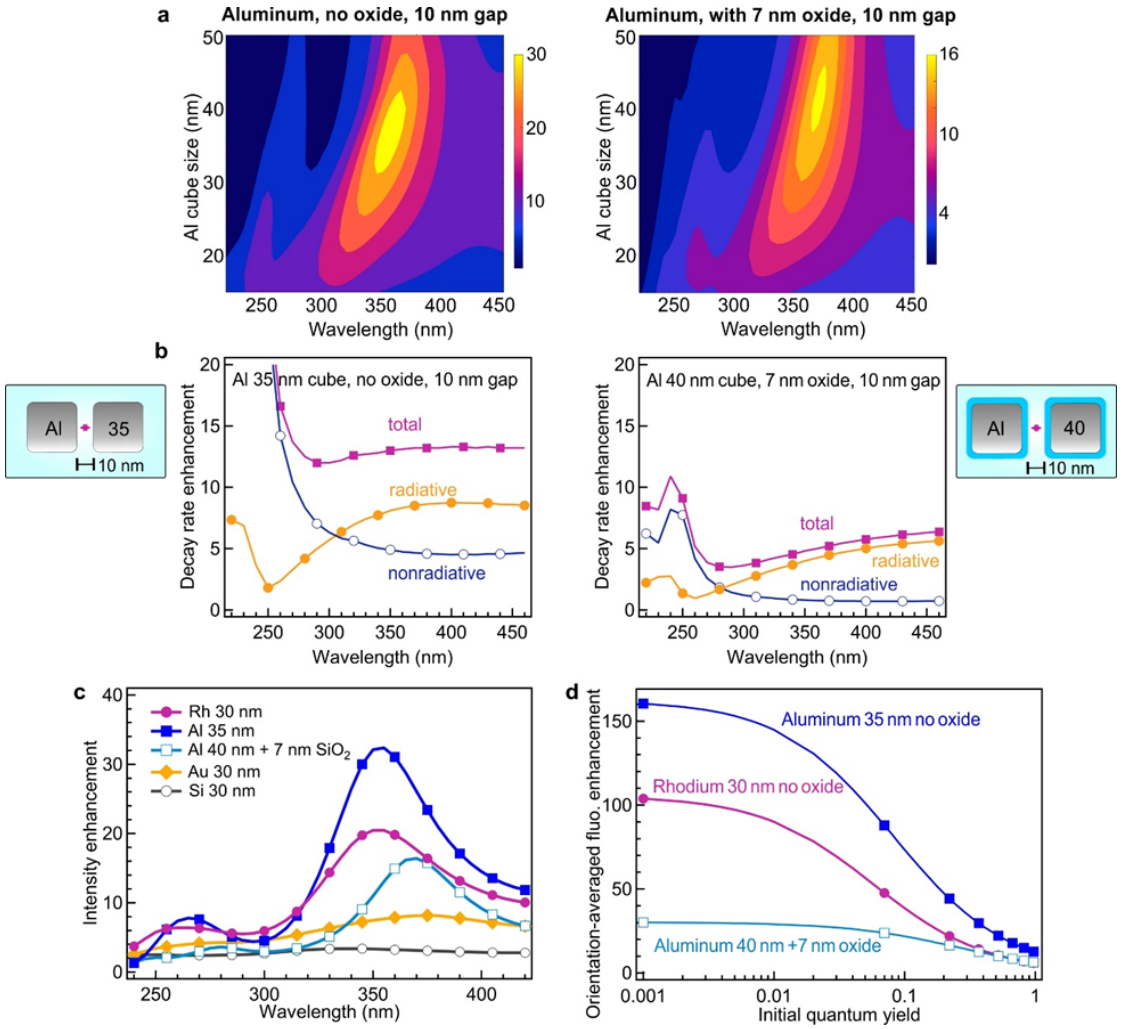

FIGURE 5.31 – Comparison of rhodium and aluminum nanocube antennas in water. (a) Spectral dependence of the intensity enhancement in the center of the nanogap as a function of the nanocube size. The gap is constant at 10 nm. (b) Decay rate enhancement for a perfect dipole emitter with parallel orientation located in the center of the 10 nm nanogap. All rates are normalized respective to the dipole radiative rate in free space. (c) Comparison of the intensity enhancement in the center of the 10 nm gap between nanocubes made of different materials. The nanocube sizes and the materials are indicated in the figure legend. We have considered amorphous silicon. (d) Comparison of the net fluorescence brightness enhancement for three different materials as a function of the emitter's initial quantum yield in free space. The gap size is kept constant at 10 nm. The excitation wavelength is 295 nm for rhodium and 266 nm for aluminum since this wavelength gives a slightly better overall enhancement. The emission wavelength is 350 nm and is averaged over the three orientation directions.

5.6.5 Protein information and sequences

S12. Fitting parameters results

Table S1. Fitting parameters for the FCS data.

Protein	STREPTAVIDIN		P-TERPHENYL		HEMOGLOBIN	
Concentration	50 µM		10 µM		50 µM	
Power (µW)	15		40		15	
Exc. Polarization	Parallel	Perpendicular	Parallel	Perpendicular	Parallel	Perpendicular
F (counts/s)	5740	4860	3370	2100	4070	2970
B (counts/s)	2100	2100	1700	1450	2200	2200
ρ_1	0.0276	--	--	--	0.028	--
ρ_2	0.0093	0.0145	0.635	0.119	0.012	0.0024
ρ_3	0.0014	--	0.034	0.027	0.0053	0.0042
τ_1 (ms)	0.042	--	--	--	0.04	--
τ_2 (ms)	0.70	0.73	0.005	0.0066	0.07	0.08
τ_3 (ms)	8	--	1.4	4.6	49	30
G(0) = ρ_1 + ρ_2	0.0369	0.014	0.635	0.119	0.040	0.0024
N_0	22.2	--	0.8	--	28	--
Q_0 (counts/s)	124	--	807	--	27.5	--
N*	0.90	22.2	0.16	0.8	1.9	28
Q* (counts/s)	987	124	6530	807	583	27.5
Q_{ref} (counts/s)	22	22	475	475	3.5	3.5
Brightness enhancement	44.9	5.6	13.75	1.7	166	7.9

FIGURE 5.32 – Information of proteins used in the study

5.6.6 Comparison of gap sizes achieved for different nanofabrication methods

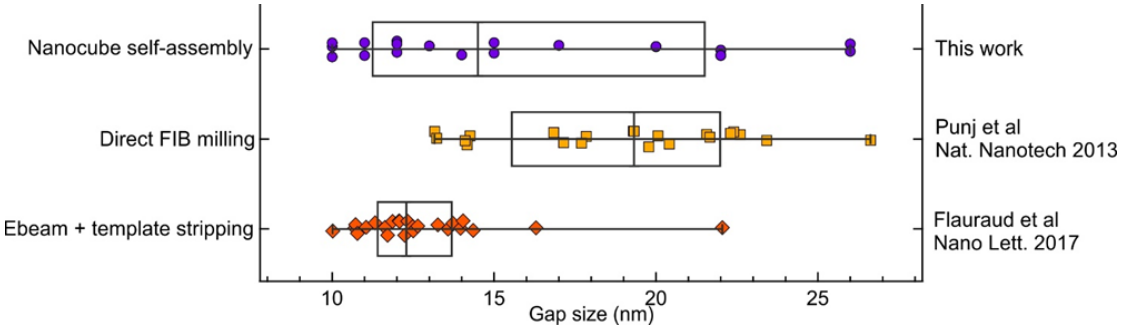

FIGURE 5.33 – Comparison of the estimated gap sizes achieved using different fabrication methods. The markers represent individual nanoantennas while the boxes and whiskers display the median, 25th and 75th percentile and the min/max values. For focused ion beam (FIB) and electron beam lithography (Ebeam) we refer to past works from our group on gold nanogap antennas. This comparison demonstrates that the gap sizes achieved using self-assembly into nanorectangles are quite comparable with other nanofabrication methods.

Conclusion and Perspective

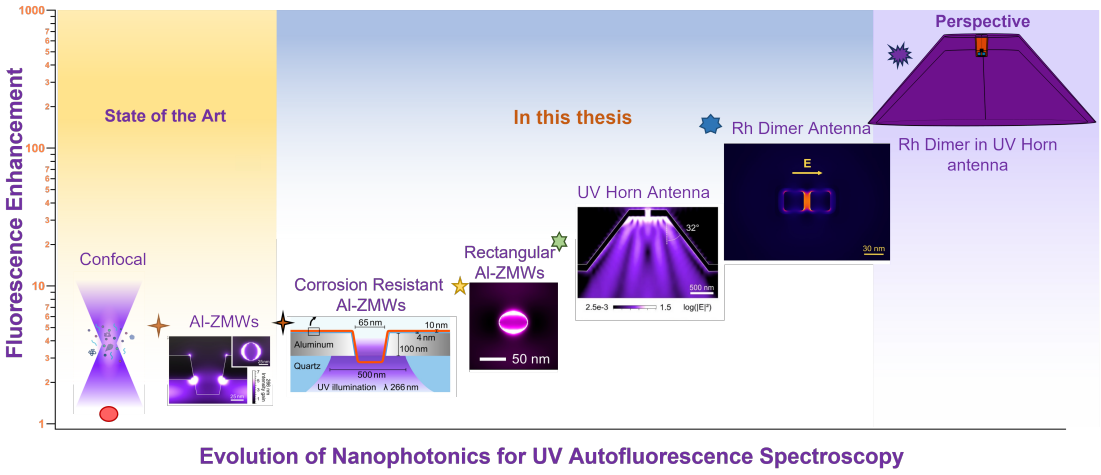

FIGURE 5.34 – Evolution of UV Nanophotonics for Autofluorescence spectroscopy

In this thesis, a robust Label-free UV autofluorescence technique with the sensitivity to detect a single protein containing a single tryptophan residue was created. This was achieved by utilising advanced nanophotonic structures, optimising buffer chemistry, and investigating non-conventional materials to protect against UV corrosion, thus making the method robust.

We began our exploration with a single molecule of β galactosidase containing 150+ tryptophan residues, which was the state-of-the-art available at the time, with the aim of achieving single-molecule-single tryptophan resolution in UV autofluorescence spectroscopy. The state of the art was achieved using Al ZMWs and photostabilizing buffers. The ZMWs provided 5X times enhancement of signal and 1000 times smaller diffraction volume. However, the technique was not adequate for sensing smaller proteins, and photo-corrosion of Al ZMWs was prominent because of the water, salt, and UV combination.

We saw in **Chapter-2** how this ZMWs work and how they enhance the total emission of proteins inside the ZMW cavity. We concluded that the total enhancement of ZMWs is the product of 1.5X excitation gain, 1.4X collection gain, and almost 2X due to LDOS modification. We further showed that by implementing silica coating on ZMWs we were able to protect it from UV corrosion, and the transparent silica layer to UV radiation did not perturb the measurements. We further studied other oxide combinations such as HfO_2, TiO_2 and $TiO_2 - Al_2O_3$ to show that different

oxide protection can be used for different purposes as they have different degrees of UV photo-corrosion. This extra protection layer provided us with the capability of using ZMWs for longer acquisition times and higher power, thus increasing the Signal-to-Noise ratio. In addition to that, oxide coated ZMWs can be used to study molecule proteins at a concentration of μ M and under physiological conditions such as high pH and high salt. We were able to show that we can detect streptavidin a protein with 24 Trp residues using Fluorescence correlation spectroscopy(FCS).

The overall enhancement was limited to 5X with ZMWs. When we look at the fluorescence enhancement equation, we can see that the fluorescence gain is determined by the excitation gain, the collection gain, and the Purcell factor. In **Chapter 3**, we concentrated on increasing the collection gain of our UV spectroscopy system. To comprehend this, we studied how an emitter behaves when it is close to a glass-and-water interface and what its far-field emission pattern looks like. Through a literature review and optical simulations, we discovered that the majority of the emission from molecules is emitted at a wide range of angles and is not collected by the objective, which has a limited numerical aperture of 0.8 in the UV. Thus, we implemented a nanophotonic reflector to steer the emission from a point-like source (protein molecule) to the objectives. The nanophotonic structure is a nanohole embedded in a conical microreflector that is analogous to a horn antenna in the microwave regime. Thus we name it UV horn antenna, this antenna increased the collection angle from 30°to 85° which increases total enhancement gain to 15X in comparison to 4-5X in ZMWs. The UV-horn antennas enable us to detect proteins that are diffusing at the single molecule level in real-time. Our colleagues also used this technology to study the denaturation of β-galactosidase in the presence of Urea, allowing us to accurately predict the Urea concentration at which the protein is denatured and breaks down into monomers with a single-molecule resolution. Furthermore, these antennas were used to detect immobilized proteins by functionalizing them with biotin-PEG-silane to bind β-galactosidase-streptavidin and pure streptavidin proteins.

We realized that the majority proteins in the human body have fewer than five tryptophans. In previous studies, we were able to detect proteins such as streptavidin with 24 Trps. To make UV spectroscopy a complete technique, we had to reach the highest possible sensitivity, which would be proteins with a single Trp residue. Utilizing confocal information and horn antenna enhancement results, we condetectionducted a simulation to assess the feasibility of FCS for single Trp proteins. The simulation results showed that the background (any emission other than protein autofluorescence) plays a critical role, and, even with the enhanced signal from the horn antenna, it was not possible to reach a single Trp sensitivity for a given signal-to-background ratio. For efficient detection, the correlation intensity of proteins should be greater than the correlation intensity of background without proteins.

We embarked on a journey to explore the background and ways to mitigate them, (any emission other than protein autofluorescence) we saw in **Chapter 4** that the main component of the background is from buffers used to stabilize proteins and gallium embedded in nanophotonic structures such as ZMW and Horn antennas due to FIB milling. Ascorbic acid, which is often used as a buffer, has a significant impact

on the background noise that we strive to reduce. Other extensively used buffer combinations of GODCAT (glucose oxidase and catalase enzymes) with glucose not only give a high background signal but also polymerize under UV light and thus affect the overall experiment. We replaced the buffer with MEA and glutathione, which provided a lower background and bubbled Ar to remove oxygen from the system replacing GODCAT. We further investigated the lifetime and spectral characteristics of all the different background components. This gave us the opportunity to separate the spectra of gallium embedded in nanostructures from the protein emission, which is red-shifted compared to the peaks of gallium oxide emission. We also applied time gating (a temporal filter) to remove the very short and very long lifetime components of the total fluorescence (protein signal plus background). This resulted in a five-fold reduction in the total background and a three-fold increase in the SBR (signal-to-background ratio). This enabled us to detect proteins such as LicT dimer (2 Trp) and TNase (1 Trp) with significant statistical precision. This was the first time that UV spectroscopy reported the sensitivity of a single molecule of a single Trp-containing protein. We enhanced the TNase signal (6 counts per molecule per second) in confocal to 70 counts/sec per molecule in a horn antenna with a correlation amplitude of 0.01, which is higher than the background correlation.

After reaching the ultimate sensitivity of UV autofluorescence spectroscopy, we strived further to find ways to enhance the signal even more. Till now we used non-resonating structures to enhance the signal and horn antenna reflector to enhance the collection; however, excitation gain and Purcell factor components were X1.4 and X2, respectively, so far. We explore the optical antenna in **Chapter 5** to incorporate a resonating structure to enhance the excitation gain and the Purcell factor. The idea was to use gap plasmons generated when two plasmonic nanostructures are a few nanometers apart, and these gap plasmons are known for very high Purcell factor and excitation enhancement. However, studies for UV plasmonic antennas are mostly simulation-based or used for proof of concept for some UV Raman or fluorescence of dyes. It was due to challenges in nanofabrication and material requirements for UV nanophotonics. Al, which is the most widely used UV plasmonic material as a pristine nanostructure was not stable in water and UV and oxide coating reduced its plasmonic response. Thus we resorted to the use of single crystalline Rh Nps which is UV material with corrosion resistance and no oxide. We simulated the Rh dimer antenna design and predicted the dimension (around 30 nm) which was then fabricated by the group at Duke University with a very narrow size distribution. In the simulation, we took into account all possible fabrication and experimental constraints thus optimizing not just for excitation but for total fluorescent enhancement where we account for radiative and non-radiative losses of the antenna.

To deal with the fabrication problem of achieving aligned Rh NPs with 10-20 nm gap size we started with FIB-milled Al rectangular ZMWs which were protected with a silica layer and used a self-assembly technique called CAPA (Capillary Assisted Particle Assembly). In this technique, a colloidal solution of Rh NPs dropped on the sample with arrays of Al Nanoapertures and the solution was dragged along and evaporated, due to capillary forces Rh NPs entered the nanoapertures and by controlling the size of

rectangular nanoapertures and conc of colloidal solution we got Rh dimer in Al nanoaperture with gap size ranging from 7-20 nm. In our optical simulation, we observed that total fluorescent enhancement could reach up to 150 times for systems with low quantum yields, such as haemoglobin (0.1% QE and 6 Trp). In the experiment, we were able to demonstrate an unprecedented 120-time enhancement of Auto-fluorescence by a UV antenna. We also observed different kinetic rates for p-Terphenyl (UV dye) (85% QE) and streptavidin (3.5% QE). This led to the first report of a UV Rh dimer antenna in an antenna-in-box configuration, providing background screening and two orders of enhancement (X15 excitation gain and X10 radiative rate enhancement). The antenna is resistant to UV corrosion and can be reused for many experiments. By using the Rh dimer antenna in UV, we were able to achieve a diffraction volume that is a million times smaller, allowing us to perform single molecule FCS at a few hundred of μM concentrations.

In this thesis we saw a development of UV spectroscopy of protein autofluorescence facilitated by nanophotonics. The journey started with detecting larger proteins with 150+ Trp residues to proteins with single Trp residues. We saw the fluorescence enhancement increase from 4 to 15 to 120 times making proteins like haemoglobin which gives 2 photons/molecule/sec in the confocal, detectable in FCS at single-molecule resolution. We achieved this by developing multiple aspects, such as the nanophotonic structure, from a simple nanohole (nanoaperture) to an advanced beam-steering antenna (horn antenna) further to an antenna-in-box plasmonic antenna, by optimizing protein stabilizing buffers and UV corrosion protection. The primary objective was to maintain the ultimate system biocompatible for single-molecule autofluorescence spectroscopy.

What further steps can be taken to improve this technique and bring it to the same level as other established label-free methods? In this thesis, we focused on nanophotonic techniques to increase collection gain, excitation gain, and Purcell factor. We had two primary designs : ZMWs plus a micro-reflector (Horn Antenna) which provided an effective collection of fluorescence, and ZMW plus an Rh dimer antenna (Antenna-in-box), which gave us excitation gain and Purcell factor enhancement. It is clear that the next step will be to combine the ZMW, micro-reflector, and Rh (Al) dimer antenna, which could result in an ultimate design with an enhancement factor of up to 500 times.

Also, one of the major limitations we have in the method, we developed is specificity; in our experiments, we have a priori information about the proteins we used, so the question arises of what will happen if we have no information about the proteins a priori or if there are a combination of different proteins in solution all having tryptophan. There are some possible solutions which we have explored and believe might be the solution

1. It is feasible to differentiate between proteins by using a UV spectrometer. The spectra can be altered by the amount of tryptophan residues, tyrosine (Tyr) and phenylalanine (Phe), the location of tryptophan, and FRET between Trp and Tyr. This means that, at the single-molecule level, different proteins can have distinct spectra

(shifted or different shapes) which can be used as a unique identifier. In the past, due to the low signal from proteins, single-molecule spectrophotometry was not possible. However, with our nanophotonic approach of enhancing UV autofluorescence signal, this is now achievable.
2. It will also be possible to use UV Resonance Raman as fingerprinting technique. When excited at 220-250 nm we can excite both UV Resonance Raman and UV Autofluorescence and we can use both the signal , Raman signal for identification and autofluorescence to study kinetics of protein molecules.
3. The plasmonic nanopore technique can be combined with nanophotonic-enabled UV autofluorescence spectroscopy. This allows us to obtain a unique electrical signal for each protein, which can then be studied through its autofluorescence to gain insight into its behaviour.

It may take a while to construct a custom microscope system with these features, though the concept is intriguing. It is clear that there is a solution to the issue of nonspecificity in nanophotonics-enabled UV autofluorescence spectroscopy; however, this requires further investigation.

In conclusion, this work focused on the development of a technique and the use of basic biophysical models such as protein denaturation and FCS on proteins to assess the technique's reliability and applicability to biophysical studies. Looking ahead, we should investigate more biologically relevant phenomena and collaborate with biologists to address real-world issues, such as the detection of proteins in liquid in vivo and more sophisticated proteomics like kinetics of binding of proteins which were mostly done either on ensemble level or with modified labels; also, the technique could be implemented for the detection of adulteration in processed food production, in chemistry to detect new biomolecules that have aromatic amino acids.

On personal notes, I believe UV spectroscopy both at the ensemble and single molecule level could be the key technique in interplanetary biology to study biomolecules on different planets where the use of labels is limited and the spectrum of sunlight(starlight) is more shifted to UV in comparison to Earth.

Author's contribution The project was carried out with the assistance of various team members due to its multidisciplinary nature. The antenna or nanophotonic strucuture fabrication which required FIB was done Jean Benoit. The Rh NPs were fabricated at Duke university and oxide deposition was done by group in CiNAM Author conducted all the COMSOL simulations and spectroscopic measurements with dyes or proteins on a UV microscope (except for some parts of Chapter 2, which author did with Alexandr, a former PhD student). Author analyzed the data presented in the paper, with guidance and help from the supervisor. Author took part in modification and debugging of microscope setup along with former PhD student(who initially built the setup). The chemistry was all performed by author and protocols were decided based on discussion with supervisior. Illustrative images on Biorender, 3D images on blender or painted images used in thesis were made by Author himself.Author also took part in planning of experiments especially in last chapters (4 and 5).

Main findings of the Dissertation

1. Zero mode waveguides (ZMWs)enhance the signal from proteins by modification of Local density of states and decay rates of proteins autofluorescence
2. UV treated Silica coating can protect ZMWs from UV corrosion of Aluminium layer. Combination TiO_2 and Al_2O_3 is the best protective layer for Al against corrosion due to salt or UV induced radical species.
3. UV horn antenna can collect forbidden light and increase the angle of collection of the 0.8 NA objective from 35 ° to 85 °. Renders 15 fold enhancement of the autofluorescence signal (confocal ref.)
4. UV Horn antenna can be used to study label-free diffusing protein with single molecule sensitivity
5. Background plays the limiting role in the single Tryptophan sensitivity of UV autofluorescence spectroscopy
6. MEA and Glutathione and bubbling Ar to remove oxygen make low background buffer combination for UV photostability of proteins
7. Single Tryptophan single-molecule sensitivity can be reached using horn antenna, spectral filter, time gating.
8. The self-assembled Rh dimer can be used to make corrosion-resistant UV nano-gap antennas for proteins.
9. Rh dimer antenna in Al nanopaerture can enhance total fluorescent by 120 times, making FCS of low quantum yield proteins feasible.

Résumé long

FIGURE 5.35 – Les UV rendent visibles les protéines invisibles

Le véritable caractère des êtres humains se révèle lorsqu'ils sont invisibles, affirmait Platon dans l'histoire de "l'Anneau de Gygès" dans le livre "La République". De même, pour découvrir la véritable nature des protéines et étudier leur cinétique, nous devons les observer lorsqu'elles sont invisibles (sans marquage) et dans leur environnement physiologique, par exemple dans de l'eau salée et à des concentrations de l'ordre du micromolaire au milli-molaire. La spectroscopie dans l'ultraviolet nous permet d'observer les protéines sans avoir besoin de les marquer, et la nanophotonique nous permet de les observer au niveau de la molécule unique avec une sensibilité remarquable.

Ces dernières années, les études biophysiques sont passées de l'étude d'ensembles à celle de molécules uniques afin de mieux comprendre les protéines au niveau moléculaire. D'autres recherches se concentrent à présent sur des études de

molécules uniques sans marquage, qui fourniront une vue inaltérée de la cinétique au niveau moléculaire.

La spectroscopie de fluorescence s'est imposée comme un outil formidable, notamment pour la biodétection, avec un avantage particulier dans le domaine de la détection des protéines. La fluorescence est un phénomène fascinant observé depuis des siècles, mais ce n'est qu'au XIXe siècle qu'elle a commencé à être comprise et étudiée scientifiquement. Le phénomène de la fluorescence remonte à l'Antiquité. Les Romains, par exemple, fabriquaient des coupes en fluorine qui brillaient dans l'obscurité lorsqu'elles étaient exposées à la lumière. Les propriétés fluorescentes de la fluorine ont ensuite été utilisées au XVIe siècle par Vincenzo Cascariolo, un cordonnier et alchimiste italien, qui a créé la "pierre de Bologne", un matériau qui, après avoir été exposé à la lumière du soleil, brillait dans l'obscurité. Le terme "fluorescence" lui-même a été inventé par Sir George Gabriel Stokes en 1852. Stokes a étudié l'émission de lumière par des substances qui avaient absorbé la lumière ou d'autres radiations électromagnétiques. Il a nommé le phénomène d'après la fluorine, un minéral qui présente cette propriété importante. L'interaction de la lumière avec les molécules est au cœur de la spectroscopie de fluorescence et peut être visualisée à l'aide d'un diagramme de Jablonski. Nommé d'après le physicien polonais Aleksander Jabłoński, ce diagramme fournit une représentation visuelle des différents états énergétiques d'une molécule et des transitions entre eux.

Bien que le marquage des protéines en spectroscopie de fluorescence fournisse des informations précieuses sur la structure, la dynamique et les interactions des protéines, il n'est pas sans limites. La perturbation de la structure et de la fonction des protéines, les effets spécifiques des sondes, les défis posés par la sélection des sites de marquage, les problèmes d'efficacité et d'homogénéité du marquage, les interactions photophysiques, la photostabilité et le photoblanchiment, ainsi que les complexités liées au multi-marquage et aux systèmes complexes, posent des défis considérables. Le dépassement de ces limites et le progrès des techniques de marquage contribueront à améliorer la précision et la fiabilité de la spectroscopie de fluorescence dans la recherche sur les protéines. Il va sans dire que nous avons besoin d'une technique qui présente des contrastes élevés, comme la spectroscopie de fluorescence, mais qui ne souffre pas des inconvénients du marquage, c'est-à-dire une technique sans marquage.
Dans cette thèse, une technique robuste d'autofluorescence UV sans marquage avec la sensibilité nécessaire pour détecter une seule protéine contenant un seul résidu de tryptophane a été créée. Ce résultat a été obtenu en utilisant des structures nanophotoniques avancées, en optimisant la chimie des tampons et en étudiant des matériaux non conventionnels pour protéger la méthode contre la corrosion par les UV, ce qui la rend robuste.

Nous avons commencé notre exploration avec une molécule unique de β galactosidase contenant plus de 150 résidus de tryptophane, ce qui représentait l'état de l'art disponible à l'époque, dans le but d'obtenir une résolution de tryptophane unique-molécule unique en spectroscopie d'autofluorescence UV. L'état de l'art a été atteint en utilisant des ZMW en aluminium et des tampons photostabilisants. Les

ZMW ont permis de multiplier le signal par 5 et le volume de diffraction par 1000. Toutefois, la technique n'était pas adaptée à la détection de protéines plus petites, et la photocorrosion des ZMW d'Al était importante en raison de la combinaison de l'eau, du sel et des UV.

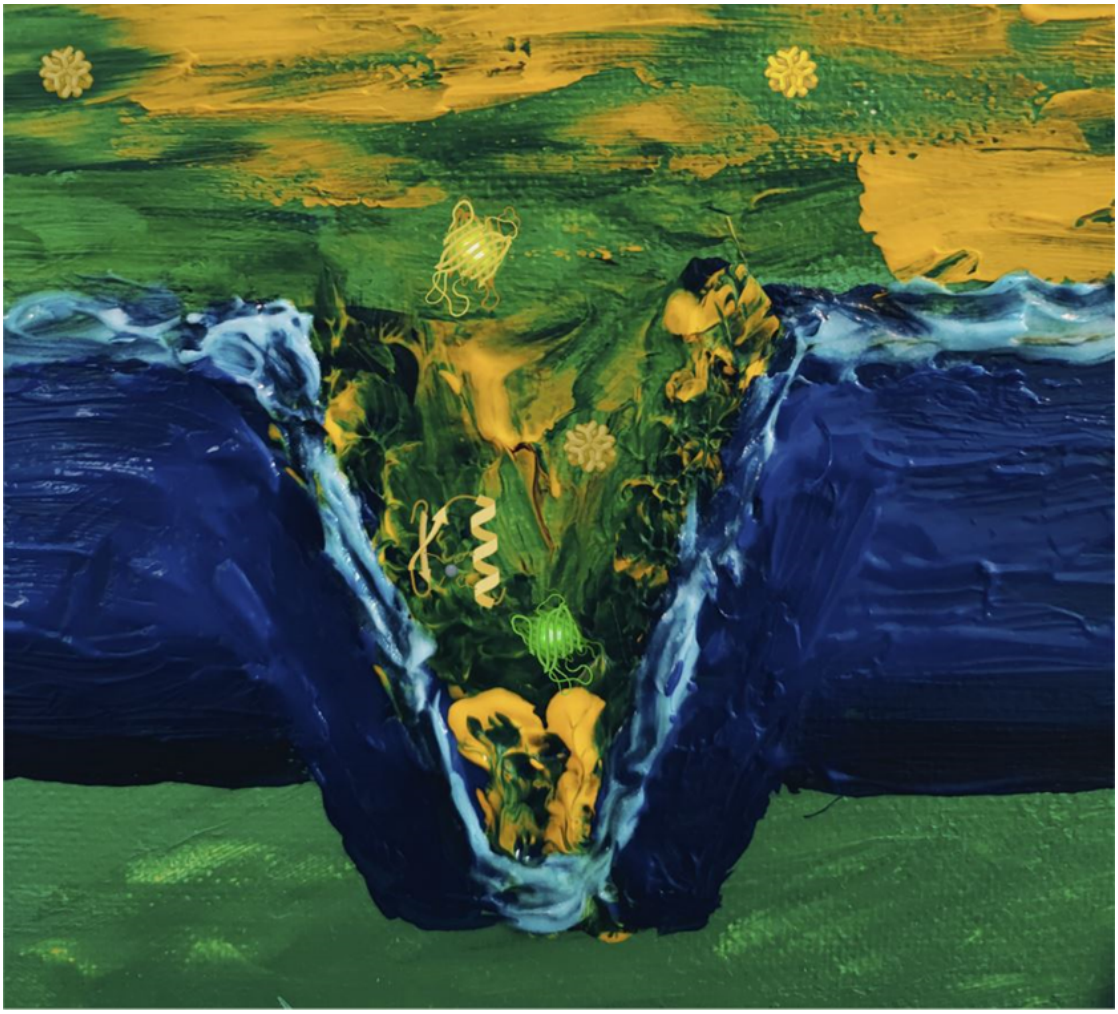

FIGURE 5.36 – Peinture à l'huile impressionniste des ZMW

Nous avons vu dans **Chapitre-2** comment ces ZMW fonctionnent et comment ils augmentent l'émission totale des protéines à l'intérieur de la cavité ZMW. Nous avons conclu que l'amélioration totale des ZMW est le produit d'un gain d'excitation de 1,5X, d'un gain de collecte de 1,4X et d'un gain de près de 2X dû à la modification du LDOS. Nous avons également montré qu'en appliquant un revêtement de silice sur les ZMW, nous avons pu les protéger de la corrosion par les UV, et la couche de silice transparente au rayonnement UV n'a pas perturbé les mesures. Nous avons également étudié d'autres combinaisons d'oxydes telles que HfO_2, TiO_2 et $TiO_2 - Al_2O_3$ pour montrer que différentes protections d'oxydes peuvent être utilisées à des fins

différentes, car elles ont des degrés différents de photocorrosion par les UV. Cette couche de protection supplémentaire nous a permis d'utiliser les ZMW pour des temps d'acquisition plus longs et une puissance plus élevée, augmentant ainsi le rapport signal/bruit. En outre, les ZMW recouverts d'oxyde peuvent être utilisés pour étudier des protéines moléculaires à une concentration de μ M et dans des conditions physiologiques telles qu'un pH élevé et une forte teneur en sel. Nous avons pu montrer que nous pouvions détecter la streptavidine, une protéine contenant 24 résidus Trp, en utilisant la spectroscopie de corrélation de fluorescence (FCS).

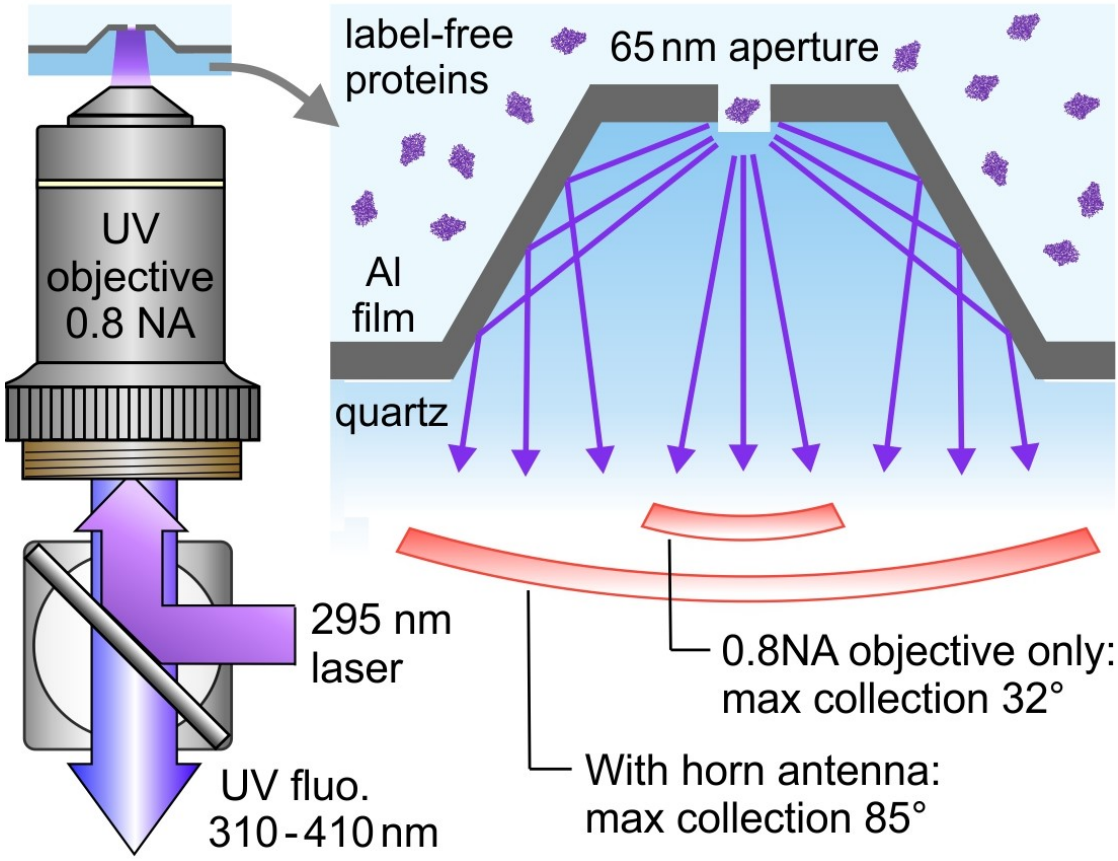

(a) Figure A

FIGURE 5.37 – Schémas de l'antenne à cornet (Horn Antenna)

L'amélioration globale a été limitée à 5X avec les ZMW. L'équation de l'amélioration de la fluorescence montre que le gain de fluorescence est déterminé par le gain d'excitation, le gain de collecte et le facteur de Purcell. Dans le **Chapitre 3**, nous nous sommes concentrés sur l'augmentation du gain de collecte de notre système de spectroscopie UV. Pour ce faire, nous avons étudié le comportement d'un émetteur lorsqu'il est proche d'une interface verre-eau et son schéma d'émission en champ lointain. Grâce à une revue de la littérature et à des simulations optiques, nous avons découvert que la majeure partie de l'émission des molécules est émise à un large

éventail d'angles et n'est pas collectée par l'objectif, dont l'ouverture numérique est limitée à 0,8 dans l'UV. Nous avons donc mis en place un réflecteur nanophotonique pour diriger l'émission d'une source ponctuelle (molécule de protéine) vers les objectifs. La structure nanophotonique est un nano-trou intégré dans un microréflecteur conique qui est analogue à une antenne cornet dans le régime des micro-ondes. Cette antenne a augmenté l'angle de collecte de 30°à 85° ce qui augmente le gain total de 15X par rapport à 4-5X dans les ZMWs. Les antennes cornet UV nous permettent de détecter en temps réel les protéines qui diffusent au niveau de la molécule unique. Nos collègues ont également utilisé cette technologie pour étudier la dénaturation de la β-galactosidase en présence d'urée, ce qui nous a permis de prédire avec précision la concentration d'urée à laquelle la protéine est dénaturée et se décompose en monomères avec une résolution de l'ordre de la molécule unique. En outre, ces antennes ont été utilisées pour détecter des protéines immobilisées en les fonctionnalisant avec de la biotine-PEG-silane pour lier la β-galactosidase-streptavidine et les protéines pures de streptavidine.

Nous avons réalisé que la majorité des protéines du corps humain contiennent moins de cinq tryptophanes. Dans des études antérieures, nous avons pu détecter des protéines telles que la streptavidine avec 24 Trps. Pour faire de la spectroscopie UV une technique complète, nous devions atteindre la sensibilité la plus élevée possible, c'est-à-dire les protéines ne comportant qu'un seul résidu Trp. En utilisant les informations confocales et les résultats de l'amélioration de l'antenne conique, nous avons effectué une simulation pour évaluer la faisabilité de la FCS pour les protéines à un seul résidu Trp. Les résultats de la simulation ont montré que le bruit de fond (toute émission autre que l'autofluorescence de la protéine) joue un rôle critique et que, même avec le signal amélioré de l'antenne conique, il n'était pas possible d'atteindre une sensibilité pour une protéine Trp unique pour un rapport signal/bruit de fond donné. Pour une détection efficace, l'intensité de corrélation des protéines doit être supérieure à l'intensité de corrélation de l'arrière-plan sans protéines.

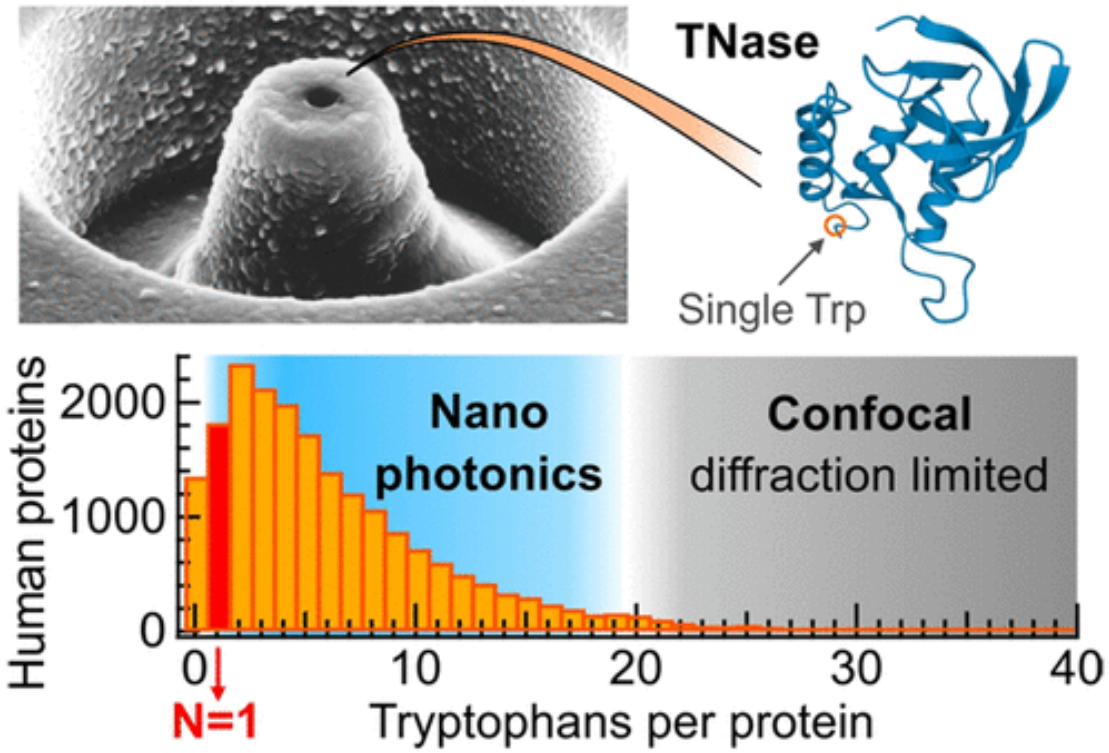

FIGURE 5.38 – Atteindre la sensibilité au Trp unique

Nous nous sommes lancés dans l'exploration du bruit de fond et des moyens de l'atténuer, (toute émission autre que l'autofluorescence des protéines) nous avons vu dans le **chapitre 4** que la principale composante du bruit de fond provient des tampons utilisés pour stabiliser les protéines et du gallium incorporé dans les structures nanophotoniques telles que les antennes ZMW et Horn en raison du fraisage FIB. L'acide ascorbique, qui est souvent utilisé comme tampon, a un impact significatif sur le bruit de fond que nous nous efforçons de réduire. D'autres combinaisons de tampons largement utilisées de GODCAT (enzymes glucose oxydase et catalase) avec du glucose donnent non seulement un signal de fond élevé, mais polymérisent également sous la lumière UV, ce qui affecte l'ensemble de l'expérience. Nous avons remplacé le tampon par de la MEA et du glutathion, ce qui a permis d'obtenir un signal de fond plus faible, et nous avons fait barboter de l'Ar pour éliminer l'oxygène du système remplaçant le GODCAT. Nous avons ensuite étudié la durée de vie et les caractéristiques spectrales de tous les différents composants de l'arrière-plan. Cela nous a permis de séparer les spectres du gallium intégré dans les nanostructures de l'émission des protéines, qui est décalée vers le rouge par rapport aux pics d'émission de l'oxyde de gallium. Nous avons également appliqué un time gating (filtre temporel) pour éliminer les composantes à très courte et très longue durée de vie de la fluorescence totale (signal de la protéine plus bruit de fond). Il en est résulté une réduction d'un facteur cinq du bruit de fond total et une augmentation d'un facteur trois du SBR (rapport signal/bruit de fond). Cela nous a permis de détecter des protéines telles que le dimère LicT (2 Trp) et la TNase (1 Trp) avec une précision statistique significative.

C'est la première fois que la spectroscopie UV rapporte la sensibilité d'une seule molécule d'une seule protéine contenant du Trp. Nous avons augmenté le signal TNase (6 coups par molécule par seconde) en confocal à 70 coups/seconde par molécule dans une antenne cornet avec une amplitude de corrélation de 0,01, ce qui est plus élevé que la corrélation de fond.

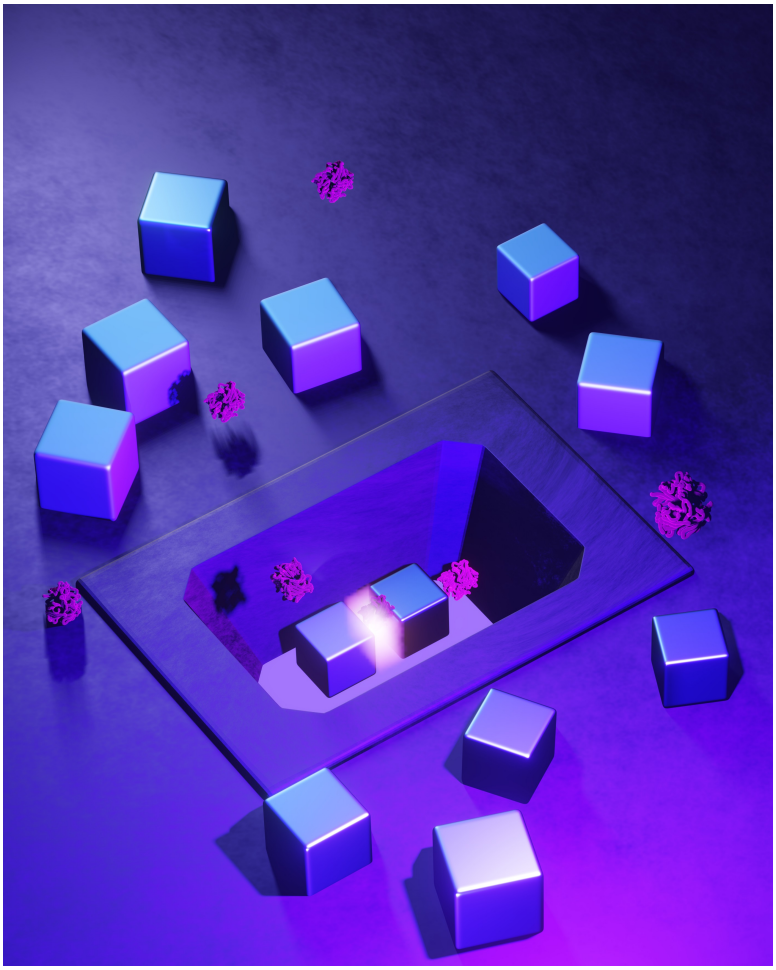

FIGURE 5.39 – Antenne dimère Rh Cube en Nano-Aperture

Après avoir atteint la sensibilité ultime de la spectroscopie d'autofluorescence UV, nous nous sommes efforcés de trouver des moyens d'améliorer encore le signal. Jusqu'à présent, nous avons utilisé des structures non résonantes pour améliorer le signal et un réflecteur d'antenne à cornet pour améliorer la collecte ; cependant, le gain d'excitation et les composantes du facteur de Purcell étaient respectivement de X1,4 et X2 jusqu'à présent. Nous explorons l'antenne optique dans le **Chapitre 5** pour incorporer une structure résonante afin d'améliorer le gain d'excitation et le facteur de Purcell. L'idée était d'utiliser les plasmons de lacunes générés lorsque deux nanostructures plasmoniques sont séparées de quelques nanomètres, et ces plasmons de lacunes sont connus pour leur facteur de Purcell très élevé et l'amélioration de

l'excitation. Cependant, les études sur les antennes plasmoniques UV sont principalement basées sur des simulations ou utilisées comme preuve de concept pour le Raman UV ou la fluorescence de colorants. Cela s'explique par les défis posés par la nanofabrication et les exigences en matière de matériaux pour la nanophotonique UVa . L'aluminium, qui est le matériau plasmonique UV le plus largement utilisé en tant que nanostructure vierge, n'était pas stable dans l'eau et le revêtement d'oxyde et d'UV réduisait sa réponse plasmonique. Nous avons donc eu recours au Rh Nps monocristallin qui est un matériau UV résistant à la corrosion et dépourvu d'oxyde. Nous avons simulé la conception de l'antenne de dimères de Rh et prédit la dimension (environ 30 nm) qui a ensuite été fabriquée par le groupe de l'université Duke avec une distribution de taille très étroite. Dans la simulation, nous avons pris en compte toutes les contraintes expérimentales et de fabrication possibles, optimisant ainsi non seulement l'excitation mais aussi l'amélioration totale de la fluorescence en tenant compte des pertes radiatives et non radiatives de l'antenne.
Pour résoudre le problème de fabrication des NPs de Rh alignées avec une taille d'espace de 10-20 nm, nous avons commencé avec des ZMW rectangulaires en Al fraisés par FIB qui ont été protégés par une couche de silice et nous avons utilisé une technique d'auto-assemblage appelée CAPA (Capillary Assisted Particle Assembly). Dans cette technique, une solution colloïdale de nanoparticules de Rh est tombée sur l'échantillon avec des réseaux de nanoparticules d'Al et la solution a été entraînée et évaporée, en raison des forces capillaires, les nanoparticules de Rh sont entrées dans les nanoparticules et en contrôlant la taille des nanoparticules rectangulaires et la concentration de la solution colloïdale, nous avons obtenu des dimères de Rh dans les nanoparticules d'Al avec une taille d'espace allant de 7 à 20 nm. Dans notre simulation optique, nous avons observé que l'augmentation totale de la fluorescence pouvait atteindre jusqu'à 150 fois pour les systèmes à faible rendement quantique, tels que l'hémoglobine (0,1% QE et 6 Trp). Au cours de l'expérience, nous avons pu démontrer une augmentation sans précédent de 120 fois de l'auto-fluorescence par une antenne UV. Nous avons également observé des taux cinétiques différents pour le p-Terphenyl (colorant UV) (85% QE) et la streptavidine (3.5% QE). Cela a conduit au premier rapport d'une antenne UV Rh dimère dans une configuration d'antenne dans une boîte, fournissant un filtrage de fond et deux ordres d'amélioration (gain d'excitation X15 et amélioration du taux radiatif X10). L'antenne est résistante à la corrosion par les UV et peut être réutilisée pour de nombreuses expériences. En utilisant l'antenne Rh dimère dans l'UV, nous avons pu obtenir un volume de diffraction un million de fois plus petit, ce qui nous a permis d'effectuer un FCS à molécule unique à quelques centaines de μM de concentration.
Dans cette thèse, nous avons vu un développement de la spectroscopie UV de l'autofluorescence des protéines facilité par la nanophotonique. Le voyage a commencé par la détection de protéines plus grandes avec 150+ résidus Trp jusqu'à des protéines avec un seul résidu Trp. Nous avons vu le renforcement de la fluorescence passer de 4 à 15 à 120 fois, ce qui a permis à des protéines telles que l'hémoglobine, qui produit 2 photons/molécule/seconde au confocal, d'être détectées au FCS avec une résolution de l'ordre de la molécule. Nous y sommes parvenus en développant de multiples as-

pects, tels que la structure nanophotonique, d'un simple nano trou (nano ouverture) à une antenne à orientation de faisceau avancée (antenne cornet) en passant par une antenne plasmonique en boîte, en optimisant les tampons de stabilisation des protéines et la protection contre la corrosion par les rayons ultraviolets. L'objectif principal était de maintenir le système ultime biocompatible pour la spectroscopie d'autofluorescence à molécule unique.

Quelles autres mesures peuvent être prises pour améliorer cette technique et l'amener au même niveau que d'autres méthodes établies sans marquage? Dans cette thèse, nous nous sommes concentrés sur les techniques nanophotoniques pour augmenter le gain de collecte, le gain d'excitation et le facteur de Purcell. Nous avions deux conceptions principales : Les ZMWs plus un micro-réflecteur (Antenne Corne) qui a permis une collecte efficace de la fluorescence, et les ZMWs plus une antenne dimère Rh (Antenne en boîte), qui nous a permis d'augmenter le gain d'excitation et le facteur de Purcell. Il est clair que la prochaine étape consistera à combiner le ZMW, le micro-réflecteur et l'antenne dimère Rh (Al), ce qui pourrait déboucher sur une conception ultime avec un facteur d'amélioration jusqu'à 500 fois.

Les principales conclusions de cette thèse sont les suivantes Les guides d'ondes à mode zéro (ZMW) améliorent le signal des protéines en modifiant la densité locale des états et les taux de décroissance de l'autofluorescence des protéines.
Le revêtement de silice traité aux UV peut protéger les ZMWs de la corrosion de la couche d'aluminium par les UV. La combinaison de TiO_2 et Al_2O_3 est la meilleure couche protectrice pour l'aluminium contre la corrosion due au sel ou aux espèces radicales induites par les UV.
L'antenne cornet UV peut collecter la lumière interdite et augmenter l'angle de collecte de l'objectif 0.8 NA de 35 ° à 85 °. Le signal d'autofluorescence est multiplié par 15 (réf. confocale).
L'antenne UV Horn peut être utilisée pour étudier les protéines diffusantes sans marquage avec une sensibilité à la molécule unique.
L'arrière-plan joue un rôle limitant dans la sensibilité de la spectroscopie d'autofluorescence UV pour un seul tryptophane.
La MEA et le glutathion, ainsi que le barbotage d'Ar pour éliminer l'oxygène, constituent une combinaison de tampons à faible bruit de fond pour la photostabilité UV des protéines.
La sensibilité d'une seule molécule de Tryptophane peut être atteinte en utilisant une antenne conique, un filtre spectral et un contrôle du temps.
Le dimère de Rh auto-assemblé peut être utilisé pour fabriquer des antennes à nanogap UV résistantes à la corrosion pour les protéines.
L'antenne de dimère de Rh dans la nanoperture d'Al peut augmenter la fluorescence totale de 120 fois, ce qui rend possible le FCS de protéines à faible rendement quantique.

Dans nos expériences, nous disposons d'informations a priori sur les protéines que nous avons utilisées. La question se pose donc de savoir ce qui se passera si nous

ne disposons d'aucune information a priori sur les protéines ou s'il y a une combinaison de différentes protéines en solution contenant toutes du tryptophane. Il y a quelques solutions possibles que nous avons explorées et que nous pensons être la solution
1. Il est possible de différencier les protéines en utilisant un spectromètre UV. Les spectres peuvent être modifiés par la quantité de résidus de tryptophane, de tyrosine (Tyr) et de phénylalanine (Phe), par l'emplacement du tryptophane et par le FRET entre Trp et Tyr. Cela signifie qu'au niveau d'une seule molécule, différentes protéines peuvent avoir des spectres distincts (décalés ou de formes différentes) qui peuvent être utilisés comme identifiant unique. Auparavant, en raison du faible signal émis par les protéines, la spectrophotométrie à l'échelle de la molécule unique n'était pas possible. Toutefois, grâce à notre approche nanophotonique de l'amélioration du signal de l'autofluorescence UV, cela est désormais possible.
2. Il sera également possible d'utiliser le Raman à résonance UV comme technique d'empreinte digitale. Lorsqu'il est excité à 220-250 nm, nous pouvons exciter à la fois le Raman de résonance UV et l'autofluorescence UV et nous pouvons utiliser les deux signaux, le signal Raman pour l'identification et l'autofluorescence pour étudier la cinétique des molécules de protéines.
3. La technique des nanopores plasmoniques peut être combinée avec la spectroscopie d'autofluorescence UV basée sur la nanophotonique. Cela nous permet d'obtenir un signal électrique unique pour chaque protéine, qui peut ensuite être étudié par autofluorescence pour mieux comprendre son comportement.

La construction d'un système de microscope personnalisé doté de ces caractéristiques peut prendre un certain temps, mais le concept est intriguant. Il est clair qu'il existe une solution au problème de la non-spécificité dans la spectroscopie d'autofluorescence UV à l'aide de nanophotonique, mais elle nécessite des recherches plus approfondies.

En conclusion, ce travail s'est concentré sur le développement d'une technique et l'utilisation de modèles biophysiques de base tels que la dénaturation des protéines et la FCS sur les protéines afin d'évaluer la fiabilité de la technique et son applicabilité aux études biophysiques. À l'avenir, nous devrions étudier des phénomènes plus pertinents sur le plan biologique et collaborer avec des biologistes pour résoudre des problèmes concrets, tels que la détection de protéines dans des liquides in vivo et une protéomique plus sophistiquée, comme la cinétique de liaison des protéines, qui a été principalement réalisée au niveau de l'ensemble ou avec des marquages modifiées ; en outre, la technique pourrait être mise en œuvre pour la détection de l'adultération dans la production d'aliments transformés, en chimie pour détecter de nouvelles biomolécules contenant des acides aminés aromatiques.
Pour ma part, je pense que la spectroscopie UV au niveau de l'ensemble et de la molécule unique pourrait être la technique clé de la biologie interplanétaire pour étudier les biomolécules sur différentes planètes où l'utilisation d'marquages est limitée et où le spectre de la lumière solaire (lumière stellaire) est plus orienté vers les UV que sur la Terre.

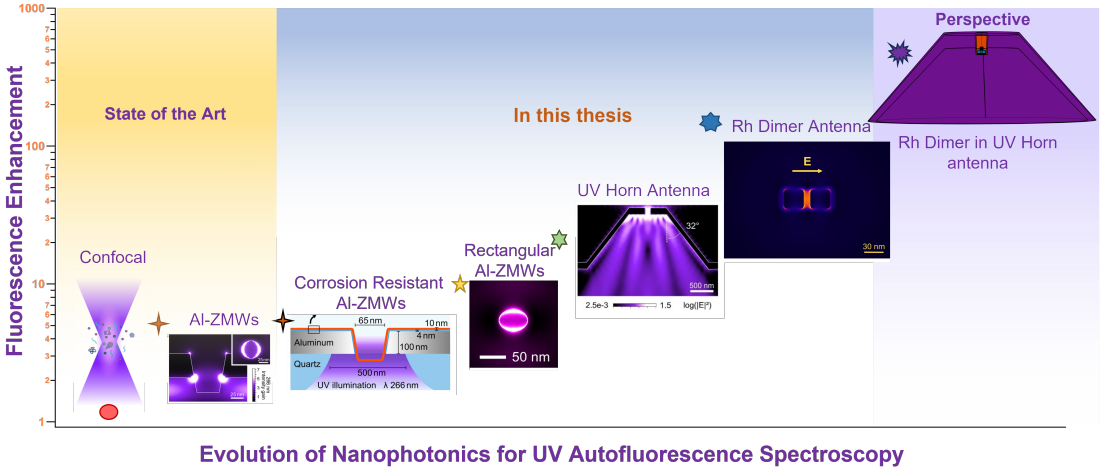

FIGURE 5.40 – Évolution de la nanophotonique UV pour la spectroscopie d'autofluorescence

Bibliographie

[Acu+12] G. P. ACUNA, F. M. MÖLLER et al. « Fluorescence enhancement at docking sites of DNA-directed self-assembled nanoantennas ». In : *Science* 338.6106 (oct. 2012), p. 506-510. ISSN : 10959203. DOI : 10.1126/SCIENCE.1228638/SUPPL{_}FILE/1228638.ACUNA.SM.PDF. URL : https://www.science.org/doi/10.1126/science.1228638 (cf. p. 163).

[AO22] Subhasis ADHIKARI et Michel ORRIT. « Progress and perspectives in single-molecule optical spectroscopy ». In : *Journal of Chemical Physics* 156.16 (avr. 2022). ISSN : 10897690. DOI : 10.1063/5.0087003 (cf. p. 21, 132).

[AC13] Mario AGIO et Diego Martin CANO. « Nano-optics : The Purcell factor of nanoresonators ». In : *Nature Photonics* 7.9 (2013), p. 674-675. ISSN : 17494885. DOI : 10.1038/nphoton.2013.219 (cf. p. 39).

[Ahm+16] Arash AHMADIVAND, Raju SINHA et al. « Rhodium Plasmonics for Deep-Ultraviolet Bio-Chemical Sensing ». In : *Plasmonics* 11.3 (2016), p. 839-849. ISSN : 15571963. DOI : 10.1007/s11468-015-0117-x (cf. p. 137).

[Ait+17] Soraya AIT-BARA, Caroline CLERTÉ et al. « Competitive folding of RNA structures at a termination-antitermination site ». In : *RNA* 23.5 (mai 2017), p. 721-734. ISSN : 14699001. DOI : 10.1261/RNA.060178.116 (cf. p. 120).

[Al +20] Abdullah AL MASUD, W. Elliott MARTIN et al. « Mixed metal zero-mode guides (ZMWs) for tunable fluorescence enhancement ». In : *Nanoscale Advances* 2.5 (mai 2020), p. 1894-1903. ISSN : 25160230. DOI : 10.1039/C9NA00641A (cf. p. 58, 60).

[Alb13] Jihad-René ALBANI. « Origin of Tryptophan Fluorescence Lifetimes. Part 2 : Fluorescence Lifetimes Origin of Tryptophan in Proteins ». In : *Journal of Fluorescence* (2013). DOI : 10.1007/s10895-013-1274-y (cf. p. 27).

[Alc+15] R. ALCARAZ DE LA OSA, J. M. SANZ et al. « Rhodium Tripod Stars for UV Plasmonics ». In : *The Journal of Physical Chemistry C* 119.22 (mai 2015), p. 12572-12580. DOI : 10.1021/acs.jpcc.5b00983 (cf. p. 136, 137).

[Alt10] Matteo ALTISSIMO. « E-beam lithography for micro-nanofabrication ». In : *Biomicrofluidics* 4.2 (2010). ISSN : 1932-1058. DOI : 10.1063/1.3437589. URL : https://pubmed.ncbi.nlm.nih.gov/20697574/ (cf. p. 64).

[Alt+22] Hatice ALTUG, Sang Hyun OH et al. « Advances and applications of nanophotonic biosensors ». In : *Nature Nanotechnology* 17.1 (2022), p. 5-16. ISSN : 17483395. DOI : 10.1038/s41565-021-01045-5 (cf. p. 38).

[And13] R. A. ANDRIEVSKII. « The role of nanoscale effects in the interaction between nanostructured materials and environments ». In : *Protection of Metals and Physical Chemistry of Surfaces* 49.5 (sept. 2013), p. 528-540. ISSN : 20702051. DOI : 10.1134/S207020511305002X (cf. p. 48).

[AK16] Jaime Ortega ARROYO et Philipp KUKURA. « Non-fluorescent schemes for single-molecule detection, imaging and spectroscopy ». In : *Nature Photonics* 10.1 (jan. 2016), p. 11-17. ISSN : 17494893. DOI : 10.1038/NPHOTON.2015.251 (cf. p. 132).

[Ass+17] Ossama N. ASSAD, Tal GILBOA et al. « Light-Enhancing Plasmonic-Nanopore Biosensor for Superior Single-Molecule Detection ». In : *Advanced Materials* 29.9 (mars 2017), p. 1605442. ISSN : 1521-4095. DOI : 10.1002/ADMA.201605442. URL : https://onlinelibrary.wiley.com/doi/full/10.1002/adma.201605442%20https://onlinelibrary.wiley.com/doi/abs/10.1002/adma.201605442%20https://onlinelibrary.wiley.com/doi/10.1002/adma.201605442 (cf. p. 66).

[Baa+22] Martin D. BAASKE, Nasrin ASGARI et al. « Nanosecond time scale transient optoplasmonic detection of single proteins ». In : *Science Advances* 8.2 (jan. 2022). ISSN : 23752548. DOI : 10.1126/SCIADV.ABL5576/SUPPL{_}FILE/SCIADV.ABL5576{_}SM.PDF. URL : https://www.science.org/doi/10.1126/sciadv.abl5576 (cf. p. 22).

[BFV14] Martin D. BAASKE, Matthew R. FOREMAN et al. « Single-molecule nucleic acid interactions monitored on a label-free microcavity biosensor platform ». In : *Nature Nanotechnology* 9.11 (nov. 2014), p. 933-939. ISSN : 17483395. DOI : 10.1038/NNANO.2014.180 (cf. p. 15).

[Bai+20a] Mikhail BAIBAKOV, Aleksandr BARULIN, Prithu ROY, Jean Benoît CLAUDE et al. « Zero-mode waveguides can be made better : Fluorescence enhancement with rectangular aluminum nanoapertures from the visible to the deep ultraviolet ». In : *Nanoscale Advances* 2.9 (sept. 2020), p. 4153-4160. ISSN : 25160230. DOI : 10.1039/D0NA00366B (cf. p. 136).

[Bai+20b] Mikhail BAIBAKOV, Aleksandr BARULIN, Prithu ROY, Jean-Benoît CLAUDE et al. « Zero-mode waveguides can be made better : fluorescence enhancement with rectangular aluminum nanoapertures from the visible to the deep ultraviolet ». In : *Nanoscale Advances* 2.9 (2020), p. 4153-4160. ISSN : 2516-0230. DOI : 10.1039/d0na00366b (cf. p. 4, 11, 47, 56, 61, 65, 85, 138).

[Bai+19a] Mikhail BAIBAKOV, Satyajit PATRA et al. « Extending Single-Molecule Förster Resonance Energy Transfer (FRET) Range beyond 10 Nanometers in Zero-Mode Waveguides ». In : *ACS Nano* 13.7 (juill. 2019), p. 8469-8480. ISSN : 1936086X. DOI : 10.1021/ACSNANO.9B04378 (cf. p. 59).

[Bai+19b] Mikhail BAIBAKOV, Satyajit PATRA et al. « Extending Single-Molecule Förster Resonance Energy Transfer (FRET) Range beyond 10 Nanometers in Zero-Mode Waveguides ». In : *ACS Nano* 13.7 (juill. 2019), p. 8469-8480. ISSN : 1936086X. DOI : 10.1021/ACSNANO.9B04378 (cf. p. 61, 123, 129).

[Bar+19a] A BARULIN, J CLAUDE et al. « Deep UV plasmonic enhancement of single protein autofluorescence in zero-mode waveguides. » In : *Nano letters* null (2019), null. DOI : 10.1021/acs.nanolett.9b03137. URL : https://www.semanticscholar.org/paper/651862180e72bde84e73ec4e5745b435dbc58b3c (cf. p. 30, 127).

[BW20a] A BARULIN et J WENGER. « Ultraviolet Photostability Improvement for Autofluorescence Correlation Spectroscopy on Label-free Proteins. » In : *The journal of physical chemistry letters* null (2020), null. DOI : 10.1021/acs.jpclett.0c00209. URL : https://www.semanticscholar.org/paper/3744f38e306506fb4e53d95ef98ffdf500e28bda (cf. p. 37).

[Bar20] Aleksandr BARULIN. « Label-free single protein fluorescence detection in the UV enhanced by aluminum plasmonic nanostructures ». Thèse de doct. 2020. URL : http://www.theses.fr/2020AIXM0384/document (cf. p. 36).

[Bar+19b] Aleksandr BARULIN, Jean Benoît CLAUDE et al. « Deep Ultraviolet Plasmonic Enhancement of Single Protein Autofluorescence in Zero-Mode Waveguides ». In : *Nano Letters* 19.10 (2019), p. 7434-7442. ISSN : 15306992. DOI : 10.1021/acs.nanolett.9b03137 (cf. p. 47, 66, 76-78, 85, 135, 136, 158).

[Bar+19c] Aleksandr BARULIN, Jean Benoît CLAUDE et al. « Deep Ultraviolet Plasmonic Enhancement of Single Protein Autofluorescence in Zero-Mode Waveguides ». In : *Nano Letters* 19.10 (oct. 2019), p. 7434-7442. ISSN : 15306992. DOI : 10.1021/ACS.NANOLETT.9B03137 (cf. p. 61).

[Bar+19d] Aleksandr BARULIN, Jean Benoît CLAUDE et al. « Deep Ultraviolet Plasmonic Enhancement of Single Protein Autofluorescence in Zero-Mode Waveguides ». In : *Nano Letters* 19.10 (oct. 2019), p. 7434-7442. ISSN : 15306992. DOI : 10.1021/ACS.NANOLETT.9B03137 (cf. p. 154).

[Bar+19e] Aleksandr BARULIN, Jean-Benoît CLAUDE et al. « Preventing Aluminum Photocorrosion for Ultraviolet Plasmonics ». In : *The Journal of Physical Chemistry Letters* (2019). DOI : 10.1021/acs.jpclett.9b02137 (cf. p. 69).

[Bar+19f] Aleksandr BARULIN, Jean-Benoît CLAUDE et al. « Preventing Aluminum Photocorrosion for Ultraviolet Plasmonics ». In : *The Journal of Physical Chemistry Letters* 10.19 (sept. 2019), p. 5700-5707. DOI : 10.1021/acs.jpclett.9b02137 (cf. p. 50, 68).

[Bar+22a] Aleksandr BARULIN, Prithu ROY, Jean Benoît CLAUDE et al. « Ultraviolet optical horn antennas for label-free detection of single proteins ». In : *Nature Communications* 13.1 (déc. 2022). ISSN : 20411723. DOI : 10.1038/S41467-022-29546-4 (cf. p. 136, 155).

[Bar+21a] Aleksandr BARULIN, Prithu ROY, Jean Benôit CLAUDE et al. « Purcell radiative rate enhancement of label-free proteins with ultraviolet aluminum plasmonics ». In : *Journal of Physics D : Applied Physics* 54.42 (oct. 2021). ISSN : 13616463. DOI : 10.1088/1361-6463/AC1627 (cf. p. 81, 123).

[Bar+21b] Aleksandr BARULIN, Prithu ROY, Jean-Benoît CLAUDE et al. « Purcell radiative rate enhancement of label-free proteins with ultraviolet aluminum plasmonics ». In : *Journal of Physics D : Applied Physics* 54.42 (oct. 2021), p. 425101. ISSN : 0022-3727. DOI : 10.1088/1361-6463/ac1627. URL : https://iopscience.iop.org/article/10.1088/1361-6463/ac1627 (cf. p. 4, 11, 38, 56, 60, 78, 97).

[Bar+22b] Aleksandr BARULIN, Prithu ROY, Jean-Benoît Benoît CLAUDE et al. « Ultraviolet optical horn antennas for label-free detection of single proteins ». In : *Nature Communications* 13.1 (déc. 2022), p. 1842. URL : https://www.nature.com/articles/s41467-022-29546-4 (cf. p. 3, 11, 62, 84, 101, 123, 158).

[BW20b] Aleksandr BARULIN et Jérôme WENGER. « Ultraviolet Photostability Improvement for Autofluorescence Correlation Spectroscopy on Label-Free Proteins ». In : *Journal of Physical Chemistry Letters* 11.6 (mars 2020), p. 2027-2035. ISSN : 19487185. DOI : 10.1021/ACS.JPCLETT.0C00209 (cf. p. 38).

[BW20c] Aleksandr BARULIN et Jérôme WENGER. « Ultraviolet Photostability Improvement for Autofluorescence Correlation Spectroscopy on Label-Free Proteins ». In : *Journal of Physical Chemistry Letters* 11.6 (fév. 2020), p. 2027-2035. ISSN : 19487185. DOI : 10.1021/acs.jpclett.0c00209 (cf. p. 118, 119).

[BH52] G. H. BEAVEN et E. R. HOLIDAY. « Ultraviolet Absorption Spectra of Proteins and Amino Acids ». In : *Advances in Protein Chemistry* 7.C (1952), p. 319-386. ISSN : 00653233. DOI : 10.1016/S0065-3233(08)60022-4 (cf. p. 26).

[Bee+15] Luther BEEGLE, Rohit BHARTIA et al. « SHERLOC : Scanning habitable environments with Raman & luminescence for organics & chemicals ». In : *IEEE Aerospace Conference Proceedings* 2015-June (2015), p. 1-11. ISSN : 1095323X. DOI : 10.1109/AERO.2015.7119105 (cf. p. 22, 26).

[BA10] Mikhail Y. BEREZIN et Samuel ACHILEFU. « Fluorescence lifetime measurements and biological imaging ». In : *Chemical Reviews* 110.5 (mai 2010), p. 2641-2684. ISSN : 00092665. DOI : 10.1021/CR900343Z/ASSET/IMAGES/MEDIUM/CR-2009-00343Z{_}0034.GIF. URL : https://

pubs-acs-org.lama.univ-amu.fr/doi/full/10.1021/cr900343z (cf. p. 16).

[Bet44] H. A. BETHE. « Theory of Diffraction by Small Holes ». In : *Physical Review* 66.7-8 (oct. 1944), p. 163. ISSN : 0031899X. DOI : 10.1103/PhysRev.66.163. URL : https://journals.aps.org/pr/abstract/10.1103/PhysRev.66.163 (cf. p. 58).

[BHH12] Paolo BIAGIONI, Jer Shing HUANG et al. « Nanoantennas for visible and infrared radiation ». In : *Reports on Progress in Physics* 75.2 (fév. 2012). ISSN : 00344885. DOI : 10.1088/0034-4885/75/2/024402 (cf. p. 135).

[BYR18] John S. BIGGINS, Sadegh YAZDI et al. « Magnesium Nanoparticle Plasmonics ». In : *Nano Letters* 18.6 (juin 2018), p. 3752-3758. ISSN : 15306992. DOI : 10.1021/ACS.NANOLETT.8B00955 (cf. p. 45).

[BG98] Laurent BINET et Didier GOURIER. « Origin of the blue luminescence of β-Ga2O3 ». In : *Journal of Physics and Chemistry of Solids* 59.8 (1998), p. 1241-1249. ISSN : 00223697. DOI : 10.1016/S0022-3697(98)00047-X (cf. p. 116).

[Bue+22] Carlos BUENO-ALEJO, M S VEGA et al. « Surface Passivation With a Perfluoroalkane Brush Improves the Precision of Single-Molecule Measurements ». In : *Acs Applied Materials & Interfaces* (2022). DOI : 10.1021/acsami.2c16647 (cf. p. 20).

[BD85] R F BUNSHAH et C V DESHPANDEY. « Plasma assisted physical vapor deposition processes : A review ». In : *Journal of Vacuum Science & Technology A : Vacuum, Surfaces, and Films* 3.3 (mai 1985), p. 553-560. DOI : 10.1116/1.572993. URL : http://dx.doi.org/10.1116/1.572993 (cf. p. 46).

[BRF03] T D BURLEIGH, C RUHE et al. « Photo-Corrosion of Different Metals During Long-Term Exposure to Ultraviolet Light ». In : *Corrosion* (2003). DOI : 10.5006/1.3277606 (cf. p. 48, 139).

[CL04] Patrik R. CALLIS et Tiqing LIU. « Quantitative Prediction of Fluorescence Quantum Yields for Tryptophan in Proteins ». In : *Journal of Physical Chemistry B* 108.14 (avr. 2004), p. 4248-4259. ISSN : 15206106. DOI : 10.1021/JP0310551 (cf. p. 120).

[Cam+11] Luis A. CAMPOS, Jianwei LIU et al. « A photoprotection strategy for microsecond-resolution single-molecule fluorescence spectroscopy ». In : *Nature Methods* 8.2 (2011), p. 143-146. ISSN : 15487091. DOI : 10.1038/nmeth.1553 (cf. p. 118).

[Cap+23a] Anna CAPITAINE, Mehrnaz BOCHET-MODARESIALAM et al. « Nanoparticle Imprint Lithography : From Nanoscale Metrology to Printable Metallic Grids ». In : *ACS Nano* 17.10 (mai 2023), p. 9361-9373. ISSN : 1936086X. DOI : 10.1021/ACSNANO.3C01156/ASSET/IMAGES/LARGE/NN3C01156{_}0007.JPEG. URL : https://pubs-acs-org.lama.univ-amu.fr/doi/full/10.1021/acsnano.3c01156 (cf. p. 54).

[Cap+23b] Anna CAPITAINE, Muhammad L FAJRI et al. « Pushing the Limits of Capillary Assembly for the Arbitrary Positioning of Sub-50nm Nanocubes in Printable Plasmonic Surfaces ». In : *Small Methods* (2023), p. 2300373. ISSN : 2366-9608. DOI : 10.1002/SMTD.202300373. URL : https://onlinelibrary.wiley.com/doi/full/10.1002/smtd.202300373%20https://onlinelibrary.wiley.com/doi/abs/10.1002/smtd.202300373%20https://onlinelibrary.wiley.com/doi/10.1002/smtd.202300373 (cf. p. 53, 54).

[Cas+22] Marion CASTILLA, Silvère SCHUERMANS et al. « Colloidal Synthesis of Crystalline Aluminum Nanoparticles for UV Plasmonics ». In : *ACS Photonics* 9.3 (mars 2022), p. 880-887. DOI : 10.1021/acsphotonics.1c01615 (cf. p. 47, 50).

[Cha+18] Pavan Kumar CHALLA, Quentin PETER et al. « Real-Time Intrinsic Fluorescence Visualization and Sizing of Proteins and Protein Complexes in Microfluidic Devices ». In : *Analytical Chemistry* 90.6 (2018), p. 3849-3855. ISSN : 15206882. DOI : 10.1021/acs.analchem.7b04523 (cf. p. 18).

[CR07] Chia-Lin CHANG et Shriram RAMANATHAN. « A Theoretical Approach to Investigate Low-Temperature Nanoscale Oxidation of Metals Under UV Radiation ». In : *Journal of the Electrochemical Society* (2007). DOI : 10.1149/1.2737347 (cf. p. 48).

[Che+18] Chang Wen CHEN, Yi LI et al. « High Spatial Resolution Nanoslit SERS for Single-Molecule Nucleobase Sensing ». In : *Nature Communications* (2018). DOI : 10.1038/s41467-018-04118-7 (cf. p. 23).

[Che72] Raymond F. CHEN. « Measurements of Absolute Values in Biochemical Fluorescence Spectroscopy ». In : *Journal of research of the National Bureau of Standards. Section A, Physics and chemistry* 76A.6 (nov. 1972), p. 593. ISSN : 0022-4332. DOI : 10.6028/JRES.076A.052. URL : https://pubmed.ncbi.nlm.nih.gov/34565885/ (cf. p. 153).

[CWM03] Yan CHEN, Li WEI et al. « Probing Protein Oligomerization in Living Cells With Fluorescence Fluctuation Spectroscopy ». In : *Proceedings of the National Academy of Sciences* (2003). DOI : 10.1073/pnas.2533045100 (cf. p. 19).

[Che+17] Yang CHEN, Yuhang CHEN et al. « Bridged Bowtie Aperture Antenna for Producing an Electromagnetic Hot Spot ». In : *Acs Photonics* (2017). DOI : 10.1021/acsphotonics.6b00857 (cf. p. 68).

[CB98] Yu CHEN et Mary D. BARKLEY. « Toward understanding tryptophan fluorescence in proteins ». In : *Biochemistry* 37.28 (juill. 1998), p. 9976-9982. ISSN : 00062960. DOI : 10.1021/BI980274N (cf. p. 80, 141).

[CDM13] Caroline CLERTE, Nathalie DECLERCK et al. « Competitive folding of anti-terminator/terminator hairpins monitored by single molecule FRET ». In : *Nucleic Acids Research* 41.4 (fév. 2013), p. 2632-2643. ISSN : 03051048. DOI : 10.1093/NAR/GKS1315 (cf. p. 120).

[CVT09] Thorben CORDES, Jan VOGELSANG et al. « On the mechanism of trolox as antiblinking and antibleaching reagent ». In : *Journal of the American Chemical Society* 131.14 (avr. 2009), p. 5018-5019. ISSN : 00027863. DOI : 10.1021/JA809117Z (cf. p. 19).

[CHL79] F. A. COTTON, E. E. HAZEN et al. « Staphylococcal nuclease : Proposed mechanism of action based on structure of enzyme-thymidine 3',5'-bisphosphate-calcium ion complex at 1.5-Å resolution ». In : *Proceedings of the National Academy of Sciences of the United States of America* 76.6 (1979), p. 2551-2555. ISSN : 00278424. DOI : 10.1073/PNAS.76.6.2551 (cf. p. 120).

[Cui+] Lingfei CUI, Xingyu YANG et al. *An achiral magnetic photonic antenna as a tunable nanosource of superchiral light*. Rapp. tech. (cf. p. 65).

[Cur+22] Kathrine CURTIN, Bethany J FIKE et al. « Recent Advances in Digital Biosensing Technology ». In : *Biosensors* (2022). DOI : 10.3390/bios12090673 (cf. p. 15).

[Dan+05] Christophe DANELON, Jean-Baptiste PEREZ et al. « Cell Membranes Suspended Across Nanoaperture Arrays ». In : *Langmuir* 22.1 (déc. 2005), p. 22-25. DOI : 10.1021/la052387v (cf. p. 61).

[De +15a] Juan DE TORRES, Petru GHENUCHE et al. « FRET enhancement in aluminum zero-mode waveguides ». In : *ChemPhysChem* 16.4 (mars 2015), p. 782-788. ISSN : 14397641. DOI : 10.1002/CPHC.201402651 (cf. p. 59).

[De +15b] Juan DE TORRES, Petru GHENUCHE et al. « FRET enhancement in aluminum zero-mode waveguides ». In : *ChemPhysChem* 16.4 (mars 2015), p. 782-788. ISSN : 14397641. DOI : 10.1002/CPHC.201402651 (cf. p. 135).

[Dea+15] Kevin M DEAN, Jennifer L LUBBECK et al. « Microfluidics-Based Selection of Red-Fluorescent Proteins With Decreased Rates of Photobleaching ». In : *Integrative Biology* (2015). DOI : 10.1039/c4ib00251b (cf. p. 19).

[Den+20] Fu DENG, Hongfeng LIU et al. « Optical Scattering of Liquid Gallium Nanoparticles Coupled to Thin Metal Films ». In : *Nanomaterials* 10.6 (mai 2020), p. 1052. ISSN : 2079-4991. DOI : 10.3390/nano10061052. URL : https://www.mdpi.com/2079-4991/10/6/1052 (cf. p. 48).

[Dey+21] Swarup DEY, Chunhai FAN et al. « DNA Origami ». In : *Nature Reviews Methods Primers* (2021). DOI : 10.1038/s43586-020-00009-8 (cf. p. 51, 52).

[DDZ23] Swayandipta DEY, Mathias DOLCI et al. « Single-Molecule Optical Biosensing : Recent Advances and Future Challenges ». In : *ACS Physical Chemistry Au* 0.0 (jan. 2023). DOI : 10.1021/acsphyschemau.2c00061 (cf. p. 135).

[Dou21] Oscar A DOUGLAS-GALLARDO. « Plasmonic Enhancement of Molecular Hydrogen Dissociation on Metallic Magnesium Nanoclusters ». In : (2021). DOI : 10.48550/arxiv.2104.00141 (cf. p. 45).

[Dua+14] Haohong DUAN, Ning YAN et al. « Ultrathin Rhodium Nanosheets ». In : *Nature Communications* (2014). DOI : 10.1038/ncomms4093 (cf. p. 148).

[Els13] Elliot L. ELSON. « Brief introduction to fluorescence correlation spectroscopy ». In : *Methods in Enzymology*. T. 518. 2013. DOI : 10.1016/B978-0-12-388422-0.00002-9 (cf. p. 108).

[EZ03] Jörg ENDERLEIN et Christoph ZANDER. « Theoretical Foundations of Single Molecule Detection in Solution ». In : *Single Molecule Detection in Solution*. 2003. DOI : 10.1002/3527600809.ch2 (cf. p. 117).

[Far+21] H FARHEEN, Till LEUTERITZ et al. « Optimization of Optical Waveguide Antennas for Directive Emission of Light ». In : (2021). DOI : 10.48550/arxiv.2106.02468 (cf. p. 40).

[Fel+12] Suren FELEKYAN, Stanislav KALININ et al. « Filtered FCS : Species auto- and cross-correlation functions highlight binding and dynamics in biomolecules ». In : *ChemPhysChem* 13.4 (2012), p. 1036-1053. ISSN : 14397641. DOI : 10.1002/CPHC.201100897 (cf. p. 32).

[Fie88] Loren J FIELD. « Atrial Natriuretic Factor-Sv40 T Antigen Transgenes Produce Tumors and Cardiac Arrhythmias in Mice ». In : *Science* (1988). DOI : 10.1126/science.2964082 (cf. p. 27).

[FM08] Holger FISCHER et Olivier J F MARTIN. « Engineering the Optical Response of Plasmonic Nanoantennas ». In : *Optics Express* (2008). DOI : 10.1364/oe.16.009144 (cf. p. 68).

[Fla+17a] Valentin FLAURAUD, Massimo MASTRANGELI et al. « Nanoscale topographical control of capillary assembly of nanoparticles ». In : *Nature Nanotechnology* 12.1 (2017), p. 73-80. ISSN : 17483395. DOI : 10.1038/nnano.2016.179. URL : http://dx.doi.org/10.1038/nnano.2016.179 (cf. p. 53, 54, 150).

[Fla+17b] Valentin FLAURAUD, Raju REGMI, Pamina M. WINKLER et al. « In-Plane Plasmonic Antenna Arrays with Surface Nanogaps for Giant Fluorescence Enhancement ». In : *Nano Letters* 17.3 (fév. 2017), p. 1703-1710. DOI : 10.1021/acs.nanolett.6b04978 (cf. p. 160).

[Fla+17c] Valentin FLAURAUD, Raju REGMI, Pamina M. WINKLER et al. « In-Plane Plasmonic Antenna Arrays with Surface Nanogaps for Giant Fluorescence Enhancement ». In : *Nano Letters* 17.3 (mars 2017), p. 1703-1710. ISSN : 15306992. DOI : 10.1021/ACS.NANOLETT.6B04978 (cf. p. 110, 123).

[Fla+17d] Valentin FLAURAUD, Raju REGMI, Pamina M. WINKLER et al. « In-Plane Plasmonic Antenna Arrays with Surface Nanogaps for Giant Fluorescence Enhancement ». In : *Nano Letters* 17.3 (mars 2017), p. 1703-1710. ISSN : 15306992. DOI : 10.1021/ACS.NANOLETT.6B04978 (cf. p. 164).

[Foq+08] Mathieu FOQUET, Kevan T. SAMIEE et al. « Improved fabrication of zero-mode waveguides for single-molecule detection ». In : *Journal of Applied Physics* 103.3 (fév. 2008). ISSN : 0021-8979. DOI : 10.1063/1.2831366. URL : /aip/jap/article/103/3/034301/902033/Improved-fabrication-of-zero-mode-waveguides-for (cf. p. 63, 64).

[GJC93] Theodorus W.J. GADELLA, Thomas M. JOVIN et al. « Fluorescence lifetime imaging microscopy (FLIM) : spatial resolution of microstructures on the nanosecond time scale ». In : *Biophysical Chem.* 48.2 (1993), p. 221-239. ISSN : 03014622. DOI : 10.1016/0301-4622(93)85012-7 (cf. p. 17).

[Gar+19] Denis GAROLI, Hirohito YAMAZAKI et al. « Plasmonic Nanopores for Single-Molecule Detection and Manipulation : Toward Sequencing Applications ». In : *Nano Letters* 19.11 (2019), p. 7553-7562. ISSN : 15306992. DOI : 10.1021/acs.nanolett.9b02759 (cf. p. 24).

[Geo+14] Florian GEORGESCAULD, Kristina POPOVA et al. « GroEL/ES Chaperonin Modulates the Mechanism and Accelerates the Rate of TIM-Barrel Domain Folding ». In : *Cell* (2014). DOI : 10.1016/j.cell.2014.03.038 (cf. p. 33).

[Gér+08] Davy GÉRARD, Jérôme WENGER et al. « Nanoaperture-enhanced fluorescence : Towards higher detection rates with plasmonic metals ». In : *Physical Review B - Condensed Matter and Materials Physics* 77.4 (jan. 2008). ISSN : 10980121. DOI : 10.1103/PHYSREVB.77.045413 (cf. p. 60).

[Ghe+15] Petru GHENUCHE, Mathieu MIVELLE et al. « Matching Nanoantenna Field Confinement to FRET Distances Enhances Förster Energy Transfer Rates ». In : *Nano Letters* 15.9 (sept. 2015), p. 6193-6201. ISSN : 15306992. DOI : 10.1021/ACS.NANOLETT.5B02535 (cf. p. 163, 164).

[GA23] Biswajoy GHOSH et Krishna AGARWAL. « Viewing life without labels under optical microscopes ». In : *Communications Biology 2023 6 :1* 6.1 (mai 2023), p. 1-12. ISSN : 2399-3642. DOI : 10.1038/s42003-023-04934-8. URL : https://www.nature.com/articles/s42003-023-04934-8 (cf. p. 17).

[Gia+11a] Vincenzo GIANNINI, Antonio I. FERNÁNDEZ-DOMÍNGUEZ et al. « Plasmonic Nanoantennas : Fundamentals and Their Use in Controlling the Radiative Properties of Nanoemitters ». In : *Chemical Reviews* 111.6 (mars 2011), p. 3888-3912. ISSN : 0009-2665. DOI : 10.1021/cr1002672 (cf. p. 38).

[Gia+11b] Vincenzo GIANNINI, Antonio I. FERNÁNDEZ-DOMÍNGUEZ et al. « Plasmonic nanoantennas : Fundamentals and their use in controlling the radiative properties of nanoemitters ». In : *Chemical Reviews* 111.6 (juin 2011), p. 3888-3912. ISSN : 00092665. DOI : 10.1021/CR1002672/ASSET/IMAGES/MEDIUM/CR-2010-002672{_}0004.GIF. URL : https://pubs-acs-org.lama.univ-amu.fr/doi/full/10.1021/cr1002672 (cf. p. 40).

[Gie+06] Ben N G GIEPMANS, Stephen R ADAMS et al. « The Fluorescent Toolbox for Assessing Protein Location and Function ». In : *Science* 312.5771 (avr. 2006), p. 217-224. DOI : 10.1126/science.1124618. URL : http://dx.doi.org/10.1126/SCIENCE.1124618 (cf. p. 18, 19).

[Gle+21] Viktorija GLEMBOCKYTE, Lennart GRABENHORST et al. « DNA Origami Nanoantennas for Fluorescence Enhancement ». In : *Accounts of Chemical Research* 54.17 (août 2021), p. 3338-3348. ISSN : 0001-4842. DOI : 10.1021/acs.accounts.1c00307 (cf. p. 135).

[Gor19] Reuven GORDON. « Biosensing with nanoaperture optical tweezers ». In : *Optics and Laser Technology* 109 (jan. 2019), p. 328-335. ISSN : 00303992. DOI : 10.1016/J.OPTLASTEC.2018.07.019 (cf. p. 61).

[Gro+18] Heiko GROSS, Joachim M. HAMM et al. « Near-field strong coupling of single quantum dots ». In : *Science Advances* 4.3 (mars 2018). ISSN : 23752548. DOI : 10.1126/SCIADV.AAR4906 (cf. p. 38).

[GZZ18] Panpan GU, Wei ZHANG et al. « Plasmonic Nanogaps : From Fabrications to Optical Applications ». In : *Advanced Materials Interfaces* 5.19 (oct. 2018). ISSN : 21967350. DOI : 10.1002/ADMI.201800648 (cf. p. 63).

[Gut+16] Yael GUTIERREZ, Dolores ORTIZ et al. « How an oxide shell affects the ultraviolet plasmonic behavior of Ga, Mg, and Al nanostructures ». In : *Optics Express* 24.18 (sept. 2016), p. 20621. ISSN : 1094-4087. DOI : 10.1364/oe.24.020621 (cf. p. 139).

[Gut+19] Yael GUTIÉRREZ, Maria LOSURDO, Pablo GARCÍA-FERNÁNDEZ et al. « Gallium Polymorphs : Phase-Dependent Plasmonics ». In : *Advanced Optical Materials* 1900307 (2019), p. 1-10. ISSN : 21951071. DOI : 10.1002/adom.201900307 (cf. p. 44).

[Gut+20] Yael GUTIÉRREZ, Maria LOSURDO, Francisco GONZÁLEZ et al. « Nanoplasmonic Photothermal Heating and Near-Field Enhancements : A Comparative Survey of 19 Metals ». In : *Journal of Physical Chemistry C* 124.13 (avr. 2020), p. 7386-7395. ISSN : 19327455. DOI : 10.1021/ACS.JPCC.0C00757 (cf. p. 42, 43).

[Gut+18] Yael GUTIÉRREZ, Rodrigo Alcaraz de la OSA et al. « Plasmonics in the Ultraviolet with Aluminum, Gallium, Magnesium and Rhodium ». In : *Applied Sciences 2018, Vol. 8, Page 64* 8.1 (jan. 2018), p. 64. ISSN : 2076-3417. DOI : 10.3390/APP8010064. URL : https://www.mdpi.com/2076-3417/8/1/64/htm%20https://www.mdpi.com/2076-3417/8/1/64 (cf. p. 42).

[HT12a] Taekjip HA et Philip TINNEFELD. « Photophysics of fluorescent probes for single-molecule biophysics and super-resolution imaging ». In : *Annual Review of Physical Chemistry* 63 (mai 2012), p. 595-617. ISSN : 0066426X. DOI : 10.1146/ANNUREV-PHYSCHEM-032210-103340 (cf. p. 19).

[HT12b] Taekjip HA et Philip TINNEFELD. « Photophysics of fluorescent probes for single-molecule biophysics and super-resolution imaging ». In : *Annual Review of Physical Chemistry* 63 (mai 2012), p. 595-617. ISSN : 0066426X. DOI : 10.1146/ANNUREV-PHYSCHEM-032210-103340 (cf. p. 37).

[HWP15] Conor M HANEY, Rebecca F WISSNER et al. « Multiply Labeling Proteins for Studies of Folding and Stability ». In : *Current Opinion in Chemical Biology* (2015). DOI : 10.1016/j.cbpa.2015.07.007 (cf. p. 18).

[HH19] Gufran A HASSAN et Jawad ul HASSAN. « Design and Study the Performance of Optical Nanoantenna ». In : *Al-Qadisiyah Journal for Engineering Sciences* (2019). DOI : 10.30772/qjes.v12i2.593 (cf. p. 68).

[HS03] Elke HAUSTEIN et Petra SCHWILLE. « Ultrasensitive investigations of biological systems by fluorescence correlation spectroscopy ». In : *Methods* 29.2 (fév. 2003), p. 153-166. ISSN : 10462023. DOI : 10.1016/S1046-2023(02)00306-7 (cf. p. 132).

[Hei+21] Jeanne HEINTZ, Nemanja MARKEŠEVIĆ et al. « Few-Molecule Strong Coupling with Dimers of Plasmonic Nanoparticles Assembled on DNA ». In : *ACS Nano* (2021). ISSN : 1936-0851. DOI : 10.1021/acsnano.1c04552 (cf. p. 52).

[HTW16] Heike HEVEKERL, Johan TORNMALM et al. « Fluorescence-Based Characterization of Non-Fluorescent Transient States of Tryptophan – Prospects for Protein Conformation and Interaction Studies ». In : *Scientific Reports* (2016). DOI : 10.1038/srep35052 (cf. p. 29).

[Hol+14] Phil HOLZMEISTER, Guillermo P. ACUNA et al. « Breaking the concentration limit of optical single-molecule detection ». In : *Chemical Society Reviews* 43.4 (fév. 2014), p. 1014-1028. ISSN : 14604744. DOI : 10.1039/C3CS60207A (cf. p. 58, 132).

[Hor+18] Michal HORÁK, Kristýna BUKVIŠOVÁ et al. « Comparative Study of Plasmonic Antennas Fabricated by Electron Beam and Focused Ion Beam Lithography ». In : *Scientific Reports* (2018). DOI : 10.1038/s41598-018-28037-1 (cf. p. 51).

[Hor+23] Michal HORÁK, Vojtěch ČALKOVSKÝ et al. « Plasmonic Properties of Individual Gallium Nanoparticles ». In : *Journal of Physical Chemistry Letters* 14.8 (mars 2023), p. 2012-2019. ISSN : 19487185. DOI : 10.1021/ACS.JPCLETT.3C00094 (cf. p. 43).

[Hsi17] Chia-Lung HSIEH. « Ultrahigh-Speed Imaging Reveals Nanoscopic Single-Molecule Dynamics ». In : *Spie Newsroom* (2017). DOI : 10.1117/2.1201611.006731 (cf. p. 20).

[HTM22] Changpeng HU, Rabia TAHIR et al. « Single-Molecule Mechanochemical Sensing ». In : *Accounts of Chemical Research* (2022). DOI : 10.1021/acs.accounts.1c00770 (cf. p. 15).

[HF15] Ali A HUMMADI et Raad S FYATH. « Performance of Modified Silicon-Based Optical Leaky-Wave Antenna Structures ». In : *International Journal of Computers & Technology* (2015). DOI : 10.24297/ijct.v14i3.2000 (cf. p. 40).

[Hum+07] Simon M HUMPHREY, Michael E GRASS et al. « Rhodium Nanoparticles From Cluster Seeds : Control of Size and Shape by Precursor Addition Rate ». In : *Nano Letters* (2007). DOI : 10.1021/nl070035y (cf. p. 44, 148).

[HYR00] Thomas R HUSER, Ming YAN et al. « Single Chain Spectroscopy of Conformational Dependence of Conjugated Polymer Photophysics ». In : *Proceedings of the National Academy of Sciences* (2000). DOI : 10.1073/pnas.97.21.11187 (cf. p. 19).

[I R+12] Christopher I. RICHARDS, Khai LUONG et al. « Live-Cell Imaging of Single Receptor Composition Using Zero-Mode Waveguide Nanostructures ». In : *Nano Letters* 12.7 (juin 2012), p. 3690-3694. DOI : 10.1021/nl301480h (cf. p. 61).

[Jam+19] Ryan M. JAMIOLKOWSKI, Kevin Y. CHEN et al. « Nanoaperture fabrication via colloidal lithography for single molecule fluorescence analysis ». In : *PLoS ONE* 14.10 (oct. 2019). ISSN : 19326203. DOI : 10.1371/journal.pone.0222964 (cf. p. 63, 149).

[Jha+12a] Shankar K. JHA, Zeeshan AHMED et al. « Deep-UV surface-enhanced resonance Raman scattering of adenine on aluminum nanoparticle arrays ». In : *Journal of the American Chemical Society* 134.4 (fév. 2012), p. 1966-1969. ISSN : 00027863. DOI : 10.1021/JA210446W (cf. p. 24, 136).

[Jha+12b] Shankar K. JHA, Zeeshan AHMED et al. « Deep-UV surface-enhanced resonance Raman scattering of adenine on aluminum nanoparticle arrays ». In : *Journal of the American Chemical Society* 134.4 (fév. 2012), p. 1966-1969. ISSN : 00027863. DOI : 10.1021/JA210446W (cf. p. 132).

[Jia+21a] Quanbo JIANG, Prithu ROY, Jean Benoît CLAUDE et al. « Single Photon Source from a Nanoantenna-Trapped Single Quantum Dot ». In : *Nano Letters* 21.16 (août 2021), p. 7030-7036. ISSN : 15306992. DOI : 10.1021/ACS.NANOLETT.1C02449 (cf. p. 135).

[Jia+21b] Quanbo JIANG, Prithu ROY, Jean-Benoît CLAUDE et al. « Single Photon Source from a Nanoantenna-Trapped Single Quantum Dot ». In : *Nano Letters* (août 2021), p. 7030-7036. ISSN : 1530-6984. DOI : 10.1021/acs.nanolett.1c02449 (cf. p. 4).

[JWB15] X JIAO, Yunshan WANG et al. « UV fluorescence enhancement by Al and Mg nanoapertures ». In : *Journal of Physics D : Applied Physics* 48 (2015), null. DOI : 10.1088/0022-3727/48/18/184007. URL : https://www.semanticscholar.org/paper/790d158515ad293e946fc8465ea200e63be7a99d (cf. p. 45).

[Jia+14] Xiaojin JIAO, Eric M. PETERSON et al. « UV Fluorescence Lifetime Modification by Aluminum Nanoapertures ». In : *ACS Photonics* 1.12 (2014), p. 1270-1277. ISSN : 23304022. DOI : 10.1021/ph500267n (cf. p. 76-78).

[Jin+13] Xing Ri JIN, Lei SUN et al. « Quantum Entanglement in Plasmonic Waveguides With Near-Zero Mode Indices ». In : *Optics Letters* (2013). DOI : 10.1364/ol.38.004078 (cf. p. 59, 60).

[Jon+19] Robin R. JONES, David C. HOOPER et al. « Raman Techniques : Fundamentals and Frontiers ». In : *Nanoscale Research Letters 2019 14 :1* 14.1 (juill. 2019), p. 1-34. ISSN : 1556-276X. DOI : 10.1186/S11671-019-3039-2. URL : https://link.springer.com/article/10.1186/s11671-019-3039-2 (cf. p. 23).

[Jos+22] Gayatri K JOSHI, Ab Q MIR et al. « Plasmon-Based Small-Molecule Activation : A New Dawn in the Field of Solar-Driven Chemical Transformation ». In : *Acs Catalysis* (2022). DOI : 10.1021/acscatal.1c05245 (cf. p. 45).

[Kaa+23] Ediz KAAN HERKERT, Domenica ROMINA BERMEO ALVARO et al. « Hybrid Plasmonic Nanostructures for Enhanced Single-Molecule Detection Sensitivity ». In : *ACS Nano* 17.9 (avr. 2023), p. 8453-8464. DOI : 10.1021/acsnano.3c00576 (cf. p. 67, 68).

[Kal+18] Megan J. KALISZEWSKI, Xiaojun SHI et al. « Quantifying membrane protein oligomerization with fluorescence cross-correlation spectroscopy ». In : *Methods* 140-141 (mai 2018), p. 40-51. ISSN : 10959130. DOI : 10.1016/j.ymeth.2018.02.002 (cf. p. 32).

[Kau+15] Abu KAUSAR, Ahmed Wasif REZA et al. « Optical Nano Antennas : State of the Art, Scope and Challenges as a Biosensor Along With Human Exposure to Nano-Toxicology ». In : *Sensors* (2015). DOI : 10.3390/s150408787 (cf. p. 68).

[Kin+09] Anika KINKHABWALA, Zongfu YU et al. « Large single-molecule fluorescence enhancements produced by a bowtie nanoantenna ». In : *Nature Photonics* 3.11 (nov. 2009), p. 654-657. ISSN : 17494885. DOI : 10.1038/nphoton.2009.187. URL : www.nature.com/naturephotonics (cf. p. 39, 135).

[KD21] Nils KLUGHAMMER et Cees DEKKER. « Palladium zero-mode waveguides for optical single-molecule detection with nanopores ». In : *Nanotechnology* 32.18 (avr. 2021), 18LT01. ISSN : 0957-4484. DOI : 10.1088/1361-6528/abd976. URL : https://iopscience.iop.org/article/10.1088/1361-6528/abd976 (cf. p. 61, 63).

[Kni+14] Mark W. KNIGHT, Nicholas S. KING et al. « Aluminum for plasmonics ». In : *ACS Nano* 8.1 (jan. 2014), p. 834-840. ISSN : 19360851. DOI : 10.1021/NN405495Q (cf. p. 132).

[Kni+12] Mark W. KNIGHT, Lifei LIU et al. « Aluminum plasmonic nanoantennas ». In : *Nano Letters* 12.11 (2012), p. 6000-6004. ISSN : 15306984. DOI : 10.1021/nl303517v (cf. p. 45, 106).

[Kol+14] Heiko KOLLMANN, Xianji PIAO et al. « Toward Plasmonics With Nanometer Precision : Nonlinear Optics of Helium-Ion Milled Gold Nanoantennas ». In : *Nano Letters* (2014). DOI : 10.1021/nl5019589 (cf. p. 51).

[Kop74a] Dennis KOPPEL. « Statistical accuracy in FCS ». In : *Physical Review A* 10.6 (1974) (cf. p. 110).

[Kop74b] Dennis E. KOPPEL. « Statistical accuracy in fluorescence correlation spectroscopy ». In : *Physical Review A* 10.6 (1974). ISSN : 10502947. DOI : 10.1103/PhysRevA.10.1938 (cf. p. 110, 111).

[KT13] Jonas KORLACH et Stephen W TURNER. « Zero-Mode Waveguides ». In : *Encyclopedia of Biophysics*. Sous la dir. de Gordon C K ROBERTS. Berlin, Heidelberg : Springer Berlin Heidelberg, 2013, p. 2793-2795. ISBN : 978-3-642-16712-6. DOI : 10.1007/978-3-642-16712-6{_}499. URL : https://doi.org/10.1007/978-3-642-16712-6_499 (cf. p. 58, 59).

[Kra+12] Alexander E. KRASNOK, Andrey E. MIROSHNICHENKO et al. « All-dielectric optical nanoantennas ». In : *AIP Conference Proceedings* 1475.June 2014 (2012), p. 22-24. ISSN : 0094243X. DOI : 10.1063/1.4750083 (cf. p. 39, 142).

[Kue+11] Cyrill KUEMIN, Richard STUTZ et al. « Precise placement of gold nanorods by capillary assembly ». In : *Langmuir* 27.10 (2011), p. 6305-6310. ISSN : 07437463. DOI : 10.1021/la2001128 (cf. p. 138, 149).

[KS22] Govind KUMAR et Ravi Kant SONI. « Rhodium concave nanocubes and nanoplates as deep-UV resonant SERS platform ». In : *Journal of Raman Spectroscopy* (nov. 2022). ISSN : 10974555. DOI : 10.1002/jrs.6427 (cf. p. 44, 136).

[Küp+23] Michelle KÜPPERS, David ALBRECHT et al. « Confocal Interferometric Scattering Microscopy Reveals 3D Nanoscopic structure and Dynamics in Live Cells ». In : *Nature Communications* (2023). DOI : 10.1038/s41467-023-37497-7 (cf. p. 20).

[Kuz+23] Maksim KUZNETCOV, Davide COMITE et al. « Half-Annular Leaky-Wave Antenna With Suppressed Open Stopband : Design and Experimental Testing ». In : *Ieee Antennas and Wireless Propagation Letters* (2023). DOI : 10.1109/lawp.2023.3236614 (cf. p. 40).

[Kuz+18] Anton KUZYK, Ralf JUNGMANN et al. « DNA Origami Route for Nanophotonics ». In : *Acs Photonics* (2018). DOI : 10.1021/acsphotonics.7b01580 (cf. p. 52).

[Lac11] JR LACKOWICZ. *Principles of Fluorescence Spectroscopy*. 2011 (cf. p. 26).

[Lak06] Joseph R LAKOWICZ. « Principles of Fluorescence Spectroscopy Third Edition ». In : (2006). URL : http://extras.springer.com. (cf. p. 15, 27, 28).

[Lal+15] Adrien LALISSE, Gilles TESSIER et al. « Quantifying the Efficiency of Plasmonic Materials for Near-Field Enhancement and Photothermal Conversion ». In : *Journal of Physical Chemistry C* 119.45 (oct. 2015), p. 25518-25528. ISSN : 19327455. DOI : 10.1021/ACS.JPCC.5B09294 (cf. p. 41).

[Lao+20] Zhaoxin LAO, Yuanyuan ZHENG et al. « Nanogap Plasmonic Structures Fabricated by Switchable Capillary-Force Driven Self-Assembly for Localized Sensing of Anticancer Medicines With Microfluidic SERS ». In : *Advanced Functional Materials* (2020). DOI : 10.1002/adfm.201909467 (cf. p. 54).

[Lar+14] Joseph LARKIN, Mathieu FOQUET et al. « Reversible Positioning of Single Molecules inside Zero-Mode Waveguides ». In : *Nano Letters* 14.10 (sept. 2014), p. 6023-6029. DOI : 10.1021/nl503134x (cf. p. 61).

[Lee+17] Junghoon LEE, Sangwoo SHIN et al. « Oil-Impregnated Nanoporous Oxide Layer for Corrosion Protection With Self-Healing ». In : *Advanced Functional Materials* (2017). DOI : 10.1002/adfm.201606040 (cf. p. 49).

[LCW21] Ji-Young LEE, Xueling CHENG et al. « Ultraviolet plasmonic enhancement of the native fluorescence of tryptophan on aluminum nano-hole arrays ». In : *Journal of Physics D : Applied Physics* 54.13 (avr. 2021), p. 135107. ISSN : 0022-3727. DOI : 10.1088/1361-6463/abd0b0. URL : https://iopscience.iop.org/article/10.1088/1361-6463/abd0b0 (cf. p. 76).

[Lev+03] H. J. LEVENE, J. KORLACH et al. « Zero-mode waveguides for single-molecule analysis at high concentrations ». In : *Science* 299.5607 (août 2003), p. 682-686. ISSN : 00368075. DOI : 10.1126/science.1079700 (cf. p. 58, 59, 61, 132).

[Li+19] Jing-Feng LI, Qing X LI et al. « Force Spectroscopic Detection of Peptide Cleavage by Thrombin Exploiting Biotin–streptavidin Interactions in a Bio-Sensing Context ». In : *Analytical Methods* (2019). DOI : 10.1039/c8ay02519c (cf. p. 15).

[Li+23] Ling LI, Shihong NIE et al. « DNA Origami Technology for Biomedical Applications : Challenges and Opportunities ». In : *Medcomm – Biomaterials and Applications* (2023). DOI : 10.1002/mba2.37 (cf. p. 52).

[LS06] Qiang LI et Stefan SEEGER. « Label-free detection of single protein molecules using deep UV fluorescence lifetime microscopy ». In : *Analytical Chemistry* 78.8 (avr. 2006), p. 2732-2737. ISSN : 00032700. DOI : 10.1021/AC052166U (cf. p. 29, 30).

[Lia+08] David LIAO, Peter GALAJDA et al. « Single Molecule Correlation Spectroscopy in Continuous Flow Mixers With Zero-Mode Waveguides ». In : *Optics Express* (2008). DOI : 10.1364/oe.16.010077 (cf. p. 59).

[Lip+02] M. LIPPITZ, W. ERKER et al. « Two-photon excitation microscopy of tryptophan-containing proteins ». In : *Proceedings of the National Academy of Sciences of the United States of America* 99.5 (mars 2002), p. 2772-2777. ISSN : 00278424. DOI : 10.1073/PNAS.052662999 (cf. p. 30).

[Lob+10] V. LOBO, A. PATIL et al. « Free radicals, antioxidants and functional foods : Impact on human health ». In : *Pharmacognosy Reviews* 4.8 (juill. 2010), p. 118. ISSN : 09737847. DOI : 10.4103/0973-7847.70902. URL : /pmc/articles/PMC3249911/%20/pmc/articles/PMC3249911/?report=abstract%20https://www.ncbi.nlm.nih.gov/pmc/articles/PMC3249911/ (cf. p. 37).

[Los+18] Maria LOSURDO, Yael GUTIERREZ et al. « Multiphase gallium-based nanoparticles for a versatile plasmonic platform ». In : *Optics InfoBase Conference Papers* Part F107- (juin 2018), p. 3-4. DOI : 10.1364/NOMA.2018.NoTh3D.4 (cf. p. 44).

[Los+21] Maria LOSURDO, Yael GUTIÉRREZ et al. « Gallium Plasmonic Nanoantennas Unveiling Multiple Kinetics of Hydrogen Sensing, Storage, and Spillover ». In : *Advanced Materials* 2100500 (2021). ISSN : 15214095. DOI : 10.1002/adma.202100500 (cf. p. 44).

[MH11] Kathryn M. MAYER et Jason H. HAFNER. « Localized Surface Plasmon Resonance Sensors ». In : *Chemical Reviews* 111.6 (juin 2011), p. 3828-3857. DOI : 10.1021/cr100313v (cf. p. 40).

[M W+15] Anne M. WATSON, Xiao ZHANG et al. « Rhodium Nanoparticles for Ultraviolet Plasmonics ». In : *Nano Letters* 15.2 (jan. 2015), p. 1095-1100. DOI : 10.1021/nl5040623 (cf. p. 136).

[Mal+07] Laurent MALAQUIN, Tobias KRAUS et al. « Controlled particle placement through convective and capillary assembly ». In : *Langmuir* 23.23 (2007), p. 11513-11521. ISSN : 07437463. DOI : 10.1021/la700852c (cf. p. 53, 150).

[Mao+10] Huibing MAO, Jiqing WANG et al. « TM and TE Propagating Modes of Photonic Crystal Waveguide Based on Honeycomb Lattices ». In : *Applied Optics* (2010). DOI : 10.1364/ao.49.006597 (cf. p. 59).

[Mao+18] Jieying MAO, Yunshan WANG et al. « Effect of Ga Implantation and Hole Geometry on Light Transmission through Nanohole Arrays in Al and Mg ». In : *The Journal of Physical Chemistry C* 122.19 (2018), p. 10535-10544. ISSN : 1932-7447. DOI : 10.1021/acs.jpcc.8b02310. URL : https://pubs.acs.org/doi/10.1021/acs.jpcc.8b02310 (cf. p. 51).

[Mar+17] W. Elliott MARTIN, Ning GE et al. « Real-Time Sensing of Single-Ligand Delivery with Nanoaperture-Integrated Microfluidic Devices ». In : *ACS Omega* 2.7 (juill. 2017), p. 3858-3867. ISSN : 24701343. DOI : 10.1021/ACSOMEGA.7B00934 (cf. p. 64).

[MSG13] Jeffrey M. MCMAHON, George C. SCHATZ et al. « Plasmonics in the ultraviolet with the poor metals Al, Ga, In, Sn, Tl, Pb, and Bi ». In : *Physical Chemistry Chemical Physics* 15.15 (mars 2013), p. 5415-5423. ISSN : 1463-9084. DOI : 10.1039/C3CP43856B. URL : https://pubs.rsc.org/en/content/articlehtml/2013/cp/c3cp43856b%20https://pubs.rsc.org/en/content/articlelanding/2013/cp/c3cp43856b (cf. p. 41, 42).

[MCA10] M. F. MELÉNDREZ, G. CÁRDENAS et al. « Synthesis and characterization of gallium colloidal nanoparticles ». In : *Journal of Colloid and Interface Science* 346.2 (2010), p. 279-287. ISSN : 00219797. DOI : 10.1016/j.jcis.2009.11.069 (cf. p. 44).

[MR11] Laurent D MENARD et J Michael RAMSEY. « Fabrication of Sub-5 nm Nanochannels in Insulating Substrates Using Focused Ion Beam Milling ». In : *Nano Letters* 11.2 (fév. 2011), p. 512-517. DOI : 10.1021/nl103369g. URL : http://dx.doi.org/10.1021/nl103369g (cf. p. 51).

[Mes+22] Troy C. MESSINA, Bernadeta R. SRIJANTO et al. « Gold Ion Beam Milled Gold Zero-Mode Waveguides ». In : *Nanomaterials* 12.10 (mai 2022). ISSN : 20794991. DOI : 10.3390/NANO12101755. URL : https://www.researchgate.net/publication/360770588_Gold_Ion_Beam_Milled_Gold_Zero-Mode_Waveguides (cf. p. 63).

[MGC16] Cédric MONGIN, Jessica H. GOLDEN et al. « Liquid PEG Polymers Containing Antioxidants : A Versatile Platform for Studying Oxygen-Sensitive Photochemical Processes ». In : *ACS Applied Materials and Interfaces* 8.36 (2016), p. 24038-24048. ISSN : 19448252. DOI : 10.1021/acsami.6b05697 (cf. p. 113).

[Mor+18] Sergii MOROZOV, Michele GAIO et al. « Metal-Dielectric Parabolic Antenna for Directing Single Photons ». In : *Nano Letters* 18.5 (2018), p. 3060-3065. ISSN : 15306992. DOI : 10.1021/acs.nanolett.8b00557 (cf. p. 135).

[Mue+12] Falk MUENCH, Cornelia NEETZEL et al. « Fabrication of Porous Rhodium Nanotube Catalysts by Electroless Plating ». In : *Journal of Materials Chemistry* (2012). DOI : 10.1039/c2jm31110k (cf. p. 148).

[Naj+11] Mohamadreza NAJIMINAINI, Fartash VASEFI et al. « Optical resonance transmission properties of nano-hole arrays in a gold film : effect of adhesion layer ». In : *Optics Express, Vol. 19, Issue 27, pp. 26186-26197* 19.27 (déc. 2011), p. 26186-26197. ISSN : 1094-4087. DOI : 10.1364/OE.19.026186. URL : https://opg.optica.org/viewmedia.cfm?uri=oe-19-27-26186&seq=0&html=true%20https://opg.optica.org/abstract.cfm?uri=oe-19-27-26186%20https://opg.optica.org/oe/abstract.cfm?uri=oe-19-27-26186 (cf. p. 64).

[NF90] T. NAKANO et A. L. FINK. « The folding of staphylococcal nuclease in the presence of methanol or guanidine thiocyanate ». In : *Journal of Biological Chemistry* 265.21 (1990), p. 12356-12362. ISSN : 00219258. DOI : 10.1016/S0021-9258(19)38354-1 (cf. p. 120).

[NKG05] Thomas NAUSER, Willem H. KOPPENOL et al. « The kinetics of oxidation of GSH by protein radicals. » In : *The Biochemical journal* 392.3 (déc. 2005), p. 693-701. ISSN : 02646021. DOI : 10.1042/BJ20050539 (cf. p. 118).

[NA16] Robert D. NEVELS et Hasan Tahir ABBAS. « Optical nanoantennas ». In : *Handbook of Antenna Technologies* 1.October 2016 (2016), p. 527-566. DOI : 10.1007/978-981-4560-44-3{_}43 (cf. p. 135).

[Ng+19] Soon Xin NG, Gediminas SENIUTINAS et al. « UV Illumination for Electron and Ion Beam Microscopy and Nanofabrication ». In : (2019). DOI : 10.1117/12.2528681 (cf. p. 148).

[Nov07] Lukas NOVOTNY. « Chapter 5 The history of near-field optics ». In : *Progress in Optics* 50 (2007), p. 137-184. ISSN : 00796638. DOI : 10.1016/S0079-6638(07)50005-3 (cf. p. 135).

[Nov12] Lukas NOVOTNY. « Optical Antennas : A New Technology that can Enhance Light-Matter Interactions ». In : *Frontiers of Engineering* 39.4 (2012), p. 100-120. ISSN : 1943-8206. DOI : 10.1364/AOP.1.000438. URL : https://www.nae.edu/Publications/Bridge/17281/17291.aspx (cf. p. 135, 139).

[NH06] Lukas NOVOTNY et Bert HECHT. « Principles of nano-optics ». In : *Principles of Nano-Optics* 9780521832243 (jan. 2006), p. 1-539. DOI : 10.1017/CBO9780511813535 (cf. p. 38, 136).

[NV11] Lukas NOVOTNY et Niek VAN HULST. « Antennas for light ». In : *Nature Photonics* 5.2 (2011), p. 83-90. ISSN : 17494885. DOI : 10.1038/nphoton.2010.237. URL : http://dx.doi.org/10.1038/nphoton.2010.237 (cf. p. 39, 40, 85).

[Nüe+22] Mark F. NÜESCH, Miloš T. IVANOVIĆ et al. « Single-molecule Detection of Ultrafast Biomolecular Dynamics with Nanophotonics ». In : *Journal of the American Chemical Society* 144.1 (jan. 2022), p. 52-56. ISSN : 15205126. DOI : 10.1021/JACS.1C09387 (cf. p. 63).

[OJ08] Alan Van ORDEN et Jaemyeong JUNG. « Review Fluorescence Correlation Spectroscopy for Probing the Kinetics and Mechanisms of DNA Hairpin Formation ». In : *Biopolymers* (2008). DOI : 10.1002/bip.20826 (cf. p. 33).

[Ort+23] Júlia Ferrer ORTAS, Pierre MAHOU et al. « Label-free imaging of red blood cells and oxygenation with color third-order sum-frequency generation microscopy ». In : *Light : Science & Applications 2023 12 :1* 12.1 (jan. 2023), p. 1-15. ISSN : 2047-7538. DOI : 10.1038/s41377-022-01064-4. URL : https://www.nature.com/articles/s41377-022-01064-4 (cf. p. 161).

[OCK16a] Jaime ORTEGA ARROYO, Daniel COLE et al. « Interferometric scattering microscopy and its combination with single-molecule fluorescence imaging ». In : *Nature Protocols* 11.4 (avr. 2016), p. 617-633. ISSN : 17502799. DOI : 10.1038/NPROT.2016.022 (cf. p. 110).

[OCK16b] Jaime ORTEGA ARROYO, Daniel COLE et al. « Interferometric scattering microscopy and its combination with single-molecule fluorescence imaging ». In : *Nature Protocols* 11.4 (avr. 2016), p. 617-633. ISSN : 17502799. DOI : 10.1038/NPROT.2016.022 (cf. p. 132).

[Pad+11] Sergi PADILLA-PARRA, Nicolas AUDUGÉ et al. « Dual-color fluorescence lifetime correlation spectroscopy to quantify protein-protein interactions in live cell ». In : *Microscopy Research and Technique* 74.8 (2011), p. 788-793. ISSN : 10970029. DOI : 10.1002/JEMT.21015 (cf. p. 33).

[Pan+16] Jiri PANEK, Eva KOZIOLOVÁ et al. « Intracellular Fate of Polymer Therapeutics Investigated by Fluorescence Lifetime Imaging and Fluorescence Pattern Analysis ». In : *Physiological Research* (2016). DOI : 10.33549/physiolres.933423 (cf. p. 33).

[PG12] Yuanjie PANG et Reuven GORDON. « Optical trapping of a single protein ». In : *Nano Letters* 12.1 (jan. 2012), p. 402-406. ISSN : 15306984. DOI : 10.1021/NL203719V (cf. p. 135).

[Pat+23] Swati J PATIL, Vladimir LOMONOSOV et al. « Tip-Enhanced Raman Imaging of Plasmon-Driven Coupling of 4-Nitrobenzenethiol on Au-Decorated Magnesium Nanostructures ». In : *The Journal of Physical Chemistry C* (2023). DOI : 10.1021/acs.jpcc.3c01345 (cf. p. 45).

[Pel+14] Jesica V. PELLEGROTTI, Guillermo P. ACUNA et al. « Controlled reduction of photobleaching in DNA origami-gold nanoparticle hybrids ». In : *Nano letters* 14.5 (mai 2014), p. 2831-2836. ISSN : 1530-6992. DOI : 10.1021/NL500841N. URL : https://pubmed.ncbi.nlm.nih.gov/24690008/ (cf. p. 135).

[Pel15] Matthew PELTON. « Modified spontaneous emission in nanophotonic structures ». In : *Nature Photonics* 9.7 (2015), p. 427-435. ISSN : 17494893. DOI : 10.1038/nphoton.2015.103. URL : http://dx.doi.org/10.1038/nphoton.2015.103 (cf. p. 38, 39).

[Per+17] Ammasi PERIASAMY, Shagufta R. ALAM et al. « FLIM-FRET image analysis of tryptophan in prostate cancer cells ». In : *Optics InfoBase Conference Papers* Part F61-E (2017), p. 1-5. ISSN : 0277-786X. DOI : 10.1117/12.2283037 (cf. p. 18).

[PS14] Marek PILIARIK et Vahid SANDOGHDAR. « Direct Optical Sensing of Single Unlabelled Proteins and Super-Resolution Imaging of Their Binding Sites ». In : *Nature Communications* (2014). DOI : 10.1038/ncomms5495 (cf. p. 20).

[Pon+19] Paolo PONZELLINI, Giorgia GIOVANNINI et al. « Metallic Nanoporous Aluminum-Magnesium Alloy for UV-Enhanced Spectroscopy ». In : *Journal of Physical Chemistry C* 123.33 (août 2019), p. 20287-20296. ISSN : 19327455. DOI : 10.1021/ACS.JPCC.9B04230 (cf. p. 45).

[Pon+18] Paolo PONZELLINI, Xavier ZAMBRANA-PUYALTO et al. « Plasmonic zero mode waveguide for highly confined and enhanced fluorescence emission ». In : *Nanoscale* 10.36 (sept. 2018), p. 17362-17369. ISSN : 20403372. DOI : 10.1039/C8NR04103B. URL : https://pubs.rsc.org/en/content/articlehtml/2018/nr/c8nr04103b%20https://pubs.rsc.org/en/content/articlelanding/2018/nr/c8nr04103b (cf. p. 61).

[Pop+08] Evgeny POPOV, Davy GÉRARD et al. « Emission and excitation contributions to enhanced single molecule fluorescence by gold nanometric apertures ». In : *Optics Express, Vol. 16, Issue 5, pp. 3008-3020* 16.5 (mars 2008), p. 3008-3020. ISSN : 1094-4087. DOI : 10.1364/OE.16.003008. URL : https://opg.optica.org/viewmedia.cfm?uri=oe-16-5-3008&seq=0&html=true%20https://opg.optica.org/abstract.cfm?uri=oe-16-5-3008%20https://opg.optica.org/oe/abstract.cfm?uri=oe-16-5-3008 (cf. p. 129).

[PW06] Aladdin PRAMANIK et Jerker WIDENGREN. « Fluorescence Correlation Spectroscopy (FCS) ». In : *Encyclopedia of Molecular Cell Biology and Molecular Medicine* (sept. 2006). DOI : 10.1002/3527600906.MCB.200300170. URL : https://onlinelibrary.wiley.com/doi/full/10.1002/3527600906.mcb.200300170%20https://onlinelibrary.wiley.com/doi/abs/10.1002/3527600906.mcb.200300170%20https://onlinelibrary.wiley.com/doi/10.1002/3527600906.mcb.200300170 (cf. p. 32, 129).

[Pre+21] Eva I PREISS, Benoit MERLE et al. « Applicability of focused Ion beam (FIB) milling with gallium, neon, and xenon to the fracture toughness characterization of gold thin films ». In : *Journal of Materials Research* 36.12 (2021), p. 2505-2514. ISSN : 2044-5326. DOI : 10.1557/s43578-020-

00045-w. URL : https://doi.org/10.1557/s43578-020-00045-w (cf. p. 63).

[Pro+13] J. PROUST, S. SCHUERMANS et al. « Synthesis of aluminum nanoparticles for UV plasmonics ». In : The Optical Society, juin 2013, JTu4A.58. DOI : 10.1364/cleo{_}at.2013.jtu4a.58 (cf. p. 45, 47).

[Puc+15a] Anastasiya PUCHKOVA, Carolin VIETZ et al. « DNA Origami Nanoantennas with over 5000-fold Fluorescence Enhancement and Single-Molecule Detection at 25 μm ». In : *Nano Letters* 15.12 (déc. 2015), p. 8354-8359. ISSN : 15306992. DOI : 10.1021/ACS.NANOLETT.5B04045/ASSET/IMAGES/LARGE/NL-2015-04045H{_}0004.JPEG. URL : https://pubs.acs.org/doi/full/10.1021/acs.nanolett.5b04045 (cf. p. 52, 96).

[Puc+15b] Anastasiya PUCHKOVA, Carolin VIETZ et al. « DNA Origami Nanoantennas with over 5000-fold Fluorescence Enhancement and Single-Molecule Detection at 25 μm ». In : *Nano Letters* 15.12 (déc. 2015), p. 8354-8359. ISSN : 15306992. DOI : 10.1021/ACS.NANOLETT.5B04045 (cf. p. 123).

[Pun+14a] Deep PUNJ, Petru GHENUCHE et al. « Plasmonic antennas and zero-mode waveguides to enhance single molecule fluorescence detection and fluorescence correlation spectroscopy toward physiological concentrations ». In : *Wiley Interdisciplinary Reviews : Nanomedicine and Nanobiotechnology* 6.3 (2014), p. 268-282. ISSN : 19390041. DOI : 10.1002/wnan.1261 (cf. p. 61).

[Pun+14b] Deep PUNJ, Petru GHENUCHE et al. « Plasmonic antennas and zero-mode waveguides to enhance single molecule fluorescence detection and fluorescence correlation spectroscopy toward physiological concentrations ». In : *Wiley Interdisciplinary Reviews : Nanomedicine and Nanobiotechnology* 6.3 (2014), p. 268-282. ISSN : 19390041. DOI : 10.1002/WNAN.1261 (cf. p. 132).

[Pun+13a] Deep PUNJ, Mathieu MIVELLE, Satish Babu MOPARTHI et al. « A plasmonic 'antenna-in-box' platform for enhanced single-molecule analysis at micromolar concentrations ». In : *Nature Nanotechnology* 8.7 (2013), p. 512-516. ISSN : 17483395. DOI : 10.1038/nnano.2013.98 (cf. p. 67, 68, 135, 149, 154, 159, 160).

[Pun+13b] Deep PUNJ, Mathieu MIVELLE, Satish Babu MOPARTHI et al. « A plasmonic 'antenna-in-box' platform for enhanced single-molecule analysis at micromolar concentrations ». In : *Nature Nanotechnology* 8.7 (2013), p. 512-516. ISSN : 17483395. DOI : 10.1038/NNANO.2013.98 (cf. p. 96).

[Pun+13c] Deep PUNJ, Mathieu MIVELLE, Satish Babu MOPARTHI et al. « A plasmonic 'antenna-in-box' platform for enhanced single-molecule analysis at micromolar concentrations ». In : *Nature Nanotechnology* 8.7 (2013), p. 512-516. ISSN : 17483395. DOI : 10.1038/NNANO.2013.98 (cf. p. 135, 164).

[Pun+13d] Deep PUNJ, Mathieu MIVELLE, Satish Babu MOPARTHI et al. « A plasmonic 'antenna-in-box' platform for enhanced single-molecule analysis at micromolar concentrations ». In : *Nature Nanotechnology 2013 8 :7* 8.7 (juin 2013), p. 512-516. ISSN : 1748-3395. DOI : 10.1038/nnano.2013.98. URL : https://www.nature.com/articles/nnano.2013.98 (cf. p. 164).

[Pun+13e] Deep PUNJ, Mathieu MIVELLE, Thomas VAN ZANTEN et al. « Plasmonic nanoantennas for enhanced single molecule analysis at micromolar conentrations ». In : *2013 Conference on Lasers and Electro-Optics Europe and International Quantum Electronics Conference, CLEO/Europe-IQEC 2013* (2013). DOI : 10.1109/CLEOE-IQEC.2013.6801867 (cf. p. 40).

[Pun+15] Deep PUNJ, Raju REGMI et al. « Self-Assembled Nanoparticle Dimer Antennas for Plasmonic-Enhanced Single-Molecule Fluorescence Detection at Micromolar Concentrations ». In : *ACS Photonics* 2.8 (août 2015), p. 1099-1107. ISSN : 23304022. DOI : 10.1021/ACSPHOTONICS.5B00152 (cf. p. 154).

[Pur46] EM PURCELL. « Spontaneous emission probabilities at radio frequencies ». In : *Phys. Rev.* 69 (1946), p. 681 (cf. p. 39).

[RSL09] Krishanu RAY, Henryk SZMACINSKI et al. « Enhanced fluorescence of proteins and label-free bioassays using aluminum nanostructures ». In : *Analytical Chemistry* 81.15 (août 2009), p. 6049-6054. ISSN : 00032700. DOI : 10.1021/AC900263K (cf. p. 136).

[Raz+23] Joseph RAZZELL HOLLIS, Sunanda SHARMA et al. « A Deep Ultraviolet Raman and Fluorescence Spectral Library of 51 Organic Compounds for the SHERLOC Instrument Onboard Mars 2020 ». In : *Astrobiology* 23.1 (jan. 2023), p. 1-23. ISSN : 15311074. DOI : 10.1089/ast.2022.0023 (cf. p. 24, 26).

[Reg+16a] Raju REGMI, Johann BERTHELOT et al. « All-Dielectric Silicon Nanogap Antennas to Enhance the Fluorescence of Single Molecules ». In : *Nano Letters* 16.8 (2016), p. 5143-5151. ISSN : 15306992. DOI : 10.1021/acs.nanolett.6b02076 (cf. p. 39).

[Reg+16b] Raju REGMI, Johann BERTHELOT et al. « All-Dielectric Silicon Nanogap Antennas to Enhance the Fluorescence of Single Molecules ». In : *Nano Letters* 16.8 (août 2016), p. 5143-5151. ISSN : 15306992. DOI : 10.1021/ACS.NANOLETT.6B02076 (cf. p. 142).

[Reg+16c] Raju REGMI, Johann BERTHELOT et al. « All-Dielectric Silicon Nanogap Antennas to Enhance the Fluorescence of Single Molecules ». In : *Nano Letters* 16.8 (août 2016), p. 5143-5151. ISSN : 15306992. DOI : 10.1021/ACS.NANOLETT.6B02076 (cf. p. 164).

[Ren+03] Bin REN, Xu Feng LIN et al. « Surface-enhanced Raman scattering in the ultraviolet spectral region : UV-SERS on rhodium and ruthenium electrodes ». In : *Journal of the American Chemical Society* 125.32 (août 2003), p. 9598-9599. ISSN : 00027863. DOI : 10.1021/JA035541D (cf. p. 44).

[Ren+20] David RENARD, Shu TIAN et al. « UV-Resonant Al Nanocrystals : Synthesis, Silica Coating, and Broadband Photothermal Response ». In : *Nano Letters* 21.1 (déc. 2020), p. 536-542. DOI : 10.1021/acs.nanolett.0c04020 (cf. p. 47).

[RV] RICHARD W. TAYLOR et V. SANDOGHDAR. *Interferometric Scattering (iSCAT) Microscopy&Related Techniques* (cf. p. 22).

[Rie+10] Jonas RIES, Zdeněk PETRÁEK et al. « A comprehensive framework for fluorescence cross-correlation spectroscopy ». In : *New Journal of Physics* 12 (2010). ISSN : 13672630. DOI : 10.1088/1367-2630/12/11/113009 (cf. p. 33).

[RS12] Jonas RIES et Petra SCHWILLE. « Fluorescence correlation spectroscopy ». In : *BioEssays* 34.5 (mai 2012), p. 361-368. ISSN : 02659247. DOI : 10.1002/BIES.201100111 (cf. p. 132).

[Rig+05] Hervé RIGNEAULT, Jérémie CAPOULADE et al. « Enhancement of single-molecule fluorescence detection in subwavelength apertures ». In : *Physical Review Letters* 95.11 (sept. 2005). ISSN : 00319007. DOI : 10.1103/PHYSREVLETT.95.117401 (cf. p. 63).

[Rin20] Emilie RINGE. « Shapes, Plasmonic Properties, and Reactivity of Magnesium Nanoparticles ». In : *Journal of Physical Chemistry C* 124.29 (juill. 2020), p. 15665-15679. ISSN : 19327455. DOI : 10.1021/ACS.JPCC.0C03871 (cf. p. 45).

[Rit06] F. RITORT. « Single-molecule experiments in biological physics : methods and applications ». In : *Journal of physics. Condensed matter : an Institute of Physics journal* 18.32 (août 2006). ISSN : 0953-8984. DOI : 10.1088/0953-8984/18/32/R01. URL : https://pubmed.ncbi.nlm.nih.gov/21690856/ (cf. p. 15).

[Rob+80] R. J. ROBBINS, G. R. FLEMING et al. « Photophysics of Aqueous Tryptophan : PH and Temperature Effects ». In : *Journal of the American Chemical Society* 102.20 (1980), p. 6271-6279. ISSN : 15205126. DOI : 10.1021/JA00540A016 (cf. p. 28).

[Rot06] Paul W.K. ROTHEMUND. « Folding DNA to create nanoscale shapes and patterns ». In : *Nature 2006 440 :7082* 440.7082 (mars 2006), p. 297-302. ISSN : 1476-4687. DOI : 10.1038/nature04586. URL : https://www.nature.com/articles/nature04586 (cf. p. 52).

[Roy+21] Prithu ROY, Clémence BADIE et al. « Preventing Corrosion of Aluminum Metal with Nanometer-Thick Films of Al2O3 Capped with TiO2 for Ultraviolet Plasmonics ». In : *ACS Applied Nano Materials* 4.7 (juin 2021), p. 7199-7205. DOI : 10.1021/acsanm.1c01160 (cf. p. 3, 11, 50, 56, 60, 136, 147).

[Roy+] Prithu ROY, Clémence BADIE et al. « Preventing Corrosion of Aluminum Metal with Nanometer-Thick Films of Al₂O₃ Capped with TiO₂ for Ultraviolet Plasmonics ». In : *ACS Applied Nano Materials* 4.7 (), p. 7199-7205. ISSN : 2574-0970. DOI : 10.1021/acsanm.1c01160 (cf. p. 139).

[RB20] Prithu ROY et Alexey D. BOLSHAKOV. « Temperature-controlled switching of plasmonic response in gallium core-shell nanoparticles ». In : *Journal of Physics D : Applied Physics* (juill. 2020). ISSN : 0022-3727. DOI : 10.1088/1361-6463/abaae2. URL : https://iopscience.iop.org/article/10.1088/1361-6463/abaae2 (cf. p. 44).

[RB21a] Prithu ROY et Alexey D. BOLSHAKOV. « A Highly Directive Ultraviolet Plasmonic "Antenna-on-Reflector" for Single-Molecule Detection ». In : *physica status solidi (RRL) – Rapid Research Letters* 15.6 (juin 2021), p. 2000579. ISSN : 1862-6270. DOI : 10.1002/PSSR.202000579. URL : https://onlinelibrary.wiley.com/doi/full/10.1002/pssr.202000579%20https://onlinelibrary.wiley.com/doi/abs/10.1002/pssr.202000579%20https://onlinelibrary.wiley.com/doi/10.1002/pssr.202000579 (cf. p. 91).

[RB21b] Prithu ROY et Alexey D. BOLSHAKOV. « A Highly Directive Ultraviolet Plasmonic "Antenna-on-Reflector" for Single-Molecule Detection ». In : *Physica Status Solidi - Rapid Research Letters* 15.6 (juin 2021). ISSN : 18626270. DOI : 10.1002/PSSR.202000579 (cf. p. 135).

[Roy+23a] Prithu ROY, Jean Benoît CLAUDE et al. « Ultraviolet Nanophotonics Enables Autofluorescence Correlation Spectroscopy on Label-Free Proteins with a Single Tryptophan ». In : *Nano Letters* 23.2 (jan. 2023), p. 497-504. ISSN : 15306992. DOI : 10.1021/ACS.NANOLETT.2C03797 (cf. p. 51, 164).

[Roy+23b] Prithu ROY, Jean-Benoît CLAUDE et al. « Ultraviolet Nanophotonics Enables Autofluorescence Correlation Spectroscopy on Label-Free Proteins with a Single Tryptophan ». In : *Nano Letters* 23.2 (jan. 2023), p. 497-504. DOI : 10.1021/acs.nanolett.2c03797 (cf. p. 3, 12, 63, 78, 104, 127).

[Roy+23c] Prithu ROY, Siyuan ZHU et al. « Ultraviolet Resonant Nanogap Antennas with Rhodium Nanocube Dimers for Enhancing Protein Intrinsic Autofluorescence ». In : *ACS Nano* 17.22 (2023), p. 22418-22429. DOI : 10.1021/acsnano.3c05008. URL : https://doi.org/10.1021/acsnano.3c05008 (cf. p. 3).

[RE12] Eric C Le RU et Pablo G ETCHEGOIN. « Single-Molecule Surface-Enhanced Raman Spectroscopy ». In : *Annual Review of Physical Chemistry* (2012). DOI : 10.1146/annurev-physchem-032511-143757 (cf. p. 22).

[Ruc+00] Thomas RUCKSTUHL, Jörg ENDERLEIN et al. « Forbidden Light Detection from Single Molecules ». In : *Analytical Chemistry* 72.9 (mars 2000), p. 2117-2123. DOI : 10.1021/ac991358k (cf. p. 40, 86).

[S N07] T Asano S NODA M Fujia. « Spontaneous-emission control by photonic crystals and nanocavities ». In : *Nature Photon.* 1 (2007), p. 449-458 (cf. p. 39).

[SMD17] Anushka S. GANGNAIK, Yordan M. GEORGIEV et al. « New Generation Electron Beam Resists : A Review ». In : *Chemistry of Materials* 29.5 (fév. 2017), p. 1898-1917. DOI : 10.1021/acs.chemmater.6b03483 (cf. p. 64).

[Sah+08] Bankanidhi SAHOO, J. BALAJI et al. « Protein aggregation probed by two-photon fluorescence correlation spectroscopy of native tryptophan ». In : *Journal of Chemical Physics* 129.7 (2008), p. 2-8. ISSN : 00219606. DOI : 10.1063/1.2969110 (cf. p. 30).

[Sam+] K T SAMIEE, M FOQUET et al. « l-Repressor Oligomerization Kinetics at High Concentrations Using Fluorescence Correlation Spectroscopy in Zero-Mode Waveguides ». In : *Biophysical Journal* 88 (), p. 2145-2153. DOI : 10.1529/biophysj.104.052795. URL : www.brenda.uni-koeln.de (cf. p. 59).

[San+13a] J. M. SANZ, D. ORTIZ et al. « UV plasmonic behavior of various metal nanoparticles in the near- and far-field regimes : Geometry and substrate effects ». In : *Journal of Physical Chemistry C* 117.38 (sept. 2013), p. 19606-19615. ISSN : 19327447. DOI : 10.1021/JP405773P/ASSET/IMAGES/JP-2013-05773P{_}M007.GIF. URL : https://pubs-acs-org.lama.univ-amu.fr/doi/full/10.1021/jp405773p (cf. p. 41).

[San+13b] J. M. SANZ, D. ORTIZ et al. « UV plasmonic behavior of various metal nanoparticles in the near- and far-field regimes : Geometry and substrate effects ». In : *Journal of Physical Chemistry C* 117.38 (sept. 2013), p. 19606-19615. ISSN : 19327447. DOI : 10.1021/jp405773p (cf. p. 42).

[San+14] Juan M. SANZ, Dolores ORTIZ et al. « Metals for UV Plasmonics ». In : The Optical Society, mars 2014, OW4D.3. DOI : 10.1364/opm.2014.ow4d.3 (cf. p. 42, 136).

[San+23] María SANZ-PAZ, Fangjia ZHU et al. « DNA Origami Assembled Nanoantennas for Manipulating Single-Molecule Spectral Emission ». In : *Nano Letters* 23 (juin 2023), p. 43. ISSN : 1530-6984. DOI : 10.1021/ACS.NANOLETT.3C01818. URL : https://doi.org/10.1021/acs.nanolett.3c01818 (cf. p. 52).

[SD21] Sonja SCHMID et Cees DEKKER. « Nanopores : A versatile tool to study protein Dynamics ». In : *Essays in Biochemistry* 65.1 (2021), p. 93-107. ISSN : 00711365. DOI : 10.1042/EBC20200020 (cf. p. 15, 24).

[SE08] Benjamin SCHULER et William A. EATON. « Protein folding studied by single-molecule FRET ». In : *Current Opinion in Structural Biology* 18.1 (fév. 2008), p. 16-26. ISSN : 0959440X. DOI : 10.1016/j.sbi.2007.12.003 (cf. p. 17).

[Sch+10] Jon A. SCHULLER, Edward S. BARNARD et al. *Plasmonics for extreme light concentration and manipulation*. 2010. DOI : 10.1038/nmat2630 (cf. p. 146).

[SH01] Petra SCHWILLE et Elke HAUSTEIN. « Fluorescence correlation spectroscopy. An introduction to its concepts and applications ». In : *Doi :10.1002/Lpor.200910041* (2001), p. 1-33. ISSN : 15206882. DOI : 10.1146/annurev.biophys.36.040306.132612. URL : http://scholar.google.com/scholar?hl=en&btnG=Search&q=intitle:Fluorescence+correlation+spectroscopy+An+introduction+to+its+concepts+and+applications#0 (cf. p. 33).

[Shi+23] Daisuke SHIMA, Hiroshi SUGIMOTO et al. « Gallium Phosphide Nanoparticles for Low-Loss Nanoantennas in Visible Range ». In : *Advanced Optical Materials* 11.12 (juin 2023). ISSN : 21951071. DOI : 10.1002/ADOM.202203107 (cf. p. 39).

[SC12] Min Ju SHON et Adam F COHEN. « Mass Action at the Single-Molecule Level ». In : *Journal of the American Chemical Society* (2012). DOI : 10.1021/ja3062425 (cf. p. 58).

[Smi+97] Alexandre SMIRNOV, Dallas R ENGLISH et al. « Photophysics and Biological Applications of 7-Azaindole and Its Analogs ». In : *The Journal of Physical Chemistry B* (1997). DOI : 10.1021/jp9630232 (cf. p. 27).

[SJZ07] Bruno F. SOARES, Fredrik JONSSON et al. « All-optical phase-change memory in a single gallium nanoparticle ». In : *Physical Review Letters* 98.15 (2007), p. 1-4. ISSN : 00319007. DOI : 10.1103/PhysRevLett.98.153905 (cf. p. 44).

[Sol+22] David SOLTI, Kyle D. CHAPKIN et al. « Plasmon-Generated Solvated Electrons for Chemical Transformations ». In : *Journal of the American Chemical Society* 144.44 (oct. 2022), p. 20183-20189. DOI : 10.1021/jacs.2c07768 (cf. p. 164).

[Špa+22] Barbora ŠPAČKOVÁ, Henrik KLEIN MOBERG et al. « Label-free nanofluidic scattering microscopy of size and mass of single diffusing molecules and nanoparticles ». In : *Nature Methods* 19.6 (juin 2022), p. 751-758. ISSN : 15487105. DOI : 10.1038/S41592-022-01491-6 (cf. p. 132).

[Sri+12] Rahul SRINIVASAN, Christopher I RICHARDS et al. « Förster Resonance Energy Transfer (FRET) Correlates of Altered Subunit Stoichiometry in Cys-Loop Receptors, Exemplified by Nicotinic A4β2 ». In : *International Journal of Molecular Sciences* (2012). DOI : 10.3390/ijms130810022 (cf. p. 59).

[Ste+15] Florian STERL, Nikolai STROHFELDT et al. « Magnesium as Novel Material for Active Plasmonics in the Visible Wavelength Range ». In : *Nano Letters* (2015). DOI : 10.1021/acs.nanolett.5b03029 (cf. p. 45).

[Sto52] George Gabriel STOKES. *XXX. On the Change of Refrangibility of Light*. 1852. DOI : 10.1098/rstl.1852.0022 (cf. p. 15).

[Str+08] Jennifer STRUNK, Jörg ENDERLEIN et al. « Probing Protein Conformations by in Situ Non-Covalent Fluorescence Labeling ». In : *Bioconjugate Chemistry* (2008). DOI : 10.1021/bc8002088 (cf. p. 19).

[Sun+21] Luzhao SUN, Guowen YUAN et al. « Chemical vapour deposition ». In : *Nature Reviews Methods Primers* 1.1 (2021), p. 5. ISSN : 2662-8449. DOI : 10.1038/s43586-020-00005-y. URL : https://doi.org/10.1038/s43586-020-00005-y (cf. p. 46).

[Sun+19] Xiaohui SUN, Xianghui AN et al. « Physical vapor deposition ({PVD}) : a method to fabricate modified g-{C}\textsubscript{3}{N}\textsubscript{4} sheets ». In : *New Journal of Chemistry* 43.17 (2019), p. 6683-6687. DOI : 10.1039/c8nj06509h. URL : http://dx.doi.org/10.1039/C8NJ06509H (cf. p. 46).

[Tan+17] Ichiro TANABE, Yoshito Y. TANAKA et al. « Far- and deep-ultraviolet surface plasmon resonance sensors working in aqueous solutions using aluminum thin films ». In : *Scientific Reports* 7.1 (2017), p. 1-7. ISSN : 20452322. DOI : 10.1038/s41598-017-06403-9. URL : http://dx.doi.org/10.1038/s41598-017-06403-9 (cf. p. 106).

[TS19] Richard W. TAYLOR et Vahid SANDOGHDAR. « Interferometric Scattering Microscopy : Seeing Single Nanoparticles and Molecules via Rayleigh Scattering ». In : *Nano Letters* 19.8 (août 2019), p. 4827-4835. ISSN : 15306992. DOI : 10.1021/ACS.NANOLETT.9B01822 (cf. p. 20).

[] *TCSPC - What is Time-Correlated Single Photon Counting?* URL : https://www.edinst.com/us/blog/what-is-tcspc/ (cf. p. 34).

[TPP12] Maria TERESA, Steffen PETERSEN et al. « UV Light Effects on Proteins : From Photochemistry to Nanomedicine ». In : *Molecular Photochemistry - Various Aspects* May 2014 (2012). DOI : 10.5772/37947 (cf. p. 119).

[Tha+14] Vivek V. THACKER, Lars O. HERRMANN et al. « DNA origami based assembly of gold nanoparticle dimers for surface-enhanced Raman scattering ». In : *Nature Communications* 5 (2014). ISSN : 20411723. DOI : 10.1038/ncomms4448. URL : www.nature.com/naturecommunications (cf. p. 96, 135).

[Tho99] George J. THOMAS. « Raman spectroscopy of protein and nucleic acid assemblies ». In : *Annual review of biophysics and biomolecular structure* 28 (1999), p. 1-27. ISSN : 1056-8700. DOI : 10.1146/ANNUREV.BIOPHYS.28.1.1. URL : https://pubmed.ncbi.nlm.nih.gov/10410793/ (cf. p. 24).

[Tiw+23a] Sunny TIWARI, Prithu ROY et al. « Achieving High Temporal Resolution in Single-Molecule Fluorescence Techniques Using Plasmonic Nanoantennas ». In : *Advanced Optical Materials* (avr. 2023). ISSN : 2195-1071. DOI : 10.1002/ADOM.202300168. URL : https://onlinelibrary.wiley.com/doi/10.1002/adom.202300168 (cf. p. 3, 102).

[Tiw+23b] Sunny TIWARI, Prithu ROY et al. « Achieving High Temporal Resolution in Single-Molecule Fluorescence Techniques Using Plasmonic Nanoantennas ». In : *Advanced Optical Materials* (avr. 2023). ISSN : 2195-1071. DOI : 10.1002/ADOM.202300168. URL : https://onlinelibrary.wiley.com/doi/10.1002/adom.202300168 (cf. p. 135).

[Tog+09] Denisio M TOGASHI, Boguslaw SZCZUPAK et al. « Investigating Tryptophan Quenching of Fluorescein Fluorescence Under Protolytic Equilibrium ». In : *The Journal of Physical Chemistry A* (2009). DOI : 10.1021/jp808121y (cf. p. 29).

[TTT03] Danyelle M. TOWNSEND, Kenneth D. TEW et al. « The importance of glutathione in human disease ». In : *Biomedicine and Pharmacotherapy* 57.3 (mai 2003), p. 145-155. ISSN : 07533322. DOI : 10.1016/S0753-3322(03)00043-X (cf. p. 118).

[Tro+23a] Kateryna TROFYMCHUK, Karol KOŁATAJ, Viktorija GLEMBOCKYTE, Fangjia ZHU, Guillermo P ACUNA et al. « Gold Nanorod DNA Origami Antennas for 3 Orders of Magnitude Fluorescence Enhancement in NIR ». In : *ACS Nano* 17.2 (jan. 2023), p. 1327-1334. ISSN : 1936-0851. DOI : 10.1021/acsnano.2c09577. URL : https://doi.org/10.1021/acsnano.2c09577 (cf. p. 52).

[Tro+22] Kateryna TROFYMCHUK, Karol KOŁATAJ, Viktorija GLEMBOCKYTE, Fangjia ZHU, Guillermo P. ACUNA et al. « Gold Nanorod DNA Origami Antennas for 3 Orders of Magnitude Fluorescence Enhancement in NIR ». In : *ACS Nano* (2022). ISSN : 1936086X. DOI : 10.1021/ACSNANO.2C09577 (cf. p. 135).

[Tro+23b] Kateryna TROFYMCHUK, Karol KOŁATAJ, Viktorija GLEMBOCKYTE, Fangjia ZHU, Guillermo P. ACUNA et al. « Gold Nanorod DNA Origami Antennas for 3 Orders of Magnitude Fluorescence Enhancement in NIR ». In : *ACS Nano* 17.2 (jan. 2023), p. 1327-1334. DOI : 10.1021/acsnano.2c09577 (cf. p. 96).

[Tse05] Ampere A TSENG. « Recent Developments in Nanofabrication Using Focused Ion Beams ». In : *Small* 1.10 (juill. 2005), p. 924-939. DOI : 10.1002/smll.200500113. URL : http://dx.doi.org/10.1002/SMLL.200500113 (cf. p. 51).

[] *Understanding Aluminum Corrosion*. URL : https://www.corrosionpedia.com/understanding-aluminum-corrosion/2/6954 (cf. p. 48, 49, 136).

[VV92] Kamil A. VALIEV et Kamil A. VALIEV. « Optical Lithography ». In : *The Physics of Submicron Lithography* (1992), p. 395-463. DOI : 10.1007/978-1-4615-3318-4{_}6 (cf. p. 149).

[VLB14] Jolien S VERDAASDONK, Josh LAWRIMORE et al. « Determining Absolute Protein Numbers by Quantitative Fluorescence Microscopy ». In : (2014). DOI : 10.1016/b978-0-12-420138-5.00019-7 (cf. p. 19).

[Wah+08] Michael WAHL, Hans Jürgen RAHN et al. « Scalable time-correlated photon counting system with multiple independent input channels ». In : *Review of Scientific Instruments* 79.12 (2008). ISSN : 00346748. DOI : 10.1063/1.3055912 (cf. p. 16).

[WT15] Dingdi WANG et Zikang TANG. « Direct Measurement of Raman Scattering Tensor of Orientation-Fixed Single Iodine Molecules ». In : *Advanced Functional Materials* (2015). DOI : 10.1002/adfm.201500763 (cf. p. 23).

[Wan+18] Juanjuan WANG, Shengli JIA et al. « Design Principles for Nanoparticle Plasmon-Enhanced Organic Solar Cells ». In : *Nanoscale Research Letters* 13 (2018). ISSN : 1556276X. DOI : 10.1186/s11671-018-2620-4 (cf. p. 38).

[Wan+16] Yunshan WANG, X JIAO et al. « UV fluorescence lifetime modification by aluminum and magnesium nanoapertures ». In : (2016). DOI : 10.1117/12.2237873. URL : https://www.semanticscholar.org/paper/6d4c56769865addb2413792fce20203d9f305aec (cf. p. 45).

[Wan+17] Yunshan WANG, E M PETERSON et al. « Magnesium as a Novel UV Plasmonic Material for Fluorescence Decay Rate Engineering in Free Solution ». In : *Journal of Physical Chemistry C* 121 (2017), p. 11650-11657. DOI : 10.1021/ACS.JPCC.7B01934. URL : https://www.semanticscholar.org/paper/e5f2bfdb953a6a141fb194f1aa139800e31eeded (cf. p. 45).

[Wat+15] Anne M. WATSON, Xiao ZHANG et al. « Rhodium nanoparticles for ultraviolet plasmonics ». In : *Nano Letters* 15.2 (fév. 2015), p. 1095-1100. ISSN : 15306992. DOI : 10.1021/NL5040623 (cf. p. 44).

[Wen19] Jérôme WENGER. « Fluorescence Spectroscopy Enhancement on Photonic Nanoantennas ». In : *Plasmonics in Chemistry and Biology* September 2017 (2019), p. 139-158. DOI : 10.1201/9780429458750-6 (cf. p. 15, 39).

[WRC23] Jerome WENGER, Prithu ROY et Jean-Benoit CLAUDE. « Deep Ultraviolet Nanophotonics to enhance the sensitivity of autofluorescence spectroscopy on label-free proteins ». In : *Conference on Lasers and Electro-Optics/Europe (CLEO/Europe 2023) and European Quantum Electronics Conference (EQEC 2023) (2023), paper eg_5_5* (juin 2023), eg_5_5. URL : https://opg.optica.org/abstract.cfm?uri=EQEC-2023-eg_5_5 (cf. p. 3).

[Wen+23] Jerome WENGER, Prithu ROY, Jean-Benoit CLAUDE et al. « Self-Assembled Deep Ultraviolet Rhodium nanogap antenna to enhance single protein autofluorescence ». In : *Conference on Lasers and Electro-Optics/Europe (CLEO/Europe 2023) and European Quantum Electronics Conference (EQEC 2023) (2023), paper eh_p_16* (juin 2023), eh_p_16. URL : https://opg.optica.org/abstract.cfm?uri=EQEC-2023-eh_p_16 (cf. p. 3).

[Wen+08] Jérôme WENGER, Davy GÉRARD et al. « Emission and excitation contributions to enhanced single molecule fluorescence by gold nanometric apertures ». In : *Optics Express* 16.5 (2008), p. 3008. ISSN : 10944087. DOI : 10.1364/OE.16.003008 (cf. p. 63).

[Wet63] D. B. WETLAUFER. « Ultraviolet spectra Of Proteins and Amino Acids ». In : *Advances in Protein Chemistry* 17.C (1963), p. 303-390. ISSN : 00653233. DOI : 10.1016/S0065-3233(08)60056-X (cf. p. 29).

[WMR95] Jerker WIDENGREN, Ülo METS et al. « Fluorescence correlation spectroscopy of triplet states in solution : A theoretical and experimental study ». In : *Journal of Physical Chemistry* 99.36 (1995), p. 13368-13379. ISSN : 00223654. DOI : 10.1021/J100036A009 (cf. p. 17).

[WRM94] Jerker WIDENGREN, Rudolf RIGLER et al. « Triplet-state monitoring by fluorescence correlation spectroscopy ». In : *Journal of Fluorescence* 4.3 (sept. 1994), p. 255-258. ISSN : 10530509. DOI : 10.1007/BF01878460 (cf. p. 37).

[Win+18] Pamina M. WINKLER, Raju REGMI et al. « Optical Antenna-Based Fluorescence Correlation Spectroscopy to Probe the Nanoscale Dynamics of Biological Membranes ». In : *Journal of Physical Chemistry Letters* 9.1 (jan. 2018), p. 110-119. ISSN : 19487185. DOI : 10.1021/ACS.JPCLETT.7B02818 (cf. p. 33).

[Win12] Christine C. WINTERBOURN. « Biological Chemistry of Reactive Oxygen Species ». In : *Encyclopedia of Radicals in Chemistry, Biology and Materials* (2012). DOI : 10.1002/9781119953678.rad077 (cf. p. 37, 118).

[Wöl14] Dominik WÖLL. « Fluorescence Correlation Spectroscopy in Polymer Science ». In : *RSC Advances* (2014). DOI : 10.1039/c3ra44909b (cf. p. 33).

[Wu+19] Meiyan WU, Wenzhao LIU et al. « Fluorescence enhancement in an over-etched gold zero-mode waveguide ». In : *Optics Express* 27.13 (2019). ISSN : 10944087. DOI : 10.1364/oe.27.019002 (cf. p. 61).

[Wu+09a] Pae C. WU, Christopher G. KHOURY et al. « Demonstration of Surface-Enhanced Raman Scattering by Tunable, Plasmonic Gallium Nanoparticles ». In : *Journal of the American Chemical Society* 131.34 (août 2009), p. 12032-12033. ISSN : 00027863. DOI : 10.1021/ja903321z (cf. p. 44).

[Wu+09b] Pae C. WU, Maria LOSURDO et al. « Plasmonic gallium nanoparticles on polar semiconductors : Interplay between nanoparticle wetting, localized surface plasmon dynamics, and interface charge ». In : *Langmuir* 25.2 (jan. 2009), p. 924-930. ISSN : 07437463. DOI : 10.1021/la802678y (cf. p. 44).

[Xia+19] Jin XIANG, Jingdong CHEN et al. « Liquid Gallium Nanospheres Emitting White Light ». In : *Laser and Photonics Reviews* 13.5 (2019), p. 1-8. ISSN : 18638899. DOI : 10.1002/lpor.201800214 (cf. p. 44).

[XNL18] Hongbao XIN, Bumseok NAMGUNG et al. « Nanoplasmonic optical antennas for life sciences and medicine ». In : *Nature Reviews Materials* 3.8 (2018), p. 228-243. ISSN : 20588437. DOI : 10.1038/s41578-018-0033-8. URL : http://dx.doi.org/10.1038/s41578-018-0033-8 (cf. p. 135).

[Yan+08] Ronghua YANG, Zhiwen TANG et al. « Noncovalent Assembly of Carbon Nanotubes and Single-Stranded DNA : An Effective Sensing Platform for Probing Biomolecular Interactions ». In : *Analytical Chemistry* (2008). DOI : 10.1021/ac801118p (cf. p. 18).

[Yan+22] Weiqing YANG, Zhihong WEI et al. « Optical Detection and Imaging of Nonfluorescent Matter at the Single-Molecule/Particle Level ». In : *The Journal of Physical Chemistry Letters* (2022). DOI : 10.1021/acs.jpclett.2c02228 (cf. p. 20).

[Yan+14] Yang YANG, Neset AKOZBEK et al. « Ultraviolet-Visible Plasmonic Properties of Gallium Nanoparticles Investigated by Variable-Angle Spectroscopic and Mueller Matrix Ellipsometry ». In : *ACS Photonics* 1.7 (juill. 2014), p. 582-589. ISSN : 23304022. DOI : 10.1021/ph500042v (cf. p. 43).

[Yan+13] Yang YANG, John M. CALLAHAN et al. « Ultraviolet nanoplasmonics : A demonstration of surface-enhanced raman spectroscopy, fluorescence, and photodegradation using gallium nanoparticles ». In : *Nano Letters* 13.6 (juin 2013), p. 2837-2841. ISSN : 15306984. DOI : 10.1021/NL401145J (cf. p. 44).

[Yar+14] Maksym YAREMA, Michael WÖRLE et al. « Monodisperse colloidal gallium nanoparticles : Synthesis, low temperature crystallization, surface plasmon resonance and Li-ion storage ». In : *Journal of the American Chemical Society* 136.35 (août 2014), p. 12422-12430. ISSN : 15205126. DOI : 10.1021/ja506712d (cf. p. 44).

[YH21] A T M YEŞILYURT et Jer-Shing HUANG. « Emission Manipulation by DNA Origami-Assisted Plasmonic Nanoantennas ». In : *Advanced Optical Materials* (2021). DOI : 10.1002/adom.202100848 (cf. p. 52).

[Yin+22] Yi Lun YING, Zheng Li HU et al. « Nanopore-based technologies beyond DNA sequencing ». In : *Nature Nanotechnology 2022 17 :11* 17.11 (sept. 2022), p. 1136-1146. ISSN : 1748-3395. DOI : 10.1038/s41565-022-01193-2. URL : https://www.nature.com/articles/s41565-022-01193-2 (cf. p. 25).

[You+18] Gavin YOUNG, Nikolas HUNDT et al. « Quantitative mass imaging of single biological macromolecules ». In : *Science* 360.6387 (avr. 2018), p. 423-427. ISSN : 10959203. DOI : 10.1126/SCIENCE.AAR5839 (cf. p. 21).

[Yu23] Qiaozhi YU. « Transient Stimulated Raman Excited Fluorescence Spectroscopy ». In : *Journal of the American Chemical Society* (2023). DOI : 10.1021/jacs.3c01995 (cf. p. 23).

[Zam+19] Xavier ZAMBRANA-PUYALTO, Paolo PONZELLINI et al. « A hybrid metal–dielectric zero mode waveguide for enhanced single molecule detection ». In : *Chemical Communications* 55.65 (août 2019), p. 9725-9728. ISSN : 1364-548X. DOI : 10.1039/C9CC04118D. URL : https://pubs.rsc.org/en/content/articlehtml/2019/cc/c9cc04118d%20https://pubs.rsc.org/en/content/articlelanding/2019/cc/c9cc04118d (cf. p. 66).

[Zan+13] Laura C ZANETTI-DOMINGUES, Christopher J TYNAN et al. « Hydrophobic Fluorescent Probes Introduce Artifacts into Single Molecule Tracking Experiments Due to Non-Specific Binding ». In : *PLoS ONE* 8.9 (sept. 2013). Sous la dir. de Paul A RANDAZZO, e74200. DOI : 10.1371/journal.pone.0074200. URL : http://dx.doi.org/10.1371/journal.pone.0074200 (cf. p. 19).

[Zha+20a] Chenyi ZHANG, Jinxin LI et al. « Nanoaperture fabrication in ultra-smooth single-grain gold films with helium ion beam lithography ». In : *Nanotechnology* 31.46 (nov. 2020). ISSN : 1361-6528. DOI : 10.1088/1361-6528/ABAE99. URL : https://pubmed.ncbi.nlm.nih.gov/32857734/ (cf. p. 63).

[Zha+23] Mohan ZHANG, Hulin TAI et al. « Resonance Raman Studies on Heme Ligand Stretching Modes in Methionine80-Depleted Cytochrome c : Fe–His, Fe–O 2 , and O–O Stretching Modes ». In : *The Journal of Physical Chemistry B* (mars 2023). ISSN : 1520-6106. DOI : 10.1021/ACS.JPCB.3C00514/ASSET/IMAGES/LARGE/JP3C00514{_}0006.JPEG. URL : https://pubs.acs.org/doi/full/10.1021/acs.jpcb.3c00514 (cf. p. 24).

[Zha+20b] Pengfei ZHANG, Guangzhong MA et al. « Plasmonic scattering imaging of single proteins and binding kinetics ». In : *Nature Methods* 17.10 (oct. 2020), p. 1010-1017. ISSN : 15487105. DOI : 10.1038/S41592-020-0947-0 (cf. p. 15).

[Zha+16] Xiao ZHANG, Pan LI et al. « Size-tunable rhodium nanostructures for wavelength-tunable ultraviolet plasmonics ». In : *Nanoscale Horizons* 1.1 (jan. 2016), p. 75-80. ISSN : 20556764. DOI : 10.1039/C5NH00062A (cf. p. 44, 136, 149).

[Zha+14] Yu ZHANG, Yu-Rong ZHEN et al. « Coherent Anti-Stokes Raman Scattering With Single-Molecule Sensitivity Using a Plasmonic Fano Resonance ». In : *Nature Communications* (2014). DOI : 10.1038/ncomms5424 (cf. p. 22).

[Zha+21a] Dong ZHAO, Zhelin LIN et al. « Recent advances in ultraviolet nanophotonics : From plasmonics and metamaterials to metasurfaces ». In : *Nanophotonics* 10.9 (juill. 2021), p. 2283-2308. ISSN : 21928614. DOI : 10.1515/NANOPH-2021-0083 (cf. p. 106, 132, 136).

[Zha+21b] Dong ZHAO, Zhelin LIN et al. « Recent advances in ultraviolet nanophotonics : From plasmonics and metamaterials to metasurfaces ». In : *Nanophotonics* 10.9 (juill. 2021), p. 2283-2308. ISSN : 21928614. DOI : 10.1515/NANOPH-2021-0083 (cf. p. 135, 136).

[Zhe+15] Yuanhui ZHENG, Alexander H SOERIYADI et al. « Reversible Gating of Smart Plasmonic Molecular Traps Using Thermoresponsive Polymers for Single-Molecule Detection ». In : *Nature Communications* (2015). DOI : 10.1038/ncomms9797 (cf. p. 23).

[Zho+21] Xiangli ZHONG, C. Austin WADE et al. « Comparing Xe+pFIB and Ga+FIB for TEM sample preparation of Al alloys : Minimising FIB-induced artefacts ». In : *Journal of Microscopy* 282.2 (mai 2021), p. 101-112. ISSN : 13652818. DOI : 10.1111/JMI.12983 (cf. p. 94).

[ZC12] Paul ZHU et Harold G. CRAIGHEAD. « Zero-mode waveguides for single-molecule analysis ». In : *Annual Review of Biophysics* 41.1 (2012), p. 269-293. ISSN : 1936122X. DOI : 10.1146/annurev-biophys-050511-102338 (cf. p. 33, 58, 59).

[Zij+19] Peter ZIJLSTRA, Rachel ARMSTRONG et al. « Single-Molecule Sensing Mediated by Localized Plasmon Resonances ». In : (2019). DOI : 10.1364/sensors.2019.sw5d.1 (cf. p. 135).

[ZPO12] Peter ZIJLSTRA, Pedro M.R. PAULO et al. « Optical detection of single non-absorbing molecules using the surface plasmon resonance of a gold nanorod ». In : *Nature Nanotechnology* 7.6 (2012), p. 379-382. ISSN : 17483395. DOI : 10.1038/NNANO.2012.51 (cf. p. 135).

[ZYT02] Aikaterini ZOUMI, Alvin YEH et al. « Imaging cells and extracellular matrix in vivo by using second-harmonic generation and two-photon excited fluorescence ». In : *Proc. Natl Acad. Sci.* 99.17 (août 2002), p. 11014-11019. ISSN : 00278424. DOI : 10.1073/pnas.172368799 (cf. p. 18).